Gyanendra Lal Shrestha

Stress induced problems in Himalayan tunnels with special reference to squeezing

Doctoral thesis
for the degree of Doktor Ingeniør

Trondheim, November 2005

Norwegian University of Science and Technology
Faculty of Engineering Science and Technology
Department of Geology and Mineral Resources Engineering

NTNU
Innovation and Creativity

NTNU
Norwegian University of Science and Technology
Doctoral thesis
for the degree doktor ingeniør
Faculty of Engineering Science and Technology
Department of Geology and Mineral Resources Engineering

ISBN 82-471-7780-3 (printed version)
ISBN 82-471-7778-1 (electronic version)
ISSN 1503-8181

Doctoral theses at NTNU, 2006:20

Printed by NTNU-trykk

Acknowledgement

This study has been carried out at the Department of Geology and Mineral Resources Engineering, Norwegian University of Science and Technology (NTNU) in Trondheim.

Professor Einar Broch has been my supervisor for this study. His vast knowledge and global scale experience have very much enriched my work. He has been always available for discussions and advices; and guided me to accomplish the objectives of this study. He has also supported rock sample transportation from Nepal, carrying out tests in the laboratory located in other Departments of the University and my trips to attend conferences. I am very grateful to him.

This study has been funded by the State Education Loan Fund of Norway. I express my gratitude to Ms Ragnhild Brakstad, Advisor / Programme Co-ordinator, Quota Programme for arranging the support from the loan fund. I am grateful to my organisation in Nepal, Butwal Power Company Ltd. and colleagues there for co-operating me in the course of my study. I am grateful to Mr Ove Rusten, Norplan A.S. for allowing me to use Melamchi rock samples and literatures for my study.

I am grateful to Mr Trond E. Larsen, NTNU Sintef, for his contribution to bring the creep test laboratory back to function and his helps to carry out tests for the mechanical properties. I am thankful to Ms Torill Sørløkk for helping me in coring and sample preparation.

I am indebted to my aunt Krishna Kumari, my father Bhakta Lal and mother Nirmala for their support throughout my life. I am grateful to my uncle Jagat Lal who inspired me to continue acquiring knowledge.

I am thankful to Professor Charlie Chunlin Li for providing very valuable comments on my thesis. I am grateful to Dr Carlos Carranza-Torres, Itasca consulting group Inc. USA, for the discussions and comments on the issues of rock engineering. I thank my office room partner Mr Krishna Panthi for being together from the first day in NTNU and going through and providing valuable comments on this thesis. I am also thankful to Mr Nghia Trinh for his valuable suggestion on my thesis.

I would like to thank my wife Sanu for moral and practical supports by taking all the social and household responsibilities, which allowed me to focus on my study. My daughter Jigyasha and son Sulabh have been very helpful to keep our home lively and that gave me freshness for the next day work.

Trondheim, November 2005

Gyanendra Lal Shrestha

Abstract

There is a huge potential of underground constructions in the Himalayan region for hydropower, transport systems and conservation of environment. However, the tectonic activities have resulted with a fragile regional geology. Moreover, the high mountainous topography causes high overburden pressure in the underground structures causing squeezing and other stability problems. Thus the huge tunnelling potential can only be materialised by applying professional and scientific approaches.

This thesis focuses on the stress induced problems with special reference to squeezing. Main objectives of this study were to review and check validity of the available tunnel stability assessment methods, to carry out relevant laboratory tests and interpret the results, and to use a numerical modelling code. In the present study, two projects have been used as case studies, both located in Nepal Himalayan region. These are Khimti1 hydropower project - a completed project; and Melamchi water supply project - yet to be constructed. Both projects include tunnels through series of weak rock mass strata with high overburden stress.

One of the factors that may cause stability problems in a tunnel is the stress level acting around the opening. A tunnel fails when the stress exceeds the strength of rock mass. If the stress level does not exceed the rock mass strength, but is sufficient up to a critical level to cause creep, it may lead to rock failure after some time. In a tunnel stability assessment, the determination of the critical stress level is important. Creep tests were carried out on the Melamchi gneiss and the critical stress level has been determined.

The resulted creep test curves were calibrated to obtain rheological parameters. Tunnel deformations including time-effect, were calculated for a given stress level. Based on the creep test results at various uniaxial stress levels, an equation is obtained for the relation between the strain rate and stress level. Back analyses have been carried out using the available empirical, semi-analytical and analytical methods and FLAC^{3D} code; the results have been found to be in close agreement with the tunnel convergence measurements in the Khimti tunnel. So these methods were used in the Melamchi tunnel design.

In the 66 squeezing tunnel cases from around the world and the Khimti case study, it was observed that the rock mass strength (corresponding to rock type) has a significant influence on squeezing phenomena. Thus the available squeezing prediction criteria based on the rock mass classification alone, need to be updated by including rock mass strength as well. Similarly, ‘valley side effect of topography’ has been found to influence the tunnel deformation in the Khimti project. It has opened an area for a further study to correlate the valley side effect of topography to the stress increase in the tunnel.

Table of contents

1 Introduction

For centuries, mankind has excavated caverns and tunnels for various purposes. Use of underground spaces and tunnels has been increasing year by year. Road and railway tunnels, water conveyance tunnels, hydropower station caverns, oil and gas storage caverns, caverns for defence, tunnels and caverns for mining, waste deposition caverns and underground sport halls are some of the examples of this kind of applications. Historically, tunnels were driven in rock by setting fires against the rock faces, which would cause expansion and spalling, often accelerated by dousing the hot rock with water (Broch, 1999). Through the development of science and technology, tunnel design and construction methods have been very much improved. It is safe to site underground constructions in hard and competent rock from a rock mechanical point of view. However, the tunnels required to meet the present day infrastructural demands cannot always be optimally sited in competent rock, so future tunnelling will to a greater extent than today be carried out in weak rock.

There is a huge potential of underground constructions in the Himalayan region for hydropower, transport systems and conservation of environment. However, it is associated with stability problems caused by the fragile regional geology and mountainous topography. These opportunity and the challenges have been the main motivations of this study. The research aims to focus on the stress induced problems with special reference to squeezing with two case studies.

When an underground excavation is made in a rock mass, the mechanical resistance, ability to transmit a force and the ability to hold a water pressure are removed in the space created. Thus it causes three primary effects:

1) Rock moves into the cavern because the resisting forces have been removed. Block may slide out depending on the rock mass discontinuities. It is a local problem and can be solved by rock bolts and shotcrete.

2) As load can not pass through the space, stress redistribution takes place. The stresses in the rock at the excavation boundary become parallel to the cavern surfaces because there are no stresses on the excavation boundary. Stress concentration caused by the stress redistribution may cause rock spalling or squeezing depending on the rock mass type. It may need systematic support.

3) Water flows into the cavern because the pressure has been reduced to atmospheric pressure at the excavation boundaries. It may need grouting or drainage if the water level is above the tunnel invert level.

Stability is the major concern in underground construction in weak rock. Besides the discontinuities of the rock masses, it is especially the stress conditions that in general

may influence the design. High or anisotropic stress condition will cause rock bursting, squeezing or other stress induced stability problems (Selmer-Olsen & Broch, 1977). Stress induced stability problems in weak and particulate rocks are characterised by squeezing. On the other hand, mountainous topography causes high overburden stress in the tunnel in the Himalayan region. Thus a combination of incompetent rock with high rock stress multiplies the squeezing problem. High mountainous ranges in the world, such as Alps, Andes and Himalayan regions are very prone to the squeezing problems. The rock stress may be due to either overburden or tectonic.

The term 'squeezing rock' originates from the pioneering days of tunnelling in the Alps during the excavation of railway tunnels between 1860 and 1910 (Kovari, 2000).

Karl Terzaghi defined rock squeezing in 1946, in his landmark paper, 'Rock defects and loads on tunnel support'. His definition states that *'Squeezing rock slowly advances into the tunnel without perceptible volume increase. Prerequisite for squeeze is a high percentage of microscopic and sub-microscopic particles of micaceous mineral or of clay minerals with a low swelling capacity'.*

In 1995, the International Society for Rock Mechanics (ISRM) Commission defined rock squeezing as: *'Squeezing of the rock is the time dependent large deformation, which occurs around the tunnel, and is essentially associated with creep caused by exceeding a limiting shear stress. Deformation may terminate during construction or continue over a long time period'.*

However, even today, with significant steps forward in geotechnical engineering, the fundamental mechanisms of squeezing are not fully understood (Steiner, 1996; Barla, 2000). Any further study in squeezing, thus, will be useful to enrich the available knowledge in this area. This study has made a literature survey to update and synthesise fundamentals of rock mechanics in squeezing condition. It has also explored the available methods that have been proposed to assess deformation caused by squeezing and to design tunnel supports.

It is evident that a tunnel fails when the stress exceeds the strength of rock mass around the opening. If the stress level does not exceed the rock mass strength, but is sufficient to cause creep, it may lead to rock failure after some time. If the creep stress level remains below the critical stress level, it does not lead to rock failure. Thus, in a tunnel stability assessment, determination of the critical stress level is important. Critical stress level has been determined by carrying out creep tests. Complete stress-strain tests were also carried out to correlate with creep test results. It gives total strain at failure and with strain rate it is possible to determine time to failure. It may replace many creep tests at various stress levels.

In this present study, two projects have been used as case studies. Those are Khimti1 hydropower project and Melamchi water supply project, both located in Nepal Himalayan region. Khimti1 hydropower project is a completed project and Melamchi water supply project is yet to be constructed. Both the projects include tunnels through series of weak rock mass strata with high overburden stress. The available methods have been used to calculate tunnel squeezing and compare it with the measured convergences in the Khimti tunnel. After evaluating the validity, those methods were used for stability analysis and squeezing estimation for the Melamchi tunnel.

Creep tests have been carried out and the critical stress level has been determined for the Melamchi augen gneiss. Tunnel stability analysis and tunnel convergence estimation was also carried out by using the numerical modelling FLAC^{3D} code. Objectives of this study are outlined in section 1.1.

1.1 Objectives

The main objectives of this study are as follows:

- Update knowledge on rock mechanics in squeezing condition and evaluate the available methods for tunnel stability assessment and support design.
- Creep tests to find out critical stress level below which creep does not cause rock fail. By using the creep test curves rheological parameters are determined.
- Complete stress-strain test to correlate it with creep test results. It gives total strain at failure.
- Tunnel stability analysis and squeezing estimation by using empirical, semi analytical and analytical methods.
- Tunnel stability analysis and squeezing estimation by using numerical modelling with and without considering time-effect.
- Recommend steps to assess and quantify squeezing and to design support.

In order to achieve the above mentioned objectives, a literature survey has been carried out. Two case projects have been studied with data and sample collection and lab tests for creep (long term deformation). FLAC^{3D} code has been used to simulate and analyse the tunnel deformation with and without time-effect.

1.2 Thesis organisation

Chapter 2 gives a review on the basic rock mechanics that explains the squeezing phenomenon in underground structures. It illustrates the phenomenon with an example from Lesotho. By using 66 tunnel squeezing cases from fifteen countries, it also gives a general graphical relationship between the rock type and the overburden height.

Review of the available methods for tunnel stability assessment and support design was an important part of this study. Chapter 3 gives review and discussion on those empirical, semi-analytical and analytical methods.

Many publications have been reviewed and referred in Chapters 2 and 3. Use of symbols has not been consistent in these 2 chapters. For the same parameter, different symbols are used in different publications. For example, R, a and ri are used to denote tunnel radius. However, consistency has been maintained in rest of this thesis.

Two case projects have been considered in this thesis and those are described in Chapter 4. The first case is the Khimti1 hydropower project. Its construction is completed and is in operation. The second case is the Melamchi water supply project. Its construction has not started yet.

Chapter 5 presents comparison of the tunnel convergences calculated and measured in the Khimti headrace tunnel. Input data have been obtained from the 'registration of the applied support' and the 'tunnel log' based on Q-method. The comparison was made for 26 tunnel sections and found to be comparable showing that the available methods are useful.

During detailed site investigation of the Melamchi water supply project, many borehole drillings were carried out and core samples were obtained. Some of the rock cores were transported to NTNU, Norway and three types of laboratory tests were carried out in different laboratories in NTNU. Those tests were for the mechanical properties, the time-dependent deformation and the complete stress-strain curves. These tests and the results are given in Chapter 6. The laboratory test results are used in the approaches discussed in Chapter 3 and stability analysis and support design are carried out for the Melamchi tunnel. Details of these analyses and design are given in Chapter 7.

Chapter 8 focuses on the numerical modelling using FLAC^{3D} for the Khimti and Melamchi tunnels. As there is no rheological data available, numerical modelling for the Khimti tunnel does not include time effect. On the other hand, numerical modelling has been carried out for the Melamchi tunnel with and without considering time effect.

Finally, Conclusions are given in Chapter 9, and on the basis of this study some recommendations are also made and included in the same chapter.

2 Rock mechanics in squeezing phenomenon

Squeezing phenomena have been observed in tunnels and caverns in various geological environments around the world. As described in Kovari (2000), the Alpine geologist Heim warned in his 1878 article that 'for each rock one needed to envisage a column so high that its weight exceeded the strength of the rock and therefore the foot of the column would be crushed'. Heim assumed that ‘the internal friction would be so reduced under the all round pressure that a stress redistribution would occur without cleavage and the rock begins to flow, just like ice flows in a glacier’. Wiesmann in 1912 discovered the error in the reasoning of Heim (in Kovari, 2000). Firstly, it is not the uniaxial, but the triaxial, compressive strength that applies to the behaviour of the rock surrounding the tunnel: 'The bearing capacity of enclosed bodies, this is the governing rock strength'. Secondly, the behaviour of a rock in a plastic state cannot be compared to that of a fluid. In a viscous (Newtonian) fluid it is only a question of time until a hydrostatic stress state develops. Due to internal friction, however, rocks behave quite differently.

In rocks with low values of uniaxial compressive strength, conditions for rock failure due to concentration of initial stress may lead to slow compression (“squeeze”) and destruction of tunnel supports rather than violent collapse (Goodman, 1989). Squeezing may occur in two main types of rock masses, namely, 'massive' (or intact) incompetent or weak (ductile, deformable) rocks and 'particulate materials' (or heavily jointed) rocks (Nilsen and Palmstrom, 2000). Hard rocks are those with maximum strain at failure of less than 2% (ASTM, 1985). Thus weak rocks fail with a strain of 2% or more. The presence of major discontinuities or of a number of joint sets does not necessarily imply that the rock mass will behave as a discontinuum (Brady and Brown, 1985). A heavily jointed rock mass also may behave as an incompetent massive rock mass. In such rocks, a solution for stresses and displacements derived from the theory of plasticity provides a useful basis for engineering work (Goodman, 1989).

The convergence of tunnel are to be analysed taking into account the immediate convergence due to the advance of the face and the time-dependent convergence due to the rheological behaviour of the rock mass (Panet, 1996). After the advance of the tunnel face, if the stress developed around the opening exceeds the strength of the rock mass, the rock mass starts squeezing instantaneously. This is called 'Instantaneous squeezing'. If the accumulated stress does not exceed the rock mass strength but is sufficient to cause creep, it will cause convergence towards the tunnel. It is called ‘Secondary squeezing’. Thus the squeezing may take place in one of two stages and it depends on the tangential stress level, rock mass properties and tunnel shape. These two types of squeezing are discussed in the following two subsections.

2.1 Instantaneous squeezing

Undisturbed ground is considered to be in equilibrium. Its inherent stress regime is one of the systems present in the ground. Stress can be characterised by magnitude and direction. The magnitude and direction of the stresses depend on many factors, including overburden, topography, rock mass and tectonic pressure (if present). All of the principal stresses are uniformly distributed across the underground mass. Figure 2.1(a) is an example of a stress map, but shows only one of the principal stresses.

When an underground opening is excavated, the existing stress regime is disturbed. As the stress cannot pass through the opening, it redistributes itself around the opening. This causes the concentration of stress along the contour of the opening (Figure 2.1(b)). When the stress developed around the opening exceeds the strength of the rock masses, the rock around the tunnel opening is squeezed. This is called 'Instantaneous squeezing'. Thus, it is a kind of stress failure condition caused by overstressing (Figure 2.1(c)).

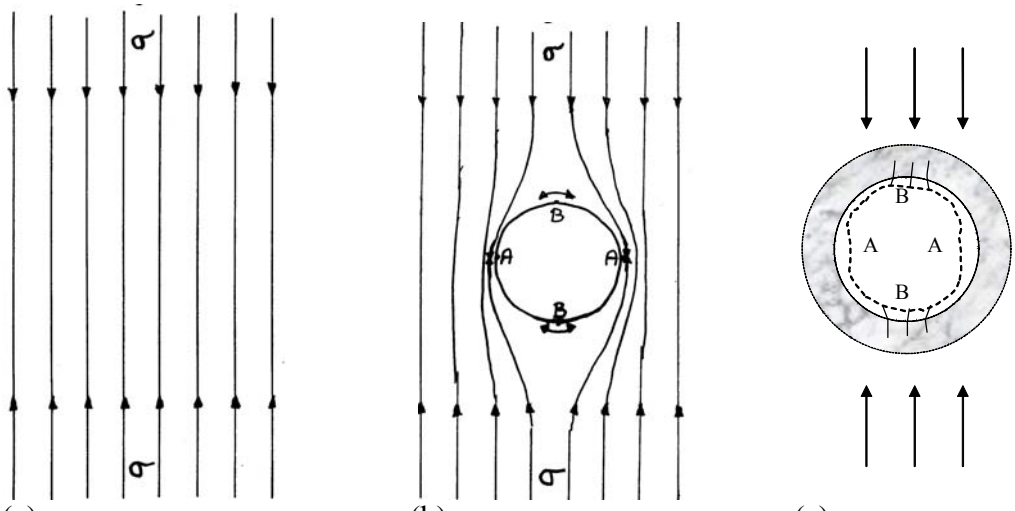

(a) (b) (c)

Figure 2.1 Vertical stress distribution (a) before excavation (b) after excavation and (c) A is squeezing failure location and B is tensile failure location indicated by the dotted lines.

The contour of an underground opening normally has two diametrically opposed areas of maximum tangential stress concentration, and two areas of minimum tangential stress. Squeezing problems normally occur at the areas of maximum tangential stress. However, if the minimum tangential stress is very low, it may also cause a problem. As a rock mass is of a discontinuous character, it can resist only a very small tensile stress. Hence, even a small tangential tensile stress may cause radial fracturing. It may result either in a new discontinuity as secondary jointing, or it may increase the opening of the existing joints.

2.2 Squeezing by creep

As defined by the ISRM, squeezing is time -dependent deformation, essentially associated with creep caused by exceeding a limiting shear stress. The complete stress-strain curve can also be used to predict rock failure as a result of creep. As shown in Figure 2.2, the locus of a creep test in stress-strain graph is a horizontal line. If the initial stress in the rock is close to the peak load, any creep will terminate in rupture when the accumulated strain intersects the falling part of the complete stress-strain curve. A creep test started at A will terminate in a rupture at point B in a relatively short time.

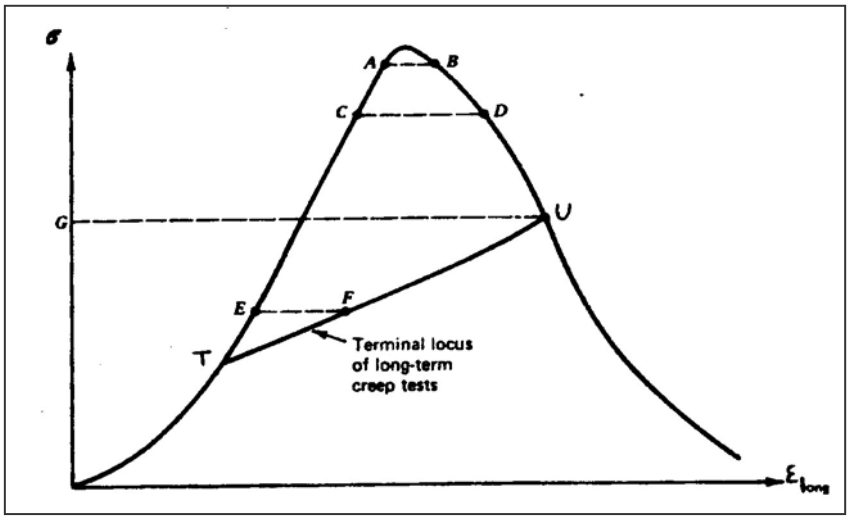

Figure 2.2 Creep in relation to the complete stress-strain curve (Goodman, 1989).

A creep test begun at C will terminate in a rupture at D after a much longer time. And a creep test initiated at E below the critical stress level G will approach point F and stops at a finite strain without rupture after a long time. Below T (creep threshold) there is no creep. If a number of creep tests are performed, each one for a different value of the applied stress (between level T and U), the results obtained can be plotted by giving the terminal locus of long term creep test (TU). The line T-U is the terminal locus of long-term creep tests. Above level U (or G), the minimum creep rate (secondary) increases with stress level and the test terminates with tertiary creep and fracture when the accumulated strain has reached a finite value, given by the descending part of the curve.

This shows that rock mass may creep to failure even if it has not failed immediately after the excavation. Failure takes place as the creep line intersects the falling part of the stress-strain curve. This is called 'secondary squeezing'. Time dependency is absent in tests with axial stress (σ_1) less than 40% of uniaxial compressive strength (q_u), and secondary creep is unimportant when σ_1 is less than 60% of q_u (Goodman, 1989).

Time dependent deformation (creep) caused tunnel sidewall spalling in 'Clarens' sandstone in Lesotho with uniaxial compressive strength (UCS) to the vertical stress ratio as high as 4 (Broch, 1996), whereas overstressing always occurred where the ratio was lower than 2.5 (section 2.6.1). These phenomena were observed several weeks after the excavation. These stress induced spalling phenomena were rather different from the violent rockbursting, which is the normal case in Scandinavian hard crystalline rocks. Similarly, the deformation in squeezing section of Taw Tunnel in Japan, continued for more than 1500 days after the completion of excavation (Aydan et al., 1996).

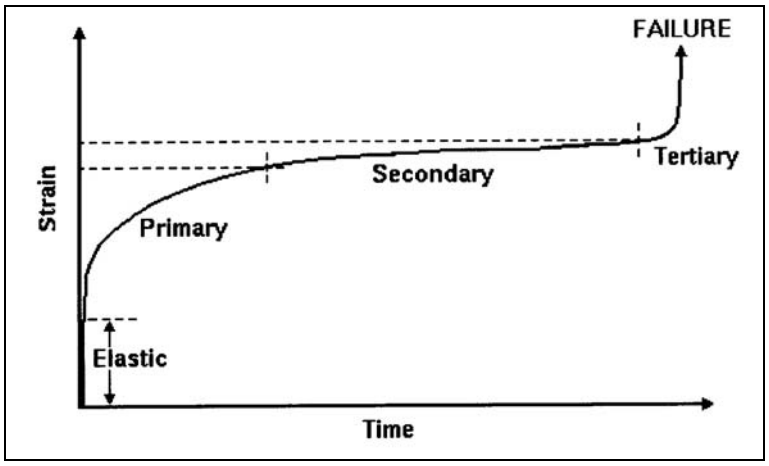

Figure 2.3 Regions of behaviour in creep (University of Saskatchewan, 2003)

The strain-time curve for a creep test has a very characteristic form. Initially, as the load is applied, the elastic strain occurs virtually instantaneously. As time passes under constant stress, the rate of strain decreases. The period of decelerating strain rate is called primary creep. The primary creep phase is followed by an extended period of slow (almost steady-state) deformation called secondary creep. At the end of this stage, the strain rate begins to accelerate and the material rapidly fails. The final stage of accelerating deformation is called tertiary creep.

Creep in rock masses is associated with crack propagation. During the primary creep phase the rock 'acclimatises' to stress and crack propagation slows to a stable, almost constant rate. During the 'steady' secondary creep stage, the material is damaged more and more until finally, in the tertiary stage, uncontrolled accelerating crack propagation leads to failure. Creep is important at low pressures only in a few rock types: shales, soft chalks and evaporite rocks (e.g. rock salts, gypsum and anhydrites). It is a major factor in the design and construction of potash mines in Saskatchewan (University of Saskatchewan, 2003).

2.2.1 Effect of water on creep

Broch (1974) showed effects of water on some isotropic (quartzdiorite and gabbro) and anisotropic (gneiss) rock with low porosity ranging from 0.3 to 1.2%. For quartzdiorite and gabbro, water saturation caused uniaxial compressive strength (UCS) decrease by 33% and 42% respectively. Similarly, for gneiss specimens cored parallel to foliation and perpendicular to foliation UCS reduction were 38% and 53% respectively. According to the results from the triaxial tests, the failure strength trend for dry and water saturated rocks were similar in case of isotropic rocks, but that was not maintained in case of gneiss specimens (Figure 2.4). Experiment results also showed that internal friction reduced in case of anisotropic rocks when it is saturated, but it did not vary in case of isotropic rocks.

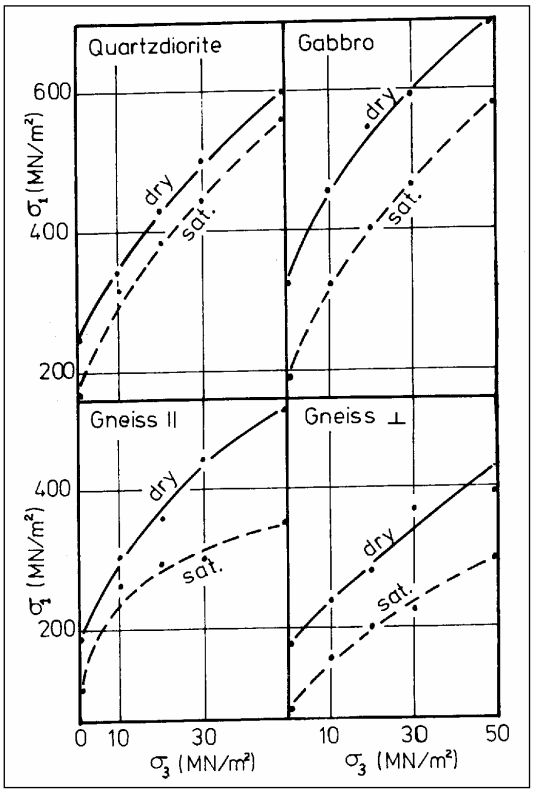

Figure 2.4 Failure curves for dry and water saturated rocks (Broch, 1974).

Presence and character of pore fluids in rocks affects their behaviour, especially in the brittle and semi-brittle rock conditions. If the pore fluid is water, two different effects are found: on the one hand, it enhances the rate of crack formation under stress, leading to increased short- and long-term deformability and a reduced long-term strength. This is considered to be partially due to water favouring stress corrosion at the crack tips and partially due to the internal (capillary and adsorption) stresses induced by changing the rock humidity.

On the other hand, as shown by Brace and Martin (1968), the effect of pore fluids can also be purely mechanical and related to the possibility of fluid drainage at a given applied strain rate. In their drained compression test with low porosity rocks, they found that at low strain rates there is sufficient time for pore pressures to dissipate, so the effect of water on strength is negligible. However, when the strain rate exceeds a certain critical value, the pore tensions created by rapid crack extension cannot dissipate and produce temporarily an internal confinement, which increases the rock strength. This effect, known as 'dilatancy hardening', has been investigated and found to apply to different kinds of rock and other cemented granular materials.

2.2.2 Effect of confining pressure on creep

Confining pressure increases the differential stress which a rock can sustain before fracturing. If a stress difference less than the fracture stress is applied, confining pressures increases the time to failure. It is thought (Kranz, 1979 in Ladanyi, 1993) that although pressure does not affect the nucleation of microcracks, it does increase the energy barrier to be overcome for continuous crack propagation. The difference between the creep test and rapid fracture test lies in the method of overcoming the energy barrier. In the fracture test, the energy is supplied by the continuously increased deviatoric stress, which drives the cracks to extend and interact. In the creep test, at a constant stress difference, cracks propagate into a stable position and stop. Further growth occurs when the energy barrier is lowered by a stress corrosion reaction at the crack tip.

Besides increasing the crack propagation energy required and the fracture toughness, confining pressure increases the mean normal pressure on any plane within the rock and results in closing the cracks. If a crack closes under pressure, the transport of fluids and gases through the rock is reduced, which has a beneficial effect on the corrosion process because during creep new crack surfaces cannot be reached by corrosive agents. In general, it is found that the effect of confining pressure is to decrease creep rates, increase static fatigue failure time and increase the amount of inelastic deformation the rock can sustain before failure (Ladanyi, 1993).

2.3 Factors influencing the squeezing phenomena

Squeezing ground conditions are influenced by many factors which contribute in different degrees. On the basis of analysis and case studies, many authors have identified and recognised those factors in different ways (Steiner, 1996; Aydan et al., 1996; Kovari et al., 2000; Gioda and Cividani, 1996; Brantmark and Stille, 1996; Max et al., 2005; and Brantmark, 1998). All those factors are compiled and mentioned and described below:

- Stress condition,
- Strength and deformability of the rock mass,
- Rock type,
- Water pressure and porosity of rock mass,
- Orientation of the geological structures,
- Construction procedures and support systems.

The ratio of rock mass strength to in situ stress plays a major role. Hence weak or strongly foliated or crushed rock may lead to squeezing even for low overburden. According to the survey of squeezing tunnels in Japan, squeezing took place when the value of this value is less than 2 (Aydan et al., 1996).

Large long-term deformations or large long-term rock pressure only occur in rocks of low strength and high deformability. Low rock mass strength gives low value for the ratio of rock mass strength to in situ stress causing overstressing condition. In addition, high deformability causes large deformation. Thus the rock mass strength and deformability directly contribute to the squeezing positively.

Phyllite, schist, serpentine, claystone, tuff, certain types of flysch, and weathered clayey and micaceous metamorphic rocks are typical examples of squeezing rock types. Fault-crushed zone is also a common location for squeezing problem, for example Lærdal tunnel in Norway (Grimstad, 2000).

The most important effect of the water is the high pore water pressure. The distribution of the water pressures may be quite complex. The pressure also increases when there is clay in a discontinuity plane which is located in the vicinity of the tunnel. Reduction of water pressure may result in the reduction of the squeezing potential with time. On the other hand, increase of the rock porosity reduces the mechanical strength of the rock.

The orientation of the geological structure relative to the underground opening affects squeezing. If the foliation or a fault (in vicinity) is parallel to the tunnel the squeezing behaviour may be an order of magnitude greater than for foliation or a fault perpendicular to the axes (John et al., 2005). Also for the structural features striking parallel to the tunnel, the dip relative to the opening is important. Overbreak due to buckling of schistose layers will occur mainly where the schistosity is parallel to the tunnel perimeter. Thus for nearly vertically dipping layers a vertical sidewall is unfavourable.

The selection of a suitable construction procedure may have beneficial effects on squeezing. The heading and benching method used in the Moffat Tunnel and at the Vereina Tunnel south permitted a very short distance between the tunnel face and the ring closure. Different support means react differently. A minimal support pressure may be necessary to stabilise the rock. Steel sets in combination with shorcrete or concrete and a circular cross-section may provide much higher support pressures than a dense pattern of rock bolts (Steiner, 1996).

Environment (for example alteration of rock), rock durability (for example slaking of mudstone) and joint filling of gouge type also may affect the squeezing phenomena.

For the assessment of the squeezing potential all the known factors must be considered and their relative influences must be evaluated. If some parameters can not be assessed quantitatively, then at least a qualitative description should be attempted.

In the following chapters, squeezing is only considered as a convergence phenomena caused by overstressing and deformation characteristics of the rock mass. Time dependent phenomenon is also included by using rheological parameters.

2.4 Factors affecting stress distribution in underground constructions

2.4.1 Influence of rock mass character on stress distribution

A simple case of a circular opening in homogeneous, isotropic and elastic rock material is considered with isostatic initial stress ($\sigma_1=\sigma_2=\sigma_3=\sigma$) condition. The stresses around the opening with radius (r_i) depend on the distance (r) from the circle centre:

Radial stresses $\sigma_r = \sigma(1 - r_i^2/ r^2)$

Tangential stresses $\sigma_\theta = \sigma(1 + r_i^2/ r^2)$

A tangential stress with a magnitude of twice the magnitude of the isostatic stress will be induced all around the periphery (Figure 2.5(a)). In situ rock stress measurements indicate that the stresses stabilise at a constant level at a distance from the tunnel contour corresponding to approximately half the tunnel width (Nilsen and Palmstrom, 2000). This constant level corresponds to the actual original or initial stress.

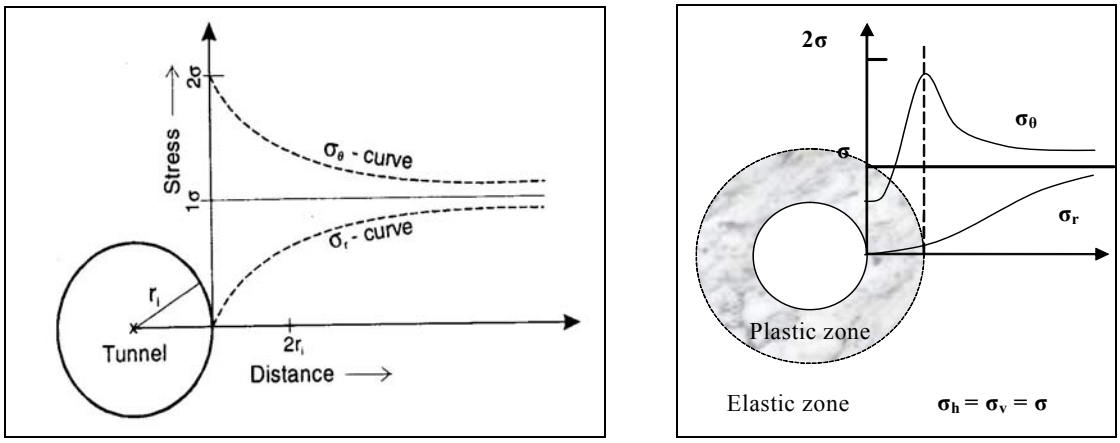

(a) (b)

Figure 2.5 Stress distribution around a tunnel in (a) elastic rock masses (Goodman, 1989) (b) plastic rock masses (Herget, 1988).

The distribution of the tangential stress will greatly depend on the mechanical properties (strength and deformation modulus) of the rock mass, and hence also on the way the excavation is carried out. In carefully blasted tunnels and TBM-bored tunnels in hard rocks, the stress peak is steep, and a distinct maximum stress value is located at the tunnel contour as shown by the curve in Figure 2.5(a). In fractured rock, and also in soft rocks, the stress peak is relatively flat, and the maximum stress value is located at some distance from the tunnel contour, as shown by the curve in the figure 2.5(b). Blasting damage will cause most drill-and-blast tunnels to exhibit this kind of stress curve.

2.4.2 Stress anisotropy

Usually, the undisturbed stress situation is often highly anisotropic. Therefore the tangential stress varies around the periphery of a circular opening. For an anisotropic stress condition, Kirsch's equations may be used for evaluating the tangential stresses. According to Kirsch the tangential stress will reach its maximum value ($\sigma_{\theta max}$) where the σ_1-direction is a tangent to the contour, and its minimum value ($\sigma_{\theta min}$) where the σ_3-direction is a tangent. Thus the actual values will be:

$\sigma_{\theta max} = 3\sigma_1 - \sigma_3$

$\sigma_{\theta min} = 3\sigma_3 - \sigma_1$

Thus, the distribution of tangential stress is strongly influenced by the degree of stress anisotropy. If the stresses are very anisotropic, the minimum tangential stress may even be negative, that is, tensile.

A characteristic feature of a fault zone is a frequent change in rock stiffness within the fault materials. During tunnel excavation, this leads to unfavourable stress concentrations in the stiffer parts of the rock mass, which may fail suddenly. In such heterogeneous rock, a reduction of displacement will also be required to reduce stress concentrations in stiffer rock parts (Schubert, 1996).

In squeezing condition, rock mass around the tunnel is usually weak or fractured and of low stiffness. The rock mass is already beyond the elastic condition and the stress peak is already shifted to the undamaged part of the rock mass. Thus stress anisotropy around the tunnel contour is not as pronounced as in strong hard rock. So the deformation due to the squeezing is not localised and it takes place around the tunnel periphery, though the quantities may not be same. On the other hand, in rockbursting condition, deformation is localised and that is based on the direction of the main principal stress.

2.4.3 Stress redistribution through support

As mentioned in section 2.1, the distribution of the tangential stress depends on the mechanical properties of the rock mass and also on the excavation method (Figures 2.5(a) and 2.5(b)). After excavation in weak rocks, if the rock strength is less than the tangential stress, it will crush (make plastic) the rock mass around the opening (MBT, 2003). The stress distribution in such a case also will be similar to figure 2.5(b). The plastic zone around the opening cannot take high stress and the stress peak moves outward, from the boundary of the opening in to the rock.

Stress conditions change with the change in the condition in opening. When support is applied to the tunnel contour, stress redistribution takes place and stress also build up on the tunnel support. In Figure 2.6, solid and dotted lines represent tangential stresses in

unsupported and supported tunnel conditions respectively. Up to 1.0 MPa stress was measured in shotcrete support in Heggura road tunnel (Norway) in 1996 after its construction in 1982 (Myrvang, 1997). If it had been a rigid concrete support it would have taken even higher stress level. The support affects the stress condition in two ways: the stress level at tunnel contour increases and the stress peak level decreases (Goodman, 1989). Support provides confining pressure (σ_3) and helps rock mass to take more stress (Mohr-Coulomb criteria). Support activates only after rock mass pushes it. However, the location of the stress peak will be same as in figure 2.5(b) as the tunnel lining cannot change the rock mass from plastic to elastic condition.

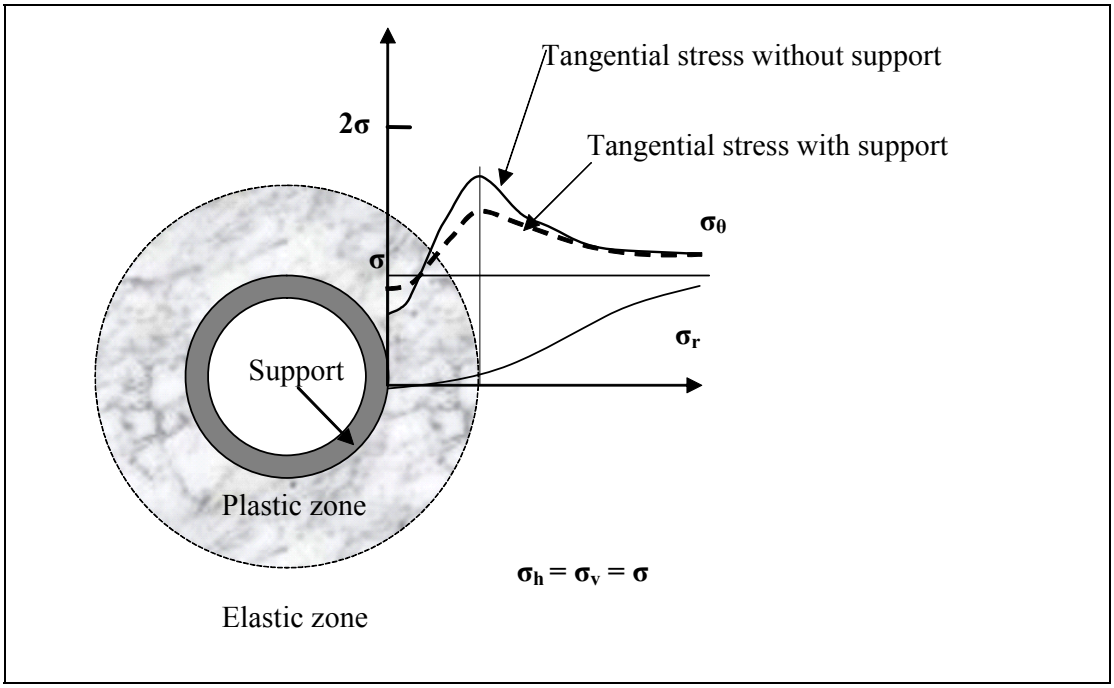

Figure 2.6: Stress distribution around a tunnel after the application of the tunnel support.

Some of the concentrated stress passes through the support as it finds support capable to stand the part of the stress, and hence partial stress relief takes place from the rock mass around the underground opening. Thus with the decrease of the tangential stress peak value, creep rate will reduce or stop, depending on the support strength. Considering these facts, thickness and residual strength of plastic zone need to be assessed for support design.

2.5 Strain energy, rockbursting and squeezing

The strain energy, or the potential energy stored in a strained body which is in equilibrium under the action of the forces, is equal to the work done by these forces acting through their displacements from the unstrained state to the position of equilibrium (Jaeger & Cook, 1976).

The strain energy per unit volume under uniaxial loading condition is

$$W = \frac{1}{2}\sigma_1\varepsilon_1 = \frac{1}{2}\frac{\sigma_1^{\,2}}{E}$$

The strain energy that can be stored in rock has also been considered as some measure of the tendency to burst. The rock burst is defined as any sudden and violent expulsion of rock from the surroundings of the opening, the phenomenon resulting from the static stress exceeding the static strength of the rock, and the result being of sufficient magnitude to create an engineering problem. The higher the maximum strain energy that can be stored in a given type of rock, the more likely the rock will be a type subject to bursting. Stress and the mechanical characteristics (such as UCS and elasticity modulus) of the rock are the factors causing rock bursting. Other mechanical characteristics such as shear strength and hardness, probably relate in some degree to bursting although data for the both parameters are scarce. The class of rock generally associated with rock bursts is qualitatively described as hard, strong and brittle.

As the strain energy per unit volume in a uniaxially loaded body of rock is $\sigma_1^2/2E$, the maximum strain energy per unit volume would be σ_c /2E, where σ_c is the uniaxial compressive strength (Obert & Duvall, 1967). Hence, on the strain energy basis, for rock types in the same stress environment with all mechanical characteristics identical except compressive strength, the type with the lowest compressive strength should be the least likely to burst.

In 1984, Broch and Sørheim presented their findings from the experience of the 5360 metre long Heggura road tunnel in Norway, subjected to heavy rockbursting. According to Broch and Sørheim (1984), the rockbursting activity increases with increasing strength of the rock, almost independent of the magnitude of the tangential stresses (Figure 2.7).

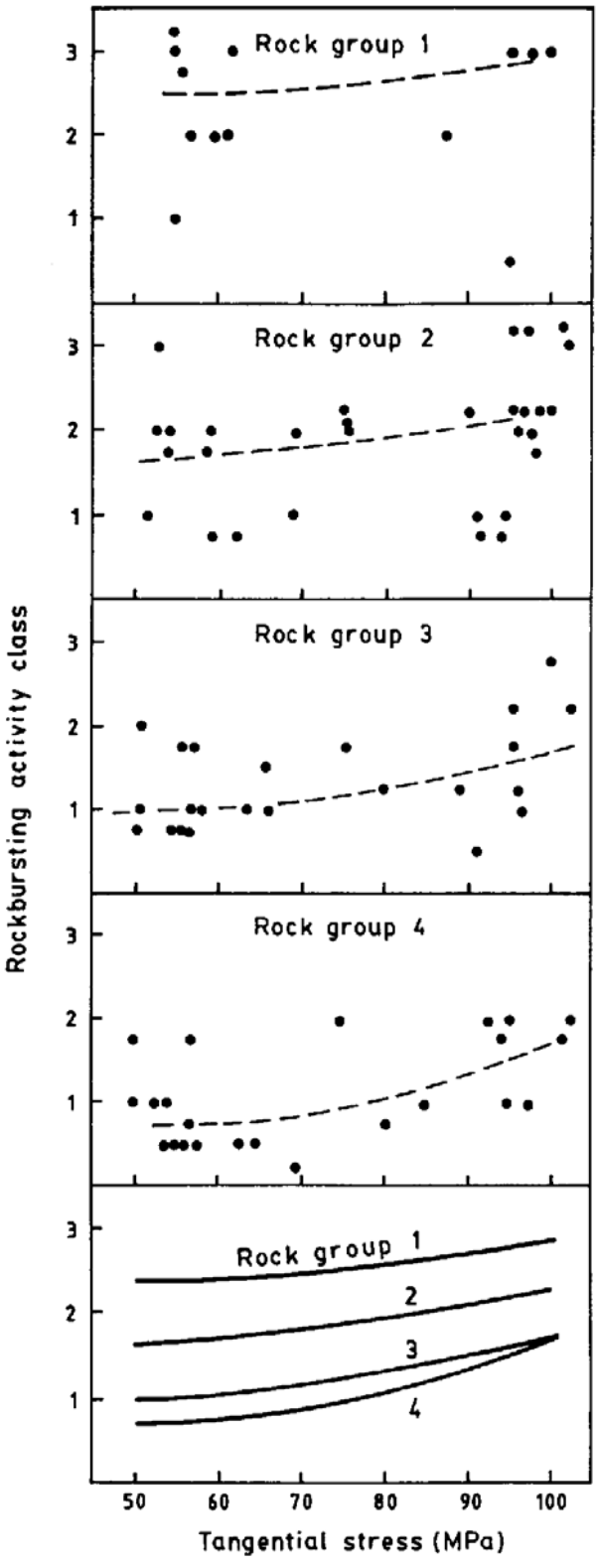

Figure 2.7 Theoretically calculated maximum tangential stresses and rockbursting activity for the rock in the Heggura tunnel (Broch and Sørheim, 1984).

In the Figure 2.7, mica and amphibolite content is increasing and strength parameters decreasing from Rock group 1 to 4. On the other hand, rockbursting activity is increasing from Class 0 to 3: Class 0 indicates no rockbursting and Class 3 high or intense rockbursting activity. Typical rock types from six stations in the tunnel were divided in four groups on the basis of strength, elasticity and content of mica and amphibole minerals. Stronger rocks were stiffer as well, and will thus be able to store more energy than weaker and softer rocks. When failure occurs, this will therefore be violent and the rockbursting will be experienced as dangerous.

On the other hand, the mechanical characteristic that seems to distinguish bursting from non-bursting rock is that the latter tends to plastically and/or visco-elastically deform under stress to the degree that failure takes place slowly. Weak rocks slowly release the pressure which can otherwise cause a rock burst, by plastic and/or visco-elastic deformation. Thus weak rocks would be the least likely to burst, because

they would reach their failure point far before they could store enough strain energy to produce a violent failure (Wahlstrom, 1973).

2.6 Some examples of squeezing problems in tunnelling

2.6.1 Time dependent stress induced problem in 'Clarens' sandstone in Lesotho

Lesotho Highlands Water Project is one of the largest underground construction projects in Africa. Through a series of five vast reservoirs and more than 200 km of tunnels, water will be diverted from the highlands of Lesotho to South Africa. Phase 1A of this ambitious long-term master plan includes construction of two dams, excavation of 82 km of about 5 m diameter tunnel and construction of an underground power station. Out of 82 km of total tunnel, the length of the Delivery Tunnel was 37 km comprising 15 km in the southern part and it was excavated in three TBM drives (Lesotho Highlands Water Project, Volume-1, 1992). The Drive-3 from Ngoajane to Vent Shaft 5 has a total length of 5690 m and time-dependent stress relief spalling occurred in this section (Figure 2.8).

This tunnel South was bored in a very uniform Clarens sandstone, partly of aeolian (wind blown desert sand) origin. It is of Jurassic age and in fact, contains a lot of dinosaur fossils (Broch, 1996). It has a high RQD rating and a compressive strength of between 50-120 MPa.

Figure 2.8 'Dog-earing' problem caused by overstressing (photo by Broch, 1993).

The stress relief spalling, locally called ‘dog-earing’ in the Drive-3 tunnel of Delivery Tunnel South was governed by the ratio of rock strength to stress. So the tunnel sections where rock strength was low and overburden was high, had severe overstressing problem. Severe ‘dog-earing’ was observed where strength/stress ratio was less than 2.5 and less severe effect for ratios between 2.5 and 4.0. The disposition of the major spalling at the 3 o’clock and 9 o’clock positions on the tunnel circumference indicates that the maximum principal stress (σ_1) is vertical (Lining for overstress, 1993).

A remarkable situation in this tunnel was that the spalling started very slowly and non-violently and at a rather late stage. It was neither as violent as in the typical rockbursting nor was there significant convergence as in squeezing. So the phenomenon can be described as a condition between rockbursting and squeezing.

The development of overstress phenomena in this area has been time dependent. Certain overstressed zones appeared immediately after excavation. These zones had the strength-stress ratio of about one. Those indicated ‘Instantaneous’ phenomena of overstressing problem. In some areas, the phenomenon of ‘dog-earing’ first appeared a month or more after excavation. It occurred in the sections where strength-stress ratio was more than one and indicated ‘Secondary’ phenomena of overstressing problem.

Two preliminary indications of overstressing were observed. One was the occurrence of excessive cutter spalling and spalling under grippers as well as small fallouts (less than 1 m) over a much longer length. Second was that the tunnel overstress has invariably been preceded by ‘dog-earing’ in sample boreholes. These are obviously subject to a double stress concentration.

2.7 Relation between rock types and overburden depths in squeezing cases

Squeezing problem has been encountered in many tunnels in different geological conditions around the world. Information are compiled from sixty six such squeezing tunnelling cases from fifteen countries and presented in Figure 2.9. The Figure is organised with the average overburden height in ascending order excluding the tunnels in Marl soil. Squeezing takes place at different overburden depths for different rock types. The dotted line shows the relation between rock types and overburden depths.

The figure shows that squeezing is frequently encountered in mudstone. Shale, schist, phyllite and tuff are the other rock types where squeezing is common. However, squeezing is observed in diorite and quartz also but only when those rock masses are altered and overburden is relatively high. Some of the squeezing cases in gneiss in the Figure 2.9, are in altered condition. Metabasics rock type in the figure is the semi-metamorphosed basic (igneous) rock with chlorite and schist nature. Many of the

squeezing cases took place in or close to fault zones. Rock types mentioned in the figure are the host rocks if there is a fault zone. However, there are some cases where squeezing took place even if there was no fault zone present.

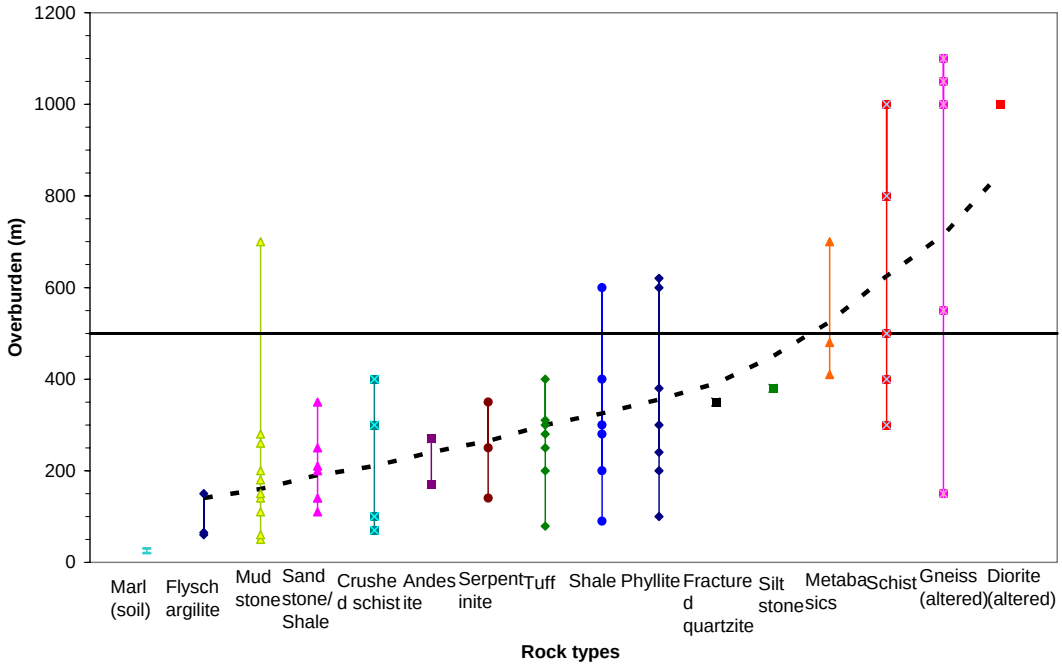

Figure 2.9 Relations between the various rock types and the overburden depths in tunnel squeezing cases. The bold straight line is the boundary line above which stress problem is expected according to Norwegian rule of thumb.

A relation can be observed between the rock type and respective overburden height. To demonstrate the trend of the relation a line is roughly fitted (no correlation analysis has been carried out). The trend line does not consider the tunnels in Marl soils; only squeezing tunnels in rock mass are considered. On the basis of the trend line, it can be noticed that squeezing takes place at lower overburden depth in weaker rocks and at higher overburden depth in stronger rocks.

According to the Norwegian rule of thumb, stress induced problems may arise when the valley side inclination exceeds 25˚ and the depth of the valley is 500 m or more. This rule of thumb is found to be valid for the stronger rocks such as schist (not crushed), gneiss and diorite (Figure 2.9). More information about the tunnelling cases is given in Appendix A.

In the figure given above, only the vertical overburden is considered. Topographical effect of valley side is not included. In case of the tunnel with steep valley side as in Figure 2.10, stress level might be much higher than induced by the vertical overburden depth alone. Squeezing cases at the low vertical overburden in Figure 2.9 might have been caused by the valley side effect. For example, in the Figure 2.10, overburden

height above the tunnel is ‘h’ but stress level around the tunnel is much higher than that is caused by ‘h’ and it would be associated with the height ‘H’.

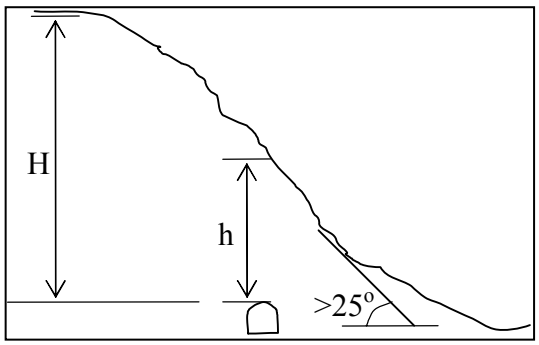

Figure 2.10 Effect of valley side on stress condition in tunnel.

Most of the squeezing problems in Japan have been overcome by using heavy and stiff support system (Yukio, et al., 2004; Kobayashi et al., 2003; Yamazaki et al., 2003). It has been done so either because of poor rock quality or from safety point of view. In case of the latter one, the strength of the rock mass around the tunnel contour would not be fully utilised.

3 Squeezing assessment and support design

Many authors have proposed a number of approaches for the assessment and support design for the squeezing phenomenon in underground constructions. Similarly, many case histories have been documented with prediction of the deformation and support requirement for squeezing rocks. These approaches can be grouped in the following four categories:

1. **Empirical methods**
2. **Semi-analytical methods**
3. **Analytical methods**
4. **Observational concept - NATM**
5. **Numerical modelling methods**

Some of the approaches for each of the above mentioned methods are discussed in the following sections. Numerical modelling is discussed in chapter 8.

3.1 Empirical methods

In empirical methods, analysis is based purely on experience and comparison. Various types of empirical approaches have been proposed by different authors for the assessment of potential squeezing phenomenon. Depending on the indicators used, the approaches can be grouped in the following three categories:

- Strength-stress ratio approach
- Strain estimation approach
- Rock mass classification approach

3.1.1 Strength-stress ratio approach

An old rule of thumb in Norway is: if the valley side height above the tunnel is 500 m or more with slope of 25˚ or steeper, there is a possibility of stress induced stability problem (Selmer-Olsen, 1965 in Broch and Sørheim, 1984). This rule of thumb was developed on the basis of repeated experiences that tunnels running parallel to fjords with steep hill sides, get rockburst problems in the tunnel wall and the part of the roof that is closest to the fjord.

Wood (1972) initially proposed the concept of Competence Factor 'F_c' to assess the stress induced stability problem in tunnel. The F_c is defined as the ratio of unconfined compressive strength of the rock mass (σ_{cm}) to overburden stress. When F_c is less than 2, the ground will be over-stressed immediately upon its exposure around the periphery of an excavation and hence the tunnel system must provide for continuous support of

the ground. This parameter has been used by many authors in many cases to recognise the squeezing potential of tunnels. This can be summarised as follows:

For squeezing condition, $$F_c = \frac{\sigma_{cm}}{\gamma H} < 2 \qquad (3\text{-}1)$$

where, γ is rock mass unit weight, and
H is overburden depth.

It is one of the simple and convenient ways to assess potential squeezing problem before the excavation is started. However, σ_{cm} needs to be estimated either on the basis of UCS of intact rock or by using some empirical relations.

3.1.2 Strain estimation approach

Saari in 1982, suggested the use of the tangential strain of tunnels as a parameter to assess the degree of squeezing of the rock, and he also suggested a threshold value of 1% for the recognition of squeezing (in Aydan et al., 1993).

Chern et al. (1998) showed that, for tunnels constructed in Taiwan, problems with tunnel stability occurred when the 'strain' exceeds about 1% (in Hoek & Marinos, 2000). This conclusion is based on the data plotted in Figure 3.1.

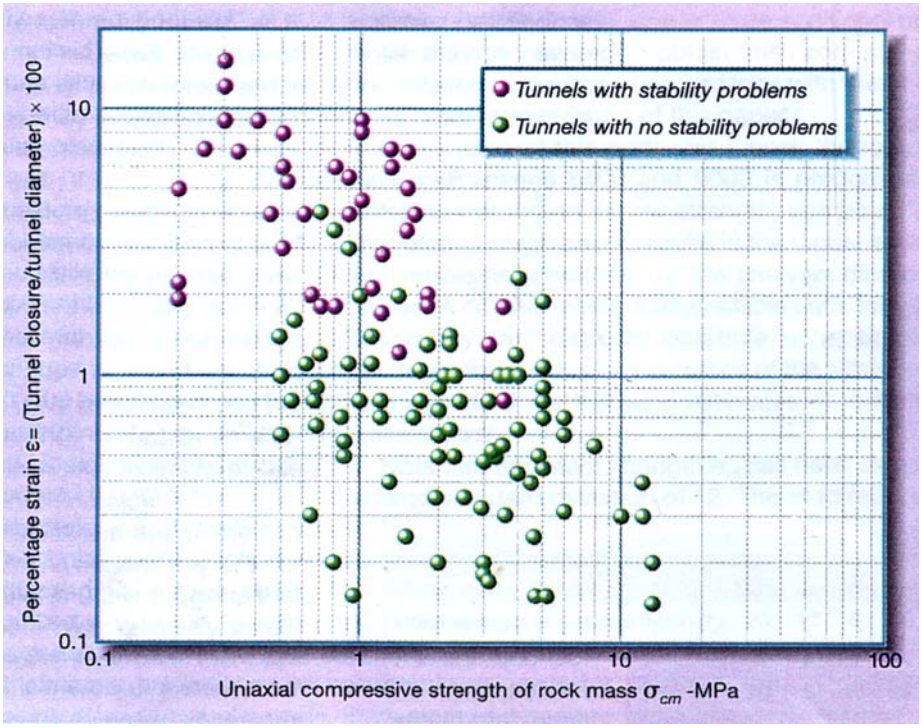

Figure 3.1 Percentage strain (tunnel closure/tunnel diameter) for different rock mass strengths. The results are for the second freeway, the Pinglin and the New Tienlun headrace tunnels in Taiwan, after Chern et al. (1998).

However, calculation of strain is a critical task before the excavation starts. Strain may have to be calculated either by using semi-analytical methods or some empirical relations.

3.1.3 Rock mass classification approach

This approach is based on the numerical value obtained from rock mass classification. Different authors have proposed different indicators using one of the available rock mass classification systems. Some of these approaches are mentioned below:

a) Singh et al. (1992) approach

Singh et al. (1992) has given a demarcation line to differentiate squeezing condition from non-squeezing condition as shown in Figure 3.2. This approach was developed by collecting data on rock mass quality Q (Barton et al.,1974) and overburden depth H based on 41 tunnel section data. Out of 41 data, 17 data were taken from case histories in Barton et al. (1974) and 24 tunnel section data were obtained from tunnels in Himalayan region.

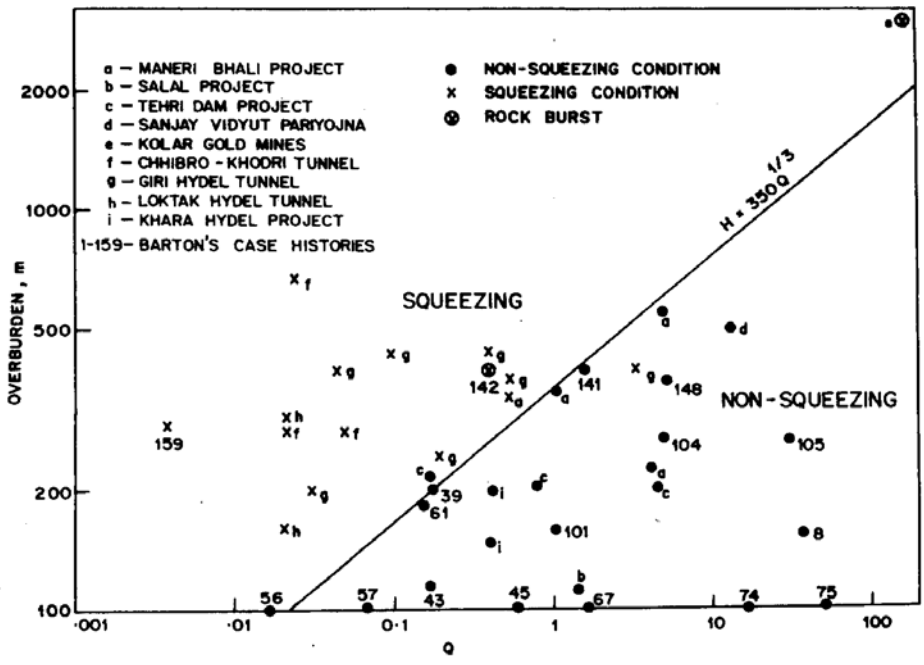

Figure 3.2 Singh et al. (1992) approach to predict squeezing condition.

The equation of the line is

$$H = 350\, Q^{1/3}\ (m) \qquad (3\text{-}2)$$

with the rock mass uniaxial compressive strength σ_{cm} estimated as

$$\sigma_{cm} = 0.7\, \gamma\, Q^{1/3}\ (MPa) \qquad (3\text{-}3)$$

where, γ is rock mass unit weight.

The data points lying above the line represent squeezing conditions, whereas those below this line represent non squeezing conditions. This can be summarised as follows:

For squeezing condition, $H > 350\,Q^{1/3}$ *(m)*

For non squeezing condition, $H < 350\,Q^{1/3}$ *(m)*

b) Goel (1994) approach

Goel (1994) developed an empirical approach based on the rock mass number N, defined as Q with SRF = 1. N was used to avoid the problems and uncertainties in obtaining the correct rating of parameter SRF in Q method.

Considering the overburden depth H, the tunnel span or diameter B, and the rock mass number N from 99 tunnel sections, Goel (1994) plotted the available data on log-log diagram (Figure 3.3) between N and $HB^{0.1}$. Out of 99 tunnel section data, 39 data were taken from Barton's case histories and 60 from projects in India. Out of those 60 data 38 data were from 5 projects in Himalayan region. All the 27 squeezing tunnel sections were observed in those 5 projects in Himalyan region. Other 72 data sets were from non-squeezing sections. As shown in the figure, a line AB distinguishes the squeezing and non squeezing cases. The equation of this line is

$$H = \left(275\,N^{0.33}\right)B^{-0.1}\,(m) \qquad (3\text{-}4)$$

The data points lying above the line represent squeezing conditions, whereas points below the line represent non-squeezing conditions.

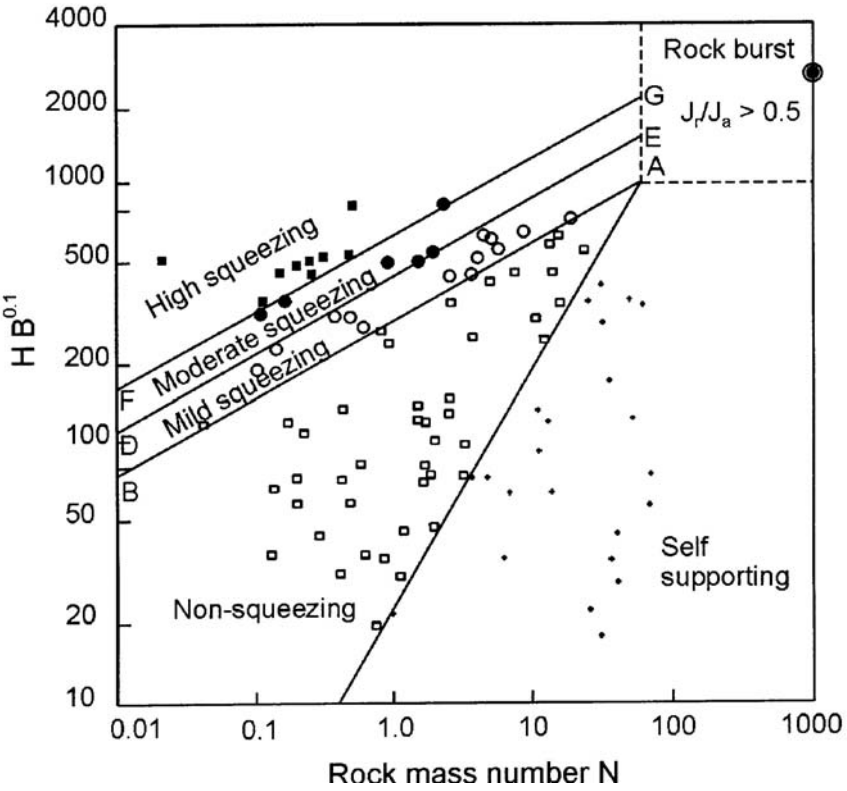

Figure 3.3 Criteria for predicting squeezing ground conditions using rock mass number N

Goel (1994) also estimated ultimate support pressure for squeezing ground condition with the following equation

$$P_{sqult}(N) = \left\{\frac{f(N)}{30}\right\} 10^{\left(\frac{H^{0.6} a^{0.1}}{50\, N^{0.33}}\right)} \qquad (3\text{-}5)$$

$$P'_{sqult}(N) = \left\{\frac{1}{30}\right\} 10^{\left(\frac{H^{0.6} a^{0.1}}{50\, N^{0.33}}\right)} \qquad (3\text{-}5a)$$

where,

$P_{sqult}(N)$ = Estimated ultimate support pressure in squeezing ground conditions in MPa using N,

$P'_{sqult}(N)$ = Estimated ultimate support pressure without correction for tunnel closure in MPa using N,

$f(N)$ = Correction factor for tunnel closure obtained from Figure 3.4,

a = Tunnel radius in cm.

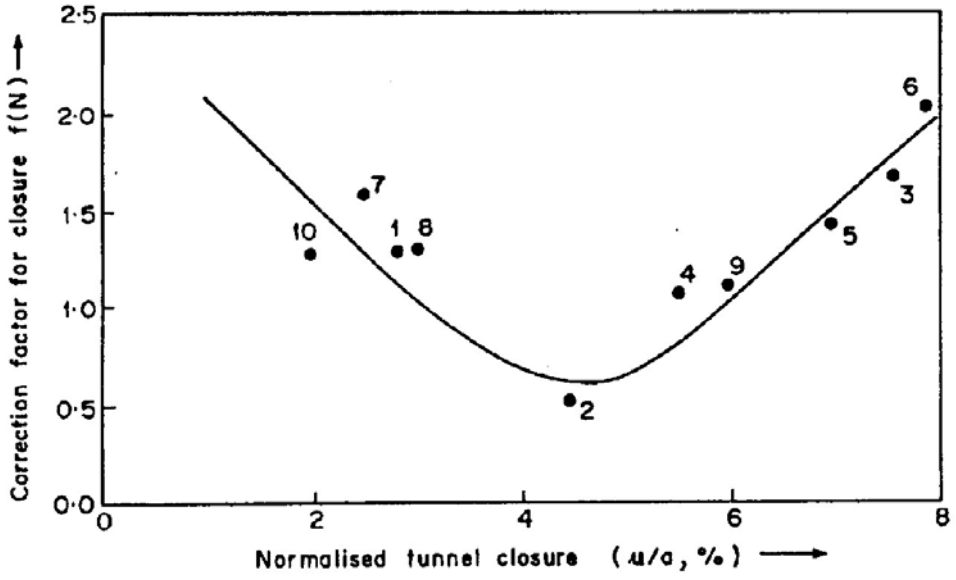

Figure 3.4 Correction factor for tunnel closure f(N).

Similarly, Goel (1994) also estimated tunnel closure for squeezing ground condition with the following equation

$$U_{sq}(N) = \frac{1}{10.5}\,\frac{a^{1.12} H^{0.81}}{N^{0.27} K^{0.62}} \qquad (3\text{-}6)$$

where,

$U_{sq}(N)$ = Estimated radial tunnel closure in cm using rock mass number N under squeezing ground condition,

a = Tunnel radius in cm,

K = Effective support stiffness in MPa.

c) RMR method, Q-system and RMi method

RMR method

This is an engineering rock mass classification system, developed by Bieniawski in 1973. It utilises following six rock mass parameters (Bieniawski, 1989):

Uniaxial compressive strength (UCS) of intact rock material.
Rock quality designation (RQD).
Spacing of discontinuities.
Condition of discontinuities.
Groundwater condition.
Orientation of discontinuities.
Once the above mentioned parameters are evaluated, rating value is assigned to each parameter. The fourth parameter 'Condition of discontinuities' is further divided into

five parameters. Thus there are, in fact, ten parameters to be evaluated in this method. This method consists of four sections and it has provision of five classes for rock masses. On the basis of the rock mass classification value, support requirement is predicted using 'RMR classification guide for excavation and support in rock tunnels' (Bieniawski, 1989).

However, RMR method does not have any provision for assessment and support design for squeezing condition in underground works.

Q-system

The Q-system for rock mass classification was developed at the Norwegian Geotechnical Institute (NGI) by Barton, Lien and Lunde in 1974. In 1993, it was updated by Grimstad and Barton by including more than 1000 cases. It is a system for estimation of the required tunnel support, based on a numerical assessment of the rock mass quality using the following six parameters:

Rock quality designation (RQD).
Number of joint sets (J_n).
Roughness of the most unfavourable joint or discontinuity (J_r).
Degree of alteration or filling along the weakest joint (J_a).
Water inflow (J_w).
Stress condition given as the stress reduction factor (SRF).

The above mentioned six parameters are grouped to give the overall rock mass quality:

$$Q = \frac{RQD}{j_n}\frac{J_r}{J_a}\frac{J_w}{SRF} \tag{3-7}$$

The Q-value is related to tunnel support requirement by defining the equivalent dimensions (D_e) of the underground opening. This equivalent dimension, which is a function of the size and type of the excavation, is obtained by dividing the span, diameter or wall height of the excavation (D_t) by a quantity called the excavation support ratio (ESR), given as:

$$D_e = \frac{D_t}{ESR} \tag{3-8}$$

ESR considers type and use of the underground construction and its rating is done as per the table given by Barton et al. in 1974. On the basis of the Q-value and D_e value, support requirement is estimated using support chart given by Grimstad and Barton (Grimstad and Barton, 1993).

Q-system refers to the Singh et al. (1992) (see section 3.1.3 a) for the assessment of potential squeezing problem. If there is squeezing, on the basis of the value of σ_θ/σ_c

ratio 'Stress reduction factor' (SRF) value is assigned as follows (σ_θ and σ_c are tangential stress and UCS of rock mass respectively.):

If σ_θ/σ_c is 1 – 5, it is mild squeezing condition and it assigns value of 5 – 10 for SRF.
If σ_θ/σ_c is > 5, it is heavy squeezing condition and it assigns value of 10 - 20 for SRF.
The tangential stress and UCS need to be calculated independently. Value of SRF affects Q value and hence the support requirement. Thus squeezing condition is addressed briefly in Q-system. Details on Q value calculation and the use of support chart, are given in Grimstad and Barton (1993).

RMi method

RMi stands for rock mass index. This method was developed by Palmstrom in 1995. RMi value is calculated by using uniaxial compressive strength of intact rock material (σ_c), block volume (V_b) and joint condition factor (jC) value. Value of jC is the function of three parameters. Thus RMi value is quantified by using the following five parameters:

Uniaxial compressive strength of intact rock material (σ_c).
Block volume (V_b).
Joint roughness factor (jR).
Joint alteration factor (jA).
Joint size factor (jL).

Joint condition factor (jC) is calculated by using the following equation:

$$jC = \frac{jR * jL}{jA} \tag{3-9}$$

In massive rock ($V_b > 8$ m^3): $RMi = 0.5\sigma_c$ (3-10)

In blocky (jointed) rock: $RMi = \sigma_c * 0.2\sqrt{jC} * V_b^D$ (3-11)

Where, $D = 0.37\, jC^{-0.2}$

The RMi method is related to tunnel support requirement by defining the continuity factor (CF), competency factor (Cg) and using ratings of the adjustment factors.

Where,

CF = Tunnel diameter / block diameter
Cg = Strength of the rock mass (RMi) / tangential stress acting

On the basis of the values of RMi and other factors mentioned above, support requirement is estimated separately for continuous ground and jointed ground, using two support charts given by Palmstrom (2000).

RMi method carries out characterisation of the rock mass in terms of continuity factor and competency factor, which assist in assessment of stress induced problem. It refers to Hoek and Brown (1980) for the tangential stress calculation, which also considers shape factor of the underground structures. 'Support requirement chart for continuous ground' is used for support estimation for underground construction in squeezing rocks. However, the support chart is in initial stage of development.

3.1.4 Application of Empirical methods

a) Strength-stress ratio approach and Strain estimation approach

The strength-stress ratio approach and strain estimation approach provide preliminary indication of potential squeezing problem. None of the approaches prescribe support requirement, so they are not complete approaches. However, some comprehensive methods have been developed on the basis of these indicators. For example, Hoek & Marinos (2000) approach uses strain estimation and rock mass classification methods such as Q and RMi use stress-strength ratio parameter.

b) Rock mass classification approaches: RMR, Q and RMi methods

All the rock mass classification approaches can be used in the whole range of underground construction works. The RMR method does not have provision to assess squeezing condition, but it has been used for rock mass classification for some of the squeezing tunnels. The Q-system and the RMi assess the squeezing phenomena and prescribe the support accordingly.

In general, the SRF describes the relation between stress and rock strength around a cavern. In order to assign rating value to SRF, the stress situation is classified in the following four categories (NGI, 1997):

(a) Weakness zones intersecting the excavation which may cause a loosening of the rock mass during excavation.

(b) Competent rock, rock stress problems.

(c) Squeezing rock; plastic flow of incompetent rock under the influence of high rock pressure.

(d) Swelling rock; chemical swelling activity depending on presence of water.

Categories (a) and (c) are related to the squeezing phenomenon. But there have been ambiguities and difficulties in estimation of SRF value and incorrect selection of SRF may result in misleading support pressure estimates.

In case of category (a), Palmstrom and Broch (2005) have given an example of difficulty to follow the use of SRF value for a weakness zone (Figure 3.5). This example considers two cases both with over burden depth of 40 m: in case A, tunnel is

excavated in competent rock. According to rating chart it belongs to category (b) and gives SRF value 1. In case B, tunnel is excavated in competent rock with a single shear zone. The rock mass type and condition are same as in case A. According to the rating chart it belongs to category (a) and gives SRF value 5. According to Q-system, the amount of rock support will be significantly higher for case B. In practice, it is opposite, as in a weakness zone the arching effect will contribute to increase stability.

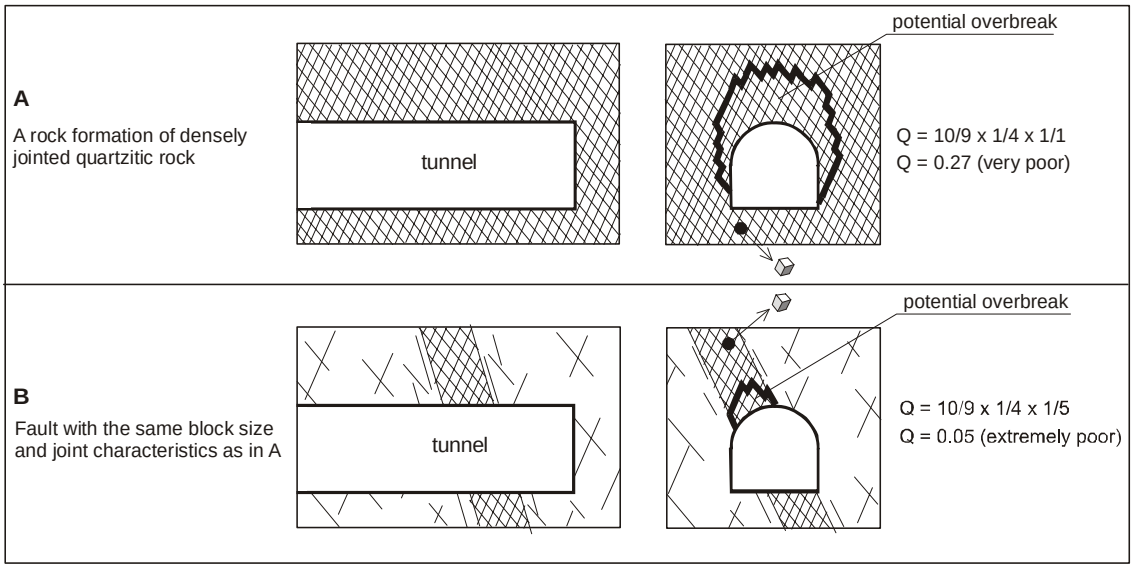

Figure 3.5 The two cases, A and B. Case A shows tunnel construction in densely jointed quartzitic rock where as case B shows tunnel intersecting a fault zone with same rock mass composition as in case A (Palmstrom and Broch, 2005).

A wide range of value for SRF is suggested if a shear zone only influences but does not intersect an excavation (Goel, 1994). Similarly there is difficulty for the tunnel which intersects weakness zone. For example, considering two tunnel sections in a similar rock mass with a single clay filled weakness zone at depths of 100 and 300 m, are assigned with the same SRF value (*i.e.* 2.5) leading to similar estimated support pressures whereas it was observed that measured support pressure increases with depth (Goel, 1994).

In case of category (c), the Q-system very briefly addresses squeezing rocks on the basis of value of the σ_θ/σ_c ratio. However, estimation of the value for σ_c is a difficult task though σ_θ can be approximated as double of overburden pressure. NGI (1997) also states 'Cases of squeezing rock may occur for depth $H > 350\ Q^{1/3}$ (Singh et al., 1992). Rock mass compression strength can be estimated as $\sigma_c = 0.7\ \gamma\ Q^{1/3}$ (MPa) where γ = rock density in kN/m^3 (Singh et al., 1993)'. But these criteria lead to the loop of dependency in the following way: above mentioned equation is used to assess squeezing potential and to do so it needs Q value which is found by estimating SRF value and; to estimate SRF value it should be known whether there is squeezing or not (Figure 3.6).

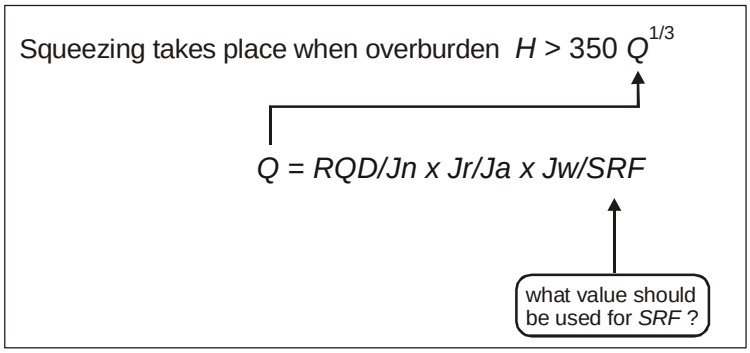

Figure 3.6 How is the value of Q in equation $H > 350\ Q^{1/3}$ found to assess squeezing? (Palmstrom and Broch, 2005).

c) Singh's approach (1992)

Q-system has been used in Himalayan tunnels and found to be useful except in cases of squeezing ground conditions (Singh, et al., 1992). Though Singh et al., have given Equation (3-2) to differentiate squeezing condition from the non-squeezing condition; it has got the problem of loop of dependency as described in the previous section. However, one of the way-outs for this problem could be to estimate Q value by assigning SRF value without considering squeezing condition. For example, in the Khimti tunnel SRF values were assigned considering 'tunnel intersecting multiple weakness zones' (*i.e.* category (a)) and assigning SRF value 10. Then the equation (3-2) was verified on the basis of 31 squeezing sections and 26 sections were found to agree with the equation.

d) Goel's approach (1994)

This approach uses Q-system for the rock mass classification. Because of the ambiguity and difficulty in estimation of SRF value (see section 3.1.4 b), this approach does not use SRF and uses only five parameters of the Q-system and that is defined as rock mass number 'N' (Equation 3-4). In order to include stress situation, it includes overburden depth. It also considers tunnel dimension and gives equations for support pressure and convergence deformation estimation. However, deformation calculation needs stiffness value and it depends on support types and it makes calculation complicated.

e) Conclusions

'Strength-stress ratio approach' is a simple and easy tool to use, so it can be used for preliminary indication of potential squeezing problems. However, 'Strain estimation approach' is not useful as preliminary indicator as strain estimation is not simple. RMi method involves many steps and further more, the support chart for squeezing is only in initial stage of development, so it may take some time before it is useful in application.

Because of the difficulty in estimating SRF value, the Q-system may not be a suitable tool to use during the construction phase. However, it has already been used for tunnel support design in many countries and found to be useful, so it can be used in the preliminary stage for support estimation. It directly leads to support estimation and can be used by a person without analytical knowledge also. It does not correlate support quantity with support pressure, hence it does not involve analytical verification. Considering the problem with SRF value in Q-system, Goel (1994) approach seems to be a suitable empirical tool as it does not use the SRF value for rock mass classification. Moreover, it addresses stress situation by including overburden depth and it also considers tunnel dimension; and gives equations for support pressure estimation.

Empirical methods are based on experience from numerous underground projects. The actual geometrical features of discontinuities and other parameters of rock mass cannot be represented in the support chart of these methods, so, an understanding of the geological condition of the rock mass is a prerequisite for using these empirical methods.

3.2 Semi-analytical method

A few semi-analytical approaches have been proposed for estimation of the deformation caused by squeezing and estimation of support pressure required in the squeezing tunnel. Three such approaches are discussed and compared in the following sections.

3.2.1 The Kovari (1998) approach

Kovari (1998) considered a circular opening and assumed isotropic, homogenous and elasto-plastic material behaviour. He gave the following equation for the displacement u_a at the boundary of the excavated opening, for a given displacement u_ρ at the boundary of the plastic zone (Figure 3.7):

$$u_a = u_\rho \left(\frac{\rho}{a} \right)^k \tag{3-12}$$

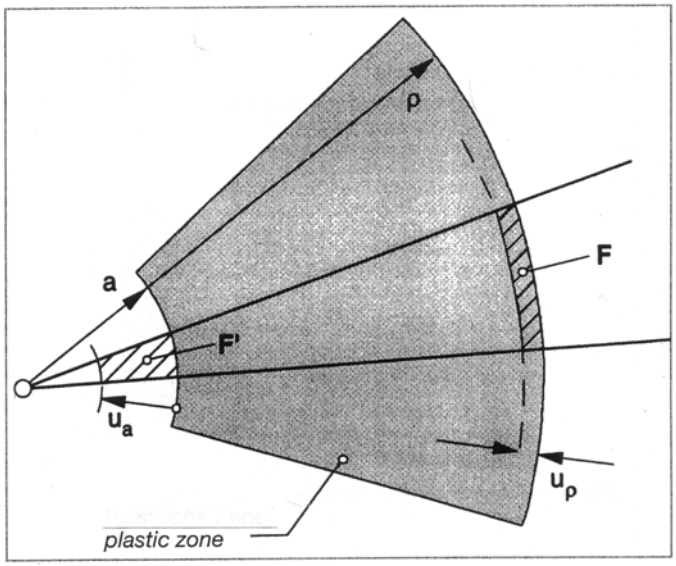

Figure 3.7 Displacement in squeezing tunnel wall (Kovari, 1998).

Where ρ and a are radius of plastic zone and the excavated opening respectively. Volume change is taken into account using the parameter k. Its value varies between 1 and (1+sinφ)/ (1-sinφ). 'k' is evaluated in reference to ρ/a ratio. The ground response curve can be represented by the following equation:

$$u_a = \left[\frac{(1+\nu)}{E}\right]\rho p'_\alpha \sin\varphi\left(\frac{\rho}{a}\right)^k \tag{3-13}$$

The following equations were given to calculate ρ and stresses:

$$\frac{\rho}{a} = \left[(1-\sin\varphi)\frac{p'_\alpha}{p'_a}\right]^{\frac{1-\sin\varphi}{2\sin\varphi}} \tag{3-14}$$

$$p'_\alpha = p_\alpha + c\cot\varphi \tag{3-15}$$

$$p'_a = p_a + c\cot\varphi \tag{3-16}$$

Thus the amount of the radial displacement u_a is controlled by altogether 8 parameters:

$$u_a = f(p_\alpha, p_a, c, \varphi, a, E, k \text{ and } \nu) \tag{3-17}$$

where:
p_α = Primary stress = unit weight * depth
p_a = Stress on the lining
c = Cohesion
φ = Angle of internal friction
E = Modulus of elasticity
ν = Poisson's ratio

For circular concrete lining with a mean radius R, lining thickness d, uniaxial compressive strength f_c and hydrostatic external loading (rock load) p, the load-bearing capacity p_o of the lining is:

$$p_o = f_c \frac{d}{R} \tag{3-18}$$

Similarly, Kovari (1998) also proposes the following equation to estimate the average load-bearing capacity (denoted by $(p_A+p_B)/2$) of a circular concrete lining under non-equally distributed rock loads:

$$\frac{(p_A + p_B)}{2} = k f_c \frac{d}{R} \tag{3-19}$$

In the above-mentioned equation, p_A and p_B describe the highest and lowest distributed rock loads respectively and the parameter k is the 'load bearing reduction factor'. 'k' describes the reduction of the permissible average rock pressure $(p_A+p_B)/2$. For a non-reinforced concrete lining the load-bearing reduction factor 'k' is given in figure 3.8(a) as a function of $p_{A/}p_B$ for three selected values of d/R. All the respective curves terminate at a constant k-value of about 50%. If these limiting values were exceeded, the concrete would react by development of cracks with the result that the assumption of an elastic material behaviour would be invalid. The effect of the reinforcements in the lining is shown in figure 3.8(b). There are virtually no limiting values for $p_{A/}p_{B,}$ as steel is now compensating for the lack of tensile strength in the concrete. 'k' does have different meanings in the deformation equation and in the load bearing capacity equation.

In both reinforced and non-reinforced concrete support, the average load-bearing capacity should correspond to the in situ $p_{A/}p_B$ ratio. Adjustment of the d/R ratio is necessary to correspond to the in situ $p_{A/}p_B$ ratio. The value of $(p_A+p_B)/2$ should be greater than the value of p'_a in the deformation equation.

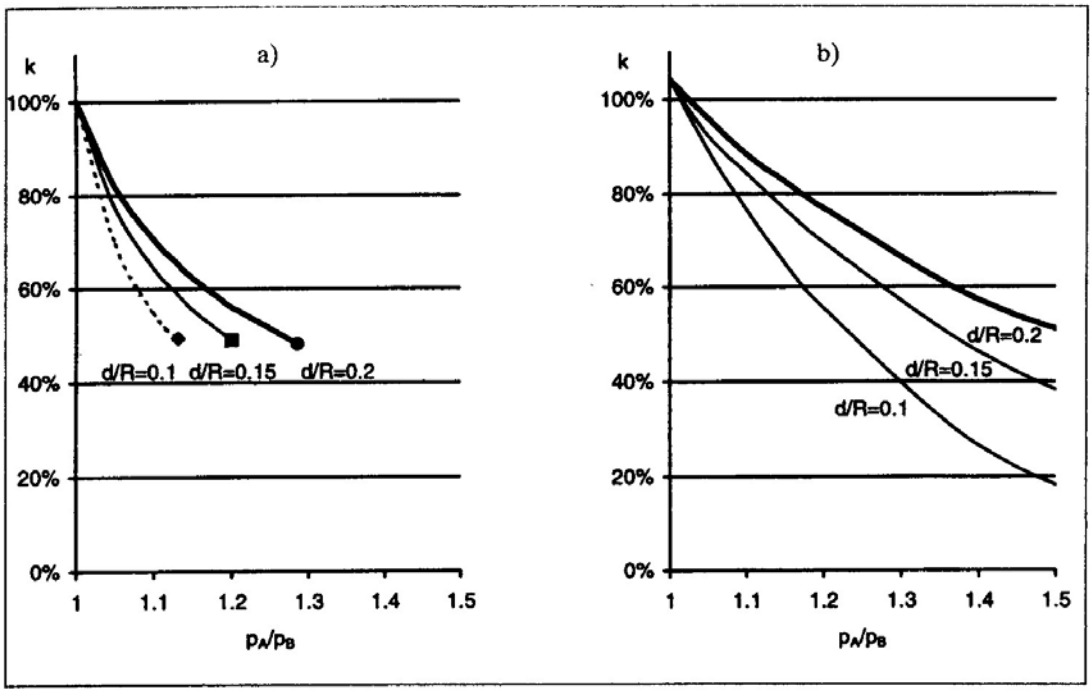

Figure 3.8 Load bearing reduction factor 'k' as a function of p_A/p_B in (a) non-reinforced concrete and (b) reinforced concrete with 0.4 % reinforcement content (Kovari, 1998).

3.2.2 The Hoek and Marinos (2000) approach

Hoek and Marinos showed that a plot of tunnel strain (ε) against the ratio σ_{cm}/p_o could be used effectively to assess tunnelling problems under squeezing conditions (Figure 3.9). Hoek and Brown's criteria for estimating the strength and deformation characteristics of rock masses assume that rock mass behaves isotropically. However, if the rock mass is heavily fractured, the continuity of the bedding surfaces will have been disrupted and the rock may behave as an isotropic mass. Thus this criterion can be adapted to weak heterogeneous rock masses too.

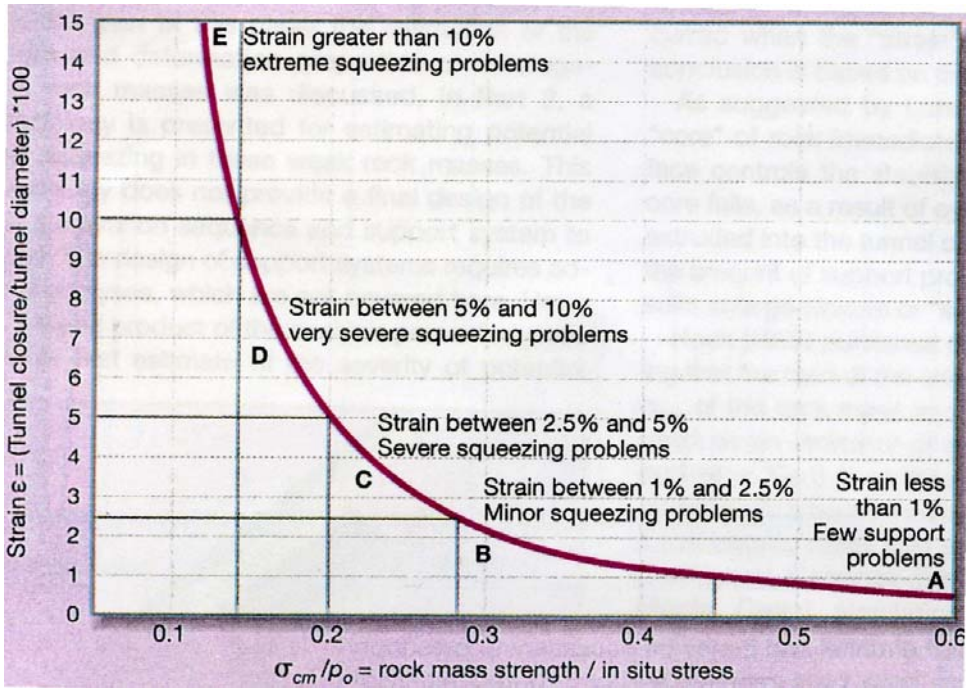

Figure 3.9 Classification of squeezing behaviour (Hoek and Marinos, 2000).

This curve can be generated using the following equation:

$$\varepsilon = \frac{\delta_i}{d_0} = \left[0.002 - 0.0025\frac{p_i}{p_0}\right]\left(\frac{\sigma_{cm}}{p_0}\right)^{\left(2.4\frac{p_i}{p_0}-2\right)} \tag{3-20}$$

In the equation given above, value of support pressure (p_i) will be zero for an unsupported condition. The value of 'p_i' should be increased until the strain reaches an acceptable range. The rock mass compressive strength (σ_{cm}) is estimated by the following equation:

$$\sigma_{cm} = \left(0.0034m_i^{0.8}\right)\sigma_{ci}\left\{1.029 + 0.025e^{(-0.1m_i)}\right\}^{GSI} \tag{3-21}$$

The size of the plastic zone can be estimated using;

$$\frac{d_p}{d_0} = \left[1.25 - 0.625\frac{p_i}{p_0}\right]\left(\frac{\sigma_{cm}}{p_0}\right)^{\left(\frac{p_i}{p_0}-0.57\right)} \tag{3-22}$$

where

σ_{ci} = Uniaxial compressive strength of intact rock elements,
m_i = A constant m_i that is defined by the frictional characteristics of the component materials in these rock elements,
GSI = A constant that relates the properties of the intact rock elements to those of the overall rock mass,
σ_{cm} = Uniaxial compressive strength of Rock mass,
p_i = Internal support pressure,

p_o = In situ stress = depth * unit weight,
δ_i = Tunnel sidewall deformation,
d_o = Original tunnel diameter in metres,
d_p = Plastic zone diameter.

According to the authors, this analysis is based upon a simple closed-form solution for a circular tunnel with hydrostatic stress field and the support is assumed to act uniformly on the entire perimeter of the tunnel. These conditions are seldom met in the field in reference to the excavation method, tunnel shape and in situ stress conditions. So, where significant potential squeezing problems have been identified, the tunnel should be subjected to numerical analyses.

3.2.3 Aydan et al. (1993) approach

Aydan et al., (1993), based on the experience with tunnels in Japan, proposed to relate the strength of the intact rock σ_{ci} in MPa to the strain levels by the following equations:

$$\eta_p = \frac{\varepsilon_p}{\varepsilon_e} = 2\sigma_{ci}^{-0.17},\ \eta_s = \frac{\varepsilon_s}{\varepsilon_e} = 3\sigma_{ci}^{-0.25},\ \eta_f = \frac{\varepsilon_f}{\varepsilon_e} = 5\sigma_{ci}^{-0.32} \qquad (3\text{-}23)$$

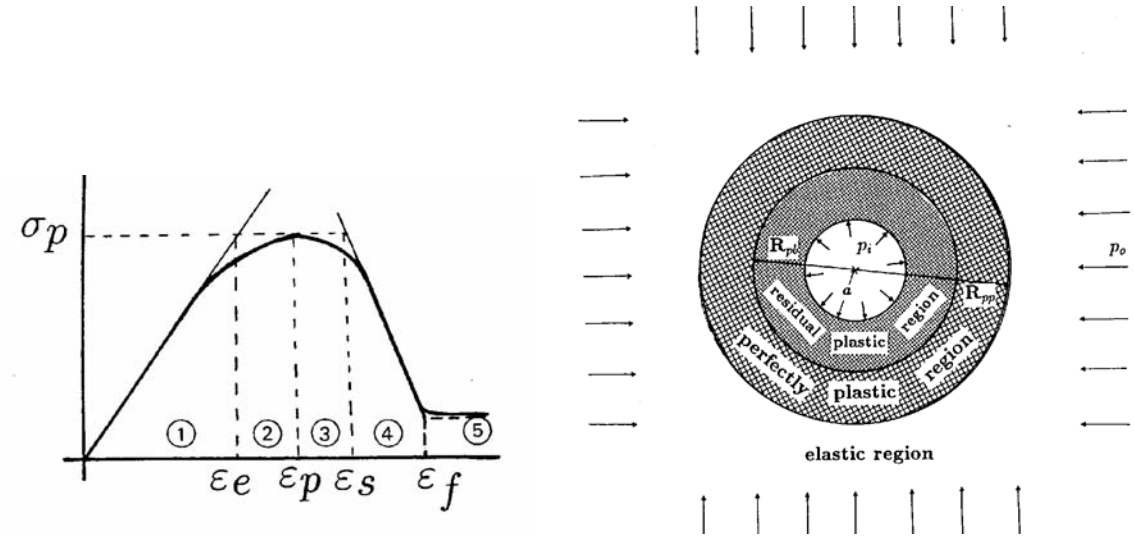

Figure 3.10 (a)Idealised stress-strain curves and (b) tunnel in squeezing rocks and notations.

η_p, η_s and η_f are normalised strain levels and other strain levels are defined in Figure 3.10. Values of the strain at different conditions are calculated using the following relations:

$$\varepsilon_e = \frac{1+\upsilon}{E}(p_0 - p_i) \qquad (3\text{-}24)$$

$$\varepsilon_p = \frac{1+\upsilon}{E}(p_0 - p_i)\frac{R_{pp}^{f+1}}{a} \quad (3\text{-}25)$$

$$\varepsilon_{sf} = \frac{1+\upsilon}{E}(p_0 - p_i)\eta_{sf}\frac{R_{pb}^{f^*+1}}{a} \quad (3\text{-}26)$$

$$\frac{\varepsilon_p}{\varepsilon_e} = f(q, \beta, \alpha, f) \quad (3\text{-}27)$$

$$\frac{\varepsilon_{sf}}{\varepsilon_e} = f(\eta_{sf}, \beta, q, \alpha, f, q^*, \alpha^*, f^*) \quad (3\text{-}28)$$

where

p_o = Hydrostatic pressure

p_i = Support pressure

R_{pp} = Radius of perfect plastic region

R_{pb} = Radius of residual plastic region

a = Radius of opening

$\eta_{sf} = (\eta_s + \eta_f)/2$

f = Ratio of radial to axial strain, (ν) for perfect plastic part

f^* = Ratio of radial to axial strain, (ν) for failed or residual plastic part

$\beta = p_i/p_o$, support pressure normalised by overburden pressure

$\alpha = \sigma_c/p_o$, competency factor

$\alpha^* = \sigma_c^*/p_o$

$q = (1+\sin\varphi)/(1-\sin\varphi)$

$q^* = (1+\sin\varphi^*)/(1-\sin\varphi^*)$

* in σ_c^* and φ^*, indicates value for plastic condition or failed rock mass.

ε_{sf} represents average of ε_s and ε_f. Thus $\varepsilon_{sf}/\varepsilon_e$ value is comparable to value of η_{sf}. Equations (3-27) and (3-28) are used to estimate the strain ratio and then degree of squeezing is found by comparing them with the values calculated from equation (3-23). If squeezing is predicted, then support (p_i) will be provided.

In addition to σ_{ci}, this method requires laboratory tests to find out Poisson's ratio for perfect plastic and residual plastic condition and friction angle for intact and failed rock mass. The fundamental concept of the Aydan et al. (1993) approach is based on the

analogy between the axial stress-strain response of rocks in laboratory tests and tangential stress-strain response of rocks surrounding tunnels. It considers $\sigma_1 = \sigma_\theta$ and $\sigma_3 = \sigma_r = p_i$.

3.2.4 Comparison of semi-analytical approaches

All the above mentioned three semi-analytical approaches consider circular opening in homogeneous rock material with a hydrostatic stress state to estimate squeezing deformation. Hoek and Marinos's and Aydan et al.'s approaches also consider the same condition for the estimation of support, whereas Kovari's approach can also accommodate anisotropic stress conditions. None of the approaches consider time-dependent deformation character. They consider only instantaneous squeezing deformation.

Hoek and Marinos's approach includes only three unknown parameters (σ_{ci}, m_i and GSI), but GSI and m_i values need to be quantified by observation of the rock mass. Kovari's approach consists of five unknown parameters (c,φ,E,k and ν) and all, except k, are evaluated by laboratory tests. Laboratory tests are carried out on intact rock samples and results needs to be correlated to rock mass condition. However, the method does not tell the exact value of k to be used in the equation. Aydan et al.'s method requires laboratory tests to find out σ_{ci}, Poisson's ratio for perfect plastic and residual plastic condition and friction angle for intact and failed rock mass. Finding parameters for failed and residual condition need advanced laboratory test facilities and there are many parameters to be used, so, this method may not be convenient to use. If detailed laboratory tests are to be carried out, analytical method also could be preferred.

Kovari proposes an average load bearing capacity of the concrete lining. The thickness of the lining should be adjusted to correspond to the in situ p_A/p_B ratio. Thus it evaluates tunnel support in terms of concrete lining thickness. On the other hand, Hoek and Marinos; and Aydan et al. adjust the support pressure p_i to give an allowable strain ratio. As these approaches consider support pressure irrespective of the support type, it may also be a convenient method to use for any type of support estimation.

The author has not come across any case study publications which mention using any of Aydan et al.'s and Kovari's methods for tunnel support design. The GSI method has been used to estimate various design parameters for many underground construction projects in the world (Kockar & Akgun, 2003; and Cai et al., 2003). As Hoek and Marinos's approach is convenient to use and it is based on the widely accepted GSI method, it can be used as a semi-analytical method for squeezing assessment and tunnel support design.

3.3 Analytical methods

Close-form analytical solutions can be categorised according to in situ stress conditions. In low stress conditions, the support is designed to resist deformation induced by dead weight of loosened rock blocks or wedges locally. Limit equilibrium method is applicable to design the support for wedges or blocks or beams for local stability. On the other hand, in high stress condition, the deformation is induced by a redistribution of the stress field in the rock mass surrounding the excavation and the corresponding rock support is usually carried out in a systematic pattern. The development of the concept of interaction of load-deformation characteristics of rock mass and support system, results in the convergence confinement method (CCM), which is often used in design of support based on idealized uniform stress field and circular opening. Similarly, in terms of Mohr-Coulomb criteria, tangential stress 'σ_θ' acts as the major principal stress 'σ_1' and radial stress 'σ_r' acts as the minor principal stress 'σ_3'. At the tunnel contour, σ_r is zero so σ_3 indicates the required tunnel support pressure 'p_i' (Duncan-Fama, 1993; and Aydan et al., 1993). Thus these two types of analytical solutions are discussed in the following sections. There is no special analytical method available for squeezing condition only. Thus the analytical methods discussed in the following sections are for general tunnel stability analysis.

3.3.1 Convergence confinement method (CCM)

Fenner carried out the first major attempt to use elasto-plastic stress analysis for determining tunnel support pressure by using the Mohr-Coulomb yield criterion. He attempted to prove theoretically that any cylindrical opening can stand on its own without supports, provided that the plastic zone is allowed unhindered expansion (Fenner, 1938 in Goel, 1994). He demonstrated, through numerical examples, that the extent of plastic zone required to ensure tunnel stability without supports was several times larger than the tunnel radius and concluded that it was desirable to install flexible supports rather than remove large volume of crushed zone. The short-term support pressure p_i due to Fenner is given by:

$$p_i = \left[P(1-\sin\varphi) + c\cot\varphi\right]\left(\frac{a}{b}\right)^{\alpha} - c\cot\varphi \qquad (3\text{-}29)$$

where,

p_i = Short term support pressure,

P = Overburden pressure,

φ = Angle of internal friction,

c = Cohesion of rock mass,

α = 2 sin φ/(1- sin φ),

a = Tunnel radius,

b = Radius of broken zone.

Goguel was the first to recognise that the failed rock mass has low cohesion and friction as compared to an intact rock mass (Goguel, 1947 in Goel, 1994). He, therefore, concluded that supports were necessary for tunnel stability. He suggested further that radial displacements may continue even after the broken zone has stabilised.

Estimation of final converged displacement and the extent of the final loosening (plastic) zone are useful information in planning and designing a tunnel. Kitagawa et al. (1991) applied Convergence Confinement method to Neogene squeezing mudstone in a squeezing tunnel, namely, Nou road tunnel in Japan, and presented good agreement between measured and calculated values of final converged displacement and the extent of the final loosening (plastic) zone.

The three basic components of the convergence-confinement method are (i) the Longitudinal Deformation Profile (LDP), (ii) the Ground Reaction Curve (GRC) and (iii) the Support Characteristic Curve (SCC). A schematic representation of these curves is shown in Figure 3.11. CCM is a procedure that allows the load imposed on a support installed behind the face of a tunnel to be estimated. When a section of support is installed in the immediate vicinity of the tunnel face, it does not carry the full load to which it will be subjected eventually. A part of the load that is redistributed around the excavation is carried by the face itself. As the tunnel and face advance (i.e., away from the installed support), this 'face effect' decreases and the support must carry a greater proportion of the load that the face had carried earlier. When the face has moved well away from the support in question, it carries effectively, the full design load.

As given in the figure, as rock mass is removed by excavation, the displacement develops from zero to maximum u_r^M . The internal stress p_i readjusts from in situ state σ_o (point O) to critical pressure p_{cr} (point E) – limit of elastic and onset of plastic stress, and finally down to zero (point M) in the rock mass surrounding the excavation. To limit the radial convergence, a confining pressure at a particular point (point D) is required on the excavation boundary. This is determined by the support characteristic line. For compatibility of deformations at the rock support interface, after the application of the support, increase in the radial displacement of the support must equal the radial displacement of the rock wall. When the support is installed at the time a radial convergence of u_r^o (point K) has occurred, stress will build up according to the stiffness of the support until the equilibrium is reached at point D and support carries the final pressure p_s^D .

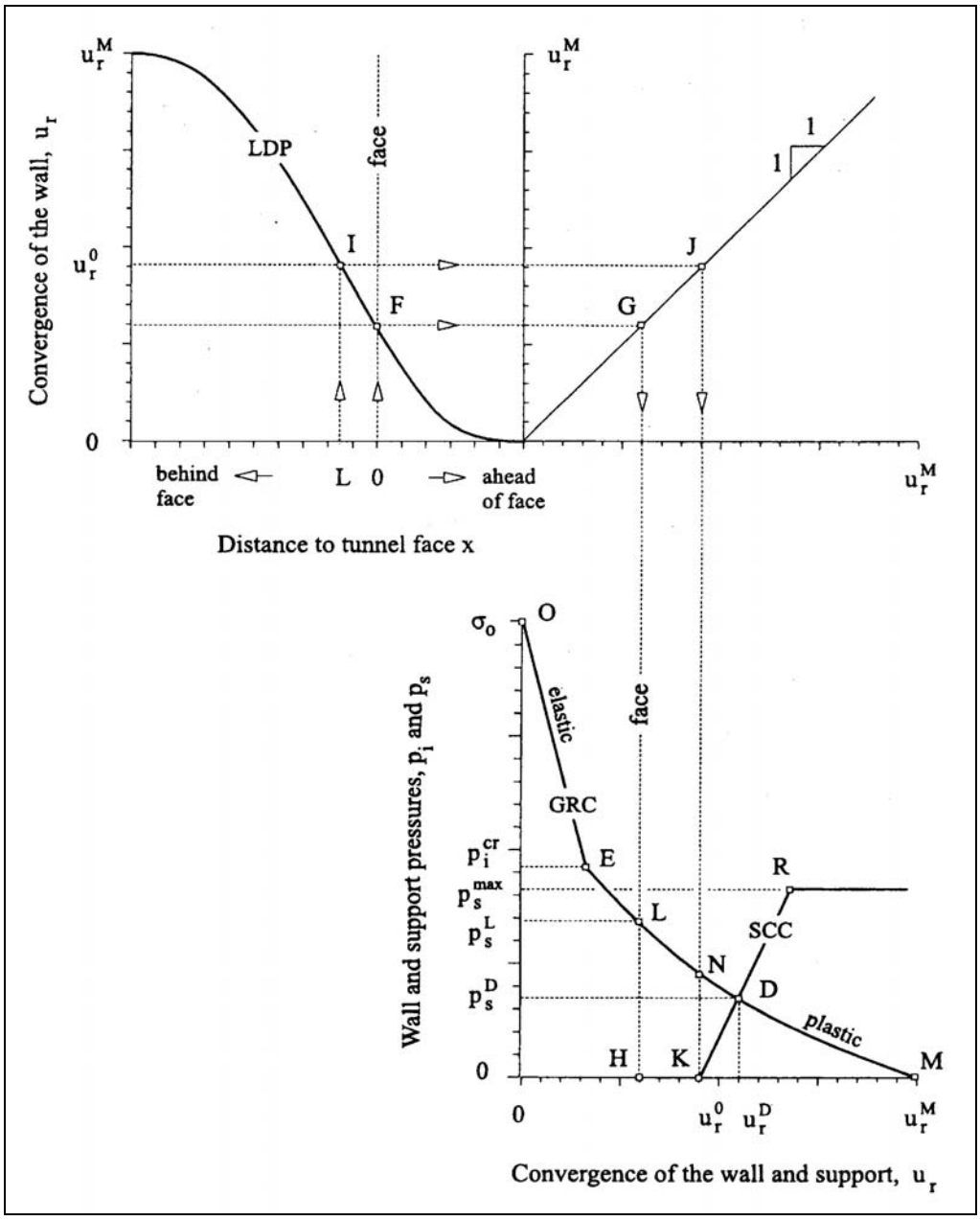

Figure 3.11 Schematic representation of the Longitudinal Deformation Profile (LDP), Ground Reaction Curve (GRC) and Support Characteristic Curve (SCC) (Carranza-Torres and Fairhurst, 2000).

The displacement and stress in rock masses surrounding an excavation are controlled mainly by the interaction of four parameters. Those are:

1. The in situ stress field σ_o (where GRC starts),
2. The mechanical behaviour of the rock mass (how GRC shape is formed as deformation develops),
3. The timing of the support installation (where the SCC starts), and

4. The stiffness of the support (how the SCC shape is formed as deformation develops).

Basic assumptions and limitations

There are two basic assumptions in the CCM: *hydrostatic stress condition and; circular cross section of the opening.* Detournay and Fairhurst (1987) considered the case of a circular cavity subjected to unequal far-field stresses and excavated in a Mohr-Coulomb material. Their results showed that for lateral stress ratio k<0.6, the CCM should not be used for such cases; otherwise, mean stress of vertical and horizontal stress can be used as σ_o in CCM. For the cases in which the cross-section area of the opening is not circular, the CCM can still be used to provide a first estimate of the extent of the plastic zone and the resulting convergence of the boundary. Carranza-Torres and Fairhurst (2000) presented a figure with curves to determine limiting value of k for given σ_o, σ_{ci} *and* φ (Figure 3.12).

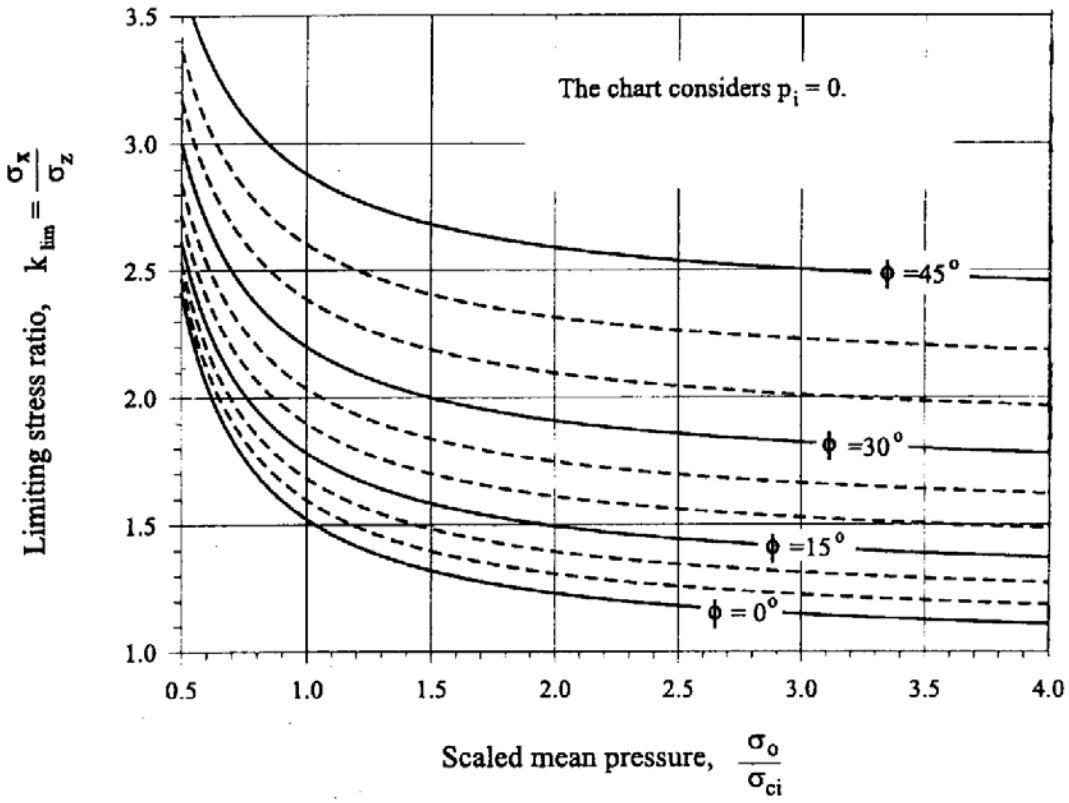

Figure 3.12 Limiting values of the horizontal to vertical stress ratio k_{lim}.

In the following sections, use of CCM in two different ways will be discussed; (a) using Hoek and Brown criteria and (b) using Mohr-Coulomb criteria.

a) CCM using Hoek - Brown criteria

Estimation of the mechanical response of a jointed rock mass is one of the fundamental problems in rock mechanics. The presence of joints and associated in situ geological effects (e.g., weathering and inhomogeneities) can considerably reduce the mechanical strength and stiffness of the rock mass compared to the corresponding properties of intact specimens taken from the mass. The Hoek-Brown criterion 'adjusts' the strength properties of intact rock cores measured in triaxial tests in order to estimate the reduced strength that the rock mass will exhibit in the field scale.

Carranza-Torres and Fairhurst (2000) presented a solution based on the 'general' form of the Hoek-Brown criterion proposed by Londe (1988). Consider a section of a cylindrical tunnel of radius R subject to uniform far-field stress σ_o internal pressure p_i shown in Figure 3.13. The rock mass is assumed to satisfy the Hoek-Brown failure criterion defined by equation (3-30); the variables characterizing the strength of the rock mass are the unconfined compressive strength of intact rock σ_{ci}, the intact rock parameter m_i, and the rock mass parameters m_b and s. Value of the parameter a is assumed to be 0.5.

$$\sigma_1 = \sigma_3 + \sigma_{ci}\left(m_b \frac{\sigma_3}{\sigma_{ci}} + s\right)^a \qquad (3\text{-}30)$$

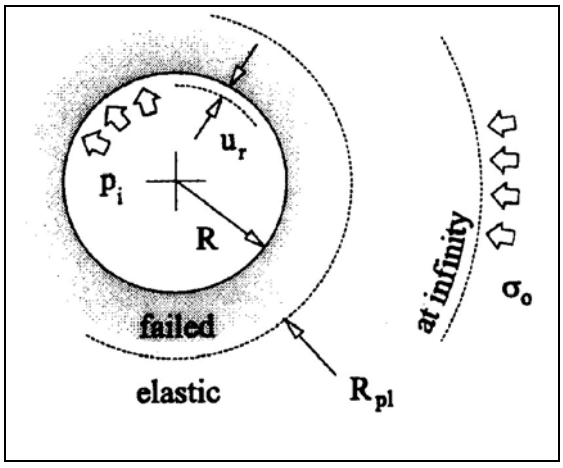

Figure 3.13 Cross-section of a cylindrical tunnel of radius R (Carranza-Torres and Fairhurst, 2000).

The uniform internal pressure p_i and far-field stress σ_o can be scaled, to give the scaled internal pressure P_i and far-field stress S_o, respectively,

$$P_i = \frac{p_i}{m_b \sigma_{ci}} + \frac{s}{m_b^2} \tag{3-31}$$

$$S_o = \frac{\sigma_o}{m_b \sigma_{ci}} + \frac{s}{m_b^2} \tag{3-32}$$

The pressure p_i^{cr}, defined by point E in the GRC of Figure 3.11, marks the transition from elastic to plastic behaviour of the rock mass-*i.e.*, for an internal pressure $p_i \geq p_i^{cr}$, the rock remains elastic, and for $p_i < p_i^{cr}$, a plastic region of radius R_{pl} develops around the tunnel (see Figure 3.13).

The scaled critical (internal) pressure P_i^{cr} for which the elastic limit is achieved is given by the following expression:

$$P_i^{cr} = \frac{1}{16}\left[1 - \sqrt{1+16S_o}\right]^2 \tag{3-33}$$

The actual (*i.e.,* non-scaled) critical pressure is found from the inverse of equation (3-31)

$$p_i^{cr} = \left[P_i^{cr} - \frac{s}{m_b^2}\right] m_b \sigma_{ci} \tag{3-34}$$

Provided $p_i \geq p_i^{cr}$, the relationship between the radial displacements u_r^{el} and internal pressure p_i in the elastic part of the GRC (*i.e.,* segment OE in Figure 3.11) is given by equation,

$$u_r^{el} = \frac{\sigma_o - p_i}{2G_{rm}} R \tag{3-35}$$

where G_{rm} is the shear modulus of the rock mass.

For values of internal pressure $p_i < p_i^{cr}$, the extent of the plastic region R_{pl} that develops around the tunnel is

$$R_{pl} = R \exp\left[2\left(\sqrt{P_i^{cr}} - \sqrt{P_i}\right)\right] \tag{3-36}$$

To define the plastic part of the GRC (EM part in the figure), a flow rule for the material is needed. The flow rule defines the relationship between the strains that produce distortion and those that produce volumetric changes, as plastic deformation occurs in the material. In underground excavation practice, the flow rule is usually assumed to be linear, with the magnitude of volumetric change characterized by a

'dilation' angle ψ, such that, if $\psi = 0^o$, the material undergoes no change in volume during plastic deformation; if $\psi > 0^o$, the volume increases during plastic deformation.

In the solution described here, the flow rule will be characterized by a dilation coefficient K_ψ, that is computed from the dilation angle, ψ, according to the expression $K_\psi = (1+\sin\psi) / (1-\sin\psi)$. Note, for example, that for $\psi = 0^o$, the dilation coefficient is $K_\psi = 1$ and for $\psi = 30^o$, the dilation coefficient is $K_\psi = 3$.

With the flow rule characterized by the dilation coefficient K_ψ, the plastic part of the GRC- *i.e.*, the segment EM in Figure 3.11- is given by

$$\frac{u_r^{pl}}{R}\frac{2G_{rm}}{\sigma_o - p_i^{cr}} = \frac{K_\psi - 1}{K_\psi + 1} + \frac{2}{K_\psi + 1}\left(\frac{R_{pl}}{R}\right)^{K_\psi + 1} + \frac{1-2\nu}{4\left(S_o - P_i^{cr}\right)}\left[\ln\left(\frac{R_{pl}}{R}\right)\right]^2$$
$$-\left[\frac{1-2\nu}{K_\psi + 1}\frac{\sqrt{P_i^{cr}}}{S_o - P_i^{cr}} + \frac{1-\nu}{2}\frac{K_\psi - 1}{\left(K_\psi + 1\right)^2}\frac{1}{S_o - P_i^{cr}}\right] x \left[\left(K_\psi + 1\right)\ln\left(\frac{R_{pl}}{R}\right) - \left(\frac{R_{pl}}{R}\right)^{K_\psi - 1} + 1\right] \tag{3-37}$$

where υ is Poisson's ratio for the rock mass.

Hoek and Brown (1997) suggest that in some cases the assumption of no plastic volume-change for the rock mass may be more appropriate. For the case of non-dilating rock-masses, characterized by the coefficient $K_\psi = 1$, Equation (3-37) becomes

$$\frac{u_r^{pl}}{R}\frac{2G_{rm}}{\sigma_o - p_i^{cr}} = \left[\frac{1-2\nu}{2}\frac{\sqrt{P_i^{cr}}}{S_o - P_i^{cr}} + 1\right]\left(\frac{R_{pl}}{R}\right)^2 + \frac{1-2\nu}{4\left(S_o - P_i^{cr}\right)}\left[\ln\left(\frac{R_{pl}}{R}\right)\right]^2$$
$$-\frac{1-2\nu}{2}\frac{\sqrt{P_i^{cr}}}{S_o - P_i^{cr}}\left[2\ln\left(\frac{R_{pl}}{R}\right) + 1\right] \tag{3-38}$$

b) CCM using Mohr-Coulomb criteria

A fundamental problem in rock mechanics is that of determining the extent of the plastic zone and radial convergence for a circular tunnel excavated in a Mohr-Coulomb perfectly plastic material subject to uniform far-field stresses. The solution to this problem has applications in the design of tunnel linings according to the Convergence-Confinement method as well. This section presents the exact solution for this fundamental problem.

The case considered is shown in Figure 3.14. A long circular tunnel of radius *a* that is subject to far-field stresses σ_o and internal pressure p_i is excavated in a perfectly-plastic Mohr-Coulomb material (plain strain conditions are considered). As a result of decreasing the internal pressure p_i below the initial value σ_o, the wall of the tunnel

converges a certain amount u_r^a. When the internal pressure p_i falls below a critical value p_i^{cr} a circular failure zone of radius R_{pl} develops (concentrically) around the tunnel.

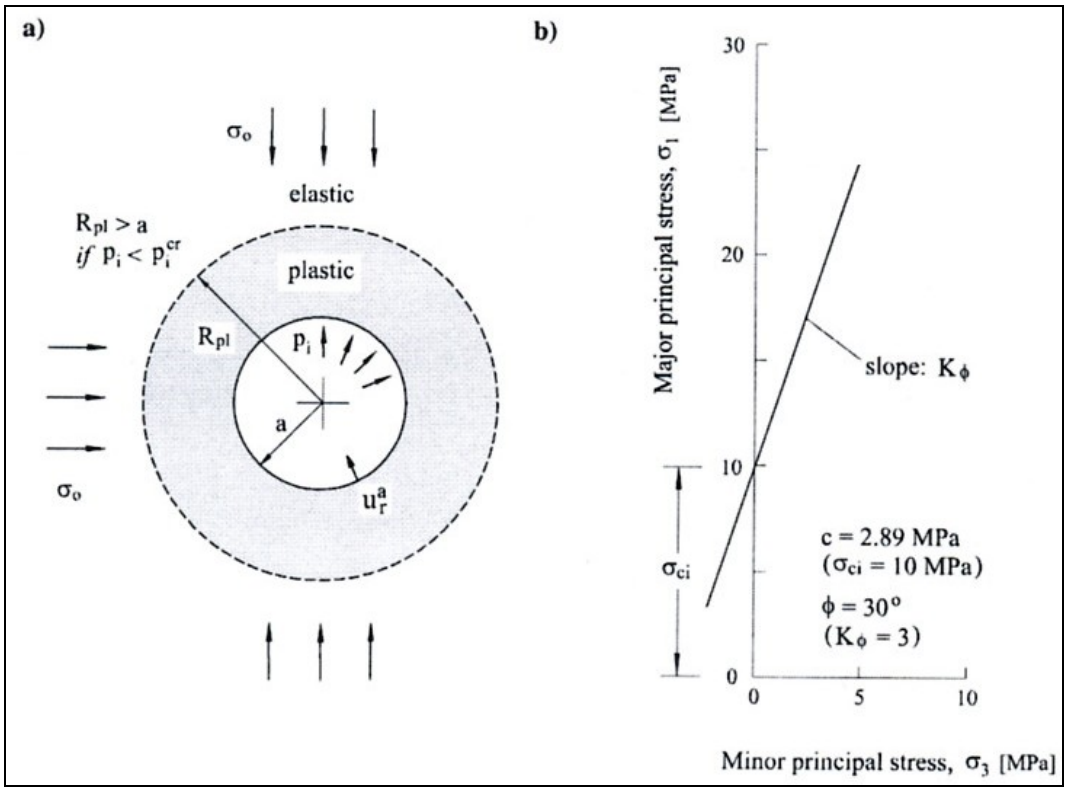

Figure 3.14 Circular tunnel in a Mohr-Coulomb elasto-plastic material subject to uniform far-field stresses and internal pressure (Carranza-Torres, 2003).

The elastic behaviour of the material is characterized by the Shear Modulus G and the Poisson's ratio ν – the Young's Modulus E is related to the Shear Modulus G according to the classical relationship $E=2G(1+\nu)$.

The plastic behaviour of the material is characterized by the internal friction angle φ, the cohesion c and the dilation angle ψ.

According to Mohr-Coulomb failure criterion, the relationship between major and minor principal stresses, σ_1 and σ_3 respectively, is given by the following relationship

$$\sigma_1 = K_\varphi \sigma_3 + \sigma_{ci} \tag{3-39}$$

where K_φ is the passive reaction coefficient, that is computed from the internal friction angle φ as follows,

$$K_\varphi = \frac{1+\sin\varphi}{1-\sin\varphi} \tag{3-40}$$

and σ_{ci} is the unconfined compressive strength that is computed from the cohesion c and the coefficient K_φ according to,

$$\sigma_{ci} = 2\, c\sqrt{K_\varphi} \tag{3-41}$$

The Mohr-Coulomb failure criterion is represented in Figure 3.14b. The coefficient K_φ is the slope of the linear failure envelope and the unconfined compression strength σ_{ci} is the intercept of the linear envelope and the vertical axis.

The volumetric response of the material is controlled by the dilation angle ψ. If the dilation angle is zero (i.e., $\psi = 0^{\circ}$) then the plastic flow rule is said to be non-associated and there is no volumetric change while the material plastifies. If the dilation angle is equal to the internal friction angle ($\psi = \varphi$), then the plastic flow rule is said to be associated and the material undergoes volumetric expansion while it plastifies. The dilation angle ψ enters the elasto-plastic formulation presented here through the parameter K_ψ, that has a similar form as the parameter K_φ, i.e.,

$$K_\psi = \frac{1+\sin\psi}{1-\sin\psi} \tag{3-42}$$

According to analytical solution given by Duncun-Fama (1993), assuming that the rock mass fails with zero plastic volume change, the critical stress level p_i^{cr} at which failure initiates is given by:

$$p_i^{cr} = \frac{2\sigma_0 - \sigma_{cm}}{K_\varphi + 1} \tag{3-43}$$

where σ_{cm} is compressive strength of rock mass. If the support pressure p_i is less than the critical pressure p_i^{cr}, the radius R_{pl} of the plastic zone and the inward deformation of the tunnel wall u_r^a are given by:

$$\frac{R_{pl}}{a} = \left[\frac{2(\sigma_0(K_\varphi - 1) + \sigma_{cm})}{(K_\varphi + 1)((K_\varphi - 1)p_i + \sigma_{cm})}\right]^{1/(K_\varphi - 1)} \tag{3-44}$$

$$\frac{u_r^a}{a} = \frac{(1+\nu)}{E}\left[2(1-\nu)(\sigma_0 - p_i^{cr})(\frac{R_{pl}}{a})^2 - (1-2\nu)(\sigma_0 - p_i)\right] \tag{3-45}$$

Where, E is the deformation modulus of Rock mass.

For the equations given by Duncun-Fama (1993), σ_{cm} needs to be replaced by σ_{ci} for the case of massive rock mass.

Carranza-Torres (2003) also presented solution using a scaling rule for Mohr-Coulomb elasto-plastic behaviour discussed by Anagnostou and Kovari (1993). Anagnostou and

Kovari showed that the cohesion c (or alternatively the unconfined compression strength σ_{ci}) can be hidden in the Mohr-Coulomb failure criterion (3-34) if the principal stresses σ_1 and σ_3 are transformed as follows:

$$S_1 = \sigma_1 + \frac{\sigma_{ci}}{K_\varphi - 1} \tag{3-46}$$

$$S_3 = \sigma_3 + \frac{\sigma_{ci}}{K_\varphi - 1} \tag{3-47}$$

With the principal stresses transformed as in Equation (3-46) and (3-47), the Mohr-Coulomb failure criterion (Equation 3-39) is written in the simpler form

$$S_1 = K_\varphi S_3 \tag{3-48}$$

According to the Equation (3-48), the failure envelope passes through the origin of the reference system so the material can be regarded as cohesionless or purely frictional. The formulation of the problem introduced in Figure 3.14 can be conveniently simplified if the stress variables entering the problem are transformed, as in equations (3-46) and (3-47). Transformed variables S_o, P_i and P_i^{cr} that are computed from the variables σ_o, p_i and p_i^{cr} respectively, as in Equations (3-46) and (3-47), i.e.,

$$S_0 = \sigma_0 + \frac{\sigma_{ci}}{K_\varphi - 1} \tag{3-49}$$

$$P_i = p_i + \frac{\sigma_{ci}}{K_\varphi - 1} \tag{3-50}$$

$$P_i^{cr} = p_i^{cr} + \frac{\sigma_{ci}}{K_\varphi - 1} \tag{3-51}$$

The transformed critical internal pressure P_i^{cr}, below which the plastic zone develops, depends on the value of transformed far-field stress S_0 and the parameter $K\varphi$ as follows

$$\frac{P_i^{cr}}{S_0} = \frac{2}{K_\varphi + 1} \tag{3-52}$$

If the given value of transformed internal pressure P_i is below the critical value P_i^{cr}, then the radius R_{pl} of the plastic zone is

$$\frac{R_{pl}}{a} = \left[\frac{P_i^{cr}}{P_i}\right]^{1/(K_\varphi - 1)} \tag{3-53}$$

For this case the radial convergence at the tunnel wall is

$$\frac{u_r^a}{a}\frac{2G}{S_0 - P_i^{cr}} = \frac{(K_\psi - 1)(K_\varphi - 1) - 2C}{(K_\psi + 1)(K_\varphi - 1)} + \frac{2(K_\psi + K_\varphi) + 2C}{(K_\psi + 1)(K_\varphi + K_\psi)}\left(\frac{R_{pl}}{a}\right)^{K_\psi + 1} + \frac{2C}{(K_\varphi + K_\psi)(K_\varphi - 1)}\left(\frac{a}{R_{pl}}\right)^{K_\varphi - 1} \tag{3-54}$$

where the constant C is

$$C = (1\text{-}\nu)(K_\varphi K_\psi + 1) - \nu(K_\varphi + K_\psi) \tag{3-55}$$

If the given value of transformed internal pressure P_i is above the critical value P_i^{cr}, then the wall convergence is given by Lame's classical solution (Jaeger and Cook, 1979),

$$\frac{u_r^a}{a}\frac{2G}{S_0} = 1 - \frac{P_i}{S_0} \tag{3-56}$$

For the equations given by Carranza-Torress (2003), σ_{ci} needs to be replaced by σ_{cm} for the case of jointed rock mass.

3.3.2 Construction of support characteristic curve

The Support Characteristic Curve (SCC) shown in Figure 3.11 can be constructed from the elastic relationship between the applied stress p_s and the resulting closure u_r for a section of the support of unit length in the direction of the tunnel.

If the elastic stiffness of the support is denoted by K_s, the elastic part of the SCC – i.e., segment KR in Figure 3.11, can be computed from the expression,

$p_s = K_s\, u_r$

Note that from the above mentioned equation, the unit of the stiffness K_s is pressure divided by length (e.g., MPa/m if the stresses are expressed in MPa and the displacements in meters). The plastic part of the SCC in the Figure 3.11 – i.e., the horizontal segment starting at point R, is defined by the maximum pressure $p_s^{\max}$ and that the support can accept before collapse.

Following different support systems are commonly used in underground construction works:

- Shotcrete or concrete lining,
- Blocked steel sets,
- Steel sets embedded in shotcrete
- Ungrouted bolts and cables and

- Grouted bolts.

The following subsections present the equations needed to compute the maximum pressure p_s^{max} and the elastic stiffness K_s for above mentioned support systems. The equations have been adapted from Hoek and Brown (1980) and Brady and Brown (1985).

a) Shotcrete or concrete rings

Considering the closed ring of shotcrete or concrete represented in Fig. 3.15a, the maximum pressure provided by the support is

$$p_s^{max} = \frac{\sigma_{cc}}{2}\left[1-\frac{(R-t_c)^2}{R^2}\right] \tag{3-57}$$

The elastic stiffness is

$$K_s = \frac{E_c}{(1-\nu_c)R}\,\frac{R^2-(R-t_c)^2}{(1-2\nu_c)R^2+(R-t_c)^2} \tag{3-58}$$

Where

E_c is Young's modulus for the shotcrete or concrete (MPa);

ν_c is Poisson's ratio for the shotcrete or concrete (dimensionless);

σ_{cc} is the unconfined compressive strength of the shotcrete or concrete (MPa);

R is the external radius of the support (m) (taken to be the same as the radius of the tunnel);

t_c is the thickness of the ring (m).

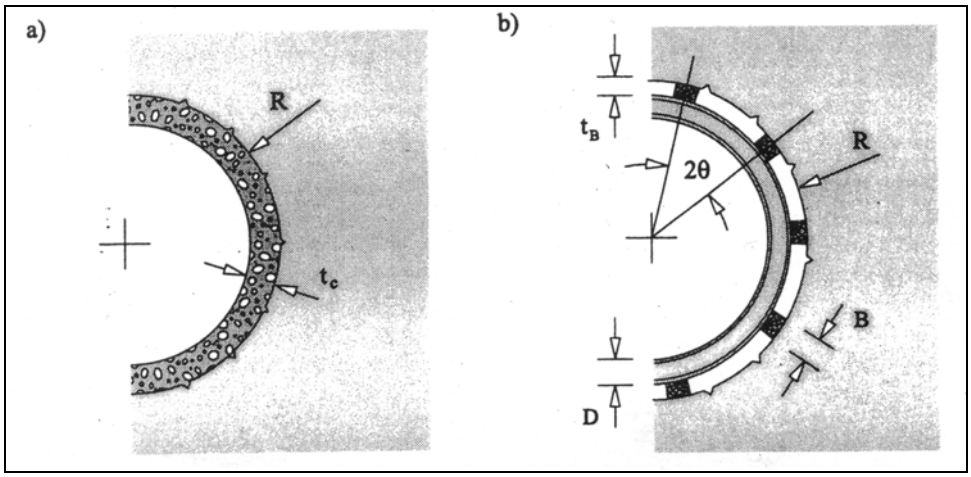

Figure 3.15 Schematic representations of sections of (a) shotcrete or concrete rings and (b) blocked steel sets (from Brady and Brown, 1985).

Typical values for σ_{cc} and E_c for wet and dry shotcrete mixtures are given in Table 3.1. Poisson's ratio for the shotcrete is usually assumed to be $\nu_c = 0.25$. The thickness t_c of the shotcrete depends on the roughness of the surface after blasting and scaling. When the shotcrete is applied as a temporary support system, the thickness usually varies between 50 and 100 mm.

Table 3.1 Values of σ_{cc} and E_c for dry and wet shotcrete mixtures after 1 and 28 days (Singh and Bortz 1975 in Carranza-Torres and Fairhurst, 2000).

Type of mixture	σ_{cc} (MPa)	E_c (MPa)
Dry (1 day)	20.3	$13.6*10^3$ - $23.4*10^3$
(28 days)	29.6	$17.8*10^3$ - $23.1*10^3$
Wet (1 day)	18.9 - 20.3	$12.3*10^3$ - $28.0*10^3$
(28 days)	33.3 – 39.4	$23.8*10^3$ - $35.9*10^3$

Maximum aggregate size 13 mm. Mix design – expressed as a percentage of total bulk weight: i) Dry mixture: 17.9% cement; 29.9% coarse aggregate; 52.2% sand. ii) Wet mixture: 16.7% cement; 27.9% coarse aggregate; 48.7% sand; 6.7% water.

For pre-cast or cast-in-place concrete support, the parameters σ_{cc} and E_c depend mainly on the type of cement and aggregate used in the mixture. Table 3.2 lists values of σ_{cc} and E_c for typical concrete mixtures used in the construction industry. Poisson's ratio ν_c for concrete varies between 0.15 and 0.25; the value $\nu_c = 0.2$ is normally used in practice. The thickness t_c for pre-cast or cast-in-place support is usually larger than that for shotcrete, partly because structural steel reinforcement is commonly used (structural steel reinforcement requires a sufficient cover of concrete to protect the steel from corrosion). Tables 3.1 and 3.2 were published three decades before. Since then significant progress has been made in terms of strength and quality of concrete and shotcrete. The values in these tables can be replaced by reliable latest values.

Table 3.2 Values of σ_{cc} and E_s for concrete mixture used in the construction industry (Leohardt, 1973 in Carranza and Fairhurst, 2000).

Designation	σ_{cc} (MPa)	E_c (MPa)
B_n 150	14.7	$25.5*10^3$
B_n 250	24.5	$29.4*10^3$
B_n 350	34.3	$33.3*10^3$
B_n 450	44.1	$36.3*10^3$
B_n 550	53.9	$38.2*10^3$

Properties after 28 days, obtained from tests on cubic samples of 200 mm side. The strength of concrete at the early age of 7 days is approximately 80% of the σ_{cc} values listed above.

b) Blocked steel set

Considering steel sets spaced a unit length apart in the direction of the tunnel axis and tightened against the rock by wood blocks that are equally spaced circumferentially-as shown in Fig. 3.15b – the maximum pressure that the system can sustain is

$$p_s^{\max} = \frac{3}{2}\frac{\sigma_{ys}}{SR\theta}\frac{A_s I_s}{3I_s + DA_s\left[R-\left(t_B+0.5D\right)\right]\left(1-\cos\theta\right)} \tag{3-59}$$

The elastic stiffness is

$$\frac{1}{K_s} = \frac{SR^2}{E_s A_s} + \frac{SR^4}{E_s I_s}\left[\frac{\theta\left(\theta+\sin\theta\cos\theta\right)}{2\sin^2\theta}-1\right] + \frac{2S\theta t_B R}{E_B B^2} \tag{3-60}$$

Where

E_s is Young's modulus for the steel (MPa)

σ_{ys} is the yield strength of the steel (MPa)

R is the external radius of the support (m) (taken to be the same as the radius of the tunnel)

t_B is the thickness of the block (m)

B is the flange width of the steel set and the side length of the square block (m)

D is the depth of the steel section (m)

A_s is the cross sectional area of the section (m^2)

I_s is the moment of inertia of the section (m^4)

S is the steel set spacing along the tunnel axis (m)

θ is half the angle between the blocking points (radians)

E_B is Young's modulus for the block material (MPa)

For the case of blocked steel sets spaced at intervals d_s other than unity, both the maximum stress and the stiffness given by the above mentioned equations should be divided by (d_s /1.0 m). Values of Young's modulus E_s and yield strength σ_{ys} for different types of steel are listed in Table 3.3. Values of D, B, A_s and I_s for typical sections of steel are given in Table 3.4. Young's modulus for the wood block depends on the type of wood used and on the tightness of the block at installation. For hard woods (e.g., ash, maple, oak) Young's modulus is typically $E_B = 10*10^3$ MPa and for conifers (e.g., pine, cypress, cedar) it is $E_B = 7*10^3$ MPa (in Carranza-Torres and Fairhurst, 2000). In order to take into account the tightness of the block at installation,

Hoek and Brown (1980) suggest the values E_B = 10,000 MPa for stiff blocking and E_B = 500 MPa for soft blocking.

Table 3.3 Values of Young's modulus Es and yield strength σ_{ys} for different steel types (Gieck, 1977 in Carranza-Torres and Fairhurst, 2000).

Designation	E_s (MPa)	σ_{ys} (MPa)
St 37 - 11	$210*10^3$	80 - 120
St 50 - 11	$210*10^3$	100 - 150
GS 38	$220*10^3$	80 - 100

The ranges of admissible stress σ_{ys} listed above are for static-compressive loads. This assumes a safety coefficient of 1.75 with respect to the yield strength.

Table 3.4 Values of D, B, A_s and I_s for typical steel sections (CONSTRADO, 1988 in Carranza-Torres and Fairhurst, 2000).

Universal beams						
Section	D (mm)	B (mm)	A_s (m^2)	I_s (m^4)	t (mm)	T(mm)
457 * 152	461	153	$9.50 * 10^{-3}$	$324.35 * 10^{-6}$	9.9	17.0
406 * 140	402	142	$5.90 * 10^{-3}$	$156.47 * 10^{-6}$	6.9	11.2
356 * 127	353	126	$4.94 * 10^{-3}$	$100.87 * 10^{-6}$	6.5	10.7
305 * 127	304	124	$4.75 * 10^{-3}$	$71.62 * 10^{-6}$	7.2	10.7
254 * 102	260	102	$3.62 * 10^{-3}$	$40.08 * 10^{-6}$	6.4	10.0
203 * 133	203	133	$3.23 * 10^{-3}$	$23.56 * 10^{-6}$	5.8	7.8
Joists						
Section	D (mm)	B (mm)	A_s (m^2)	I_s (m^4)	t (mm)	T(mm)
203 * 102	203	102	$3.23 * 10^{-3}$	$22.94 * 10^{-6}$	5.8	10.4
152 * 89	152	89	$2.18 * 10^{-3}$	$8.81 * 10^{-6}$	4.9	8.3
127 * 76	127	76	$1.70 * 10^{-3}$	$4.76 * 10^{-6}$	4.5	7.6
102 * 64	102	64	$1.23 * 10^{-3}$	$2.18 * 10^{-6}$	4.1	6.6
89 * 89	89	89	$2.94 * 10^{-3}$	$3.07 * 10^{-6}$	9.5	9.9
76 * 76	76	76	$1.63 * 10^{-3}$	$1.59 * 10^{-6}$	5.1	8.4

Universal beams, in contrast to joists, have flanges of the same thickness throughout. A typical joist section has non-parallel flanges (the thickness T is measured at the mid-distance on the flange). Note that the values of moment of inertia I_s listed above are with respect to the axis x-x indicated in the figure. This considers that the shortest side (the flange of width B) is in contact with the wood block placed between the rock

surface and the steel section (see Fig. 3.15 b). Thickness of the web has been defined by 't'.

c) Steel sets embedded in shotcrete

Maximum pressure provided by the support is

$$p_s^{\max} = \frac{A_s.\sigma_{ys}}{R.S} \tag{3-61}$$

The elastic stiffness is

$$\frac{1}{K_s} = \frac{S.R^2}{E_s.A_s} + \frac{d}{E_c} \tag{3-62}$$

Where

E_c is Young's modulus for the shotcrete or concrete (MPa);

d is mean overbreak thickness filled with shotcrete.

Two equations given above for 'steel sets embedded in shotcrete' need to be verified.

d) Ungrouted bolts and cables

The sketches in Fig. 3.16 represent mechanically anchored bolts installed in the rock-mass surrounding a circular tunnel of radius R. Assuming that the bolts are equally spaced in the circumferential direction, the maximum support pressure provided by this support system is

$$p_s^{\max} = \frac{T_{bf}}{s_c s_l} \tag{3-63}$$

The stiffness is

$$\frac{1}{K_s} = s_c s_l \left[\frac{4l}{\pi d_b^2 E_s} + Q \right] \tag{3-64}$$

where

d_b is the bolt or cable diameter (m)

l is the free length of the bolt or cable (m)

T_{bf} is the ultimate load obtained from a pull-out test (MN)

Q is a deformation-load constant for the anchor and head (m/MN)

E_s is Young's modulus for the bolt or cable (MPa)

s_c is the circumferential bolt spacing (m)

s_l is the longitudinal bolt spacing (m)

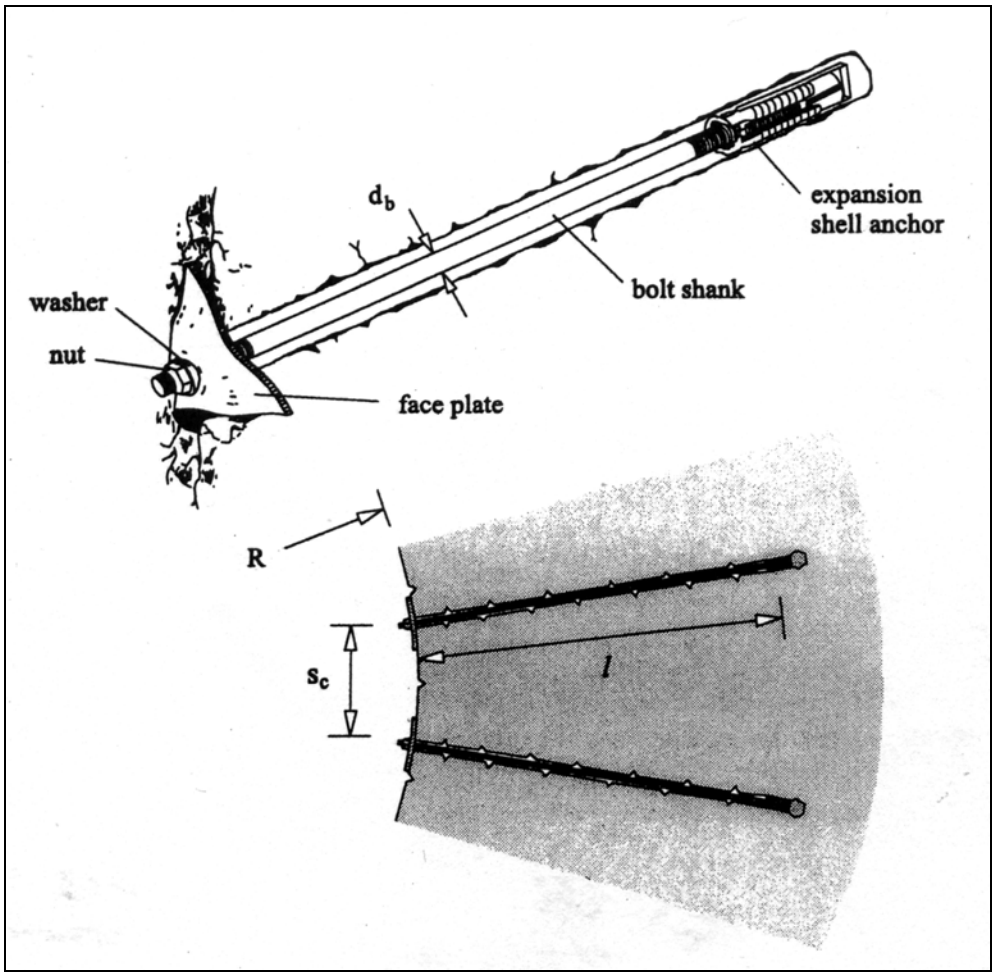

Figure 3.16 Representation of an ungrouted mechanical-anchored bolt (from Stillborg, 1994 and Hoek and Brown, 1980).

Equation (3-64) assumes that the reaction forces developed by the bolt are concentrated at the ends of the bar; therefore the equation should not be applied in the case of grouted bolts – for which the load transfer is distributed throughout the length of the shank. The circumferential bolt spacing s_c in Equations (3-63) and (3-64) can be computed as $s_c = 2\pi R / n_b$, where n_b is the total number of equally spaced bolts or cables installed in the cross-section.

Typical values of Young's modulus for the steel are listed in Table 3.3.

To illustrate how the constants T_{bf} and Q are obtained from testing of bolts, consider the diagram in Fig 3.17. This shows the results of a pull-out test performed by Stillborg (1994) on a mechanically anchored bolt 16 mm in diameter and 3 m long installed in a concrete block of compressive strength σ_{cc} = 60 MPa. The line OE corresponds to the elastic deformation of the deformation measured at the wall of the concrete block – this includes the deformation of the shank, anchor, plate, washer and nut.

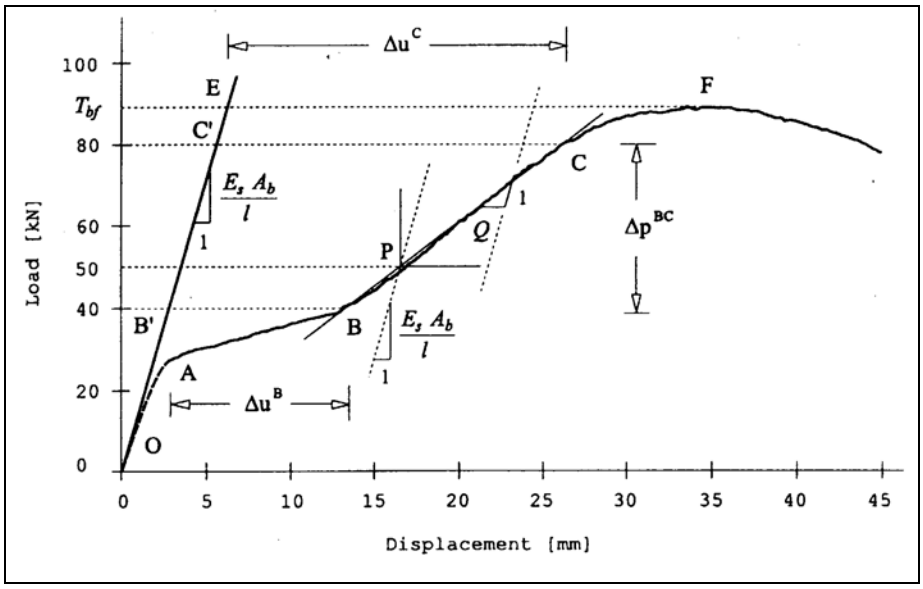

Figure 3.17 Results of a pull-out test performed on a mechanically anchored bolt (from Stillborg 1994).

The high rate of displacement over the portion AB of the curve is associated with the initial compliance of the plate, washer and nut assembly. The steeper portion BC is associated with deformation of the bolt shank and the anchor. At point C in the curve, the bolt starts to yield and at point F the bolt fails. The constant T_{bf} in equation (3-63) is therefore defined by point F in Fig 3.17.

In practice, the bolt will usually be pre-tensioned during installation, in order to avoid the initial 'flat' segment AB associated to compliance of the plate and its associated components. The level of pre-tension should be sufficient to fully 'seat' the plate, washer and nut. For the results presented in Figure 3.17, for example, an appropriate level of pre-tensioning would be between 40 and 60 kN. Thus if a pre-tension of 50 kN is applied, the effect is to move the origin of the (subsequent) load-deformation curve from point O to point P. The constant Q in Equation (3-64) is the rate of deformation for the portion BC in Fig 3.17 – this regards the elastic deformation of the shank that is already accounted by the first term within brackets in equation (3.64). Considering the magnitudes Δp^{BC}, Δu^{B} and Δu^{C} indicated in the diagram, the constant Q can be computed as

$$Q = \frac{\Delta u^{C} - \Delta u^{B}}{\Delta p^{BC}} \qquad (3\text{-}65)$$

Ideally the values of T_{bf} and Q should be obtained from pull-out tests performed directly on bolts installed on the rock in situ. The values obtained in this way will depend on the type of rock and the mechanical characteristics of the bolt being tested. Hoek and

Brown (1980) list reference values for T_{bf} and Q obtained from test in different rock types. Some of these values are presented in Tables 3.5.

Table 3.5 Values of the ultimate load T_{bf} and the deformation-load constant Q for bolt of different diameters d_b and lengths l (from Hoek and Brown, 1980).

D_b (mm)	*l (m)*	T_{bf} (MN)	Q (m/MN)
16	1.83	0.058	0.241
19	1.83	0.089	0.024
22	3.00	0.196	0.042
25	1.83	0.254	0.143

Values determined for expansion shell bolts in field tests. The rock types are: i) shale for the 16 mm bolt; ii) sandstone for the 22 mm bolt; iii) granite for the 25 mm bolt.

e) Grouted bolts

The rock-support interaction concepts, applied to the support systems discussed in the preceding sections, cannot be applied to grouted rockbolts or cables. This is because they do not act independently of the rock mass and hence the deformations which occur in both rock mass and support system cannot be separated. According to Hoek and Brown (1980), the support action grouted rockbolts or cables arises from internal reinforcement of the rock mass in much the same way as the presence of reinforcing steel casts in reinforced concrete. By knitting the rock mass together and by limiting the separation of individual blocks the grouted reinforcing elements limit the dilation in the rock mass immediately surrounding the tunnel. This has the effect of limiting the extent to which the original rock mass material constants m and s reduce to m_r and s_r. Sensitivity studies of the influence of the values of m_r and s_r upon the required support line for the rock surrounding a tunnel show that the deformation u_i is sharply reduced for relatively modest increase in m_r and s_r.

A rockbolt is mainly composed of a steel bar having axial and shear modulus (stiffness) higher than the rock. The rockbolt has a high tensile strength, while the rock mass is usually regarded as having no tensile strength. When the rockbolt is embedded in the rock mass, a new composite material will be formed with enhanced deformation modulus and higher ductility than the original rock mass. The steel bar offers confining stress to the rock when the rockbolt is prestressed or by the load induced by the deformation of the rock. The confining pressure increases the bearing capacity or the shear strength of the rock mass. When the rockbolt crosses joints or discontinuities, it offers tensile and shear resistances to the dilation and the shear of the joints. These effects form the base for the construction of the Ground Reaction Curve (GRC) of a

rock mass reinforced by grouted rockbolts. Thus it is not considered in the construction of Support Characteristic Curve (SCC).

Aydan (1989) presented the contribution of elastic and shear deformation modulus of rockbolt to deformation properties of isotropic rock mass in a local Cartesian coordinate system as

$$\Delta E_x = (E_b - E_m)n \tag{3-66}$$

$$\Delta G_y = (G_b - G_m)n \tag{3-67}$$

$$\Delta G_z = (G_b - G_m)n \tag{3-68}$$

where

E_m, E_b = elastic modulus of rock mass and steel bar, respectively

G_m, G_b = shear modulus of rock mass and steel bar, respectively

$n = A_b/A_t$

A_b = cross section of the steel bar

A_t = cross section of the representative volume

In numerical analysis, the rockbolt is represented by an embedded reinforcement element that adds stiffness to the surrounding rock mass element.

Regarding the performance and use of grouted rockbolt, Broch et al. (1996) presented an interesting observation from the construction of Gjovik Olympic Mountain Hall in Norway, which has a span of 61 meter, a length of 91 m and a maximum height of 25 m. Six instrumented, fully grouted 6-m-long rockbolts with 25 mm diameter, in most cases show very low (about 60 kN) to zero load; and furthermore, that when load build-up occurs, it is in the lower end of the bolt, i.e., close to the cavern surface. The observations also indicate that the need for the 12-m-long grouted bolts is questionable. The authors believe that in a rock mass such as that in Gjovik, grouted rockbolts with lengths of 3-4 m set in a pattern of 2-3 m together with 100 mm steel-fibre-reinforced shotcrete will do the supporting job, even for spans of 50-60 m. In this cavern, the roof is an overall self-supporting structure because of the favourable horizontal stresses.

3.3.3 Time-dependent deformation

Pan and Dong (1991), and Sulem et al.(1987) have presented models for time depending tunnel-convergence using CCM. Pan and Dong used visco-elastic model and Sulem et al. used curve fitting method.

Assume the tunnel is in a state-of-plane strain, as for the Kirsch solution to the elastic problem, and that it has been excavated in a Burgers material in distortion, which

behaves elastically in hydrostatic compression. The principal stresses in the plane perpendicular to the tunnel are p_1 and p_2. The material creeps and the strains and displacements will change with time. The radial displacement u_r of a point at coordinates r, θ is described by Goodman (1989)

$$u_r(t) = \left(A - C + B\frac{d_2}{d_4} \right)\frac{m}{q} + \left(\frac{B\left(d_2/G_1 - d_1\right)}{G_1 d_3 - d_4} - \frac{A-C}{G_1} \right) e^{-(G_1 t/\eta_1)} + B\left(\frac{d_2(1-m/\alpha) + d_1(m-\alpha)}{G_2(G_1 d_3 - d_4)} \right) e^{-(\alpha t/\eta_1)} + \frac{A - C + B/2}{\eta_2} t \qquad (3\text{-}69)$$

where

$$A = \frac{p_1 + p_2}{4}\frac{a^2}{r}$$

$$B = (p_1 - p_2)\frac{a^2}{r}\cos 2\theta$$

$$C = \frac{(p_1 - p_2)}{4}\frac{a^4}{r^3}\cos 2\theta$$

$m = G_1 + G_2$ $\qquad$ $d_3 = 6K + 2G_2$

$q = G_1 G_2$ $\qquad$ $d_4 = 6Km + 2q$

$d_1 = 3K + 4G_2$ $\qquad$ $\alpha = \dfrac{3Km + q}{3K + G_2}$

$d_2 = 3Km + 4q$

For the tunnel in an axisymmetric (hydrostatic) stress field (*i.e.* $p_1 = p_2 = p_0$) at $r = a$ in the above mentioned equation, we use A = $p_0 a/2$, $B = C = 0$, *giving*

$$u_r(t) = \frac{p_0 a}{2}\frac{G_1 + G_2}{G_1 G_2} - \frac{p_0 a}{2G_1} e^{-(G_1 t/\eta_1)} + \frac{p_0 a}{2\eta_2} t$$

or,
$$u_r(t) = \frac{p_0 a}{2G_2} + \frac{p_0 a}{2G_1} - \frac{p_0 a}{2G_1} e^{-(G_1 t/\eta_1)} + \frac{p_0 a}{2\eta_2} t \qquad (3\text{-}70)$$

The first term in the right hand side of the equation, $p_0 a/2G_2$ gives elastic deformation and rest three terms are for rheological (time-dependent) deformation. If tunnel support is provided with internal pressure p_i, it will cause deformation in opposite direction. If the support is provided immediately after the excavation, radial deformation can be calculated by the above mentioned equation with $p_0 - p_i$ instead of p_0. However, lining will not be constructed until the instantaneous elastic displacement has already occurred

(face has moved ahead and face effect is not there), the first term will have p_0 only and other three terms will have p_0 - p_i giving

$$u_r(t) = \frac{p_0 a}{2G_2} + \frac{(p_0 - p_i)a}{2G_1} - \frac{(p_0 - p_i)a}{2G_1} e^{-(G_1 t/\eta_1)} + \frac{(p_0 - p_i)a}{2\eta_2} t \qquad (3\text{-}71)$$

Rheologic parameters can be obtained for the condition between elastic and plastic if secondary phase curve is obtained. Thus time-dependent deformation can be calculated even if the rock mass is in plastic condition but the stress level has not reached the failure level yet. In Ground Reaction Curve (GRC), elastic limit can be estimated but estimation of the total tunnel convergence before the failure is not possible. It can be estimated if failure strain is determined by other methods.

3.3.4 Coulomb's shear strength criterion and Mohr's failure envelope

Coulomb in 1776 postulated that the shear strengths of rock and of soil are made up of two parts – a constant cohesion and a normal stress-dependent frictional component. (Actually, Coulomb presented his ideas and calculations in terms of forces; the concept of stress that we use today was introduced later.) Thus, the shear strength (σ_s or τ) that can be developed on a plane such as *ab* in Figure 3.18 is

$$\sigma_s = c + \sigma_n \tan \varphi \qquad (3\text{-}72)$$

where c = cohesion and φ = angle of internal friction.

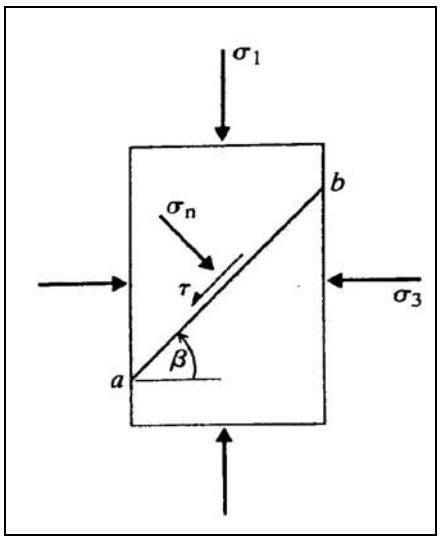

Figure 3.18 Shear failure on plane a,b.

Applying the stress transformation equations to the case shown in Figure 3.18 gives

$$\sigma_n = \frac{1}{2}(\sigma_1 + \sigma_3) + \frac{1}{2}(\sigma_1 - \sigma_3)\cos 2\beta \qquad (3\text{-}73)$$

$$\tau = \frac{1}{2}(\sigma_1 - \sigma_3)\sin 2\beta \tag{3-74}$$

Substituting for σ_n and σ_s (= τ) and rearranging them gives the limiting stress condition on any plane defined by β as

$$\sigma_3 = \frac{\sigma_1(\sin 2\beta - \tan\varphi - \cos 2\beta * \tan\varphi) - 2c}{(\sin 2\beta + \tan\varphi - \cos 2\beta * \tan\varphi)} \tag{3-75}$$

In 1882 Otto Mohr developed a very useful technique for graphing the state of stress of differently oriented planes in the same stress field. The stresses (σ_n and σ_s) on a plane plots as a single point, with σ_n measured on the horizontal axis and σ_s (or τ) on the vertical axis (Figure 3.19). A key feature of the Mohr diagram is that for a given set of principal stresses as the points, it represents the states of stress on all possible planes perpendicular to the σ_1 - σ_3 plane graph as a circle. This is called the Mohr circle. As seen in the Figure 3.19, the Mohr circle intersects the σ_n axis at values equal to σ_3 and σ_1. The radius is $(\sigma_1-\sigma_3)/2$ and the centre is at $(\sigma_1 + \sigma_3)/2$.

The Mohr circles at failure under different confining pressures together define a boundary called the *Mohr envelope* or *failure envelope* for a particular rock (Figure 3.19). The failure envelope is an empirically derived characteristic that expresses the combination of σ_1 and σ_3 magnitudes that will cause a particular rock to fracture.

There will be a critical plane on which the available shear strength will be first reached as σ_1 is increased. The Mohr circle construction (Figure 3.19) gives the orientation of this critical plane as (Brady and Brown, 1985)

$$2\beta = \frac{\pi}{2} + \varphi \tag{3-76}$$

The angle between the fracture plane and the σ_3 direction (angle β) can be determined by measuring angle 2β directly off the Mohr diagram (Figure 3.19). At intermediate confining pressure the fracture strength usually increases linearly with increasing confining pressure, producing a failure envelope with straight lines (Rowland and Duebendorfer, 1994).

For the critical plane, sin 2β = cos φ, cos 2β = -sin φ and equation (3-75) reduces to

$$\sigma_3 = \frac{\sigma_1(1-\sin\varphi) - 2c\cos\varphi}{1+\sin\varphi} = \frac{\sigma_1 - \frac{2c\cos\varphi}{1-\sin\varphi}}{K_\varphi} \tag{3-77}$$

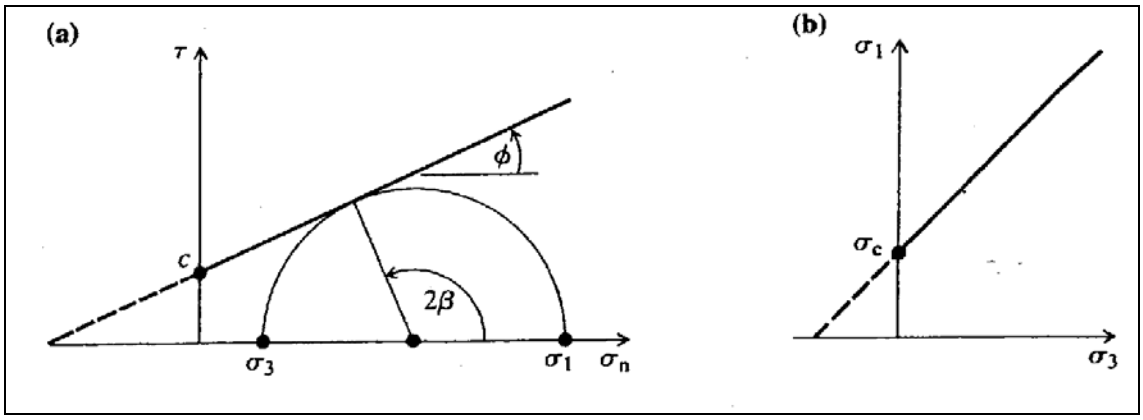

Figure 3.19 (a) Mohr circle (b) principal stresses.

Tunnel support design by using Mohr-Coulomb criteria

Mohr-Coulombs equation 3-39 can be rewritten as

$\sigma_3 = (\sigma_1 - \sigma_{ci})/ K_\varphi$. (3-78)

Value for σ_{ci} is obtained by carrying out simple UCS test. Value for φ can be determined either by tri-axial test or estimated empirically. However, it considers the intact rock condition. For jointed rock mass condition, σ_{ci} in the equation (3-78) needs to be replaced by 'rock mass strength' σ_{cm} giving the following equation:

$\sigma_3 = (\sigma_1 - \sigma_{cm})/ K_\varphi$. (3-79)

Comparing it with Equation (3-77), for critical plane,

$$\sigma_{cm} = \frac{2c\cos\varphi}{1-\sin\varphi} = 2c\sqrt{K_\varphi} \quad (3\text{-}80)$$

Hoek and Brown (1997) also proposed that the rock mass strength σ_{cm} should be estimated from the above mentioned Mohr-Coulomb relationship.

Aydan et al. (1993) considered the concept of the analogy between the axial stress-strain response of rocks in laboratory tests and tangential stress-strain response of rocks surrounding opening in the tunnels. For a circular tunnel in homogeneous isotropic rock under hydrostatic pressure (p_o) and without (or with $p_i < p_o$) support application, tangential stress 'σ_θ' acts as the major principal stress 'σ_1' and radial stress 'σ_r' acts as the minor principal stress σ_3. At the tunnel contour, σ_r is zero so σ_3 indicates the required tunnel support pressure p_i (Duncan-Fama, 1993; Aydan et al., 1993). Thus Equation (3-79) can be rewritten as

$$p_i = \frac{\sigma_\theta - 2c\sqrt{K_\varphi}}{K_\varphi} = \frac{2\sigma_0 - 2c\sqrt{K_\varphi}}{K_\varphi} = \frac{2\sigma_0 - \sigma_{cm}}{K_\varphi} \quad (3\text{-}81)$$

It is interesting to notice that this equation is similar to the Equation (3-43) given by Duncan-Fama (1993) which was used by Hoek (1998). The nominators in both the equations are same, but denominators are different. Equation (3-81) is slightly conservative as it considers unconfined condition whereas only tunnel side of the rock mass is unconfined.

Values for c and φ for the above mentioned equation refers to those of rock mass if jointed rock mass is considered. Hoek et al. (2002) have given the equations to determine c and φ for the stress range $\sigma_t < \sigma_3 < \sigma_{ci/4}$ (σ_t is the tensile strength). Using the equations for c and φ, following equation for rock mass strength is obtained:

$$\sigma_{cm} = \sigma_{ci} \cdot \frac{\left(m_b + 4s - a\left(m_b - 8s\right)\right)\left(m_b/4 + s\right)^{a-1}}{2\left(1+a\right)\left(2+a\right)} \tag{3-82}$$

Note that the value of σ_{3max}, the upper limit of confining stress over which the relationship between the Hoek-Brown and the Mohr-Coulomb criteria is considered, has to be determined for each individual case. The issue of determining the appropriate value of σ_{3max} for use in equations for c and φ, depends upon the specific application. The results of the studies for deep tunnels are plotted and the fitted equation is:

$$\frac{\sigma_{3\max}}{\sigma_{cm}} = 0.47\left(\frac{\sigma_{cm}}{\gamma H}\right)^{-0.94} \tag{3-83}$$

This equation applies to all underground excavations, which are surrounded by a zone of failure that does not extend to surface. In cases where the horizontal stress is higher than the vertical stress, the horizontal stress value should be used in place of γH.

In the Hoek-Brown criteria, GSI parameter is quantified by direct observation of rock mass. Alternative way of GSI value estimation is correlating it to RMR value. If the 1989 version of Bieniawski's RMR is used, then

$$GSI = RMR_{89} - 5 \tag{3-84}$$

where RMR_{89} has the Groundwater rating set to 15 and the Adjustment for Joint Orientation set to zero.

According to Hoek and Brown (1997), for very poor quality rock masses (GSI < 25) the value of RMR is very difficult to estimate, consequently, Bieniawski's RMR classification should not be used for estimating the GSI values for poor quality rock masses. The difficulty was that relatively few intact core pieces longer than 100 mm are recovered and it becomes difficult to determine a reliable value for RMR. However, RQD can be estimated from 'Volumetric joint count' (J_v). J_v is the number of joints intersecting a rock mass volume of 1 m^3.

$$RQD = 115 - 3.3\ J_V \tag{3-85}$$

3.3.5 The importance of pore pressure

Many rocks contain a significant amount of pores filled with fluids. These fluids support some of the load that would otherwise be supported by the rock matrix. The failure envelope in Figure 3.20 is actually derived from experiments with unfractured Weber Sandstone (Rowland and Duebendorfer, 1994). This Sandstone is subjected to the following principal stresses: $\sigma_1 = 40$ MPa and $\sigma_3 = 13$ MPa. The dashed Mohr circle in the Figure represents this state of stress. Then, 10 MPa pore pressure is added to the rock. This has effect of lowering the principal stresses by 10 MPa. Fluid pressure is hydrostatic (equal in all directions), so all principal stresses are equally affected. The Mohr circle remains the same size; it merely moves to the left on the horizontal axis a distance equal to the increase in pore pressure (Figure 3.20). Thus calculated support pressure should be increased by the amount of the increased pore pressure (*pp*) as in the following equation:

$$p_i = \frac{\sigma_\theta - 2c\sqrt{K_\varphi}}{K_\varphi} + pp \tag{3-86}$$

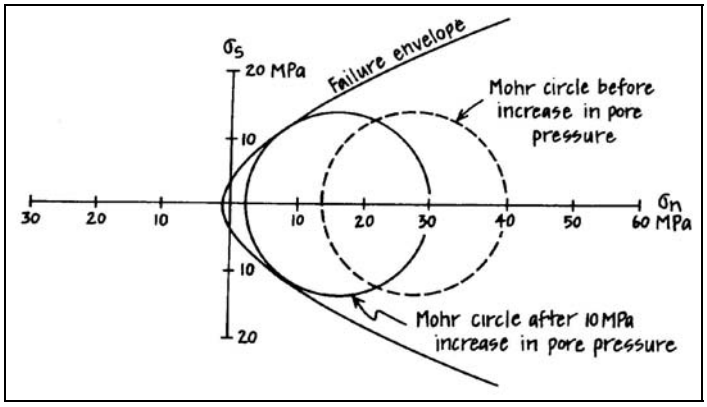

Figure 3.20 Effect of pore pressure on brittle failure. Dashed Mohr circle is based on measured principal stresses (Rowland and Duebendorfer, 1994).

Pore pressure *pp* needs to be considered in case of impermeable support system only such as for steel lining and water-tight concrete lining. Otherwise water pressure around the opening is at atmospheric, so, no need to include in equation.

3.3.6 Comparison of the analytical methods

Two types of analytical methods have been described for tunnel support design in sections 3.3.1 and 3.3.4. Those were Convergence-Confinement Method (CCM) and simple use of Mohr-Coulomb criteria.

Mohr-Coulomb and Hoek-Brown, both the criteria can be applied in CCM. Duncan-Fama (1993) presented analytical solution based on the Mohr-Coulomb criteria that can be used in CCM. It uses rock mass strength 'σ_{cm}'. Rock mass strength can be estimated

by empirical or semi-analytical methods. For massive rock mass, σ_{cm} needs to be replaced by σ_{ci}. In case of massive rock mass it is a convenient method. Carranza-Torres (2003) presented similar solution by scaling some parameters. However, it overestimates the rock mass quality giving light tunnel support as it uses σ_{ci}. It does not give any additional advantage in comparison to Duncan-Fama (1993) solutions. Carranza-Torres and Fairhurst (2000) have presented CCM of tunnel design for rock masses that satisfy the Hoek-Brown failure criterion (section 3.3.1 a). As Hoek-Brown criterion uses rock mass properties and utilizes UCS of intact rock to evaluate overall rock mass quality, this method provides direct solution. Especially for jointed rock mass, CCM with Hoek-Brown criterion is convenient. One aspect to bear in mind in using CCM is that many case studies have revealed that strain up to 1% does not cause squeezing problem (Hoek and Marinos, 2000). So support can be designed with maximum allowable strain at 1% though it may exceed elastic strain limit. All these three solutions can include rheologic properties of rock mass giving time-dependent deformation. Even if the rock mass is in plastic condition, time-dependent deformation calculation may be possible if the stress level is below failure stress level.

An analogy can be considered between the axial stress-strain response of rocks in laboratory tests and tangential stress-strain response of rocks surrounding opening in the tunnels (Duncan-Fama, 1993; Aydan et al., 1993). Thus Mohr-Coulomb equation can be rewritten in terms of tangential stress and support pressure (Equation 3-81). In tunnel, rock mass is exposed only at the tunnel side and other sides are confined. Thus in situ rock mass compressive strength is higher than uniaxial compressive strength given by Equation (3-80). σ_{cm} in the Equation (3-81) is in situ rock mass compressive strength. This simple equation estimates support pressure only.

Based on the discussion in the preceding paragraphs, for a massive rock mass Duncan-Fama (1993) solution and for jointed rock mass Carranza-Torres and Fairhurst (2000) solution would be convenient to use. They give the required parameters to draw Ground Reaction Curve (GRC). These solutions also can include time-dependent deformations. However, Equation (3-81) is helpful for quick estimate of required tunnel support, but it does not give deformation estimation, so, cannot include time-dependent deformation.

3.4 Observational approach – NATM

The selection of the support of a tunnel is a process which begins at the design stage, but does not end until geological conditions are known in detail and construction is complete. During the feasibility stage, only preliminary estimates of the amount and type of support requirement can be made. Only as the construction proceeds and the actual geological condition becomes known, deformation and support performance are observed, then the appropriate support can be determined (Shrestha and Thanju, 1997).

Observational method is adopted to assess the stability of tunnel, performance of the primary support and necessity of additional support. In situ observation and use of instrumentation to monitor deformation of the rock mass and building up of the load in support system characterize the observational approach. New Austrian Tunnelling Method (NATM) is an observational approach, and today it is a widespread concept.

NATM was introduced by Racewicz in 1964. The main contributors to the work were Rabcewicz, Muller and Pacher. The essential features of this philosophy are the conservation and mobilization of the strength of the rock mass and the formation of a largely self-supporting ring of rock mass around the tunnel. Primary support is placed so as to help the ground support itself. In order to perform this function satisfactorily, the primary support must have suitable load-deformation characteristics and be placed at the correct time (Brown, 1981). According to Muller (1978), there are 22 principles which characterize the NATM. He listed five of these as being the most important and summaries of those five principles are given below:

1. *Mobilization of the strength of the surrounding rock mass*: Preliminary support and final lining have a confining function only.
2. *Prevention of rock mass from loosening and extensive deformation*: It is done by applying shotcrete.
3. *Instrumentation to assess the influence of time on the behavior of the rock mass (and support system)*:
4. *Permanent support and lining must be thin-walled to minimize bending moment*: Necessary strengthening must be done by means of ribs, anchors not by thickening the lining.
5. *Statically, the tunnel is considered as a thick-walled tube, consisting of rock and the support and/or lining*: It needs to be assessed whether the ring is closed with rock mass or support to be provided on invert.

Kovari (1994) claims that nothing in this definition was not known and practiced long before the NATM was introduced. According to Kovari the concept of a ground arch or supporting ring was first introduced as far back as in 1882 by Engesser. In 1912 Wiesmann talked about a protective zone which supports the tunnel. Kovari claims that the ground response can not undergo loosening to the extent which has been shown by Pacher. In order to permit the optimal support to be installed, the timing of the installation should be based on measurements. Now Kovari claims that since the loosening indicated by Pacher is illogical and practically impossible, the entire argumentation for an optimal support at an optimal time becomes irrelevant.

Brown (1981) pointed out that the NATM is an approach or philosophy rather than a set of specific excavation and support methods. NATM is useful for squeezing tunnel as it considers complicated ground behaviours (Palmstrom and Broch, 2005).

4 Descriptions of the case projects

In this thesis, two case projects have been considered for stability analysis and support design for the tunnel components of the projects. The projects are: Khimti1 hydropower project and Melamchi water supply project. The construction works for the Khimti1 hydropower project is already completed. The Melamchi water supply project has been planned for construction in the near future. Squeezing is one of the main problems encountered in the Khimti tunnel. Squeezing related data has been collected and some of the available approaches have been used to analyse the squeezing phenomena that occurred in the Khimti headrace tunnel. Validity of those approaches has been checked. These two projects are located in Lesser Himalaya midlands zone and have got similar mountainous topography and regional geology. So approaches which are suitable to Khimti have been selected to assess squeezing potential and tunnel support design for the Melamchi tunnel. These outcomes can be used for the construction of the Melamchi tunnel in the future.

This chapter consists of the descriptions of these two projects and analyses are given in the following chapters.

Figure 4.1 Site locations of Melamchi and Khimti projects.

4.1 Khimti1 Hydropower Project

4.1.1 Introduction

Khimti1 hydropower project is located in Janakpur zone, central development region of Nepal. The river Khimti khola forms the boundary between the Ramechhap and

Dolakha districts. The project is located approximately 100 km east of Kathmandu (Figure 4.1).

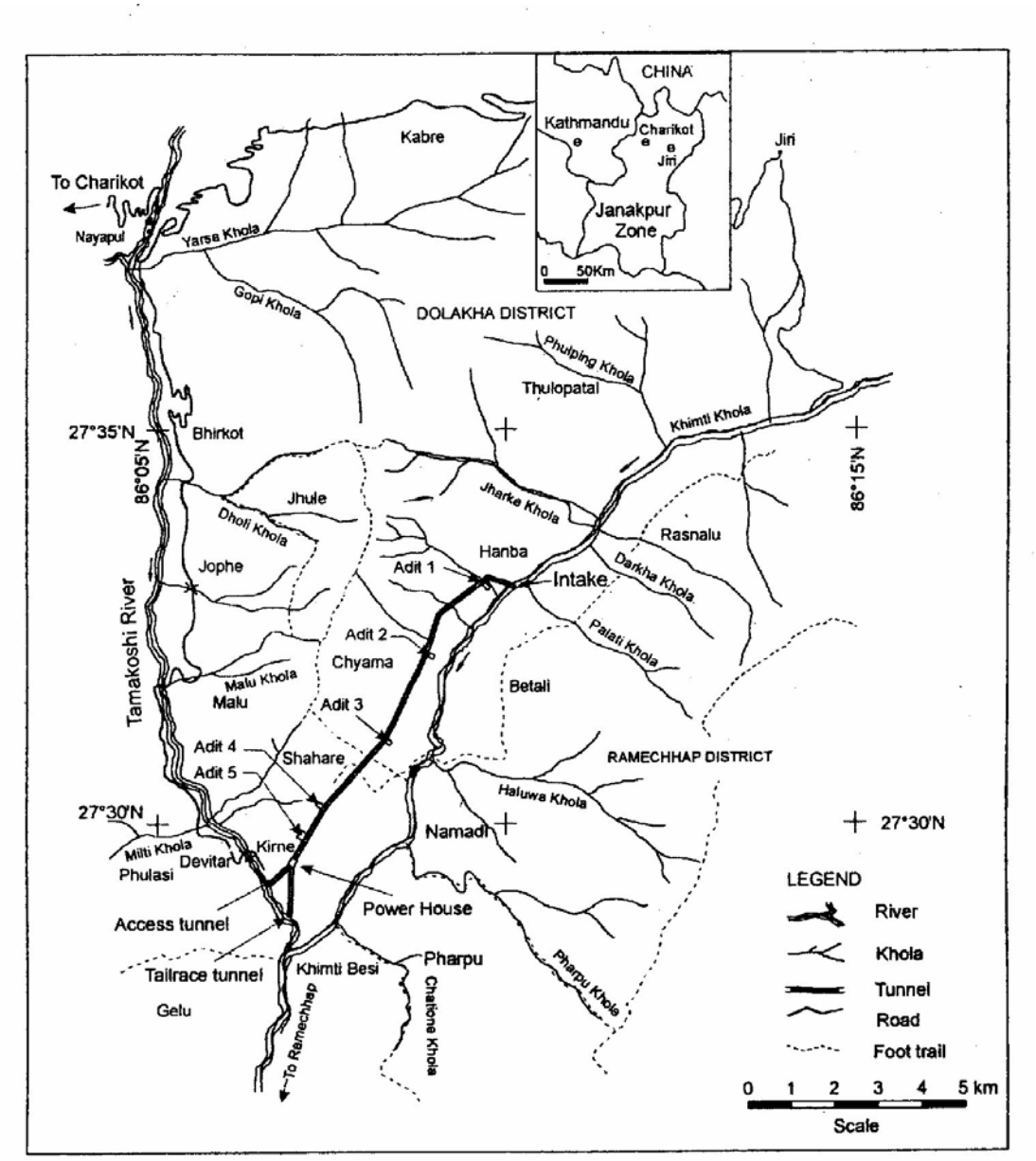

Figure 4.2 Location and layout map of Khimti1 Hydropower project (BPC, 1993).

It is a 'run of the river' type of hydroelectric power project with an installed generating capacity of 60 MW. It consists of five horizontal pelton turbines. The power plant utilises a drop from 1272 m to 586 m a.m.s.l. in the Khimti khola with the highest head in Nepal. A concrete diversion weir diverts up to 10.75 m^3/second of water from the river into a 7.9 km long headrace tunnel, and then through a 913 m long, steel lined penstock shaft inclined at 45^o to an underground powerhouse (70 m long, 11 m wide and 10 m high) cavern and finally the water discharges to Tamakoshi river though a 1.4 km

long tailrace tunnel (Figure 4.2). The powerhouse cavern is 420 m under the ground surface and 893 m inside from the entrance portal.

Himal Power Ltd. is the owner of the Khimti1 hydropower project. Project design was carried out by Statkraft Engineering (Norway) and BPC Hydroconsult (Nepal); civil construction was carried out by Statkraft Anlegg (Norway) and Himal Hydro & General Construction Ltd. (Nepal); and Equipment supply and installation was carried out by ABB Kraft (electrical) and Kværner Energy (mechanical) of Norway.

4.1.2 Geology of the project area

The project area lies in the Midland Schuppen zones of the Melung Augen Gneiss (Figure 4.3). The rocks in this zone are represented mainly by grey, coarse-to very coarse-grained, porphyroblastic augen gneiss (63%), occasionally banded gneiss (12%), and granitic gneiss (7%) with bands of very weak, green chlorite and bright grey talcose schist (18%) parallel to the foliation at intervals of 5 to 15 m. Structurally the zone is bounded by two major faults: the Midland Thrust and the Jiri Thrust to the south and north, respectively.

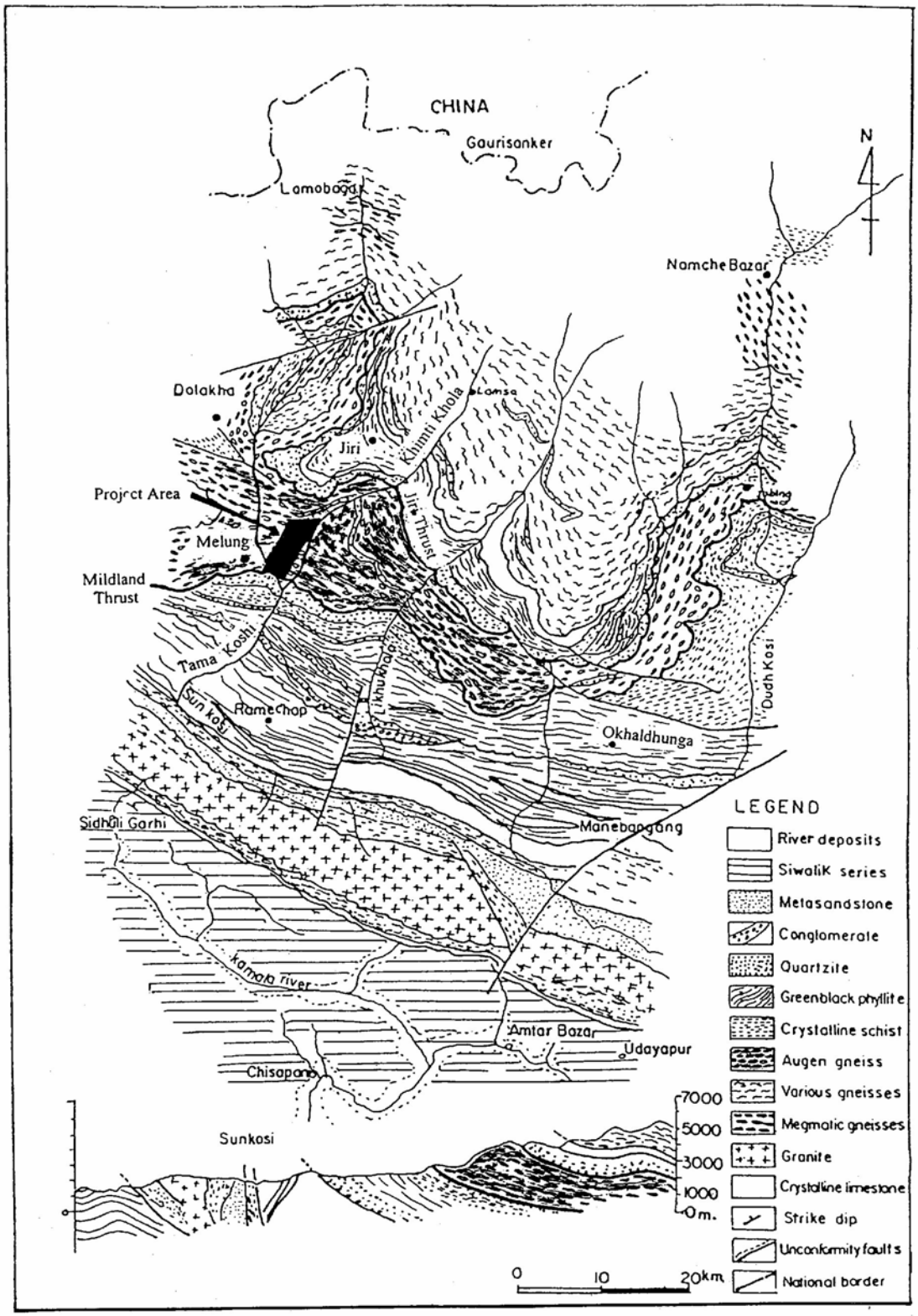

Fugure 4.3 Geological map and profile of the Ramechhap-Okhaldhunga region (After Ishida and Ohta, 1973).

The area is also influenced by several minor thrust faults characterised by very weak sheared schist with clay gouge (Figure 4.4) running parallel to the foliation plane. The foliation at the tailrace to the Adit 4 (the saddle of Pipal Danda) has steep dips (45^{o} to 60^{o}), whereas it is gently dipping (15^{o} to 35^{o}) in the area between Pipal Danda and the headworks.

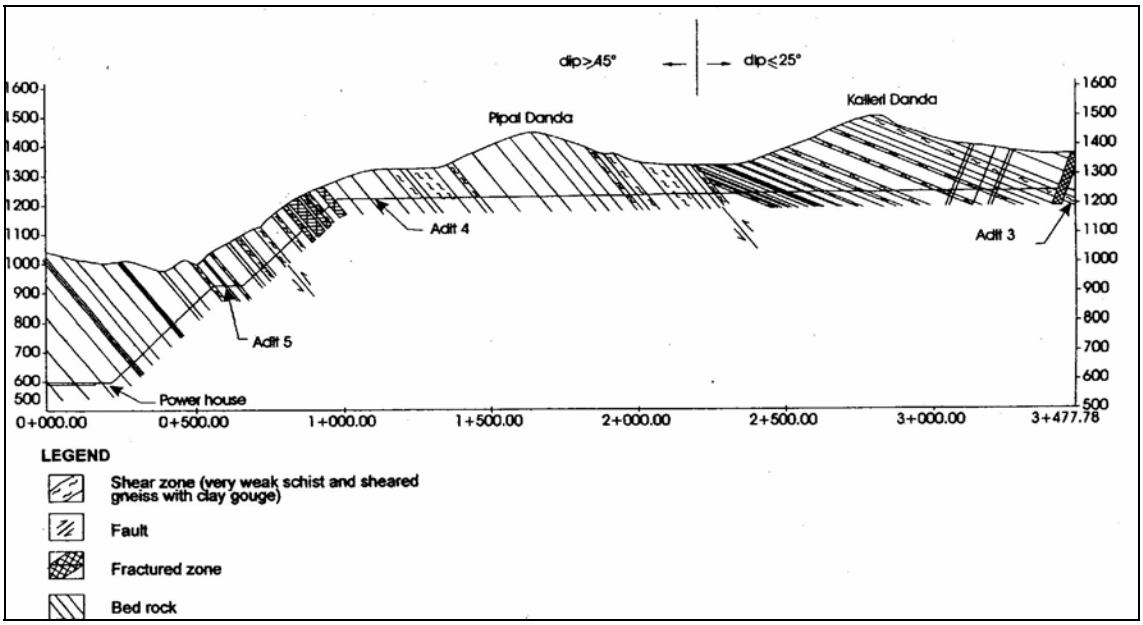

Figure 4.4 Geological cross section showing faults along the tunnel alignment (Sunuwar et al., 1999).

4.1.3 Basis for tunnel support design

The Q-method was used to classify the rock mass and to estimate the tunnel support requirement. In the Khimti project, the rock masses along the tunnel were divided into five classes based on the Q-value assigned to it. On the basis of the Q-value, tunnel support was provided using the support chart given by Grimstad and Barton (1993). Five rock classes and required tunnel support for each class are given in Table 4.1.

Table 4.1 Recommended tunnel support for Khimti1 hydropower project (for tunnel width 4 m considering ESR =1.6).

Class	**Q-value** **RMR value**	**Support**	**Description**
I Fair & Good rock	>4 >56	Spot bolting or unsupported.	Mainly competent and stable rock.
II Poor rock	1-4 44-56	Bolts in pattern 1.5*1.5 m. In fractured rock area, and mostly at crown 5 cm fibre shotcrete shall be applied.	Jointed and fractured strong rock with limited clay and water.
III Very poor rock	0.1-1 23-44	Bolts in pattern 1.0*1.5 m. Fibre shotcrete: crown 10 cm and wall 5 cm. Spiling c/c 0.5 m in crown for Q<0.4. Spiling length 4 m, or pull +1.5m at 10-15^0 & end fixed.	Heavily jointed/ fractured medium strong to weak rock. Support to be applied not more than 1 pull behind face. Reduced pull normally not needed.
IV Extre-mely poor rock	0.01-0.1 3-23	Bolts in pattern 1.0*1.2 m. Fibre shotcrete: crown 15 cm and wall 10 cm. Spiling c/c 0.4 m in crown & 1 m in walls. Spiling length 4 m, or pull +1.5m at 10-15^0 & end fixed with bolts or straps.	Weathered/weak rock, may be peeled with pocket knife. Support to be applied immediately. Reduced pull be utilised. Max pull length 2.5 m if water in-leakage.
V Except-ionally poor rock	<0.01 <3	Bolts in pattern 1.0*1.0 m. Fibre shotcrete: 20 cm thick. Spiling c/c 0.3 m in crown & 0.7 m in walls. Spiling length 3 m, or pull +1.5m. If needed 2 layers one at 10-15^0 & second at 30-45^0 & end fixed with bolts or straps.	Very weak rock normally containing >60% clay, easily separated by fingers. Schist with water. Support to be applied immediately. Reduced pull be utilised. Max pull length 2.0 m if water in-leakage.

Distribution of the rock mass classes for the total tunnel length of the project is given in Figure 4.5. According to the distribution, it consists of 7-8 % 'exceptionally poor rock', 21-22% 'extremely poor rock', 43-44% 'very poor rock', and 27-28% 'fair to poor rock'. It shows that the weak rock (i.e. Q<1) content is about 72%.

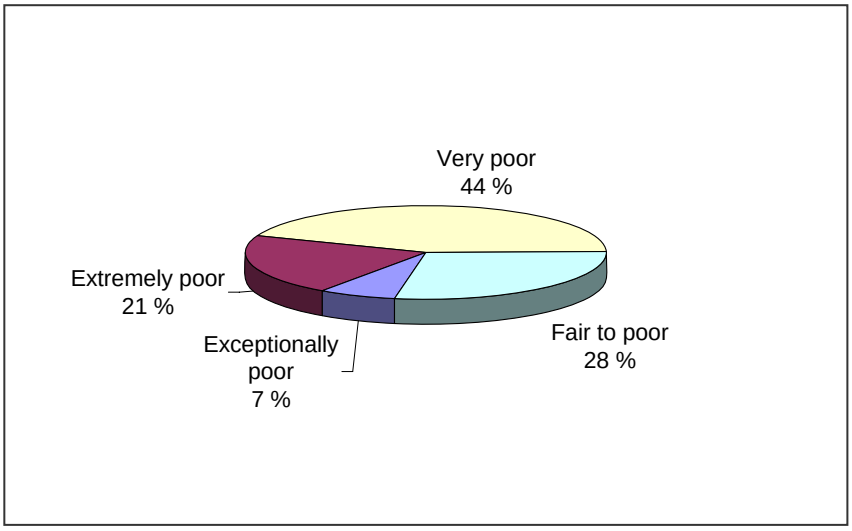

Figure 4.5 Distribution of the rock mass classes based on the Q-value for the total tunnel length.

During the tunnelling, some stability problems were encountered with the initially adopted support system (Table 4.1). So the initial support system was supplemented by adopting adjustments based on the site-specific experiences. Those adopted adjustments are summarised in Table 4.2. It was found to be practical and effective.

Table 4.2 Supplementary design principles for squeezing ground.

1. Concrete invert for the rock class V.
2. Concrete invert for the rock class IV also if the deformation measurement do not clearly indicate stable condition.
3. If the shotcrete in the squeezing areas is highly cracked and deformed, scaling and replacing with the steel fibre reinforced shotcrete. If just minor cracks exist, add a layer (30 mm) of shotcrete.

Tunnel support estimate and support review were done in three steps: 1) a tunnel log was prepared and Q-value was estimated after each round of blast, 2) support amount was recommended according to the established system and; 3) observation, monitoring in the problematic sections and support audit were carried out. Additional supports were provided where needed as per the observation and monitoring.

4.2 Melamchi Diversion Project

The Melamchi Water Supply Project (MWSP) is designed to solve a major water supply shortage in the Kathmandu valley. The overall objective of the project is to provide an efficient and safe potable water supply, improved health conditions and economic development in the Kathmandu Valley.

In 1988 Binnie and Partners identified the MWSP as the best of twenty proposed alternatives. After that several studies have concluded same. The Melamchi Diversion Scheme (MDS) is one of four components in the MWSP. The MDS shall transfer the water from Melamchi River near Nakotegaon to the Water Treatment Plant in the Kathmandu Valley.

The first phase of the MDS will be designed to transfer water from the Melamchi River to the Kathmandu Valley. 170 MLD (1.96 m^3/s) water will be the demand from MDS up to 2012. Thereafter it is assumed that additional water will be transferred from Yangri River and from year 2018 also from Larke River.

4.2.1 Location and Layout of MDS

The Melamchi Diversion Scheme project area is located in Bagmati zone, the Central Development region of Nepal. The project area stretches from the outlet to the water treatment plant near Sundarijal, around 14 km north-east of Kathmandu, to the intake, 26 km further north-east (see Figure 4.1). The intake site is located at the Melamchi River, at the confluence with Ribarma stream, at elevation of 1425 m.a.s.l. Most of the project area lies in the Sindhupalchok District. The southern end of the tunnel is in the Kathmandu District.

This project consists of a 26.3 km long tunnel with 3 adits and intake structures. Maximum tunnel overburden is about 1,200 m. Including the three adits, namely Ambathan, Gyalthum and Sindhu, access will be provided to seven working areas along the tunnel alignment. Locations of adits have been optimised considering the ground conditions for portals and to evenly distribute timing of tunnel strings. Theoretical cross-sectional area of tunnel is 12.7 m^2, except for adits and tunnel section upstream of Ambathan adit with 18.4 m^2. Tunnel gradients vary between 1.2 and 6 %, except for tunnel between Ambathan adit and intake with 44 %. Location of tunnel alignment was also important to provide sufficient rock overburden under depression in the terrain.

4.2.2 Project geology

The project area is located within the Precambrian Bhimphedi Group of the Kathmandu Complex. Geological formations along the tunnel have been assessed from the intake to outlet as (Figure 4.6):

- Timbu formation, 0 – 6.6 km in tunnel, with migmatite and banded gneiss, intensely deformed and folded, with subordinate quartzite and schist.
- Bolde quartzite, 6.6 – 8.2 km in tunnel, with massive quartzite and sporadic schist bands.
- Gyalthum formation, 8.2 – 19.5 km in tunnel, with alternation of laminated quartzite and banded schist.
- Shivapuri injection Gneiss zone, 19.5 – 26.3 km in tunnel, with banded gneiss, augen gneiss and granitic gneiss.

The rock masses along the tunnel are expected in general to be highly influenced by the intense tectonic activity connected to the orogeny of the Himalayas. When these rocks were exposed to the tectonic forces, corresponding movements were to a large extent directed along foliation planes, reducing the strength along these planes and creating a diffused weakened rock mass rather than sharply delineated thrust faults.

The rocks have, to various degrees, been affected by thrust faulting. Rock mass quality in regard to tunnelling is found to be inferior in the central part of the tunnel (Gyalthum formation) compared to rock mass quality in the Shivapuri Injection gneiss zone in the south and Timbu formation in the north (Norplan, 2002).

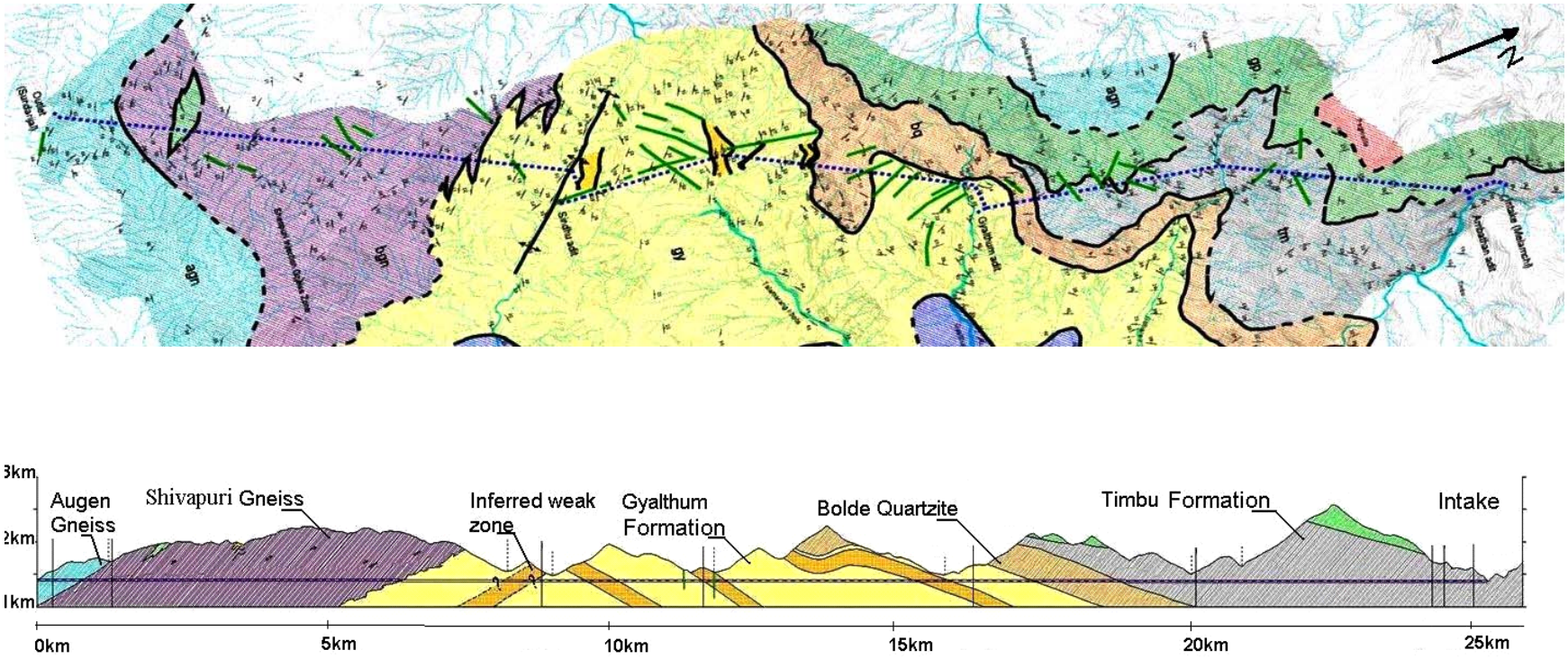

Figure 4.6 Geological map and the longitudinal profile along the Melamchi tunnel (BPC, 2001).

4.2.3 Investigations and tests

In the course of Melamchi project development, various types of investigations were carried out at different periods. Geological mapping and exploratory diamond core drilling were carried out in the first detailed study by Snowy Mountain Engineering Corps (SMEC, 1992). Similarly, geological mapping and seismic refraction study were carried out during the second detailed study by BPC Hydroconsult (BPC, 1996).

During the third (present) detailed study (Norplan, 2002), following investigations were carried out for the final design:

Exploratory diamond core drillings at tunnel / adit portals and along the tunnel. Total 33 holes with lengths up to 200 m.

Permeability testing by packer tests in exploratory holes.

Rock mechanical testing of core samples.

Average RQD values found for core samples from holes in the Timbu formation and in the Shivapuri injection gneiss zone classify as Poor (25 – 50%), while in the Gyalthum formation as Very Poor (0 – 25%).

Packer testing showed low (0.1 – 1 L) to medium (1 – 10 L) conductivities in the deep exploratory holes. No clear difference is observed between the various geological formations.

4.2.4 Collection of samples for laboratory tests

Among the four rock groups, Gyalthum formation has been considered to be the weakest one. Moreover, it is inferred that it has three weak zones and the maximum overburden above the tunnel elevation in this formation is about 550 m. Hence, this rock formation is expected to undergo squeezing problems. It would be ideal to have laboratory test such as UCS test, on the samples from this formation, but the RQD of the drilled cores is very poor (0 – 25%) and tests samples could not be obtained. Among the rest of the rock formations, Shivapuri gneiss is found to have the lowest uniaxial compressive strength, i.e. 30 MPa; and it has good RQD so that test samples have been obtained from the cores drilled in this formation. As the overburden above the tunnel level in this formation goes up to 850 m, squeezing may take place in this zone as well.

Study on creep or long term deformation of rock has been carried out with laboratory tests in NTNU laboratory in Norway as a part of this research work. In order to carry out the research, specimens were used from the core samples from bore hole TDH 1 (Figure 4.7). It is one of the six bore holes drilled along the tunnel alignment.

Figure 4.7 Drilled cores in the boxes 10 and 11 from where samples were taken for laboratory tests at NTNU (EDCO, 2001).

Some features of the exploratory hole TDH 1 are given in the following table.

Table 4.3 Some features of the exploratory hole TDH 1 and cores from it.

Location, chainage	Main tunnel alignment at Shivapuri, 25.250 km
Length, orientation	150 m, vertical
Elevation, Coordinates	1640 m, 641212 E, 3073435 N
Overburden thickness to bedrock	10.3 m
Average RQD	35
Depth to ground water	1.0 m
Average core loss	21 %
Average Point load index Is(50)	Diametric 3.7, Axial 4.3
Average UCS (M Pa)	30.0

Details of the tests carried out in NTNU laboratories in Norway, results and discussions are given in the chapter 6.

4.3 Comparison between the two projects

4.3.1 Location and Topography

The main purpose of the tunnel in the Khimti1 hydropower project and Melamchi project, is the transfer of water. Both the projects are located in the northern hilly districts of the central development region of Nepal. Both the project areas lie in the midland zone of the Lesser Himalaya having the upstream border with Higher Himalaya, hence topographies are also similar (Figure 4.8). Intakes for the Khimti and the Melamchi projects, are located at 1272 and 1425 m.a.s.l. respectively. Thus in terms of the location, topography and elevation, these two projects are similar.

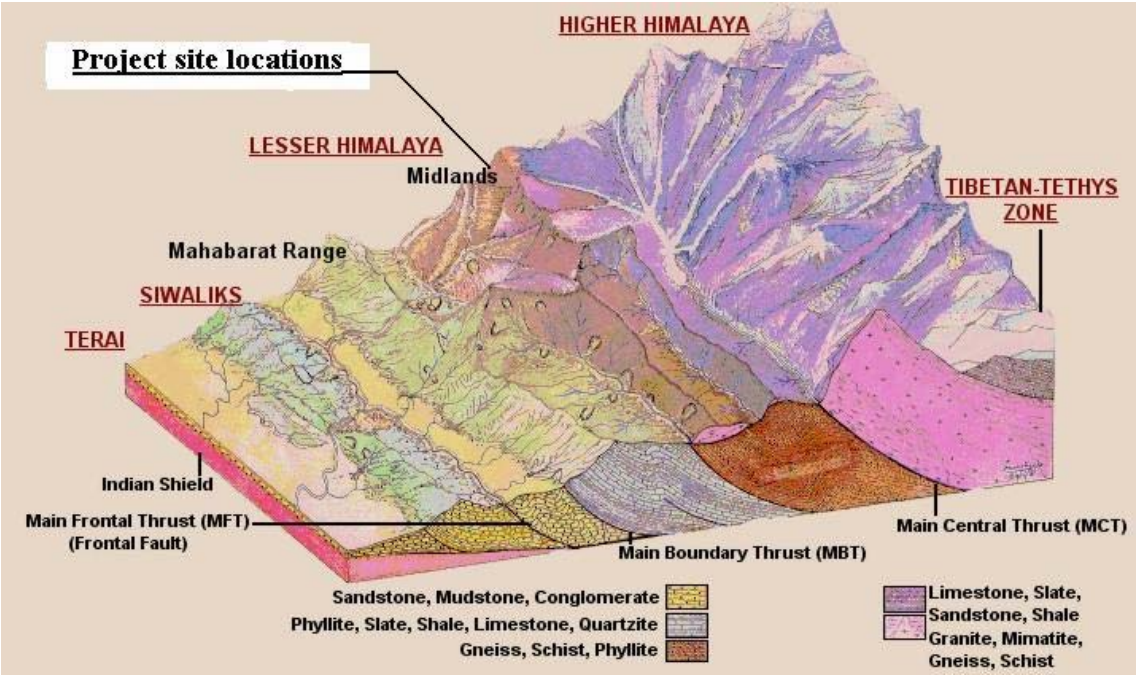

Figure 4.8 Topographical setting of the project site locations (After Galay, 1991).

4.3.2 Geology

The Khimti tunnel has been constructed through the augen gneiss with weak bands of schist. Similarly the Melamchi tunnel also has been planned through the banded gneiss, quartzite and weak schist. Some local faults and weak zones have been encountered in the Khimti tunnel and similarly such geological structures are suspected to be present in Melamchi tunnel also (Figures 4.4 and 4.6). Thus both the project areas have the combination of strong and weak rocks with local faults and weak zones.

The other common significant geological feature is that both the project areas are located on the north side of the Main Central Thrust (MCT) (Figure 4.9).

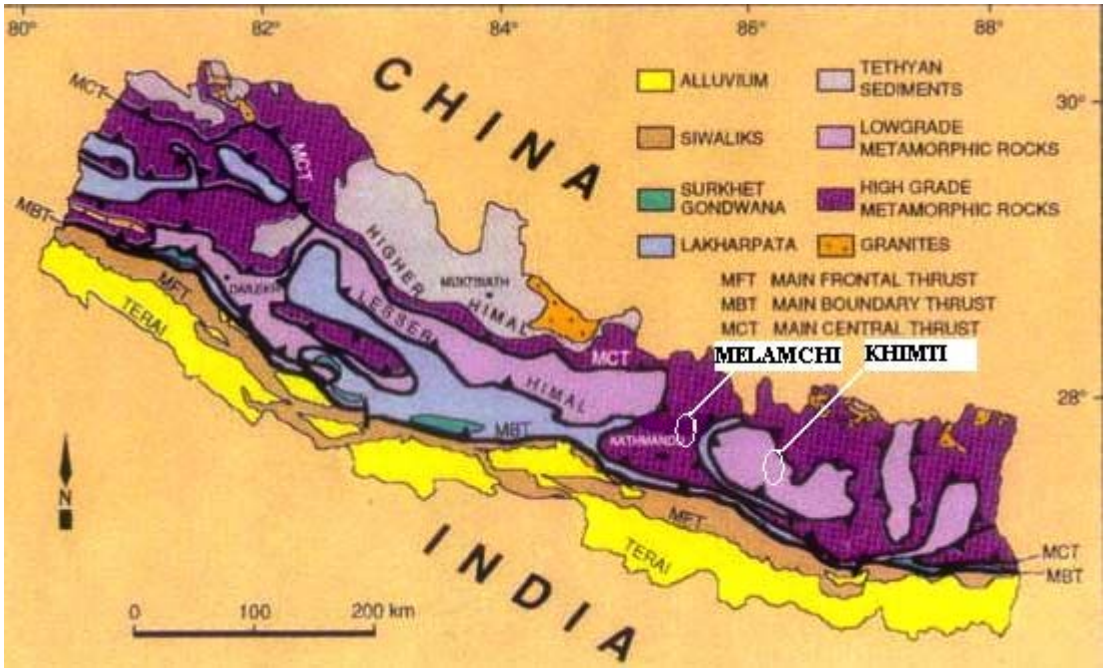

Figure 4.9 Project site locations in reference to the MCT line (www.petroleumnepal.com.np).

4.3.3 Squeezing in Khimti and Melamchi tunnels

a) Squeezing phenomena in the Khimti tunnel

Tunnel support was provided according to Table 4.1 and 4.2. Then the applied support was monitored in the locations where the rock classes were III, IV, and V, at first by visual inspection and then by convergence measurement by using tape extensometer.

Tunnel stability problems were encountered during 1997 and the beginning of 1998 (Statkraft Eng & BPC, 2001). Tunnel squeezing was one of the major problems. It was noticed in different locations of the tunnels after two weeks and 20 m behind the face mainly in the location with schist or decomposed gneiss.

b) Potential squeezing problem in the Melamchi tunnel

The planned tunnel system at Melamchi is situated in rock masses that are highly variable both regarding strengths and regarding occurrence of discontinuities, and also with highly variable rock stress conditions. A defect in the rock mass affecting the stability is the in general gently dipping foliation, disturbed and weakened by thrust movements. Gravitational failures (block falls) are anticipated to be more prominent in zones with such defects. Highest frequency of such failures is expected in the schistose sections, such as in the Gyalthum formation (Norplan, 2002).

Weak rocks and clayey zones, with risk of squeezing or creep, are also expected to be more frequently met in the Gyalthum formation. Tunnel sections with high effective overburden are expected to have pronounced rock spalling activity. Average overburden above tunnel level in this formation is of about 300 m, and the maximum overburden thickness goes up to 550 m. These conditions may be enough to cause squeezing. Test samples for UCS, could not be obtained from the schist rock of this formation as the RQD is very low. Similarly, Shivapuri gneiss zone has average overburden above tunnel level of about 600 m, and the maximum overburden goes up to 850 m. This zone may also have squeezing problems as the average uniaxial compressive strength of intact rock samples is only 30 MPa.

The alignment of the tunnel system of this project runs partly along the watershed line, partly in the valley side and at few places under the saddles. Thus some parts of the tunnel may experience the topographical effect of the valley side, which may contribute to squeezing phenomenon.

Assessment of rock support needs, used as basis for the Bills of Quantities of rock support, is based on a tentative rock mass classification based on the Q classification system. Rock bolting (both end-anchored rock bolts and rock dowels) in combination with sprayed concrete is considered to be the main method for rock support. In case of more severe stability problems, use of long spiling bolts, bar reinforced shotcrete ribs, or cast reinforced concrete lining and/or invert are anticipated.

5 Tunnel squeezing in Khimti1 hydropower project

Tunnel squeezing was one of the major problems in the Khimti1 Hydropower project. Monitoring was carried out by using tape extensometer especially in rock squeezing areas to record the convergence during the period of September 1998 to July 1999. The squeezing phenomena were noticed in different locations of the tunnels after 2 weeks and 20 m behind the face mainly in the location with schist or decomposed gneiss with 80 m to 420 m overburden depth. The maximum convergence recorded was 160.2 mm at Adit1-downstream Chainage 500 m. Details about the project and basis for support systems are given in chapter 4.

5.1 Adopted methods and approaches

Based on the discussions in chapter 3, the following methods and approaches have been adopted to analyse the squeezing problems that occurred in the Khimti tunnel:

Empirical method: *Goel (1994)'s approach based on N value*.

Empirical method: *Singh et al. (1992); and Grimstad & Barton (1993) approaches based on Q-method.*

Semi-analytical method: *Hoek and Marinos (2000)'s approach*.

Analytical method: *Carranza-Torres & Fairhurst approach (2000) using Hoek-Brown criteria.*

Analytical method: *Duncan-Fama approach (1993) using Mohr-Coulomb criteria.*

Simplified analytical solution: *using Mohr-Coulomb criteria*.

Numerical modelling method: *using FLAC^{3D} code*.

For every method mentioned above, there are more than one approach available. In this thesis, for each method at least one approach has been used. Main equations used in the analyses in this chapter, are given below; and with details in the Chapter 3. Details on the use of FLAC^{3D} and results are discussed in Chapter 8.

Equations for Goel(1994)'s approach:

$$H = \left(275\,N^{0.33}\right)B^{-0.1}\left(m\right) \tag{3-4}$$

$$P'_{sqult}(N) = \left\{\frac{1}{30}\right\}10^{\left(\frac{H^{0.6}\alpha^{0.1}}{50\,N^{0.33}}\right)} \tag{3-5}$$

where,

H = Overburden depth (m),

B = Tunnel span or diameter B (m),

N = Rock mass number, defined as Barton et al.(1974) Q with SRF = 1,

$P'_{sqult}(N)$ = Estimated ultimate support pressure in squeezing ground conditions in MPa using N,

a = Tunnel radius in cm,

N will be estimated from the assumed value of GSI by using the following equation:

GSI = 9 Log_e Q' + 44 (Hoek et al., 1995). Here Q' = (RQD/J_n)*(J_r/J_a). For dry or minor inflow (< 25 l/min), J_w = 1. Hence Q' and N are same for J_w = 1, it can be rewritten as follows:

GSI = 9 Log_e N + 44 (5-1)

Where, GSI = Geological strength index.

Equations for Hoek and Marinos(2000)'s approach:

$$\sigma_{cm} = \left(0.0034 m_i^{0.8}\right)\sigma_{ci}\left\{1.029 + 0.025 e^{(-0.1 m_i)}\right\}^{GSI} \quad (3\text{-}21)$$

$$\varepsilon = \frac{\delta_i}{d_0} = \left[0.002 - 0.0025\frac{p_i}{\sigma_0}\right]\left(\frac{\sigma_{cm}}{\sigma_0}\right)^{\left(2.4\frac{p_i}{\sigma_0}-2\right)} \quad (3\text{-}20)$$

$$\frac{d_p}{d_0} = \left[1.25 - 0.625\frac{p_i}{\sigma_0}\right]\left(\frac{\sigma_{cm}}{\sigma_0}\right)^{\left(\frac{p_i}{\sigma_0}-0.57\right)} \quad (3\text{-}22)$$

where
σ_{ci} = Uniaxial compressive strength of intact rock
m_i = A constant that is defined by the frictional characteristics of the component materials in these rock elements
GSI = A constant that relates the properties of the intact rock elements to those of the overall rock mass
σ_{cm} = Uniaxial compressive strength of rock mass
p_i = Support pressure
σ_o = In situ stress = depth * unit weight
δ_i = Tunnel sidewall deformation
d_o = Original tunnel diameter in metres
d_p = Plastic zone diameter.

Equations for Analytical method using Hoek-Brown criteria (Carranza-Torres & Fairhurst, 2000):

$$P_i = \frac{p_i}{m_b \sigma_{ci}} + \frac{s}{m_b^2} \tag{3-31}$$

$$S_o = \frac{\sigma_o}{m_b \sigma_{ci}} + \frac{s}{m_b^2} \tag{3-32}$$

$$P_i^{cr} = \frac{1}{16}\left[1 - \sqrt{1+16S_o}\right]^2 \tag{3-33}$$

$$p_i^{cr} = \left[P_i^{cr} - \frac{s}{m_b^2}\right] m_b \sigma_{ci} \tag{3-34}$$

$$u_r^{el} = \frac{\sigma_o - p_i}{2G_{rm}} R \tag{3-35}$$

$$R_{pl} = R \exp\left[2\left(\sqrt{P_i^{cr}} - \sqrt{P_i}\right)\right] \tag{3-36}$$

$$\frac{u_r^{pl}}{R}\frac{2G_{rm}}{\sigma_o - p_i^{cr}} = \left[\frac{1-2\upsilon}{2}\frac{\sqrt{P_i^{cr}}}{S_o - P_i^{cr}} + 1\right]\left(\frac{R_{pl}}{R}\right)^2 + \frac{1-2\nu}{4\left(S_o - P_i^{cr}\right)}\left[\ln\left(\frac{R_{pl}}{R}\right)\right]^2 - \frac{1-2\nu}{2}\frac{\sqrt{P_i^{cr}}}{S_o - P_i^{cr}}\left[2\ln\left(\frac{R_{pl}}{R}\right) + 1\right] \tag{3-38}$$

where,

P_i, S_o and P_i^{cr} are scaled form of p_i, σ_o and p_i^{cr}
m_b and s are Hoek-Brown parameters
σ_o = Far-field stress
σ_{cm} = Compressive strength of rock mass
σ_{ci} = Uniaxial compressive strength of intact rock
G_{rm} = Shear modulus of rock mass
v = Poisson's ratio
p_i = Support pressure
p_i^{cr} = Critical pressure
R_{pl} = Radius of the plastic zone
R = Radius of unsupported tunnel
u_r^{pl} = Inward radial deformation of the tunnel wall in plastic condition
u_r^{el} = Inward radial deformation of the tunnel wall in elastic condition.

Equations for Analytical method using Mohr-Coulomb criteria (Duncan-Fama, 1993):

$$p_i^{cr} = \frac{2\sigma_0 - \sigma_{cm}}{K_\varphi + 1} \tag{3-43}$$

$$\frac{R_{pl}}{R} = \left[\frac{2(\sigma_0 (K_\varphi - 1) + \sigma_{cm})}{(K_\varphi + 1)((K_\varphi - 1) p_i + \sigma_{cm})} \right]^{1/(K_\varphi - 1)} \tag{3-44}$$

$$\frac{u_r^{pl}}{R} = \frac{(1+\nu)}{E} \left[2(1-\nu)(\sigma_0 - p_i^{cr})(\frac{R_{pl}}{R})^2 - (1-2\nu)(\sigma_0 - p_i) \right] \tag{3-45}$$

$$u_r^{el} = (\sigma_0 - p_i) \frac{R}{2G_{rm}} \tag{3-56}$$

where

$K_\varphi = \frac{1+\sin\varphi}{1-\sin\varphi}$, and φ is the internal friction angle.

σ_o = Far-field stress
σ_{cm} = Compressive strength of rock mass
E = Modulus of deformation of rock mass
ν = Poisson's ratio
p_i = Support pressure
p_i^{cr} = Critical pressure
R_{pl} = Radius of the plastic zone
R = Radius of unsupported tunnel
u_r^{pl} = Inward radial deformation of the tunnel wall in plastic condition
u_r^{el} = Iinward radial deformation of the tunnel wall in elastic condition.

Equation for Simplified solution using Mohr-Coulomb criteria

$$p_i^{cr} = \frac{2\sigma_0 - \sigma_{cm}}{K_\varphi} \tag{3-81}$$

where

$K_\varphi = \frac{1+\sin\varphi}{1-\sin\varphi}$, and φ is the internal friction angle.

σ_o = Far-field stress
σ_{cm} = Compressive strength of rock mass
p_i^{cr} = Critical pressure.

5.2 Data collection for squeezing analysis

In order to analyse the squeezing phenomena in the Khimti tunnel, twenty six tunnel sections of the headrace tunnel have been considered. Three documents namely, tunnel logs, registration of applied support and convergence measurement records have been used as source for data collection. These main three documents are parts of the 'Khimti1 hydropower project: project completion report' (Statkraft Eng & BPC, 2001) and are described in the following sections:

5.2.1 Tunnel logs

Tunnel log of each tunnel was recorded just after the excavation and mucking. The logs include graphical representation of geological structures, rock types and attitudes. It also includes estimated values of the parameters that are needed to estimate Q and RMR values, and required rock support type. A typical 'Tunnel log' sheet is given in Figure 5.1.

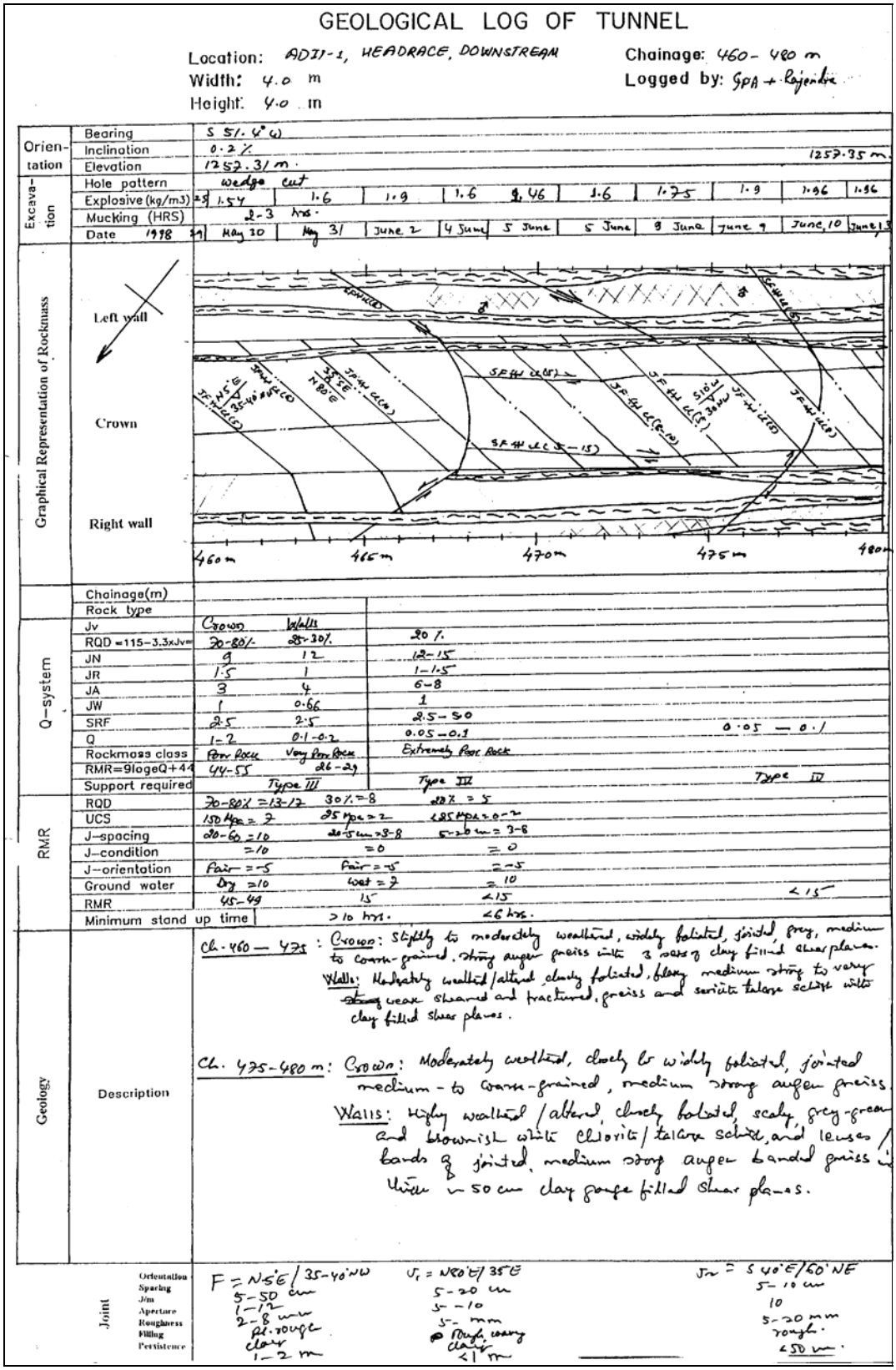

Figure 5.1 A typical 'Tunnel log' of Khimti headrace tunnel.

Squeezing related data are extracted from the tunnel logs of the twenty six tunnel sections. Those data are tabulated in Table 5.1a and Table 5.1b.

Table 5.1a Khimti tunnel data from the squeezing sections.

Location Chainage (m)	Over burden (m)	Tunnel width (m)	Rock type	Q value	Average Q value	RQD (%)	Jn	Jr	Ja	Jw	SRF
Adit1 d/s 475	98	4.0	AG/STS	0.05 - 0.1	0.08	20	12-15	1-1.5	6-8	1	2.5-5.0
Adit1 d/s 500	100	4.2	sheared SCS	0.01	0.01	10	15-20	1-1.5	6-8	1	10
Adit1 d/s 515	100	4.2	Sheared SCS	0.003 - 0.006	0.0045	<10	20	0.5-1	8	1	10
Adit1 d/s 580	111	4.3	Sheared TCS	0.006 - 0.01	0.008	10	12	1	8	0.66-1	10
Adit1 d/s 665	112	4.0	AG / S	0.03 - 0.08	0.06	20-25	15-20	1	4-6	1	5
Adit 2 d/s 441	126	4.0	AG	0.2 - 0.4	0.3	50	12-15	0.5-1	3-4	0.66	2.5
Adit 2 d/s 601	138	4.0	STS	0.01 - 0.015	0.013	10-15	15	1	6-8	1	10
Adit 2 d/s 895	198	4.0	G & CS	0.07 - 0.2	0.14	30-40	9-12	1.5	4-6	0.66-1	7.5
Adit 2 u/s 1283	212	4.4	AG/SCS	0.03 - 0.05	0.04	20-25	15	0.5-1	6-8	0.66	2.5
Adit 2 u/s 1357	261	4.0	BG / CS	0.08-0.1	0.095	30-35	12-15	1-1.5	3	0.66	5
Adit 2 u/s 1730	95	4.0	AG/AG with clay gauge	0.05 - 0.08	0.065	30-40	12-15	1-1.5	6	0.66	5
Adit 3 u/s 15	130	5.0	2m shear band of AG&S	0.1-0.3	0.2	30-35	9	1-1.5	3-4	1	5
Adit 3 u/s 59	158	4.1	AG/S	0.15 - 0.3	0.23	25-30	9-12	1	4	1	2.5
Adit 3 u/s 200	276	5.0	AG	0.2 - 0.3	0.25	30-40	9	1	3-4	1	5
Adit 3 u/s 210	276	5.0	AG	0.15 - 0.4	0.28	30-40	6-9	1	3-4	1	5
Adit 3 d/s 220	140	4.0	S	0.009	0.009	10	20	1.5	8	1	10
Adit 3 u/s 235	284	5.0	G	0.08 - 0.1	0.09	30-35	12	1	4	0.66	5
Adit 3 u/s 340	300	5.0	AG & SS	0.07 - 0.1	0.09	20-30	9	1	4-6	1	2.5
Adit 3 u/s 345	300	5.0	AG & SS	0.02 - 0.07	0.05	10-20	15	1	4-6	1	5
Adit 4 u/s 503	225	4.0	GG & STS	0.12 - 0.15	0.14	30-40	15	1.5	4-6	1	5
Adit 4 u/s 550	218	4.0	CSS	0.05 - 0.1	0.07	20-30	12-15	1.5	4	1	10
Adit 4 u/s 852	114	4.0	BG	0.35-0.6	0.47	45-55	9-12	1.5	4	1	2.5-5.0
Adit 4 u/s 876	114	4.0	BG with shear planes	0.5 - 0.68	0.6	45-55	12	1.5	4	1	2.5
Adit 4 u/s 974	112	4.0	sheared AG	0.006 - 0.009	0.008	10	20	1	6-8	1	10
Adit 4 u/s 1013	112	4.0	sheared CTS with multiple SP	0.006	0.006	<10	20	0.5-1	8	1	10
Adit 4 u/s 1045	112	4.0	Sheared AG with clay fill	0.006 - 0.01	0.008	10-15	20	1	6-8	1	10

AG=Augen Gneiss, BG=Banded Gneiss, GG=Granitic Gneiss, G=Gneiss, STS=Sericite Talcose Schist, TCS=Talcose Chlorite Schist, CS=Chlorite Schist, SS=Sericite Schist, CSS=Chlorite Sericite Schist, S=Schist, SP=Shear Plane

***Note**: In the fourth column of Tables 5.1a and b, rock type defined as AG/STS means rock type in crown is AG and that in walls is STS.*

There have been ambiguities about the evaluation of SRF in the Q-system (Palmstrom & Broch, 2005 and; Goel, 1994). However, in the Khimti project, SRF was evaluated on the basis of 'weakness zones intersecting excavations' and found to be convenient. The

field data have been also used to estimate N (Goel'94) and GSI values. Those are given in Table 5.1b.

Table 5.1b Khimti tunnel data from the squeezing sections.

Location Chainage (m)	Over burden (m)	Tunnel width (m)	Rock type	N (Goel'94)	Q'	GSI from Q'	Average RMR	σci (MPa)	Support provided	Measured converge nce (mm)
Adit1 d/s 475	98	4.0	AG/STS	0.2	0.20	30	<15	<25	IV	30.9
Adit1 d/s 500	100	4.2	sheared SCS	0.1	0.10	23	<17	<25	IV with concwall	160.2
Adit1 d/s 515	100	4.2	Sheared SCS	0.045	0.05	16	<7	<5	V with concwall	110.0
Adit1 d/s 580	111	4.3	Sheared TCS	0.08	0.12	25	<7	<5	V	32.3
Adit1 d/s 665	112	4.0	AG / S	0.3	0.30	33	15-20	25-50	III	11.8
Adit 2 d/s 441	126	4.0	AG	0.75	1.14	45	<38	<100	III	1.3
Adit 2 d/s 601	138	4.0	STS	0.13	0.13	26	13-18	<5	V	7.5
Adit 2 d/s 895	198	4.0	G & CS	1.05	1.59	48	<21	25-50	IV	11.5
Adit 2 u/s 1283	212	4.4	AG/SCS	0.1	0.15	27	<17	<25	IV	1.0
Adit 2 u/s 1357	261	4.0	BG / CS	0.475	0.72	41	<21	<50	IV	6.1
Adit 2 u/s 1730	95	4.0	AG/AG with clay gauge	0.325	0.49	38	15-20	<25	IV but not applied	11.6
Adit 3 u/s 15	130	5.0	2m shear band of AG&S	1	1.00	44	20-25	25-50	III	17.0
Adit 3 u/s 59	158	4.1	AG/S	0.575	0.58	39	25-30	25-50	III	13.2
Adit 3 u/s 200	276	5.0	AG	1.25	1.25	46	32-37	<50	III	38.7
Adit 3 u/s 210	276	5.0	AG	1.4	1.40	47	20-25	25-50	III	18.2
Adit 3 d/s 220	140	4.0	S	0.09	0.09	22	8	<5	V	32.0
Adit 3 u/s 235	284	5.0	G	0.45	0.68	41	19	50	IV	62.0
Adit 3 u/s 340	300	5.0	AG & SS	0.225	0.23	31	23-25	25-50	V	14.0
Adit 3 u/s 345	300	5.0	AG & SS	0.25	0.25	32	12-20	<25	V	9.0
Adit 4 u/s 503	225	4.0	GG & STS	0.7	0.70	41	24-28	5-25	III	9.7
Adit 4 u/s 550	218	4.0	CSS	0.7	0.70	41	<27	25	IV	5.5
Adit 4 u/s 852	114	4.0	BG	1.175	1.18	45	32-35	50	III	1.0
Adit 4 u/s 876	114	4.0	BG with shear planes	1.5	1.50	48	32-41	50	III	9.7
Adit 4 u/s 974	112	4.0	sheared AG	0.08	0.08	21	18-23	<1	V with mesh	7.9
Adit 4 u/s 1013	112	4.0	sheared CTS with multiple SP	0.06	0.06	19	<18	<1	IV mess@cr own	47.7
Adit 4 u/s 1045	112	4.0	Sheared AG with clay fill	0.08	0.08	21	<19	<5	V	4.0

AG=Augen Gneiss, BG=Banded Gneiss, GG=Granitic Gneiss, G=Gneiss, STS=Sericite Talcose Schist, TCS=Talcose Chlorite Schist, CS=Chlorite Schist, SS=Sericite Schist, CSS=Chlorite Sericite Schist, S=Schist, SP=Shear Plane

σ_{ci} is the uniaxial compressive strength of intact rock estimated in the tunnel, as one of the parameters for RMR method. However, the value of the σ_{ci} has been evaluated by visual observation and using knife and geological hammer, but without any laboratory tests. Thus the values of σ_{ci} are very rough estimations. There may be consequent effect of using this value for calculating the squeezing pressure and tunnel convergence.

5.2.2 Registration of applied supports

Applied tunnel supports were recorded by a joint team of staff from the consultant and the contractor sides. Rock bolts and fibre-reinforced shotcrete were used as the main supports in the Khimti tunnels. Occasionally, reinforced ribs of shotcrete, rock bolt straps, concrete invert, concrete wall and complete concrete lining were also used as the tunnel supports. A typical 'Tunnel support registration' is given in Figure 5.2.

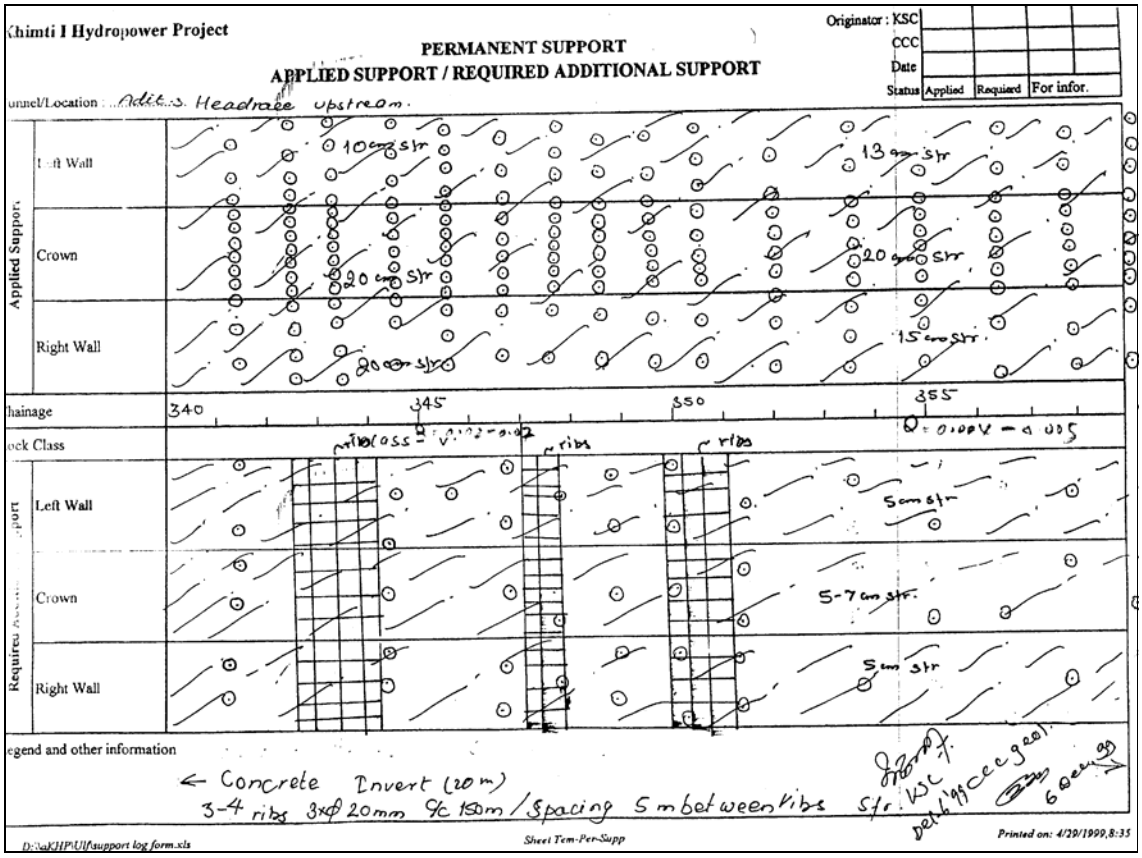

Figure 5.2 A typical 'Tunnel support registration' *of Khimti headrace tunnel.*

Thickness of the applied shotcrete was measured by drilling and measuring thickness in the drilled hole, and similarly, rock bolts were counted and their spacings were measured. These information were recorded in the registration of applied supports. Using these recorded data in the equations given in Hoek and Brown (1980), stiffness and the maximum pressure that the support can sustain are calculated for shotcrete and rock bolt separately. Then the combined effect of the rock bolt and shotcrete is calculated in terms of the maximum support pressure according to the method given in Carranza-Torres & Fairhurst (2000) (Table 5.2).

Table 5.2 Tunnel support provided.

Location Chainage (m)	Type of support proveded	Shotcrete				Rock bolts				Combined support effect		
		Thickn-ess (m)	Max pressu-re (MPa)	Stiffn-ess (MPa/m)	Max deform-ation (m)	Spaci-ng (m*m)	Max pressu-re (MPa)	Stiff-ness (MPa /m)	Max deform-ation (m)	Max deform-ation (m)	Stiff-ness (MPa)	Max press-ure (MPa)
Adit1 d/s 475	IV	0.10	1.219	927	0.0013	1.5*1.8	0.037	6	0.0065	0.0013	933	1.213
Adit1 d/s 500	IV with concwall	0.10	1.219	927	0.0013	-				0.0013	927	1.205
Adit1 d/s 515	V with concwall	0.20	2.375	1930	0.0012	1.2*1.5	0.056	9	0.0065	0.0012	1939	2.327
Adit1 d/s 580	V	0.20	2.375	1930	0.0012	1.2*2	0.042	6	0.0065	0.0012	1936	2.323
Adit1 d/s 665	III	0.05	0.617	454	0.0014	2*2.2	0.023	4	0.0065	0.0014	458	0.641
Adit 2 d/s 441	III	0.05	0.617	454	0.0014	1.5*1.5	0.044	7	0.0065	0.0014	461	0.645
Adit 2 d/s 601	V	0.20	2.375	1930	0.0012	2*2	0.025	4	0.0065	0.0012	1934	2.321
Adit 2 d/s 895	IV	0.10	1.219	927	0.0013	1.5*1.5	0.044	7	0.0065	0.0013	934	1.214
Adit 2 u/s 1283	IV	0.10	1.219	927	0.0013	2*2	0.025	4	0.0065	0.0013	931	1.210
Adit 2 u/s 1357	IV	0.10	1.219	927	0.0013	1.2*2	0.042	6	0.0065	0.0013	933	1.213
Adit 2 u/s 1730	IV but not applied	-				-					0	0.000
Adit 3 u/s 15	III	0.10	1.219	927	0.0013	1.2*1.5	0.056	9	0.0065	0.0013	936	1.217
Adit 3 u/s 59	III	0.07	0.86	641	0.0013	1.2*1.5	0.056	9	0.0065	0.0013	650	0.845
Adit 3 u/s 200	III	0.10	1.219	927	0.0013	1*1.2	0.083	13	0.0065	0.0013	940	1.222
Adit 3 u/s 210	III	0.07	0.86	641	0.0013	1.2*1.2	0.069	11	0.0065	0.0013	652	0.848
Adit 3 d/s 220	V	0.15	1.805	1420	0.0013	1.0*1.5	0.067	10	0.0065	0.0013	1430	1.859
Adit 3 u/s 235	IV	0.07	0.86	641	0.0013	1.2*1.5	0.056	9	0.0065	0.0013	650	0.845
Adit 3 u/s 340	V	0.15	1.805	1420	0.0013	1*1.5	0.067	10	0.0065	0.0013	1430	1.859
Adit 3 u/s 345	V	0.15	1.805	1420	0.0013	1*1.5	0.067	10	0.0065	0.0013	1430	1.859
Adit 4 u/s 503	III	0.08	0.98	735	0.0013	2*2	0.025	4	0.0065	0.0013	739	0.961
Adit 4 u/s 550	IV	0.07	0.86	641	0.0013	1.5*1.5	0.044	7	0.0065	0.0013	648	0.842
Adit 4 u/s 852	III	0.06	0.739	547	0.0014	1.2*1.5	0.056	9	0.0065	0.0014	556	0.778
Adit 4 u/s 876	III	0.10	1.219	927	0.0013	1.2*1.5	0.056	9	0.0065	0.0013	936	1.217
Adit 4 u/s 974	V with mesh	0.20	2.375	1930	0.0012	0.8*1.5	0.083	13	0.0065	0.0012	1943	2.332
Adit 4 u/s 1013	IV mess@crown	0.07	0.86	641	0.0013	1*1.5	0.067	10	0.0065	0.0013	651	0.846
Adit 4 u/s 1045	V	0.08	0.98	735	0.0013	0.8*1.2	0.104	16	0.0065	0.0013	751	0.976

5.2.3 Convergence measurement records

Tunnel convergence was measured by using tape extensometer at more than fifty tunnel sections covering the entire tunnels. However, other necessary data are available only for twenty six tunnel sections. These twenty six sections also include sections with significant squeezing phenomena. The convergence measurement records include date of record, convergence measurement up to tenth of millimetre and graphical presentation of the records. The measured tunnel convergences are given in Table 5.1b.

5.3 Squeezing analysis

5.3.1 Squeezing prediction criteria

Two out of the six approaches, have a provision for squeezing prediction criteria. Those criteria and the formulae are given below:

1) Singh et al. (1992) criteria based on Q value.

According to this criteria, squeezing occurs when overburden depth $H > 350\ Q^{1/3}$.

2) Goel (1994) criteria based on N value.

According to this criteria, squeezing occurs when overburden depth $H > 275\ N^{0.33}\ B^{-0.1}$ where, B is tunnel width in metre.

All the twenty six tunnel sections are evaluated by using the above mentioned two criteria. The calculated 'maximum permissible overburden depth' for non-squeezing condition and the existing overburden depths are given in the Table 5.3.

Table 5.3 Permissible overburden depths according to the two criteria and the existing overburden depths.

Location Chainage (m)	Tunnel width (m)	Rock type	Average Q value	N (Goel' 94)	Overbur-den limit for Singh'92 (m)	Overb-urden limit for Goel'94 (m)	Overburd-en at squeezing sections (m)	Overburd-en at non-squeezing sections (m)	Measured converg-ence (mm)
Adit1 d/s 515	4.2	Sheared SCS	0.0045	0.05	58	86	100		110.0
Adit 4 u/s 1013	4.0	sheared CTS with multiple SP	0.006	0.06	64	95	112		47.7
Adit1 d/s 580	4.3	Sheared TCS	0.008	0.08	70	103	111		32.3
Adit 4 u/s 974	4.0	sheared AG	0.008	0.08	70	104		112	7.9
Adit 4 u/s 1045	4.0	Sheared AG with clay fill	0.008	0.08	70	104		112	4.0
Adit 3 d/s 220	4.0	S	0.009	0.09	73	108	140		32.0
Adit1 d/s 500	4.2	sheared SCS	0.01	0.1	75	111	100		160.0
Adit 2 d/s 601	4.0	STS	0.013	0.13	82	122		138	7.5
Adit 2 u/s 1283	4.4	AG/SCS	0.04	0.1	120	111		212	1.0
Adit 3 u/s 345	5.0	AG & SS	0.05	0.25	129	148		300	9.0
Adit1 d/s 665	4.0	AG / S	0.06	0.3	137	161		112	11.8
Adit 2 u/s 1730	4.0	AG/ AG with clay gauge	0.065	0.33	141	165		95	11.6
Adit 4 u/s 550	4.0	CSS	0.07	0.7	144	213		218	5.5
Adit1 d/s 475	4.0	AG/STS	0.08	0.2	151	141	98		30.9
Adit 3 u/s 235	5.0	G	0.09	0.45	157	180	284		62.0
Adit 3 u/s 340	5.0	AG & SS	0.09	0.23	157	143		300	14.0
Adit 2 u/s 1357	4.0	BG / CS	0.095	0.48	160	187		261	6.1
Adit 2 d/s 895	4.0	G & CS	0.14	1.05	182	243		198	11.5
Adit 4 u/s 503	4.0	GG & STS	0.14	0.7	182	213		225	9.7
Adit 3 u/s 15	5.0	2 m shear band of AG & S	0.2	1	205	234		130	17.0
Adit 3 u/s 59	4.1	AG /S	0.23	0.58	214	199		158	13.2
Adit 3 u/s 200	5.0	AG	0.25	1.25	220	252	276		38.7
Adit 3 u/s 210	5.0	AG	0.28	1.4	229	262		276	18.2
Adit 2 d/s 441	4.0	AG	0.3	0.75	234	218		126	1.3
Adit 4 u/s 852	4.0	BG	0.47	1.18	272	252		114	1.0
Adit 4 u/s 876	4.0	BG with shear planes	0.6	1.5	295	274		114	9.7

Figure 5.3 has been plotted to assess the validity of these two criteria in Khimti tunnels. Singh et al. criterion defines eight sections as non-squeezing (convergence <20mm); and in reality seven sections did not squeeze and squeezing took place only in one section. Similarly, Goel criterion defines ten non-squeezing sections, out of them, only two sections squeezed. Thus both the criteria are found to be valid and similar to define non-squeezing sections.

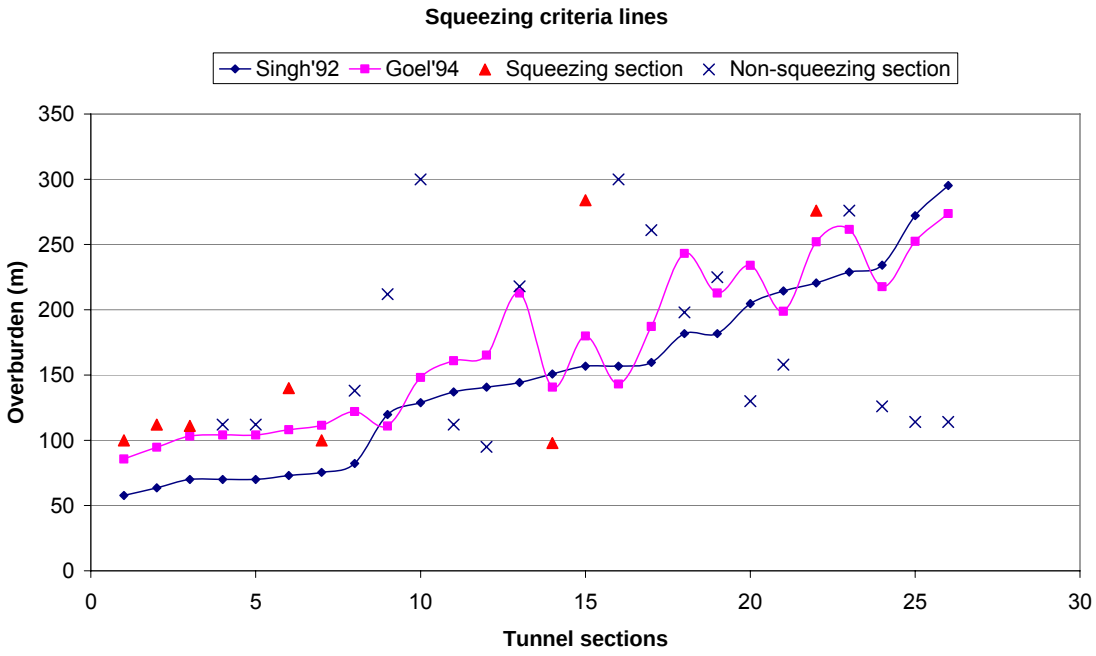

Figure 5.3 Squeezing prediction using two squeezing criteria.

According to Singh et al. criterion, eighteen sections to be squeezed (convergence >20mm) but squeezing took place only in seven sections and no squeezing in eleven sections. Similarly, according to Goel criterion, sixteen sections were supposed to squeeze, but squeezing took place only in six sections and no squeezing in ten sections. Thus, both the criteria are found to be conservative to define squeezing sections. However, it should be noted here, that tunnel convergence was measured after the tunnel support was provided, hence there is contribution of the tunnel support to minimise the convergence. Some of the non-squeezed tunnel sections could have squeezed if those sections had not been supported. Thus both the criteria may not be as conservative as they seem to be.

5.3.2 The Squeezing pressures

All the six approaches have provision for calculating squeezing pressure. Field data have been used in Grimstad and Barton (1993) and; Goel (1994) approaches to estimate squeezing pressures. Similarly, the available field data were used to estimate GSI values

for generating further data so that, squeezing pressures can be estimated also by using Hoek and Marinos (2000), Mohr-Coulomb criterion, Duncan-Fama (1993) and; Carranza-Torrres and Fairhurst (2000) approaches.

In Grimstad and Barton (1993) approach, squeezing pressure 'P' (in kg/cm^2) is estimated using the following equation:

$$P = \frac{2J_n^{1/2}Q^{-1/3}}{3J_r}$$

Where, J_n and J_r are the joint set number and the joint roughness number respectively in Q method.

The equations used in the other five methods are given in chapter 7. Above mentioned six approaches are used to calculate pressure that causes squeezing in the twenty six sections and given in Table 5.4. This pressure is the required support pressure for the given sections. The maximum support pressure provided by the combined support system at each section (from Table 5.2), is compared with the squeezing pressures estimated by the six different methods (Table 5.4).

Table 5.4 Squeezing pressures estimated by the six different approaches and the provided support pressures.

	Estimated required support pressures by different approaches (MPa)						Provided support pressure (MPa)	Measured converg-ence (mm)
Location Chainage (m)	Goel'92	Grimstad & Barton'93	Hoek & Marinos	Mohr-Coulomb	Duncan-Fama	CTorres and Fairhurst		
Adit1 d/s 475	0.27	0.45	1.50	1.07	0.81	0.71	1.21	30.9
Adit1 d/s 500	0.48	1.04	1.65	2.21	1.48	1.36	1.21	160.2
Adit1 d/s 515	1.07	2.41	1.70	2.49	1.62	1.47	2.33	110.0
Adit1 d/s 580	0.71	1.15	1.90	2.41	1.62	1.53	2.32	32.3
Adit1 d/s 665	0.24	0.71	0.00	-0.16	-0.12	0.35	0.64	11.8
Adit 2 d/s 441	0.16	0.49	0.00	-1.54	-1.24	0.17	0.65	1.3
Adit 2 d/s 601	0.64	1.10	2.30	3.04	2.06	2.01	2.32	7.5
Adit 2 d/s 895	0.21	0.28	2.00	0.69	0.55	0.71	1.21	11.5
Adit 2 u/s 1283	2.22	1.01	3.50	4.43	3.01	2.81	1.21	1.0
Adit 2 u/s 1357	0.56	0.43	3.50	1.92	1.51	1.38	1.21	6.1
Adit 2 u/s 1730	0.19	0.49	1.00	0.19	0.15	0.33	0.00	11.6
Adit 3 u/s 15	0.15	0.27	0.00	-0.42	-0.33	0.30	1.22	17.0
Adit 3 u/s 59	0.24	0.35	1.00	0.17	0.14	0.51	0.85	13.2
Adit 3 u/s 200	0.29	0.32	2.70	1.07	0.86	1.02	1.22	38.7
Adit 3 u/s 210	0.27	0.28	3.00	1.31	1.06	1.10	0.85	18.2
Adit 3 d/s 220	0.96	0.96	2.50	3.10	2.13	2.31	1.86	32.0
Adit 3 u/s 235	0.73	0.52	3.50	1.51	1.19	1.23	0.85	62.0
Adit 3 u/s 340	1.84	0.45	4.30	2.95	2.25	1.97	1.86	14.0
Adit 3 u/s 345	1.60	0.70	4.70	3.67	2.82	2.63	1.86	9.0
Adit 4 u/s 503	0.32	0.33	3.40	2.29	1.80	1.66	0.96	9.7
Adit 4 u/s 550	0.31	0.40	3.40	3.63	2.58	2.43	0.84	5.5
Adit 4 u/s 852	0.12	0.19	0.00	-0.97	-0.78	0.19	0.78	1.0
Adit 4 u/s 876	0.11	0.18	0.00	-1.08	-0.87	0.17	1.22	9.7
Adit 4 u/s 974	0.71	1.49	1.90	1.81	1.34	1.38	2.33	7.9
Adit 4 u/s 1013	0.96	2.19	2.00	2.55	1.73	1.80	0.85	47.7
Adit 4 u/s 1045	0.71	1.49	1.80	1.58	1.17	1.03	0.98	4.0

The comparison given in the Table 5.4 is plotted in Figures 5.4a and 5.4b. The plotting has been done in two figures to make comparison visually convenient.

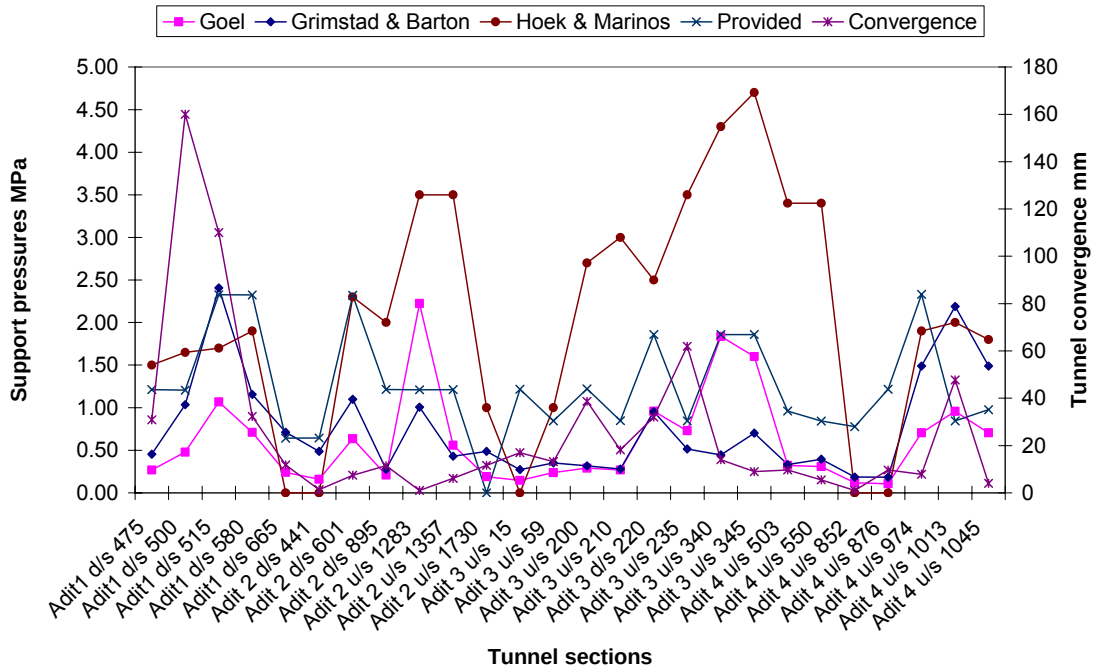

Figure 5.4a Comparison between the provided support pressures and estimated squeezing pressures calculated by two empirical and one semi-analytical methods.

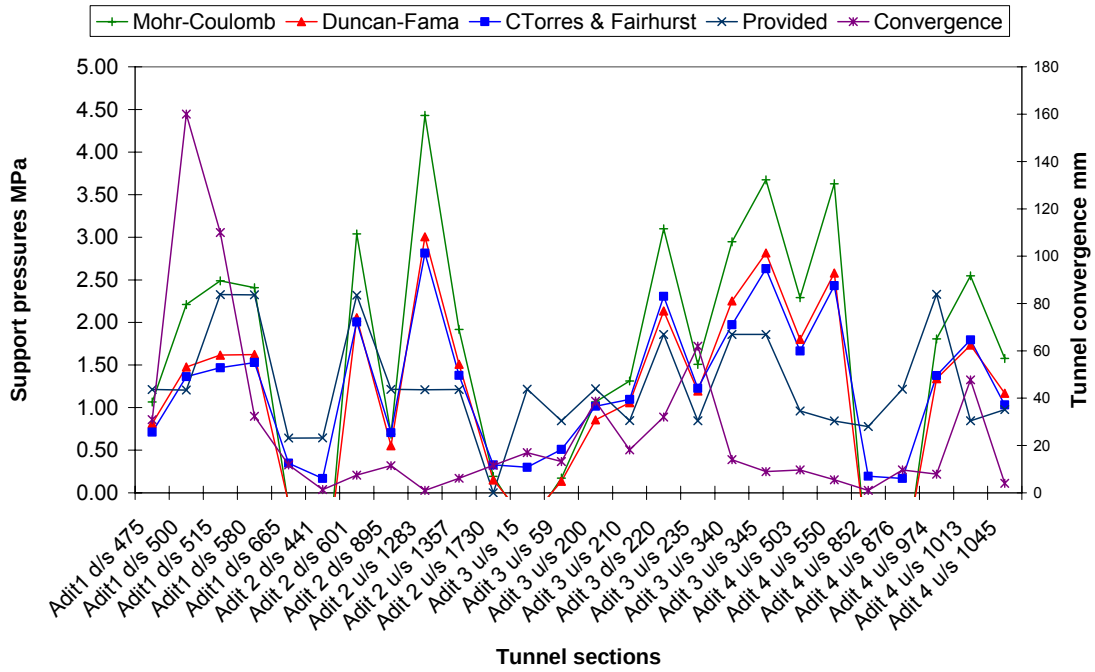

Figure 5.4b Comparison between the provided support pressures and the estimated squeezing pressures calculated by three analytical methods.

In the Khimti project, instrumentation was not carried out to measure the squeezing pressure. So there has been absence of the measured value of squeezing pressure to compare with the estimated squeezing pressures. Therefore the validity of the squeezing pressures estimated by the various approaches, is assessed on the basis of the measured convergences.

In ideal condition, there might be squeezing where the provided support is less than the estimated requirement. Similarly, there should not be significant squeezing where the provided support is more than the estimated requirement. Number of sections where estimated squeezing pressures are valid, is given for each approach in Table 5.5.

Table 5.5 Number of sections where estimated squeezing pressures are valid.

Approaches	Goel (1994)	Grimstad & Barton (1993)	Hoek & Marinos (2000)	Mohr-Coulomb	Duncan Fama (1993)	CTorres & Fairhurst (2000)
Number of sections where estimated squeezing pressures are valid.	16	15	7	14	13	13

None of the approaches has given valid squeezing pressures for all the twenty six sections. Among the six approaches, Goel approach has given the highest number of sections and; Hoek & Marinos approach has given the lowest number of sections where the estimated squeezing pressures are valid. Three out of the rest four approaches, are analytical. One of the analytical approaches uses the Mohr-Coulomb criterion. It has given one more section than that given by the other two approaches, where the estimated squeezing pressure is valid. However, this approach is conservative for many sections (Figure 5.4b). The curve given by the Carranza-Torres & Fairhurst approach is smoother than that given by the Duncan-Fama approach.

5.3.3 The convergence caused by the squeezing

Only three out of the six approaches, namely, Hoek and Marinos (2000), Duncan-Fama (1993) and; Carranza-Torrres and Fairhurst (2000) approaches have provision for calculating the convergences in the supported tunnel condition. Those calculated tunnel convergences for the twenty six sections are given in Table 5.6.

In the Khimti project tunnel, the convergences were measured by using tape extensometer. Thus the validity of the tunnel convergence calculated by the three approaches has been assessed by comparing with the measured tunnel convergences.

Table 5.6 Measured and the calculated tunnel convergence by the three different approaches.

	Estimated convergences by using different approaches (mm)						Measured
Location Chainage (m)	Hoek & Marinos		Duncan-Fama		CTorres and Fairhurst		Converge-nce (mm)
	w/o supt	with supt	w/o supt	with supt	w/o supt	with supt	
Adit1 d/s 475	47.7	7.0	18.4	7.0	22.1	7.3	30.9
Adit1 d/s 500	330.1	18.0	107.7	11.2	108.5	10.7	160.2
Adit1 d/s 515	591.5	-0.7	292.7	7.6	226.9	8.6	110.0
Adit1 d/s 580	361.8	-0.1	110.0	6.2	115.2	6.5	32.3
Adit1 d/s 665	4.1	3.5	6.3	5.5	7.4	5.1	11.8
Adit 2 d/s 441	1.0	1.2	3.4	3.3	3.1	2.6	1.3
Adit 2 d/s 601	494.3	3.9	153.9	8.0	156.2	8.0	7.5
Adit 2 d/s 895	6.8	5.0	5.2	4.0	6.1	4.0	11.5
Adit 2 u/s 1283	286.9	83.1	113.2	32.9	121.1	27.8	1.0
Adit 2 u/s 1357	18.4	11.9	11.8	8.2	14.2	8.2	6.1
Adit 2 u/s 1730	6.1	6.1	5.3	5.3	6.4	6.4	11.6
Adit 3 u/s 15	3.2	2.9	4.9	4.3	5.3	3.9	17.0
Adit 3 u/s 59	5.2	4.3	6.4	5.4	7.6	5.2	13.2
Adit 3 u/s 200	9.7	7.7	8.9	7.2	10.5	7.1	38.7
Adit 3 u/s 210	11.9	9.9	9.2	7.6	10.8	7.7	18.2
Adit 3 d/s 220	1770.5	23.4	616.5	20.0	642.8	21.2	32.0
Adit 3 u/s 235	14.3	11.7	12.7	10.5	15.3	10.5	62.0
Adit 3 u/s 340	42.7	19.8	32.0	18.1	39.1	18.0	14.0
Adit 3 u/s 345	123.3	42.2	57.0	24.0	65.3	23.3	9.0
Adit 4 u/s 503	55.5	30.1	19.3	11.1	22.1	10.8	9.7
Adit 4 u/s 550	90.2	47.7	26.3	13.2	29.7	12.0	5.5
Adit 4 u/s 852	1.4	1.6	3.3	3.1	3.2	2.6	1.0
Adit 4 u/s 876	1.2	1.5	2.8	2.6	2.6	2.2	9.7
Adit 4 u/s 974	415.7	0.0	134.6	13.5	141.7	12.3	7.9
Adit 4 u/s 1013	1453.4	150.9	549.3	48.5	510.2	46.8	47.7
Adit 4 u/s 1045	103.9	21.5	50.1	15.9	55.7	15.6	4.0

The comparison given in Table 5.6 is plotted in Figures 5.5. Tunnel convergences calculated by using the Duncan-Fama and; Carranza-Torrres and Fairhurst approaches, are almost the same. Fourteen out of the twenty six values, are very close (with difference less than 10 mm) to the convergences measured in the tunnel. Convergences calculated by the Carranza-Torrres and Fairhurst approach have been found to be closer to the measured values than those from the Duncan-Fama approach. Hoek and Marinos approach has given larger convergences than the other two methods. Twelve out of the twenty six values calculated by this method, are very close (with difference less than 10 mm) to the convergences measured in the tunnel.

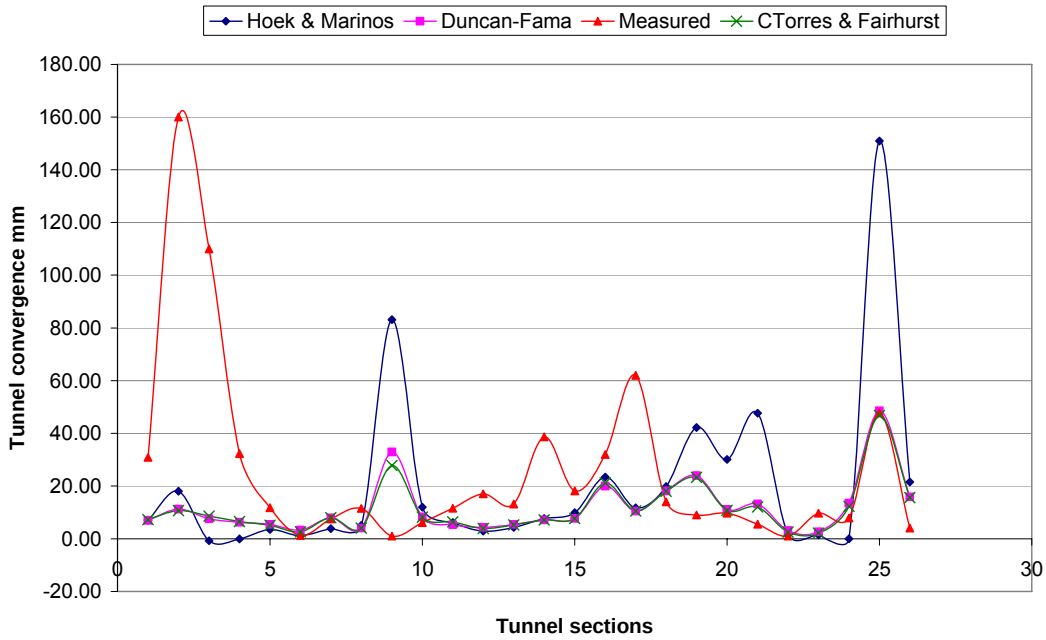

Figure 5.5 Comparison between measured and the calculated tunnel convergences by using three different approaches.

5.4 Discussions on squeezing analyses

5.4.1 Squeezing prediction criteria

Singh et al. (1992) and Goel (1994) squeezing prediction criteria have been used to estimate maximum overburden for which squeezing will not take place. Both the criteria have been found to be valid and similar to define non-squeezing sections. However, both the criteria have been found to be slightly conservative to define squeezing sections. As the Goel's approach does not need parameter SRF, it avoids the ambiguity which may arise in the evaluation of the SRF. Thus Goel's approach can be used as a quick check for squeezing possibility.

The two empirical criteria mentioned above are based on the cases including those from the Himalayan region. The Khimti project area is also located in the Himalayan region. This might be one of the reasons for these criteria to be valid for many of the 26 tunnel sections. However, it is to be noted that only vertical overburden (above the tunnel section) is considered in both the criteria. Topographical effect of valley side is not included. In case of the tunnel with steep valley side (as in Figure 2.10 in Chapter 2), stress level might be much higher than induced by the vertical overburden depth alone. In such cases, the above mentioned equations for the limiting overburden height needs to be modified to consider the topographical effect of the valley side.

5.4.2 Estimation of squeezing pressure

Among the six approaches, Goel approach has given the highest and the Hoek & Marinos approach has given the lowest number of sections where the estimated squeezing pressures are valid. Out of the remaining four approaches, three are analytical, namely, Mohr-Coulomb, Duncan-Fama; and Carranza-Torres & Fairhurst approaches. The validity of the squeezing pressures estimated using these three analytical approaches are similar (Table 5.5). The curve given by the Carranza-Torres & Fairhurst approach is smoother than those given by the other two approaches. On the basis of the discussion given above and in section 5.2.2, Goel approach and Carranza-Torres & Fairhurst approaches can be used if only few approaches are to be used.

The curves given by the two empirical and the one semi-analytical approaches (Figure 5.4a) are different from each other. It might be because of the different input parameters used in the analyses. Hoek and Marinos approach uses σ_{ci} which has been roughly estimated. The curves given by the three analytical approaches are similar in nature. It might be because the same input parameters are used in the analyses.

5.4.3 Convergence caused by squeezing

Hoek and Marinos (2000), Duncan-Fama (1993); and Carranza-Torrres and Fairhurst (2000) approaches have been used here to calculate a convergence for the supported tunnel sections. Hoek and Marinos approach has given larger tunnel convergences than the other two approaches. Convergences from the Carranza-Torrres and Fairhurst approach have been found to be closer to the measured values than those from the Duncan-Fama approach.

The equations in the Hoek & Marinos approach have been developed on the basis of the cases more in siltstone flysch rock mass from Greece (Hoek & Marinos, 2000). These equations have given higher values for the squeezing pressures and the convergences than those measured in the Khimti project. One of the reasons may be that the rock type (weak schist and gneiss) in Khimti is mechanically rather different from that in Greece.

5.4.4 Some remarks on the tunnel squeezing in Khimti

- It has been observed that squeezing is larger in the weaker rock type such as schist than that in gneiss though they have similar Q-values. For examples, tunnel sections at Adit4 u/s 974 m, 1013 m and 1045 m have Q values 0.008, 0.006 and 0.008 respectively. The section at Adit4 u/s 1013 m consists of sheared schist whereas other two sections consist of sheared gneiss. Convergences measured in those tunnel sections are 7.9, 47.7 and 4.0 mm respectively (Tables 5.1a and 5.1b). Rock type difference is not considered in the Q-system.

- In the ninth section (Adit 2 –upstream Chainage 1283 m) in Figure 5.5, the measured convergence trend is opposite to the estimated one. It may be because of augen gneiss present in the crown and upper part of the wall and; weak sericite chlorite schist in the lower part of the wall. For the analysis purpose, the parameters for the weaker rock mass have been used, hence giving higher pressure and convergence values than the measured ones.
- The tunnel sections at Adit1 d/s 500 m, 515 m, 580 m, and; at Adit4 u/s 974 m, 1013 m and 1045 m have similar Q-values and situated on the valley side of topography under the similar vertical overburden. However, these two groups have different maximum topographical overburden heights. The former group has 1100 m and the latter has about 270 m. The convergence range for the sections with the higher overburden is 32-160 mm and that for the sections with the lower overburden is in 4-47 mm (Table 5.7). This difference in the tunnel convergence might have been caused by the difference in the maximum topographical heights.

Table 5.7 The valley-side effect of topography on the Khimti tunnel convergence at six tunnel sections.

Location Chainage m	Q-value	Vertical overburden m	Total topographical overburden m	Tunnel convergence mm
Adit1 d/s 500	0.01	100	1100	160.2
Adit1 d/s 515	0.0045	100	1100	110.0
Adit1 d/s 580	0.008	111	1100	32.3
Adit4 u/s 974	0.008	112	270	7.9
Adit4 u/s 1013	0.006	112	270	47.7
Adit4 u/s 1045	0.008	112	270	4.0

These observations are plotted in Figure 5.6. using two out of the six above mentioned topographical sections. In Table 5.7, the convergences at the sections Adit1 d/s 580 m and Adit4 u/s 1013 m are not compatible in the respective groups. Relatively low tunnel convergence at the section Adit1 d/s 580 m might have been caused by the absence of the shear plane at that section whereas all the other five sections are crossed by the shear planes. The section at Adit4 u/s 1013 m is crossed by the multiple shear planes with clay filling up to 25 cm thick. It might have caused the relatively higher tunnel convergence at Adit4 u/s 1013 m.

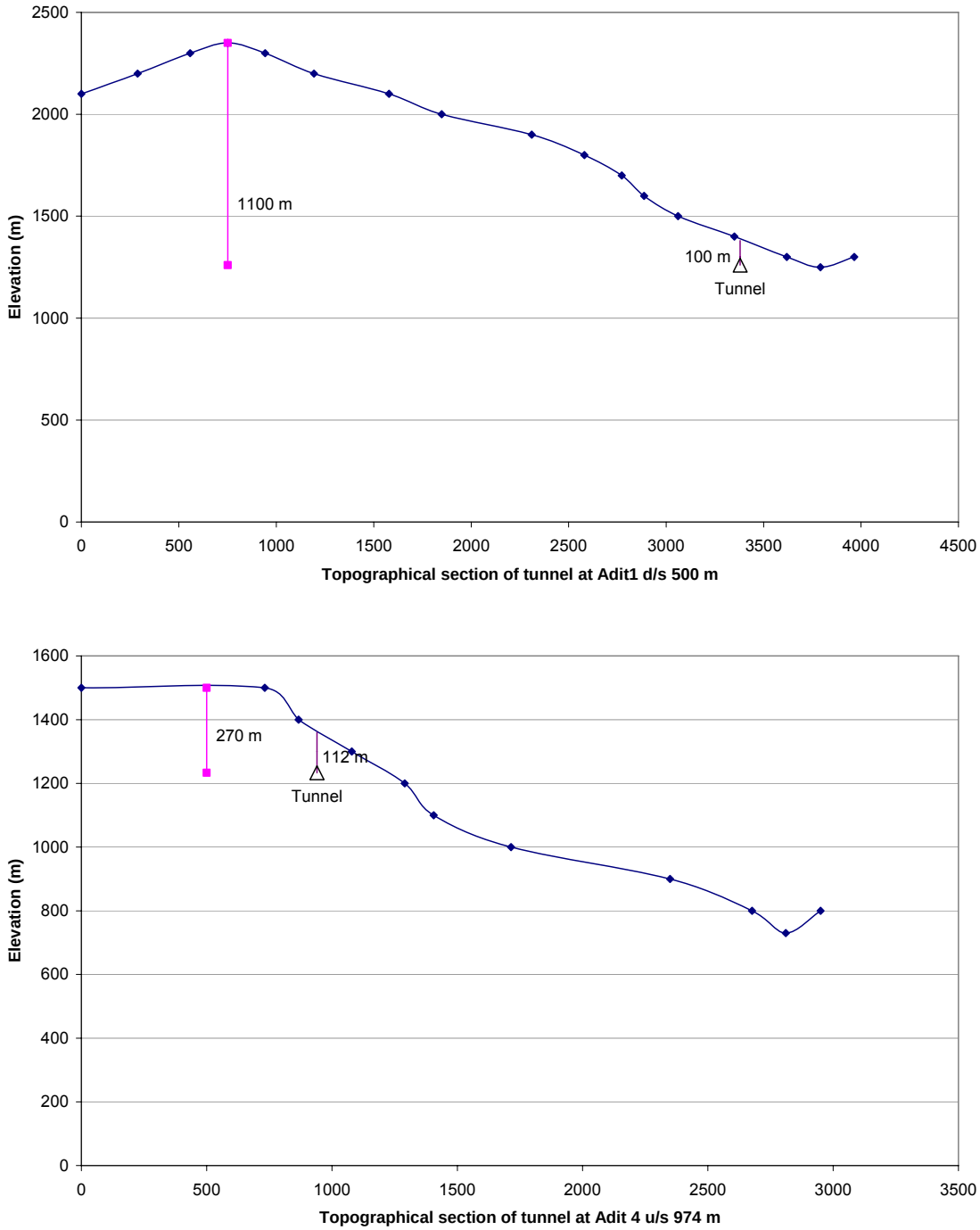

Figure 5.6 The valley-side effect of topography on the Khimti tunnel convergence at Adit 1 d/s 500 m (above) and Adit 4 u/s 974 m (below) respectively.

- In Figure 5.3, according to the Goel's squeezing criteria, ten tunnel sections fall under the criterion line showing that squeezing would not occur in those sections. It was so for eight sections only and significant squeezing took place at the rest two sections, namely, Adit1 d/s 475 m and 500 m. In both the sections,

the maximum topographical overburden heights are much larger than the vertical overburden. The squeezing criteria (Section 5.2.1) might have not considered the valley-side effect of topography though it has considered the vertical overburden above the tunnel level. Figure 5.7 shows that the higher the total overburden (1100 m) the larger the tunnel convergence (160 mm) is and the lower the total overburden (270 m) the smaller the tunnel convergence (7.9 mm) is. These observations given in Figure 5.6, are combined and compared in Figure 5.7.

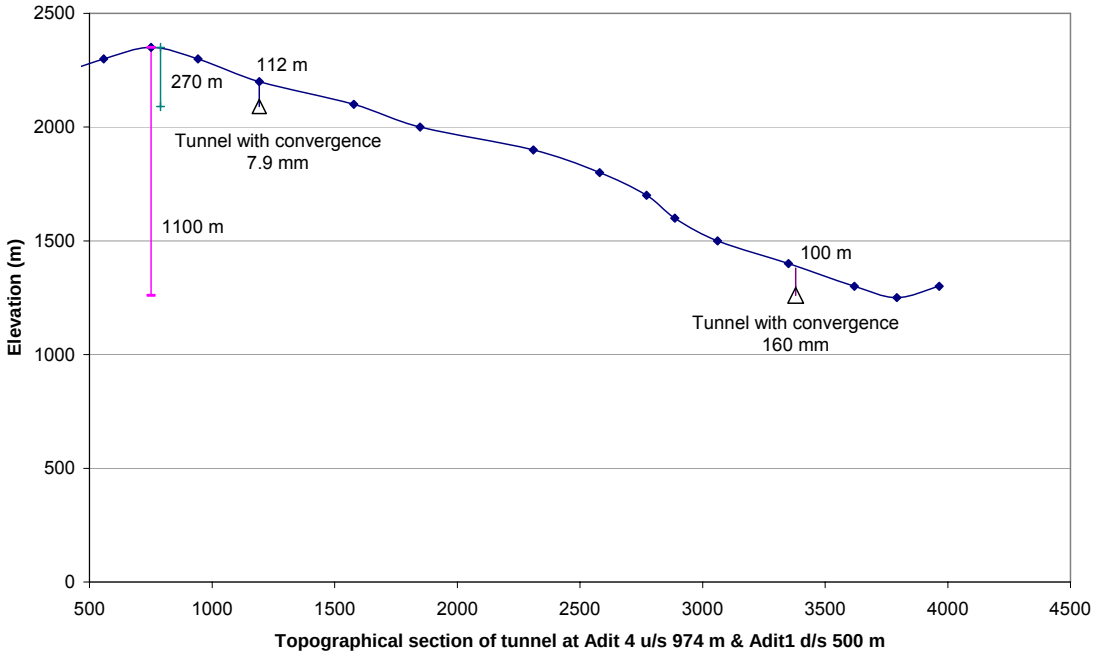

Figure 5.7 Influence of the valley-side effect of topography on the convergence at Adit 4 u/s 974 m and Adit 1 d/s 500 m respectively (shown in the same figure).

The valley-side effect of topography has been assessed by using a simple numerical model in Phase2 code. The input data used and the results obtained are given in the Table 5.8.

Table 5.8 The major principal stress(σ_1) at two locations with same vertical overburden (100 m) but different maximum topographical height; Results of the Phase2 analysis for the valley-side effect of topography.
(Input data: Cohesion=0.3 MPa, Friction angle=20^o, E modulus=1000 MPa and unit weight=0.027 MN/m^3.)

σ_h/σ_v	σ_1 at location with 240 m topographical height (MPa)	σ_1 at location with 1150 m topographical height (MPa)
0.5	3.4	15.6
1.0	2.9	36.5
1.5	2.6	57.4

The graphical results of the Phase2 analyses are given in the Figure 5.8.

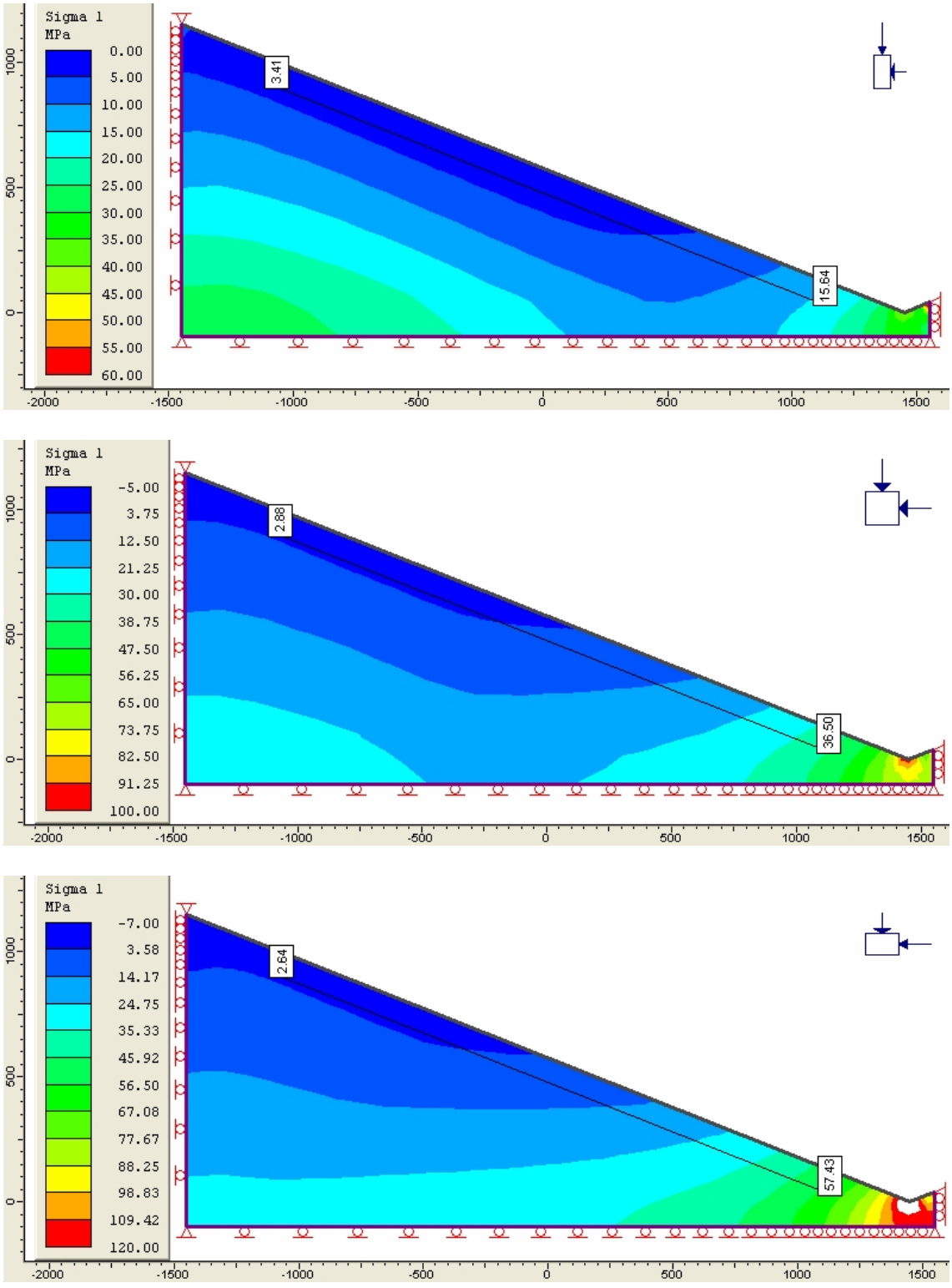

Figure 5.8 The major principal stresses for the two locations with the different maximum topographical overburden with σ_h/σ_v ratio 0.5, 1.0 and 1.5 respectively.

6 Laboratory tests on Melamchi samples

As a part of site investigation, six bore holes were drilled along the alignment of the Melamchi diversion tunnel (EDCO, 2001). Five drill holes were drilled to the depth of 150 m and one drill hole (TDH 4) was drilled to the depth of 200m. Because of the high overburden, the drill holes do not reach the tunnel level. To represent rock mass and potential problems, weak rock type with low strength is to be chosen. Jointed and weak rock usually does not yield good Rock Quality Designation (RQD). However, high RQD is needed for obtaining cores, so that they are long enough to carry out the laboratory tests. So during the sample selection process, the following criteria were followed:

- Weak rock type: Project area consists of migmatite, granitic gneiss, gneiss and schist. Attention has been given to select the samples from the weaker rock type such as schist or weak gneiss.
- Rock core with low compressive strength: Summary of the laboratory tests results (EDCO, 2001) was studied to identify the rock mass with the lower Uniaxial compressive strength (UCS).
- Rock core with high RQD: High RQD was needed for obtaining long enough samples to carry out the laboratory tests.

Considering the above mentioned factors, rock cores from the two bore holes TDH 1 and TDH 2 were found to be relatively suitable for the creep test. Brief description of the rock cores from these two bore holes are as follow:

TDH 1: Augen (few mm to few cm size) gneiss, dark grey, coarse grain, fresh, hard and crystalline. Muscovite and biotite are present. Occasional white quartzite vein is also present.

TDH 2: Gneiss, light brownish grey, medium grain, fresh, strong, hard and crystalline. Muscovite and biotite are present. Quartzite layer (few mm to one cm thick) rarely present.

Total 12 pieces of cores were collected from the 2 bore holes; 4 from the TDH 1 and 8 from the TDH 2 in summer 2003. The 12 pieces rock cores were placed in PVC pipes and transported to NTNU. Brief description of the collected rock cores are given in the following table:

Table 6.1 Core sample description.

Bore hole	Core box no	Depth (m)	Length (mm)	Dia (mm)	Usable core length (mm)	Core broken during transport
TDH 1	10	36,2	115	62	110	1 piece
TDH 1	10	36,4	410	62	125, 55, 165	3 pieces
TDH 1	10	37,0	230	62	75, 60, 55	3 pieces
TDH 1	10	37,25	360	62	160, 45, 100	3 pieces
TDH 2	11	49,3	250	47.4	75, 160	2 pieces
TDH 2	11	49,8	180	47.4	100, 40	2 pieces
TDH 2	17	82,3	180	47.4	110, 35	2 pieces
TDH 2	17	83,5	120	47.4	115	1 piece
TDH 2	18	84,4	290	47.4	65, 125, 60	3 pieces
TDH 2	18	84,8	140	47.4	130	1 piece
TDH 2	18	86,3	90	47.4	85	1 piece
TDH 2	18	87,1	80	47.4	55	1 piece

Some more samples were collected and brought to NTNU in summer 2004 too. This time samples were first individually wrapped by cushion plastic and placed with polystyrene cushion materials in a box. There was not much breakage this time.

a) Specimen preparation

Laboratory tests were to be carried out for creep, mechanical properties and complete stress-strain curve. Acceptable range of length and diameter for test specimen are given in the following table:

Table 6.2 Acceptable specimen length, diameter and their ratio.

S No	Test	Specimen Length mm	Specimen dia mm	L/D ratio
1	Creep	70 - 82	25-50	-
2	E,ν and UCS	Ideally 2.5-3 d	32-62	2.5-3
3	Complete Stress-Strain curve	Ideally 2.5-3 d	32-62	2.5-3

Creep test sets have limitation of 50 mm for maximum specimen diameter. So, 33 mm diameter specimens were cored out of all the sample cores of 62 mm diameter. Coring was carried out with 500 rpm speed. Only the longest core with 165 mm length broke into two pieces giving 90 mm and 65 mm long usable cores.

6.1 Creep test

Creep is the time-dependent strain or deformation under constant axial stress. The engineering stress (load divided by original cross-sectional area) will therefore be constant, while the true stress (load divided by actual cross-sectional area at the time) will decrease somewhat during the test as the cross-sectional area increases. Standard practice in creep testing is to maintain constant load (constant engineering stress) because of the experimental difficulties in controlling the load to maintain a constant true stress (ASTM, 1985).

This test was carried out according to ASTM D 4341 - 84 (1985). This test method covers the determination of the creep behaviour of intact cylindrical rock core specimens subjected to uniaxial compression. Load system and strain recording system are the main components of the laboratory equipment.

6.1.1 Set up for test

a) Load system

The loading device is specified to maintain constant axial load. A constant fluid pressure is created by a hanging weight acting on a hydraulic cylinder. This fluid pressure in turn acts on hydraulic cylinders mounted in connection with a balance-lever system as shown in Fig. 6.1. Thus a constant load is acting on the rock specimens. To insure axial pressure, the load is transferred to the specimen via steel balls.

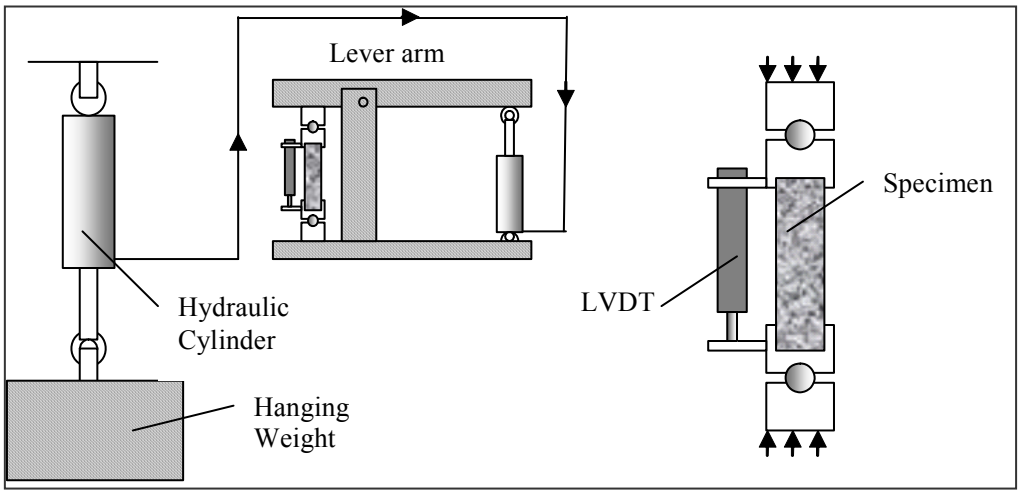

Figure 6.1 Principal sketch of load system and strain recording system.

In the hydraulic cylinders, pistons move very slowly during the test period. The pistons are provided with teflon seals to avoid variability of load acting on the specimens.

Load calibration was carried out to provide required stress to the sample. Load was calculated corresponding to the required stress for the given sample diameter. In order to apply required constant stress level, load cell was placed in the testing equipment. A 20 ton capacity load cell was used for this calibration. The load cell was connected to the computer through the data logger. Then the load was provided until the required load was reached.

b) Load application methods

The following two load application methods of conducting laboratory creep experiments are available (Malan, 1998):

- Specimens are loaded to a pre-determined, constant stress level. This stress level may, for instance, be the stress level expected around an underground excavation for a tunnel. The creep strain and the time to failure are monitored. If the material properties varies considerably, it may be difficult to determine the time to failure for the material when loaded to a particular stress or critical stress level (the stress below which failure will not occur). It may happen that a specimen loaded to a certain stress level fails after a few days while another loaded to the same stress level does not fail after a period of months.
- The same specimen is loaded to different stress levels by starting at a low value and increasing the stress in steps, allowing a certain time interval for creep. The obvious advantage of this approach is that the creep strain may be monitored for an 'identical' material at different stress levels and that each specimen will be tested to failure within a reasonable time. The total test duration is determined by the choice of the stress level of the first creep stage, the duration of each creep stage and the magnitude of subsequent stress level increases.

The creep test set which has been used, does not have mechanism to control the loading rate, so, the constant load application method has been used in the present study.

c) Strain recording system

Linear Variable Differential Transformer (LVDT), a common type of transducer, was used to measure axial deformation of the rock specimen. The LVDT used, was W1T3 inductive displacement probe type (Figure 6.2) with the technical specification given in the Table 6.3.

Table 6.3 Technical specification of W1T3 inductive displacement probe.

Version	probe
Nominal displacement (mm)	± 1
Type of connection	half bridge
Sensitivity (mV/V)	± 80
Linearity deviation in %	± 0.2
Carrier frequency (kHz)	4.8
Nominal temperature range (^{o}C)	-20 to +80

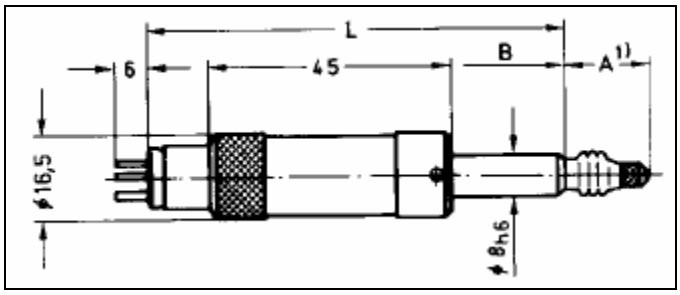

Figure 6.2 LVDT W1T3 deformation recorder, where, L = 78.5 mm, A[1)] (probe in mid position) = 16 mm, B = 20 to 24 mm.

d) Test room

The strain recording system is very sensitive to temperature changes. It is therefore of basic importance that the air temperature is kept constant during the test. The test room of the laboratory is situated in the basement and is well insulated from the surroundings with mineral wool. It is not supplied with artificial air condition. During test periods the air temperature has been constant at 20°C (± 0.5 °C) with humidity 65 to 70%.

6.1.2 Creep test results

Creep tests were carried out on the intact rock samples for Melamchi augen gneiss from TDH1 drill holes of Melamchi project. Following table summarises the results of the creep tests carried out on the samples of 33 mm diameter (Table 6.4). All the samples except sample 1, were saturated by placing in water for 48 hours. Sample 1 was in air-dry condition.

Table 6.4 Results of creep test on the 33 mm diameter rock cores of Melamchi augen gneiss.

Sample No	Length (mm)	Stress applied (MPa)	Time taken to failure	Deformation (mm)	Axial Strain (%)
2-4	82	27	25 seconds	0.0674 (-1.1545 to -1.0871)	0.082
4-2	81	25	1 hour	0.5028 (-1.2349 to -0.7321)	0.62
4-4	83	24	1hour 10 minutes	0.0306 (-1.4457 to -1.4151)	0.038
1	81	25 (already used in cyclic loading)	1 minute	0.184 (-1.432 to -1.248)	0.23
412	79	20	12 hours	0.5068 (-0.5127 to -0.0059)	0.64
41	79	19.2 (Load applied at once.)	7 seconds	0.5601 (-1.2031 to -0.643)	0.709 at failure
42	82.2	22	4 minutes	0.2075 (-1.2756 to -1.0681)	0.25
43	82	15 - 16	Did not break	0.1021 (-1.2581to -1.156)	0.12
45	82	15 - 16	Did not break	0.2323 (-1.122 to -0.8897)	0.28
410	79.5	20.5 (already used in progressive creep)	3 minutes	0.106 (-1.2103 to -1.1043)	0.133

6.1.3 Processing the creep test results

a) Critical stress level for creep failure

Sample 412 failed in 12 hours after it was subjected to the constant stress level of 20 MPa. It is the lowest stress level that caused the creep failure. Average UCS of these samples was 39 MPa. According to the test results, samples subjected to 50% or higher of uniaxial compressive strength (UCS) of intact rock samples failed by the creep. Thus the critical stress level for creep failure for this rock is 20 MPa.

b) Determining visco-elastic constants for time-dependent deformation

Burgers visco-elastic creep model is selected to represent the creep behaviour based on the laboratory test results of weak rock mass (Yu *et al., 2000)*.

The simplest procedure for evaluating visco-elastic constants is through unconfined compression of cylindrical rock specimens over prolonged periods (Goodman, 1989). This requires constant stress and constant temperature and humidity over the whole test duration, which may be hours, weeks, or longer. Load may be applied by dead weights acting through levers bearing directly on the specimen or through an oil pressure. Servo-controlled hydraulic pressure systems and compressed springs are also used.

The axial strain with time $\varepsilon_1(t)$ in a Burgers body subjected to constant axial stress σ_1, is

$$\varepsilon_1(t) = \frac{2\sigma_1}{9K} + \frac{\sigma_1}{3G_2} + \frac{\sigma_1}{3G_1} + \frac{\sigma_1}{3G_1} e^{-(G_1 t/\eta_1)} + \frac{\sigma_1}{3\eta_2} \qquad (6\text{-}1)$$

Where $K = E/[3(1-2v)]$ is the bulk modulus, assumed to be independent of time and η_1, η_2, G_1 and G_2 are properties of the rock to be evaluated as follows.

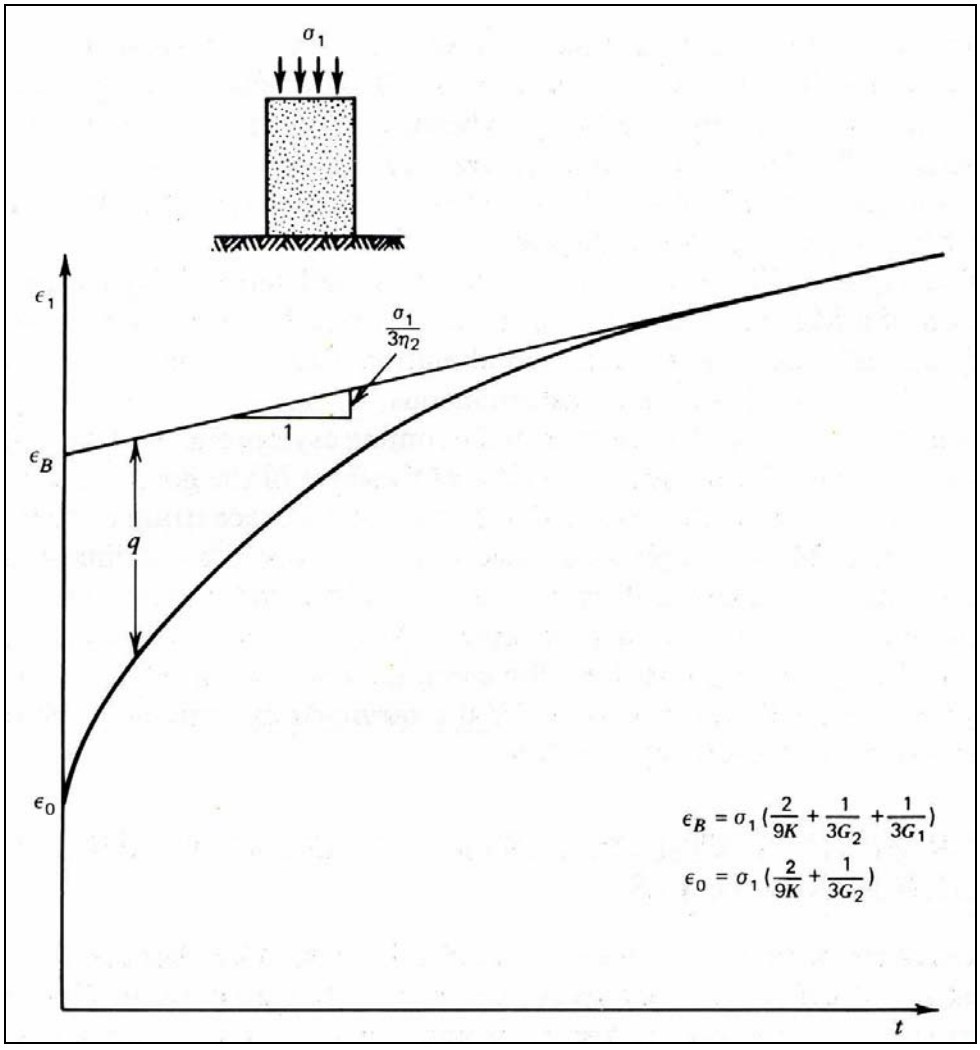

Figure 6.3 Creep in uniaxial compression of a rock that behaves as a Burgers body under deviatoric stress.

Figure 6.3 is a graph of ε_1 versus t corresponding equation (6-1). At $t = 0$, there is an intercept $\varepsilon_0 = \sigma_1 (2/9K + 1/3G_2)$ while strain at large t falls along the line with intercept $\varepsilon_B = \sigma_1 (2/9K + 1/3G_2+1/3G_1)$ and slope $\sigma_1/3\eta_2$. Value of the slope $\sigma_1/3\eta_2$ is obtained by using trend of the assymtote line. Load cannot be applied instantaneously and it may be preferable in practice to find the intercept ε_0 by regression. Let q equal the positive distance between the creep curve and the line asymptotic to the secondary creep curve (Figure 6.3) giving

$$q = \frac{\sigma_1}{3G_1} e^{-\frac{G_1 t}{\eta_1}} \tag{6-2}$$

Then

$$\log_{10} q = \log_{10}\left(\frac{\sigma_1}{3G_1}\right) - \frac{G_1 t}{2.3\eta_1} \tag{6-3}$$

A semilog plot $\log_{10} q$ versus t has intercept $\log_{10} (\sigma_1/3G_1)$ and slope $-G_1/2.3\ \eta_1$ determining $G_1$and η_1. In alternative, values of the constants $\sigma_1/3G_1$ and G_1/η_1 are obtained by using trend line of the q-curve.

If lateral strains ε_3 are monitored as well as axial strains ε_1, the volumetric strain is determined by $\Delta V/V = \varepsilon_1+2\ \varepsilon_3$ while the mean stress is $\sigma_1/3$. Therefore K can be calculated by

$$K = \frac{\sigma_1}{3(\varepsilon_1 + 2\varepsilon_3)} = \frac{E}{3(1-2\upsilon)} \tag{6-4}$$

and G_2 can be calculated from

$$\frac{\sigma_1}{3G_2} = \varepsilon_B - \sigma_1\left(\frac{1}{3G_1} + \frac{2}{9K}\right) \tag{6-5}$$

c) Effect of stress level on the secondary phase creep rate

For soft rocks the steady-state creep rate depends on the stress level (Lama and Vutukuri, 1978). It is also true for the creep of the hard rocks (Malan, 1998). The most widely used law for the steady-state creep of rock is (Dusseault and Fordham, 1993)

$$\dot{\varepsilon}_{ss} = A(\sigma_1 - \sigma_3)^n e^{-\frac{Q}{RT}} \tag{6-6}$$

Where $\dot{\varepsilon}_{ss}$ is the steady-state creep rate, A is a constant, σ_1 and σ_3 are the major and minor principal stresses respectively, R is the universal gas constant, T is the temperature in degrees Kelvin and Q is the creep activation energy. Q is different for the various creep mechanisms and should be calculated from creep tests at different temperatures. For dislocation creep, Q is the energy required by dislocations to overcome obstacles in their path.

For the experiments conducted at a constant temperature and under uniaxial conditions, the above mentioned equation can therefore be reduced to

$$\dot{\varepsilon}_{ss} = A'\sigma^n \qquad (6\text{-}7)$$

Where $A' = Ae^{-\frac{Q}{RT}}$ with units $Pa^{-n}\,s^{-1}$ and $\sigma = \sigma_1$ is the applied stress. The equation (6-7) can be arranged in log as follows.

$$\log \dot{\varepsilon}_{ss} = \log\left(A'\sigma^n\right) = \log A' + \log \sigma^n = \log A' + n \log \sigma \qquad (6\text{-}8)$$

The coefficient n can be determined from the slope of the curve of a log $\dot{\varepsilon}_{ss}$ versus log σ plot. The plot has intercept log A' determining A'.

Figure 6.4 illustrates the steady-state creep rates for the different rock specimens at three stress levels. Test results show that higher stress levels lead to higher creep rates (Table 6.5).

Table 6.5 Creep test data for calculating effect of stress level on the creep rates.

Sample	Stress (Pa)	Steady-state creep rates
45	1.5 E+07	1.7 E-06
412	2.0 E+07	40 E-06
4-2	2.5 E+07	800 E-06

Using the test results given in the Table 6.5, values for A' and n have been determined according to the method mentioned above and details are given in chapter 7.

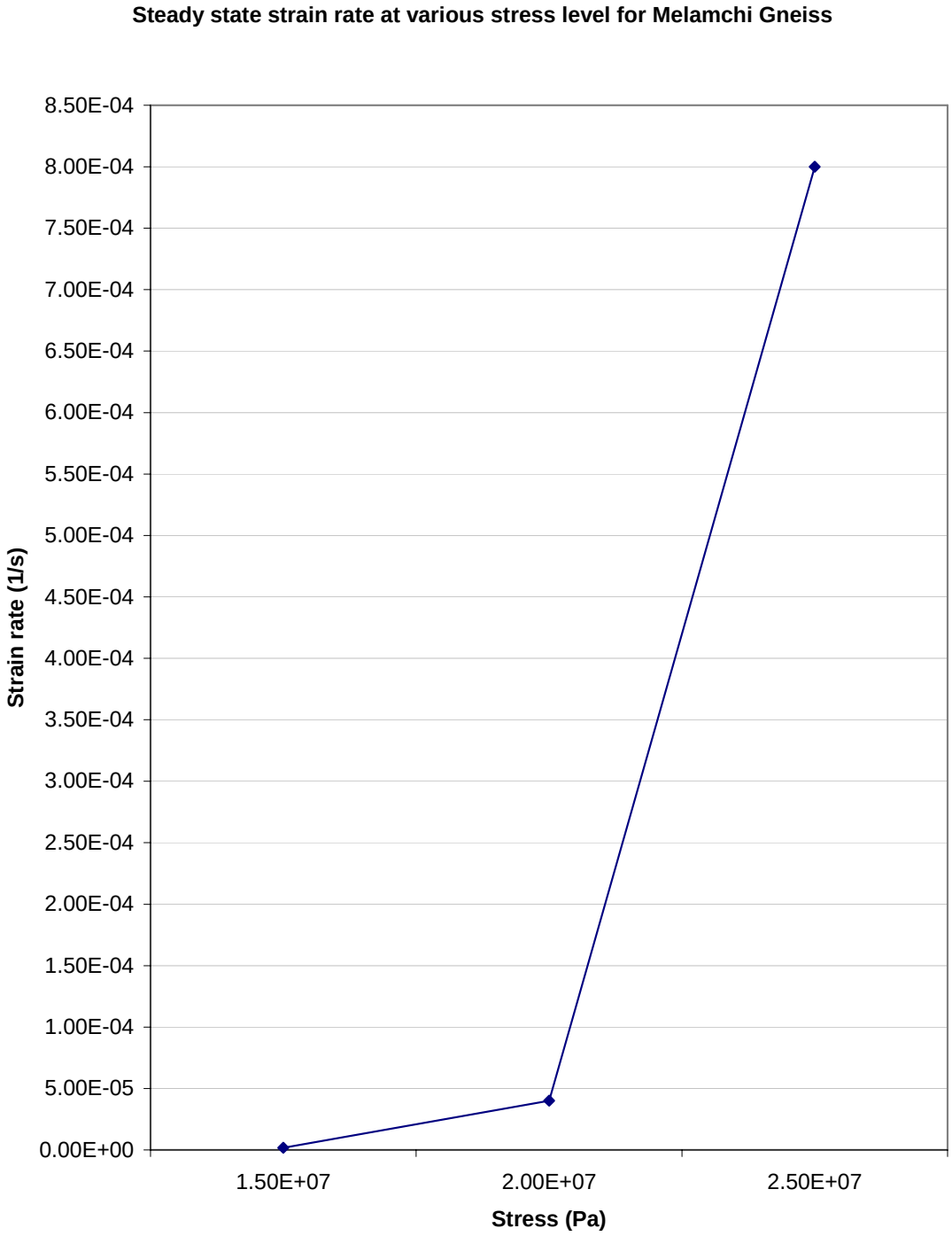

Figure 6.4 Relation between steady-state strain rate and stress level.

d) Remarks on the creep tests

The main objectives of the tests were to obtain; 1) the critical stress level above which rock fails for creep, 2) strain-time curves for calculating time-dependent deformation and secondary creep rate.

Though these objectives have been achieved, complete data set (i.e. tests with stress level up to 90% of the UCS) could not be obtained. In the ideal condition, the time to failure should decrease with the increase of stress level applied for the creep test. This trend is maintained in test results given in Table 6.4 except for the case of 22 MPa stress level.

Some of the possible reasons for the above mentioned problems could be: (1) the samples are heterogeneous and the heterogeneity varies from one sample to another, (2) the load was applied manually and there was no control on the loading rate, which might have caused impact on the sample.

When a sample previously used for a test but not broken, is subjected for another test it fails relatively in lower stress level. Sample 1 was used for cyclic loading test and after some months, when it (air dry) was subjected to creep it broke at 25 MPa. Similarly, Sample 410 was loaded for unsuccessful stepped up creep test for 5 weeks and it was taken out unbroken. It was saturated again and subjected to creep but broke at 20.5 MPa. In the light of these observations, progressive creep test may overestimate the steady-state creep rate for the various stress level. It was also observed in case of the Sample 45; it broke at 19.5 MPa when the stress level was increased from 15 to 20 MPa. Separate creep test with Sample 412 at 20 MPa survived for 12 hours.

6.2 Tests for rock material properties

6.2.1 Density and P wave velocity measurement

Density and P wave velocity for air-dry condition were measured for the rock cores from both bore holes. Then the cores were kept in water for 48 hours to get them fully saturated. Then again for all the cores density and P wave velocity were measured. With the increase in water content in the samples, P wave velocity increased and the results are presented in the following table.

Table 6.6 Density and P wave velocity for rock cores in ordinary and wet condition.

Sample No.	Depth (m)	Leng-th (mm)	Weight in room temp (g)	Density (kg/m3)	P wave travel time (μsec)	P wave velocity (m/sec)	P wave travel time for wet (μsec)	P wave velocity for wet (m/sec)	Weight in wet condn (g)
Bore hole: TDH 1; Sample diameter: 33 mm.									
1	36.2	100.7	232.5	2699	25.3	3980	20.8	4841	232.8
2-1	36.4	100.5	230.9	2686	26.2	3836	21.7	4631	231.1
2-2	36.4	50	115.2	2694	13.2	3788	10.8	4630	115.3
2-3	36.4	66.5	150.7	2650	17.1	3889	14.4	4618	151
2-4	36.4	82.3	190.9	2712	24	3429	18.5	4449	191.2
3-1	37	72.4	166.8	2694	17.8	4067	15	4827	167.1
3-2	37	60	137.7	2683	15.7	3822	12.1	4959	137.8
3-3	37	54.7	125.8	2689	16.4	3335	13	4208	125.9
4-1	37.25	75.1	173.1	2695	18	4172	15.4	4877	173.2
4-2	37.25	81.3	188.1	2705	19.6	4148	16.4	4957	188.2
4-3	37.25	43.5	100.1	2690	10.5	4143	9.1	4780	100.2
4-4	37.25	100.9	232.6	2695	24.4	4135	20.9	4828	232.9
41	40	81	185.2	2673	22.3	3632			
42	40	86	196.4	2670	22.8	3772			
43	40	86	200.9	2731	24.1	3568			
44	40	84	192.7	2682	23.0	3652			
45	40	86	197.8	2689	23.2	3707			
46	40	86	199.1	2707	25.0	3440			
47	41	84	196.7	2738	25.6	3281			
48	41	87	200.1	2689	24.8	3508			
49	41	87	202.6	2723	25.2	3452			
410	42	80	183.4	2680	21.8	3670			
411	42	82	191.0	2723	20.9	3923			
412	42	80	184.7	2699	20.1	3980			
413	42	79	184.7	2733	21.4	3691			
414	42	80	183.3	2679	21.7	3687			
Bore hole: TDH 2; Sample diameter: 47.4 mm.									
1-2	49.3	120.7	591.5	2777	28	4311	24.1	5008	592.2
2-1	49.8	90.8	447.6	2794	29.1	3120	20.8	4365	448.1
3-1	82.3	91	431	2684	36.3	2507	24.2	3760	431.8
4	83.5	90.4	428.3	2685	24.5	3690	20.3	4453	428.9
5-1	84.4	68.5	329	2722	21	3262	19.9	3442	329.6
5-2	84.4	90.5	430.7	2697	26.8	3377	15.6	5801	431.5
6	84.8	120.8	573.2	2689	30.5	3961	24.8	4871	574.4
7	86.3	88.5	422	2702	32.4	2731	22.4	3951	422.5

P wave velocity increases with the increase of water content. This was confirmed by the measurements. Figure 6.5 shows the percentage increase of P wave velocity versus increase in water content (% of sample weight). For these augen gneiss samples, the average increase in P-wave velocity is in the order of 20 – 30% for a small increase (0.05 – 0.2% of sample weight) in porosity (or water absorption). Average density of the saturated Melamchi augen gneiss from TDH1 has been found to be 2694 kg/m^3.

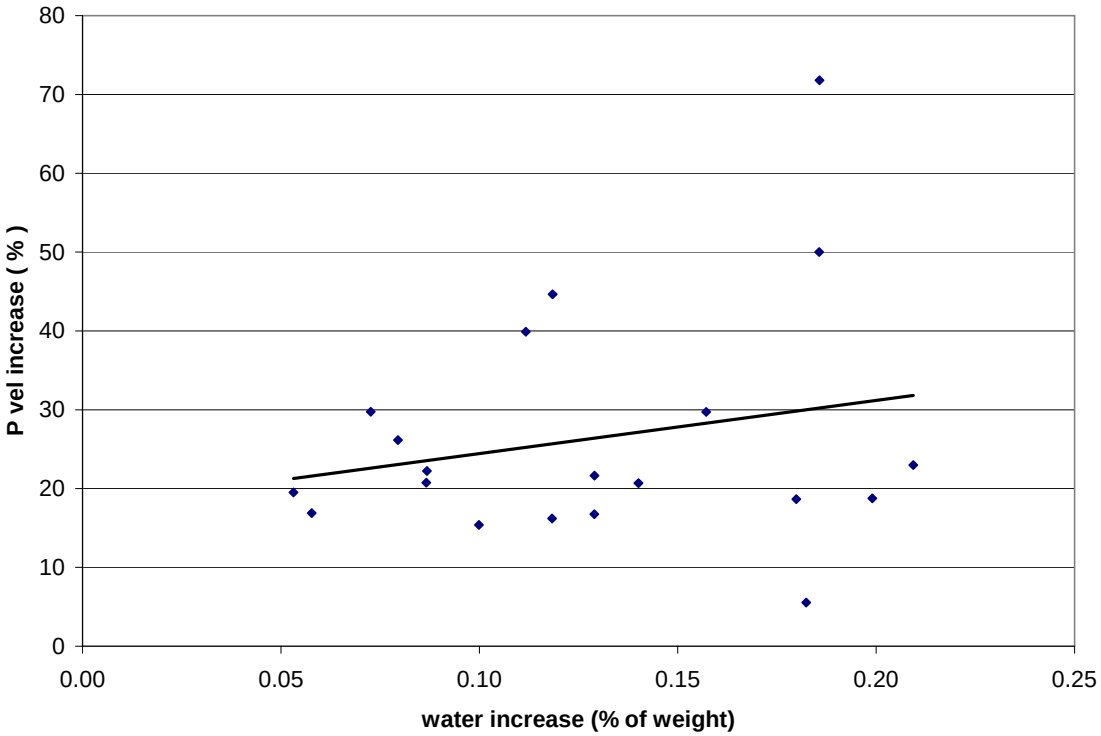

Figure 6.5 Increase in P wave velocity with the water absorption increase.

6.2.2 Mechanical properties test results

Laboratory tests were carried out on wet samples for Uniaxial Compressive Strength (UCS), Elasticity modulus (E) and Poisson's ratio (ν). Two samples were used for UCS and other two samples for E and ν values for each bore holes. A set of data for UCS and E modulus has been obtained from a test carried out in the tri-axial test set without confining pressure. The results from these tests are given in the following table:

Table 6.7 Elasticity modulus and uniaxial compressive strength tests results.

Bore hole	Sample No.	Core box No.	Depth (m)	Length (mm)	Dia (mm)	UCS (MPa)	Fracture and angle	Elasticity modulus (E) GPa	Poisson's ratio (ν)
TDH 1	2-3	10	36.4	66.5	33	38.8	Crushing layers at 25˚ & partly along mica layer.	-	-
TDH 1	3-2	10	37.0	60	33	34.8	Crushing layers at 22˚.	-	-
TDH 1	1	10	36.2	100.7	33	-	-	34	0.19
TDH 1	2-1	10	36.4	100.5	33	-	-	33	0.23
TDH 1	49	11	41.7	82.9	33	41.7	-	24.7	-
TDH 2	3-1	17	82.3	91.0	47.4	72.7	Crushing layers at 22˚.	-	-
TDH 2	5-1	18	84.4	68.5	47.4	92.4	Crushing layers at 29˚.	-	-
TDH 2	1-2	11	49.3	120.7	47.4	-	-	40.7	0.1
TDH 2	6	18	84.8	120.8	47.4	-	-	40.25	0.12

6.2.3 Point load test

Point load tests were carried out to supplement data for compressive strength. Following table gives the details of the point load test carried out on the wet (surface dry) samples from the boreholes TDH1 and TDH2.

Table 6.8 Point load test results.

Sample No.	Core box No.	Depth (m)	Length (mm)	Point load 'kp' (kgf)	Point load strength I_s (P/D_e^2=kp*0.1/D_e^2) MPa	Point load strength I_{s50}= I_s*(De/50)^0.45 MPa	Average I_{s50} (MPa)	Average UCS (MPa) (I_{s50}*22)
TDH 1, De=3.3 cm								
2-2	10	36.4	50	430	3.9	3.3	3.4	74
2-2	10	36.4	50	490	4.5	3.7		
2-2	10	36.4	50	400	3.7	3.0		
4-3	10	37.25	43.5	450	4.1	3.4		
TDH 2, De=4.74 cm								
1-1	11	49.3	>47.4	900	4.0	3.9	3.6	78
1-2	11	49.3	>47.4	2000	8.9	8.7		
2-2	11	49.8	>47.4	190	0.8	0.8		
3-2	17	82.3	>47.4	500	2.2	2.2		
3-2	17	82.3	>47.4	500	2.2	2.2		

Variation in the point load strength (I_{s50}) for samples from TDH1 is not significant but it is significant for the samples from TDH2. The significant variation might have been caused by the size effect as the length were not longer than the specimen diameter; and the samples were from the different depths (49m and 82m) of the bore hole TDH2.

6.2.4 Maximum strain before failure

This section only compiles the maximum strain values before the failure of saturated core specimens (except TDH1 sample 1) resulted by various tests (Table 6.9).

Table 6.9 Percentage strain at failure for various kinds of tests.

Sample No.	Length (mm)	Test set & failure condition	Axial micro strains	Radial micro strain	Deformation (mm)	Axial Strain (%)
TDH2 sample 6	120.8	E test set: one go loading, at 59 MPa	1668/ 2566	1736		0.26[1]
TDH2 sample1-2	120.7	E test set: cyclic loading upto 57 MPa(1Mpa/Sec)	2911/ 5510	612		0.55[1]
TDH2 sample 4	83	Creep test set: while loading, at 57 MPa			0.2473 (-1.3321 to -1.0848)	0.30
TDH2 sample 5-2	84	Creep test set: while loading, at 48 MPa			0.3147 (-1.4012 to -1.0865)	0.37
TDH1 sample 2-1	100.5	E test set: one go loading, at 19 MPa (0.1 MPa/Sec)	744/ 1152	426		0.11[1]
TDH1 sample 2-4	82	Creep test set: while loading, at 27 MPa			0.0674 (-1.1545 to -1.0871)	0.082
TDH1 sample 4-2	81	Creep test set: 1hour creep, at 25 MPa			0.5028 (-1.2349 to -0.7321)	0.62
TDH1 sample 4-4	83	Creep test set: 1hour 10 minutes creep, at 24 MPa			0.0306 (-1.4457 to -1.4151)	0.038
TDH1 sample 1	81	Creep test set: 1minute creep, at 25 MPa			0.184 (-1.432 to -1.248)	0.23
TDH1 sample 412	79	Creep test set: 12 hours creep, at 20 MPa			0.5068 (-0.5127 to -0.0059)	0.64
TDH1 sample 41	79	Creep test set: 7 seconds creep, at 19.2 MPa			0.5601 (-1.2031 to -0.643)	0.709 (load applied at once)
TDH1 sample 42	82.2	Creep test set: 4 minutes creep, at 22 MPa			0.2075 (-1.2756 to -1.0681)	0.25
TDH1 sample 410	79.5	Creep test set: 3 minutes creep, at 20.5 MPa			0.106 (-1.2103 to -1.1043)	0.133 (used in progressiv creep)
TDH1 sample 49	82.9	Tri-axial test set: 37 minutes with stress increase up to 41.7 until broke.				0.222

***Note**: 1) Maximum axial strain is considered to be the failure causing strain.*

6.3 Complete stress-strain curve

The term ‘complete stress-strain curve’ refers to the displacement of the specimen ends from initial loading, through the linear elastic prepeak region, through the onset of significant cracking, through the compressive strength (when the stress-strain curve has zero gradient), into the postpeak failure locus, and through to the residual strength. When the measured force is scaled by the original specimen area and the measured displacement is scaled by the original specimen length, a nominal stress-strain curve can be plotted.

A complete stress-strain curve for rock is shown in Figure 6.6. The prepeak portion is the region OA. Two types of curve are observed in terms of the characteristic of the postpeak region: either the curve monotonically increases in strain or it does not. The former, curve OAF in the figure is termed a class I curve; the latter, curve OABE is termed a class II curve. Cylindrical specimens that exhibit class I behaviour tend to be somewhat ductile in nature when loaded axially; whereas specimens that exhibit class II behaviour tend to respond in a brittle fashion to axial loading.

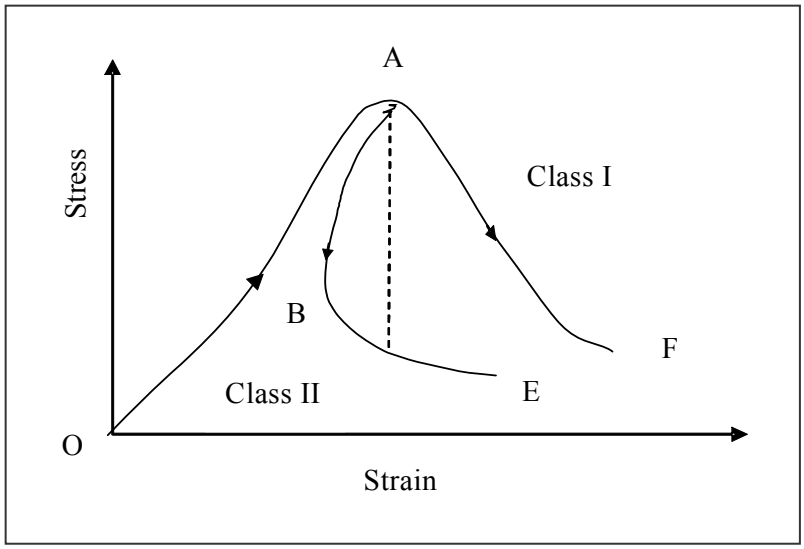

Figure 6.6 Classification of class I and class II behaviour of rock failure in uniaxial compression.

The complete stress-strain curve of an intact rock specimen, is useful in understanding the total process of intact rock specimen deformation, cracking and eventual disintegration, and can provide insight into potential in situ rock mass behaviour. However, certain extremely brittle specimens, even under the most favourable testing conditions (e.g. stiff testing frame, slow loading rate, circumferential strain feed-back, low length/diameter ratio), may fail abruptly or even explosively when tested without confinement. It should be tested in a confined state (ISRM, 1999).

The complete stress-strain curve is used to predict the long-term strength of a rock. The creep failure occurs when the rock has been strained a critical amount. The critical cumulative strain is provided by the complete stress-strain curve, containing both ascending and descending parts, as shown in Figure 6.6. Such a complete curve for a brittle rock can be obtained only in a very stiff testing machine.

6.3.1 Complete stress – strain test results

The total deformation in a creep test of a rock sample, can be correlated with the respective deformation in the complete stress-strain curve. Theoretically the total creep strain should correspond to the respective strain indicated by the falling part of the complete stress-strain curve for the same stress level.

Tests for complete stress-strain curves were carried out in the laboratory in Department of Petroleum Engineering and Applied Geophysics, NTNU. It would be ideal to correlate the total creep deformations to the complete stress-strain curve for a uniaxially loaded test, i.e. at a zero confining pressure. But a complete stress-strain curve could not be achieved at zero confining pressure with a controlled axial deformation rate of 0.000001 mm/mm/sec. The sample broke with a bang after giving a short falling part of the curve and stress instantly dropped to zero. It was technically difficult to carry out tests with a controlled radial deformation rate (no test had been carried out with a 'controlled radial deformation rate' in the laboratory, so that, laboratory staff were not confident to do so). Thus additional two tests were carried out with 1.5 MPa and 3 MPa confining pressures. The latter two tests were successful in obtaining the complete stress-strain curves. Three complete stress-strain curves have been produced with 0, 1.5 and 3 MPa confining pressures (Figure 6.7).

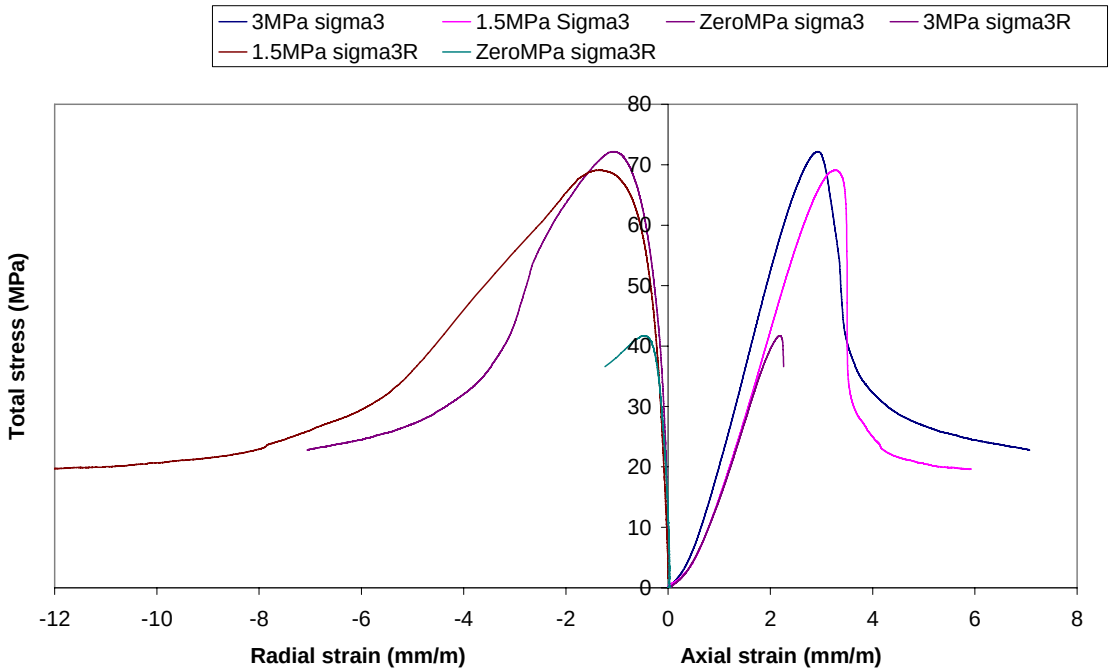

Figure 6.7 Complete stress-strain curves for 0, 1.5 and 3MPa confining pressures.

7 Squeezing analysis for the Melamchi tunnel

Excavation causes changes in stress system around the opening. Effect of the changed stress condition is reflected in ground response which subsequently influences support pressure and tunnel closure. Prediction of ground condition, support pressure and tunnel closure are very important for a cost-effective and trouble free tunnel construction.

Several methods have been developed for squeezing analysis and tunnel support design. These methods range from empirical to numerical modelling (Chapter 3). Due to the simplicity, the empirical methods are widely used. However, as far as possible, it is good to use several methods and compare the results.

7.1 Deformation and support design

The methods and approaches used to assess squeezing potential and design support in this section does not include time effect. Time effect in tunnel stability and tunnel convergence is included in the analysis in section 7.2.

7.1.1 Adopted methods and approaches

The following methods and approaches have been adopted to assess squeezing potential and to design tunnel support for the Melamchi tunnel:

Empirical method: *Goel (1994)'s approach based on N value*.

Semi-analytical method: *Hoek and Marinos (2000)'s approach*.

Analytical method: *Carranza-Torres & Fairhurst approach (2000) using Hoek-Brown criteria*.

Analytical method: *Duncan-Fama approach (1993) using Mohr-Coulomb criteria*.

Simplified analytical solution: *using Mohr-Coulomb criteria*.

Numerical modelling method: *using FLAC^{3D} code*.

For every method mentioned above, there are more than one approach available. In this thesis, for each method at least one approach has been used. Main equations used in this chapter are given in chapter 5; and their details in Chapter 3. Details on the use of FLAC^{3D} and results are discussed in Chapter 8.

7.1.2 Input parameters for analysis

In Melamchi project area rock mass condition varies in a short distance from Massive (or very less jointed) rock mass condition to very jointed rock mass condition. So in this chapter analyses have been carried out for massive and jointed rock mass conditions separately. In order to analyse for two types of rock mass conditions, two separate sets of data have been obtained by having two different GSI values (in RocLab software) and keeping all other input parameters the same.

a) Data from laboratory tests

As mentioned in Chapter 4, the Melamchi water supply project consists of 26.3 km long tunnel. The maximum overburden above the tunnel level is 1,200 m. The required input data are generated mainly by laboratory tests on the samples from Nepal. All the results given below are from the tests on saturated specimens (33-mm-diameter) from the bore hole TDH1.

In order to determine the mechanical properties of rock materials, tests were carried out in NTNU Sintef laboratory. Details of the laboratory tests are given in Chapter 6. The test results needed for squeezing analysis, are given in Table 7.1.

Table 7.1 Laboratory test results for general mechanical properties of Melamchi augen gneiss.

Sample	Length, (mm)	Diameter, (mm)	Uniaxial compressive strength (UCS), σ_{ci} (MPa)	Elasticity modulus, E (GPa)	Poisson's ratio, ν	Wet density γ (MN/m^3) (from 12 tests)
49	82.86	33	43			
2-3	66.5	33	38.8	-	-	
3-2	60	33	34.8	-	-	
1	100.7	33	-	34	0.19	
2-1	100.5	33	-	33	0.23	
						0.027

b) 'RocLab' generated data

The Hoek-Brown criterion for rock masses uses input parameters, namely σ_{ci}, GSI, m_i and D. Value for σ_{ci} has been obtained from the laboratory tests (Table 7.1), but the values for GSI, mi and D are assumed as follows:

σ_{ci} = 39 MPa (Average value from Table 7.1)

GSI = 45 (from RocLab reference - considering 'very blocky and fair' condition for jointed rock mass condition)

GSI = 70 (from RocLab reference - considering 'massive and fair' condition for massive rock mass condition).

m_i = 23 (from RocLab reference for Gneiss)

D = 0 (from RocLab reference for smooth blasting condition)

Table 7.2 Data generated from RocLab software for jointed rock mass.

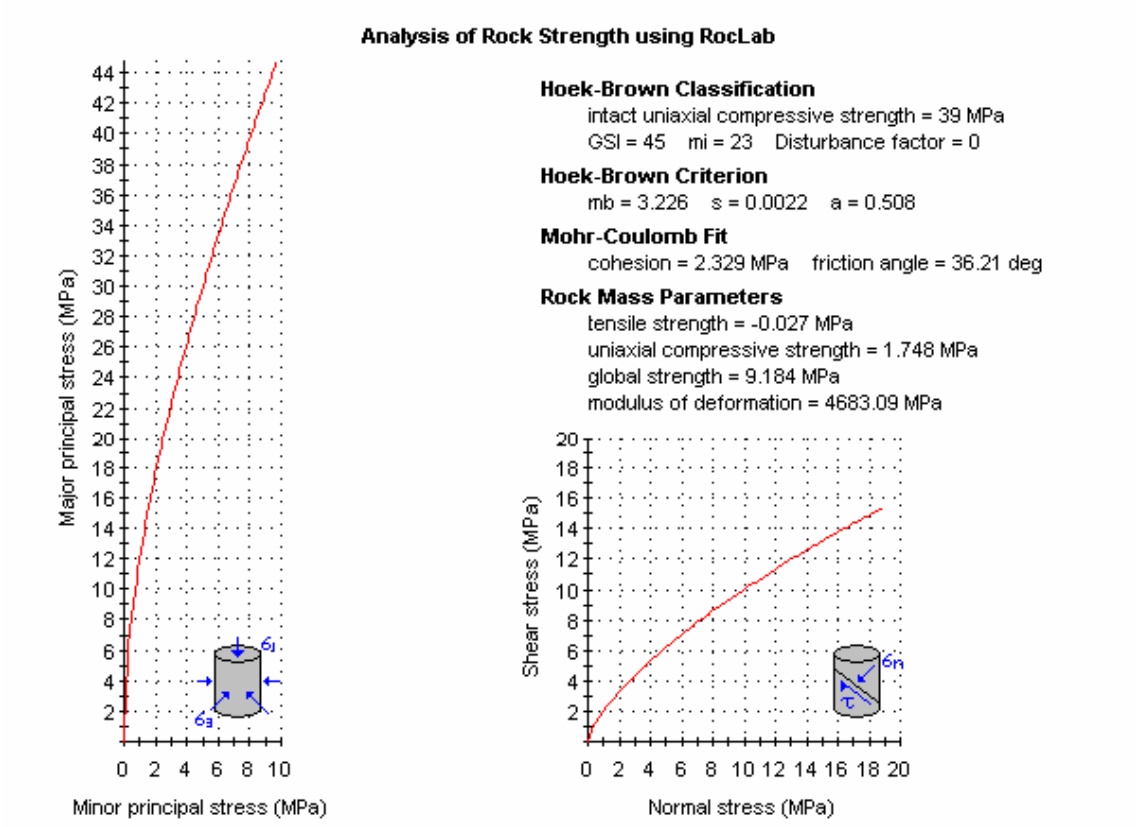

By using the above mentioned values for σ_{ci}, GSI, m_i and D in RocLab software, additional data have been generated for a jointed and massive rock mass condition; and those are given in Table 7.2 and Table 7.3 respectively.

N will be estimated from the assumed value of GSI by using the following equation:

GSI = 9 Log_e Q' + 44 (Hoek et al., 1995). Here Q' = $(RQD/J_n)*(J_r/J_a)$. For dry or minor inflow (< 25 l/min), J_w = 1. Hence Q' and N are same for J_w = 1, it can be rewritten as follows:

$GSI = 9 \text{Log}_e N + 44$ (5-1)

Where, GSI = Geological strength index.

For GSI = 45, N value by using the equation given above is 1.12.

For GSI = 70, N value by using the equation given above is 17.97.

Table 7.3 Data generated from RocLab software for massive rock mass.

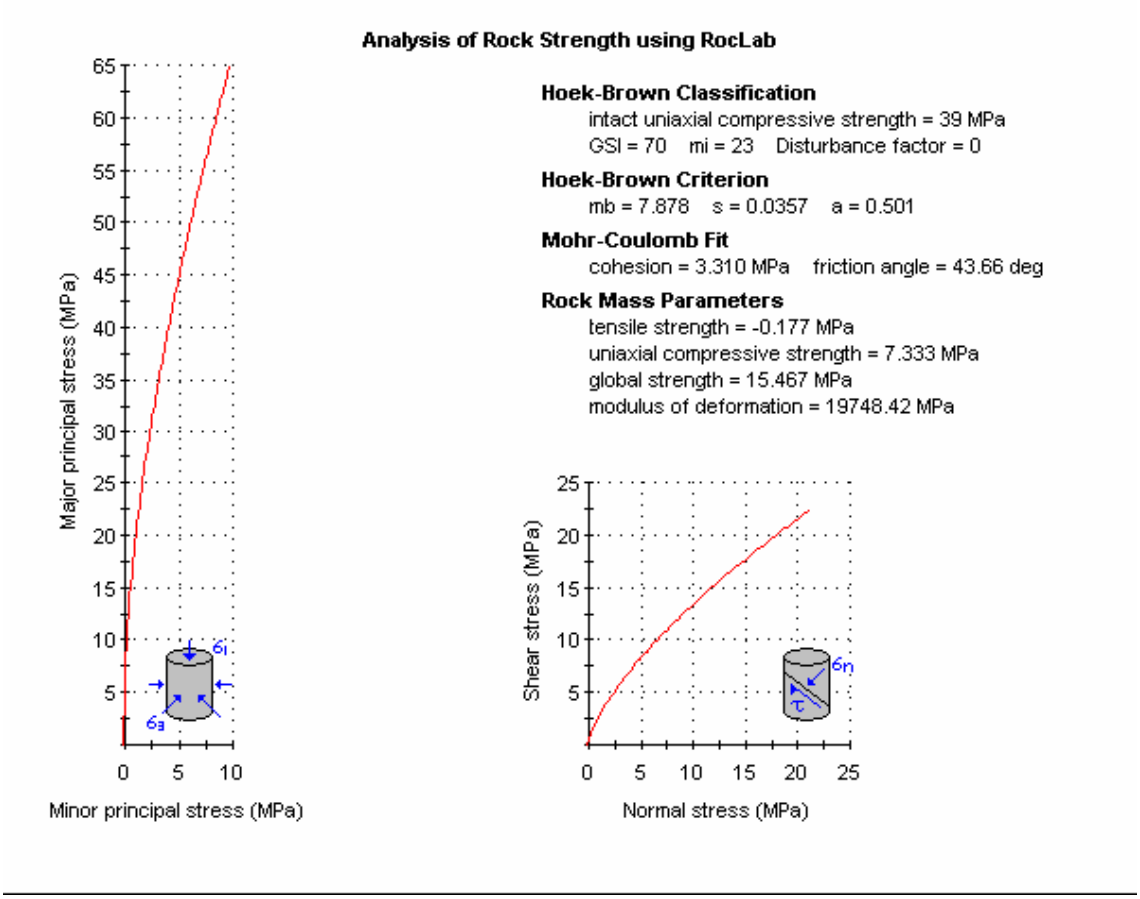

7.1.3 Squeezing deformation and support pressure calculation

A circular tunnel with hydrostatic stress condition has been considered and the support is assumed to act uniformly on the entire perimeter of the tunnel (Figure 7.1). The deformations are calculated by using the five different approaches (section 7.1.1) for a circular tunnel of 2.5 m. in radius. Separate analyses have been carried out for jointed and massive rock mass conditions.

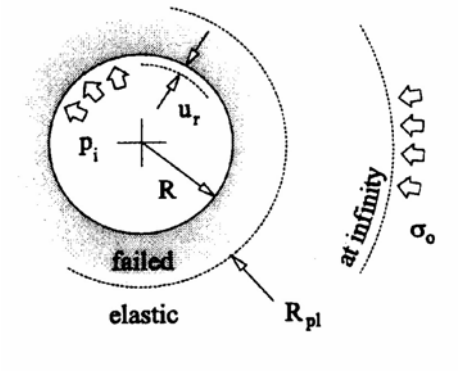

Figure 7.1 Cross-section of a cylindrical tunnel of radius R.

Squeezing deformations and required support pressures have been calculated by using the input data from section 7.1.2 and the equations from section 5.1. Various overburden depths and respective hydrostatic stress levels have been considered for squeezing assessment and support calculations. The squeezing deformations have been calculated assuming jointed rock mass condition with GSI value 45. Summary of the calculations are given in Table 7.4.

Table 7.4 Squeezing deformations and required support pressure calculated by using the five different approaches for jointed rock mass.

Overburden (m)	Stress σo (MPa)	Goel (1994)	Hoek & Marinos (2000)		Carranza-Torres & Fairhurst (2000)			Duncan-Fama (1993)			Mohr-Coulomb
		p_i^{cr} (MPa)	p_i for 1% u (MPa)	Total u% at pi=0	p_i^{cr} (MPa)	p_i for 1% u (MPa)	Total u% at pi=0	p_i^{cr} (MPa)	p_i for 1% u (MPa)	Total u% at pi=0	p_i^{cr} (MPa)
100	2.7	0.11	0	0.03	0.18	0	0.07	-0.77	0	0.08	-0.97
200	5.4	0.21	0	0.13	0.68	0	0.16	0.33	0	0.14	0.42
300	8.1	0.35	0	0.30	1.40	0	0.27	1.44	0	0.23	1.81
400	10.8	0.55	0	0.54	2.28	0	0.40	2.54	0	0.34	3.19
500	13.5	0.82	0	0.84	3.29	0	0.55	3.65	0	0.48	4.58
600	16.2	1.19	0.9	1.21	4.40	0	0.72	4.75	0	0.63	5.97
700	18.9	1.69	2.5	1.65	5.60	0	0.91	5.86	0	0.81	7.36
800	21.6	2.34	3.9	2.16	6.87	0.2	1.12	6.96	0.1	1.01	8.75
900	24.3	3.20	5.3	2.73	8.21	0.7	1.36	8.07	0.9	1.22	10.14
1000	27	4.31	6.7	3.37	9.60	1.5	1.62	9.17	1.7	1.46	11.53
1100	29.7	5.74	8.1	4.08	11.04	2.5	1.91	10.28	2.7	1.71	12.92
1200	32.4	7.56	9.5	4.85	12.53	3.8	2.22	11.38	3.75	1.97	14.31
1300	35.1	9.87	10.9	5.69	14.05	5.2	2.56	12.49	4.9	2.26	15.70
1400	37.8	12.78	12.3	6.60	15.62	6.7	2.94	13.59	6.2	2.56	17.09
1500	40.5	16.44	13.7	7.58	17.21	8.3	3.34	14.70	7.6	2.88	18.48

According to Equation (3-4) by Goel (1994), squeezing takes place in the jointed rock mass, when the overburden depth exceeds 243m.

Calculations for squeezing potential and support requirements have been carried out for a massive rock with GSI value 70 as well and the summary of the results are given in Table 7.5.

Table 7.5 Squeezing deformations and required support pressures calculated by using the five different approaches for massive rock mass.

Overburden (m)	Stress σo (MPa)	Goel (1994)	Hoek & Marinos (2000)		Carranza-Torres & Fairhurst (2000)			Duncan-Fama (1993)			Mohr-Coulomb
		p_i^{cr} (MPa)	p_i for 1% u (MPa)	Total u% at pi=0	p_i^{cr} (MPa)	p_i for 1% u (MPa)	Total u% at pi=0	p_i^{cr} (MPa)	p_i for 1% u (MPa)	Total u% at pi=0	p_i^{cr} (MPa)
100	2.7	0.05		0.01	-0.08		0.02	-1.56		0.02	-1.84
200	5.4	0.07		0.03	0.18		0.03	-0.72		0.03	-0.85
300	8.1	0.09		0.06	0.56		0.05	0.11		0.05	0.13
400	10.8	0.10		0.11	1.06		0.07	0.95		0.07	1.12
500	13.5	0.12		0.18	1.65		0.09	1.79		0.09	2.11
600	16.2	0.14		0.26	2.33		0.12	2.62		0.11	3.10
700	18.9	0.16		0.35	3.08		0.14	3.46		0.14	4.09
800	21.6	0.18		0.46	3.90		0.17	4.29		0.16	5.08
900	24.3	0.21		0.58	4.78		0.20	5.13		0.19	6.07
1000	27.0	0.23		0.71	5.72		0.23	5.97		0.22	7.06
1100	29.7	0.26		0.86	6.71		0.26	6.80		0.25	8.05
1200	32.4	0.29		1.03	7.74		0.30	7.64		0.29	9.04
1300	35.1	0.32		1.21	8.82		0.33	8.47		0.32	10.03
1400	37.8	0.36		1.40	9.93		0.37	9.31		0.36	11.01
1500	40.5	0.40		1.61	11.09		0.41	10.15		0.40	12.00

According to Equation (3-4) by Goel (1994), squeezing takes place in the massive rock mass, when the overburden depth exceeds 607m.

Total deformation

Total tunnel deformation can be calculated by using three out of the five approaches mentioned in section 7.1.1. For both of the jointed and massive rock masses, all the three deformation curves are of non-linear nature. The Hoek & Marinos approach has given the largest deformation in comparison to other two analytical approaches (Figure 7.2).

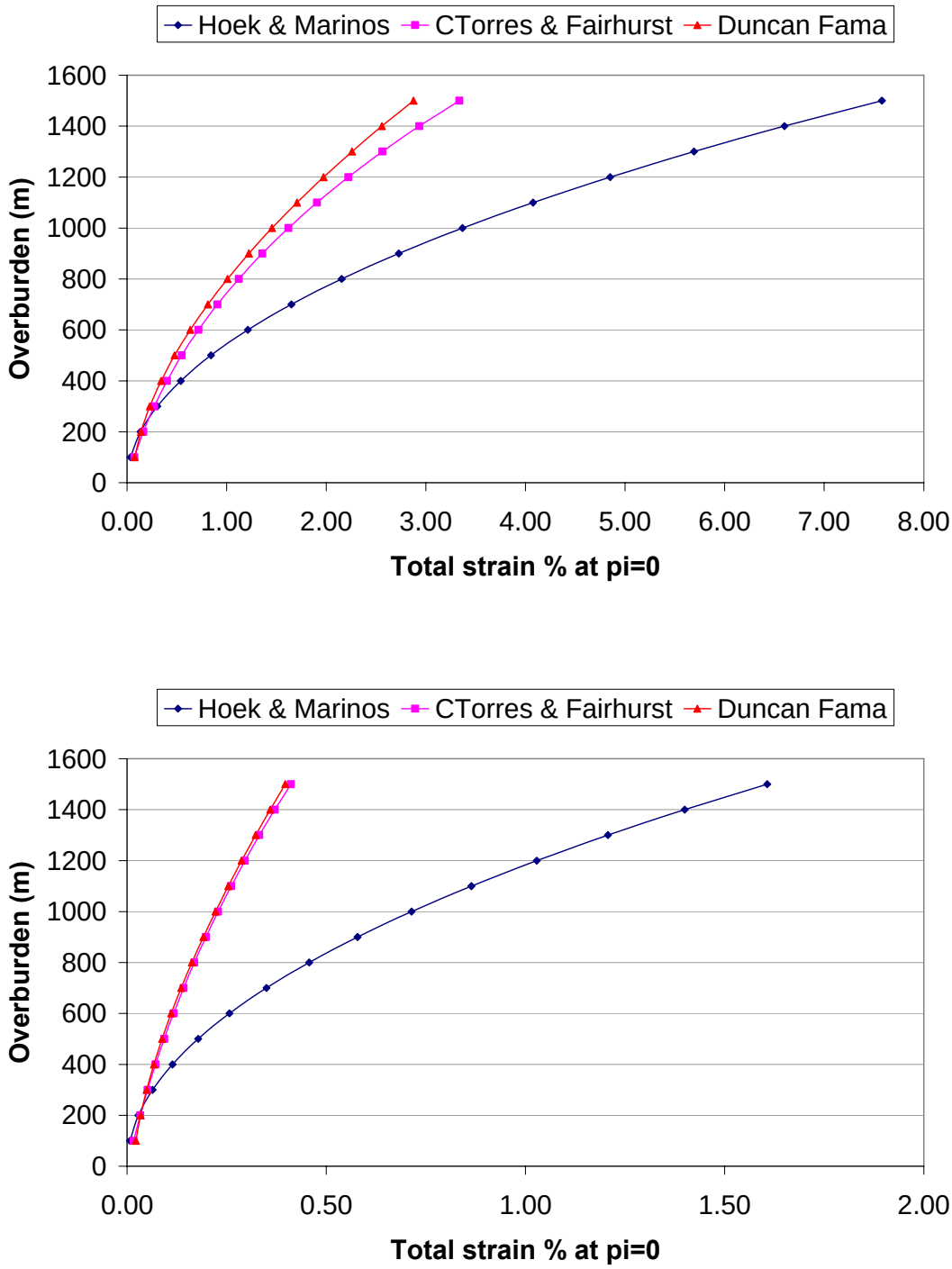

Figure 7.2 Total strain for an unsupported tunnel calculated by using a semi-analytical and two analytical methods for jointed (GSI=45) and massive (GSI=70) rock mass condition respectively.

Critical support pressure

Four of the five approaches, have the provision for critical support pressure calculation. For both the rock mass conditions, the results of these calculations are not very different from each other, except for Goel approach (Figure 7.3).

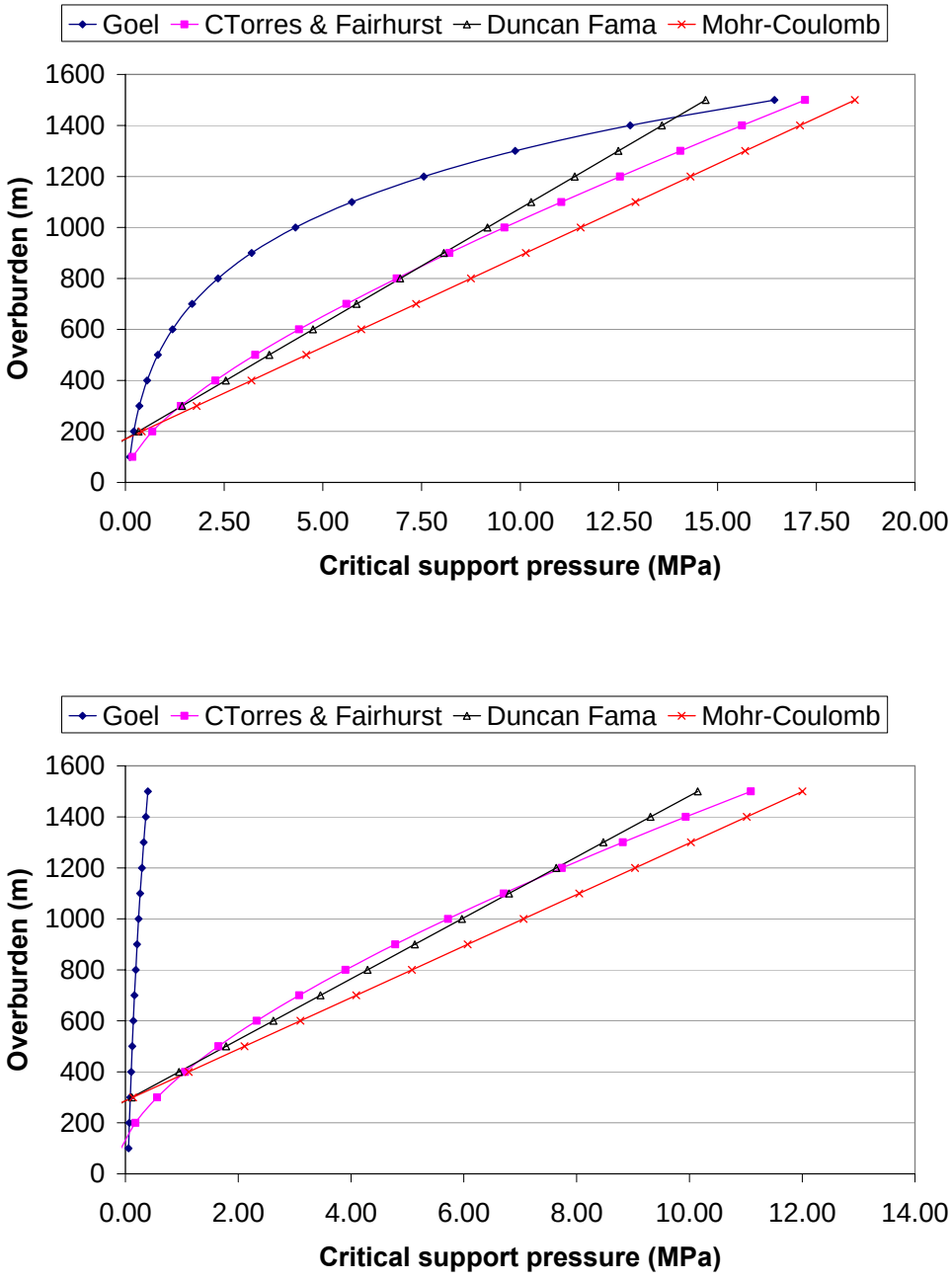

Figure 7.3 Critical support pressures required for various overburden depths calculated using an empirical and three analytical methods for jointed (GSI=45) and massive (GSI=70) rock mass condition respectively.

Duncan-Fama and Mohr-Coulomb solutions have given linear type of curves whereas Goel and Carranza-Torres and Fairhurst approaches have shown non-linear relationship between overburden and critical support pressure requirement. However, Hoek-Marinos approach does not have provision for the critical support pressure calculation. For the jointed rock mass condition with a low value of 1.12 for rock mass number N Goel approach is found to be sensitive, but for massive rock mass condition with relatively higher value of 17.97 for rock mass number N Goel approach is found to be not sensitive. For the massive rock mass condition, according to Equation (3-4), squeezing starts at an overburden of 607 m, but that is not reflected in Figure 7.3 (b) as required critical support pressures did not increase accordingly.

Support pressure for 1% strain

For the massive rock mass condition, the total strain is less than 1% except for Hoek-Marinos approach. So Figures 7.4 and 7.5 are given for only the jointed rock mass condition.

Out of the five approaches three have a provision for calculating support pressure for the 1% strain. Hoek-Marinos approach has been found to be conservative in estimation of the total strain and also in the calculation of support pressure for the 1% strain (Figures 7.2 & 7.4). It has given a linear relationship between overburden and support pressure.

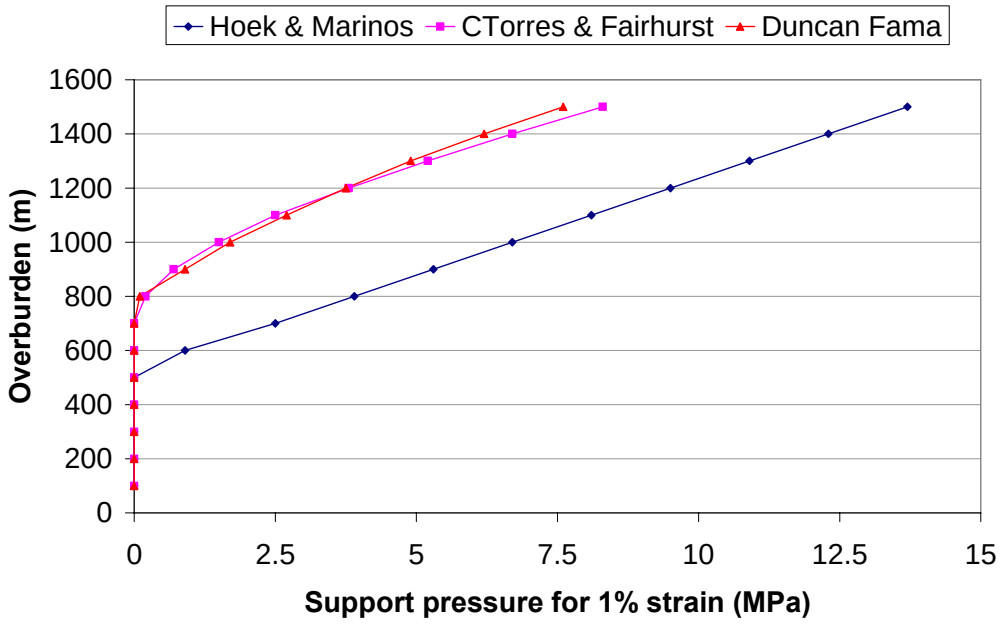

Figure 7.4 Support pressures for the 1% strain for various overburden depths using three different methods.

It is interesting to observe that two different analytical approaches have given nearly equal and identical curves for the critical support pressure and the support pressure for the 1% strain. When 1% strain is allowed, tunnel support is required only for overburden over 900m. Still those support pressures are about 30% of the respective critical support pressure or less (Figure 7.5). On the other hand, tunnel support is required even for 200m overburden if only elastic strain is allowed. The main important fact is that it reduces support pressure by more than 70 % and moreover, this reduced support is needed for a shorter tunnel section only.

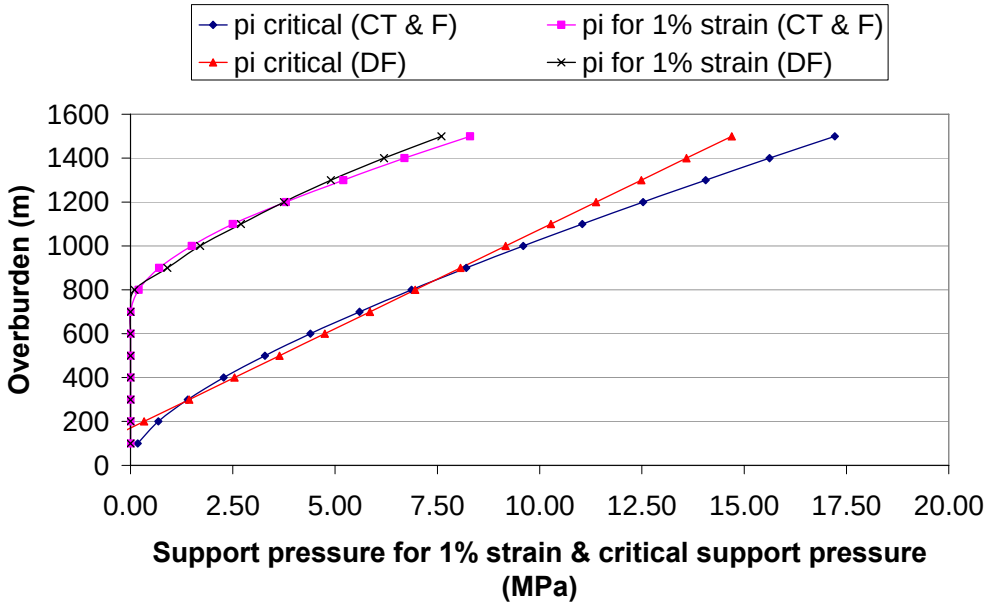

Figure 7.5 Support pressure for 1% strain and critical support pressure for two analytical methods only.

General comments

All the curves indicating the relationship between overburden and the total strain are of non-linear nature (Figure 7.2). However, non-linear relationship between overburden and critical support pressure has been obtained only in case of Carranza-Torres & Fairhurst approach (Figure 7.3).

Even by allowing a 1% tunnel strain, it reduces support pressure by more than 70 % and this reduced support is needed for a shorter tunnel section only. Thus it will reduce tunnel cost significantly.

Solutions for the two analytical and the one semi-analytical approaches were developed for circular tunnel under hydrostatic stress condition. So these approaches are applicable for those given conditions, but other two approaches, namely, Goel (1994)'s approach and the simplified solution using Mohr-Coulomb criteria can be used in anisotropic stress conditions and also for tunnels of any shape.

7.2 Time-dependent responses

7.2.1 The critical stress level for creep failure

Even if the tangential stress level around the tunnel is below the rock mass strength, it still may cause creep. Aydan et al. (1993) considered the concept of the analogy between the axial stress-strain response of rocks in laboratory tests and tangential stress-strain response of rocks surrounding opening in the tunnels. The 'critical stress level' is the minimum stress level which causes rock failure by creep after a certain time (also see section 2.2). Thus in a tunnel stability assessment, the determination of the critical stress level is important. The critical stress level has been determined by carrying out creep tests at various axial stress levels.

Creep (long-term deformation) tests were carried out in the laboratory of Department of Geology and Mineral Resources Engineering, NTNU. Creep test results given in Table 6.4 in Chapter 6, are presented in Figure 7.6. All the samples, except one at 15 MPa stress level, failed after a certain period of time. The symbol 'x' at the end of the curves indicates the samples failed at the end of the creep tests.

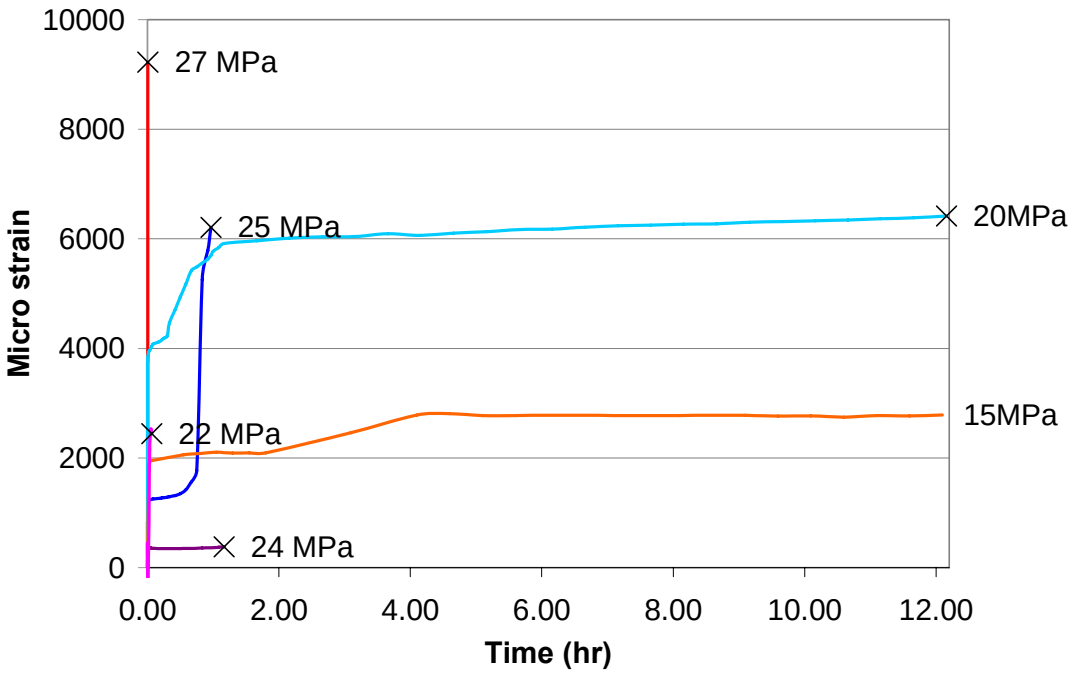

Figure 7.6 Strain – time curves for creep on Melamchi augen gneiss at different stress levels.

Sample 412 failed in 12 hours after it was subjected to the constant stress level of 20 MPa. It is the lowest stress level that caused the creep failure. Average UCS of these

samples was 39 MPa. According to the test results, samples subjected to 50% or higher of uniaxial compressive strength (UCS) of intact rock samples failed by the creep. Thus the critical stress level for creep failure for this rock is 20 MPa. Primary, secondary and tertiary phases of the creep were supposed to be observed in the Figure. However, strain data were recorded in the long interval in most of the tests, so tertiary phase is not seen for most of the curves.

In the ideal condition, the time to failure should decrease with the increase of stress level applied for the creep test. This trend is maintained in test results given in Figure 7.6 except for the case of 22 MPa stress level. Two possible reasons for it are: (1) the samples are heterogeneous and the heterogeneity varies from one sample to another, (2) the load was applied manually and there was no control on the loading rate, which might have caused impact on the sample.

7.2.2 Time-dependent tunnel deformation

Tunnel deformation calculated in section 7.1.3, does not include time-dependent (creep) effect (Carranza-Torres & Fairhurst, 2000). Thus time-dependent deformation needs to be added on to it in case that the stress level is above the 'Critical stress level'.

The time-dependent tunnel deformation is calculated by using rheological parameters of the rock. These parameters have been quantified by calibrating the strain-time curve obtained by creep tests. The calibration is carried out for Burgers substance in axial loading condition as described in Goodman (1989). Out of the six curves in the Figure 7.6, only three representative strain-time curves, namely those for 15, 20 and 25 MPa stress levels, have been calibrated. A set of calibration calculation (for sample 412) is given in the Appendix B. The stress level and the respective calibrated rheological parameter values are given in Table 7.6.

Table 7.6 Rheological parameters from creep test at different stress levels.

Sample	Stress level (MPa)	Shear modulus, G_1 (Pa)	Shear modulus, G_2 (Pa)	Viscosity, η_1 (Pa-hr)	Viscosity, η_2 (Pa-hr)
45	15	$5.4054*10^9$	$3.027*10^9$	$6.3593*10^9$	$2.2425*10^{12}$
412	20	$2.666*10^9$	$2.087*10^9$	$8.333*10^8$	$1.6648*10^{11}$
4-2	25	$1.282*10^{10}$	$2.961*10^{10}$	$1.068*10^8$	$3.754*10^{10}$

The rheological parameters given in Table 7.6 correspond to the intact rock condition loaded under constant stress level in 20˚ Centigrade temperature and with the humidity range of 65 - 70 %. Here also a circular tunnel with hydrostatic stress condition has

been considered and the support is assumed to act uniformly on the entire perimeter of the tunnel of 2.5m radius.

Equation (3-70) has been used to calculate deformations for an unsupported tunnel and Equation (3-71) for a tunnel with support pressure p_i *(Goodman, 1989)*.

$$u_r(t) = \frac{\sigma_0 R}{2G_2} + \frac{\sigma_0 R}{2G_1} - \frac{\sigma_0 R}{2G_1} e^{-(G_1 t/\eta_1)} + \frac{\sigma_0 R}{2\eta_2} t \qquad (3\text{-}70)$$

$$u_r(t) = \frac{(\sigma_0 - p_i) R}{2G_2} + \frac{(\sigma_0 - p_i) R}{2G_1} - \frac{(\sigma_0 - p_i) R}{2G_1} e^{-(G_1 t/\eta_1)} + \frac{(\sigma_0 - p_i) R}{2\eta_2} t \qquad (3\text{-}71)$$

The constant stress in the creep test corresponds to the tangential stress in the tunnel contour. For the sake of simplicity the tangential stress σ_θ is estimated to be double of the overburden pressure. Hence a tangential stress of 15, 20 and 25 MPa correspond to the hydrostatic stress (σ_o) of 7.5, 10 and 12.5 MPa respectively. Calculations are carried out for the total deformation including instantaneous and time-dependent deformations. In both the equations given above, the first part in the right hand side gives the instantaneous deformation and the rest 3 parts give the time-dependent deformation. Total radial deformation calculated for the Melamchi tunnel at hydrostatic stress levels of 12.5, 10 and 7.5 MPa are given in the Table 7.7.

Table 7.7 Total radial deformation (mm) calculated for Melamchi tunnel at three different tangential stress levels.

Time (hr)	Tangential stress 25 MPa	Tangential stress 20 MPa	Tangential stress 15 MPa
0	0.53	5.99	3.10
0.25	1.85	8.59	3.43
0.5	1.95	9.77	3.70
0.75	2.06	10.31	3.92
1	2.16	10.56	4.09
2	2.58	10.82	4.52
3	3.00	10.90	4.71
4	3.41	10.98	4.79
5	3.83	11.05	4.83
6	4.24	11.13	4.85
7	4.66	11.20	4.86
8	5.08	11.28	4.86
9	5.49	11.35	4.87
10	5.91	11.43	4.87
11	6.33	11.50	4.88
12	6.74	11.58	4.88
13	7.16	11.65	4.89
14	7.57	11.73	4.89
15	7.99	11.80	4.89
16	8.41	11.88	4.90
17	8.82	11.95	4.90
18	9.24	12.03	4.91
24	11.74	12.48	4.93

Figure 7.7 shows the response of the total deformation with time. The total deformation includes instant and time-dependent deformation. It can be observed that with the increase of the stress level, the deformation rate also increases, being 0.004, 0.08 and 0.41 mm/hr for 15, 20 and 25 MPa tangential stress levels. Similar trend applies to the case of instantaneous deformation also. These amounts have been found to be 3.1 and 5.99 mm for 15 and 20 MPa respectively. However, it occurred only 0.53 mm in case of 25 MPa tangential stress level, whereas it was supposed to be more than 5.99 mm. This discrepancy might be caused by two reasons: firstly, rock anisotropy varies from one sample to another; and secondly, the creep test set did not have a provision for controlling the loading rate.

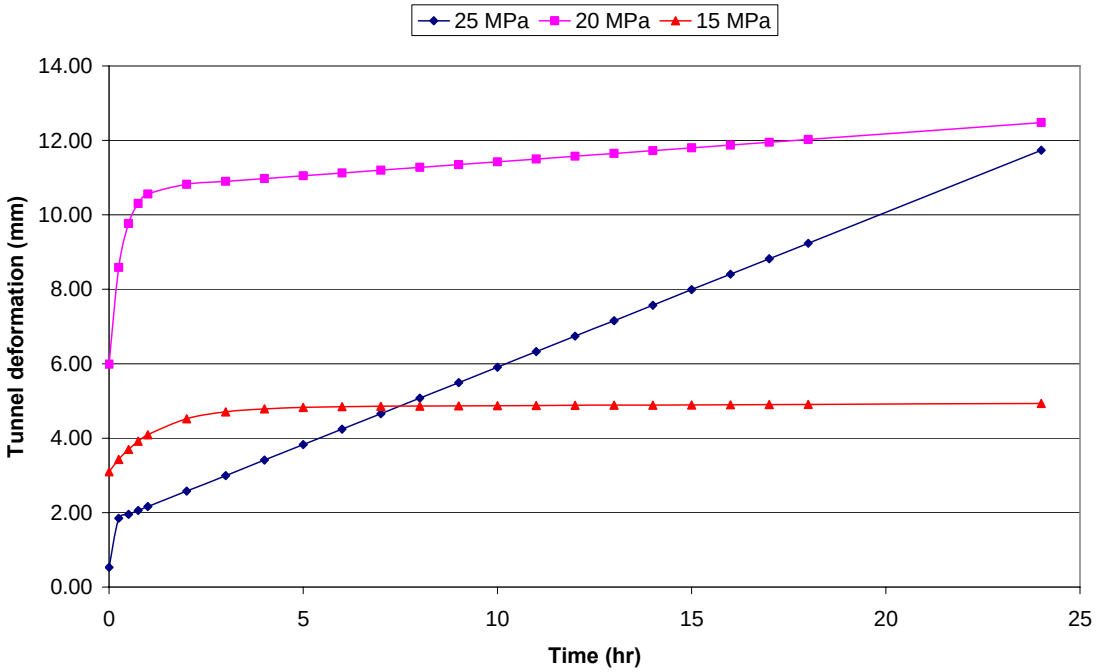

Figure 7.7 Comparison of time-dependent deformations for the Melamchi tunnel for three different tangential stress levels.

Total deformation for the unsupported and supported tunnel condition are calculated only for 10 MPa hydrostatic stress level and summary of the calculations is given in the Table 7.8.

Table 7.8 Squeezing deformation including time effect for the unlined and lined tunnels at 10 MPa hydrostatic stress level.

Time (hr)	Radial deformation in mm	Radial deformation in % of radius	Radial deformation in mm (with pi=5 MPa)	Radial deformation in % of radius (with pi=5 MPa)
0	5.99	0.24	2.99	0.12
0.25	8.59	0.34	4.29	0.17
0.5	9.77	0.39	4.88	0.20
0.75	10.31	0.41	5.15	0.21
1	10.56	0.42	5.28	0.21
2	10.82	0.43	5.41	0.22
3	10.90	0.44	5.45	0.22
4	10.98	0.44	5.49	0.22
5	11.05	0.44	5.53	0.22
6	11.13	0.45	5.56	0.22
7	11.20	0.45	5.60	0.22
8	11.28	0.45	5.64	0.23
9	11.35	0.45	5.68	0.23
10	11.43	0.46	5.71	0.23
11	11.50	0.46	5.75	0.23
12	11.58	0.46	5.79	0.23
13	11.65	0.47	5.83	0.23
14	11.73	0.47	5.86	0.23
15	11.80	0.47	5.90	0.24
16	11.88	0.48	5.94	0.24
17	11.95	0.48	5.98	0.24
18	12.03	0.48	6.0	0.24

Deformation has been calculated for the tunnel of 2.5m radius. The comparison of the calculated tunnel deformations for supported and unsupported conditions are plotted in Figure 7.8.

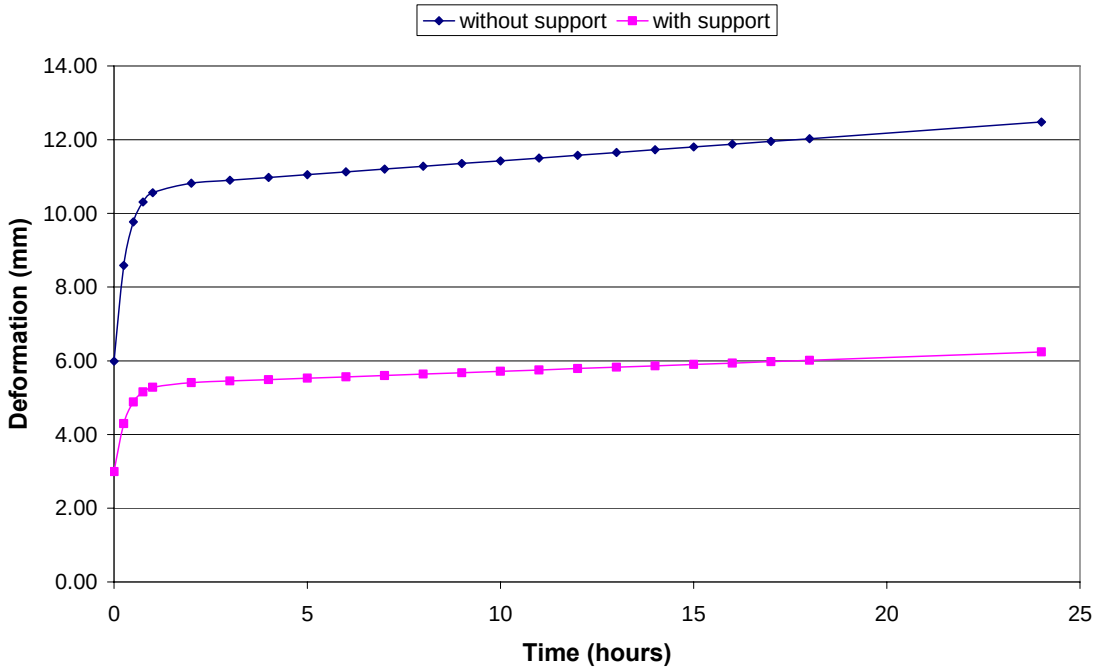

Figure 7.8 Time-dependent tunnel deformations with and without support.

In Figure 7.8, it is interesting to observe that not only the deformation amount but also the deformation rate of the supported tunnel is less than those of the unsupported tunnel. For example, instantaneous deformations are 3 and 6 mm for lined and unlined tunnel respectively. After 2 hours the deformation rate for unsupported tunnel is 0.08 mm/hour and for supported tunnel it is only 0.04 mm/hour. Thus the tunnel support reduces the instantaneous deformation and the deformation rate also.

7.2.3 Steady-state deformation rate

The steady-state creep rate is almost constant for a given stress level. Thus this rate multiplied by time gives the steady-state deformation for the respective time period. The total deformation for a given time period can be estimated by adding instant and steady-state deformations together. However, it will underestimate the total deformation as it does not include the primary-state creep deformation.

The steady-state strain rate itself is useful information. It helps in predicting tunnel convergence rate. On the basis of creep test results, an equation can be established for calculating the stress dependent steady-state strain rate. Necessary creep test results for the calculation are given in the Table 7.9. Test results show that higher stress levels lead to higher creep rates.

Table 7.9 Creep test data for calculating effect of stress level on the steady-state creep rates.

Sample	Stress (Pa)	Log_{10} Stress (Pa)	Steady-state creep rates	Log_{10} creep rates (1/s)
45	1.5 E+07	7.176	1.7 E-06	-5.769
412	2.0 E+07	7.301	40 E-06	-4.398
4-2	2.5 E+07	7.398	800 E-06	-3.097

Equations (5-2) and (5-3) are applicable to calculate steady-state creep rate at various stress levels. Details about these equations are given in Chapter 6.

$$\dot{\varepsilon}_{ss} = A'\sigma^{n} \tag{5-2}$$

$$\log \dot{\varepsilon}_{ss} = \log A' + n \log \sigma \tag{5-3}$$

Figure 7.9 shows the plotting of $\log \dot{\varepsilon}_{ss}$ versus log σ. The values of log A' and n are given by the intercept and slope of the line in Figure 7.9.

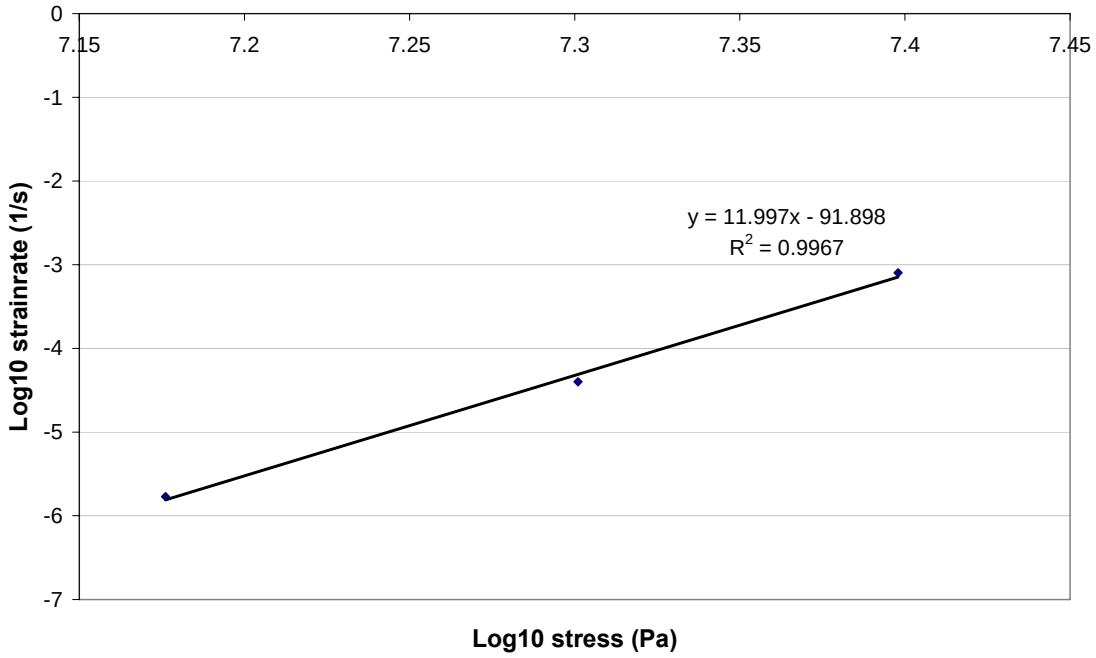

Figure 7.9 Log (creep rate) versus Log (stress) for gneissic rock samples from bore hole TDH1 of Melamchi project.

Figure 7.9 gives values 11.997 for n and -91.898 for log_{10} A'. Accordingly it assigns value 1.2647E-92 to A'. Replacing values of n and A' in Equation (5-2), it gives

$$\dot{\varepsilon}_{ss} = 1.265 * 10^{-92} \sigma^{12} \qquad (7\text{-}1)$$

By using Equation (7-1), the steady-state strain rate can be estimated for any constant stress level for the rock samples from the bore hole TDH1.

7.3 Correlating the total creep to the complete stress-strain diagram

The total deformation in a creep test of a rock, can be correlated with the respective deformation in the complete stress-strain curve. Theoretically the total creep strain should correspond to the respective strain indicated by the falling part of the complete stress-strain curve for the same stress level.

Tests for complete stress-strain curves were carried out in the laboratory in Department of Petroleum Engineering and Applied Geophysics, NTNU. It would be ideal to correlate the total creep deformations to the complete stress-strain curve for a uniaxially loaded test, i.e. at a zero confining pressure. But a complete stress-strain curve could not be achieved at zero confining pressure with controlled axial deformation rate. The sample broke with a bang after giving a short falling part of the curve and stress instantly dropped to zero. Three complete stress-strain curves have been produced with 0, 1.5 and 3 MPa confining pressures. The total creep strain for 20 MPa constant stress level, have been compared with the respective strain in the falling part of the complete stress-strain curve at 1.5 MPa confining pressure (Figure 7.10).

The total creep strain and the final strain at failure on the complete curve are comparable. The total creep strain is slightly larger than that given by the complete stress-strain test.

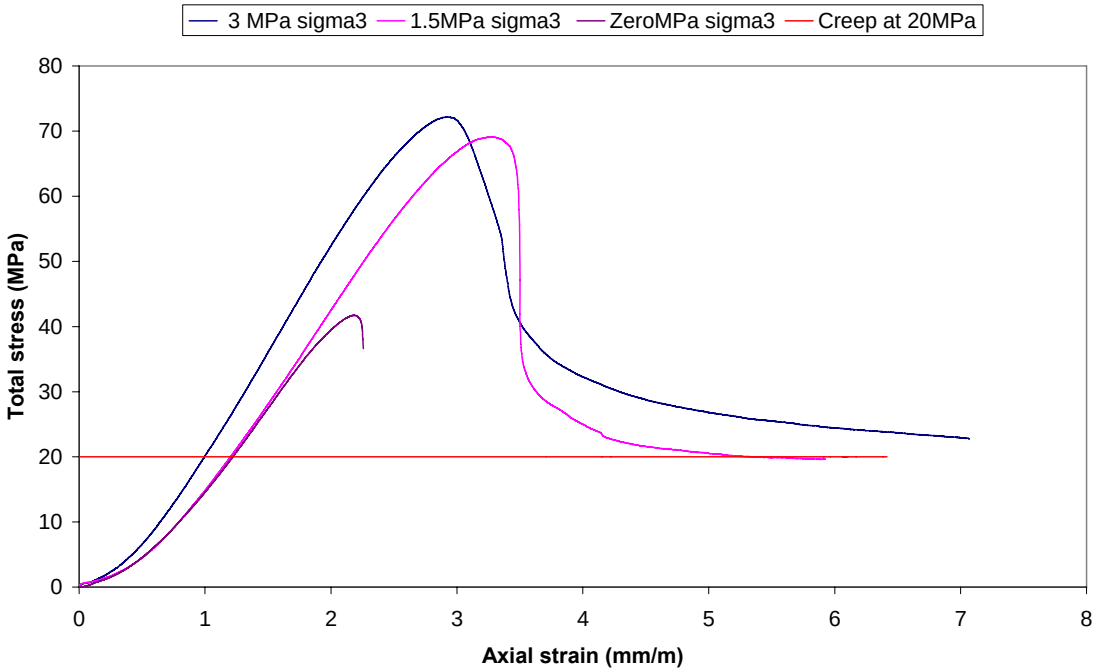

Figure 7.10 Correlation between total creep deformation and the respective total deformation in the complete stress-strain curve at 0, 1.5 and 3 MPa confining pressures.

8 Numerical modelling

8.1 Introduction

Design problems in rock mechanics practices can be dealt with by using one of the three analytical methods: *Physical models, Mathematical models and Numerical models.*

A major detraction from the use of physical models of any sort for prediction of the rock mass response is their high cost in time and effort. Similarly, complex geometry, non-homogeneity of the rock mass and non-linear constitutive behaviour of the medium cannot be dealt with by mathematical (closed form solution) models. Thus solution to the more complex excavation design problems may usually be obtained by use of numerical modelling procedures. The use of these techniques is now firmly embedded in rock mechanics practice (Brady and Brown, 1985). Numerical modelling can be used for analysing rock stress, deformations and many other parameters.

Numerical modelling means discretization of the rock mass into a large numbers of individual elements and simulate them for analysis. There are two main categories of numerical models: continuous and discontinuous models. In squeezing analysis, rock mass is considered continuous and time-dependent deformation is also to be considered. FLAC (Fast Langrangian Analysis of Continua) is a continuous model and it can incorporate time-dependent behaviour as well. In this thesis, FLAC^{3D} code has been used for numerical modelling.

8.2 FLAC numerical modelling code

FLAC is an explicit finite-difference program (FDM) and available in two and three dimensional analysis. The drawbacks of the explicit formulation (small time step and choice of damping) are overcome in this code, by automatic inertia and automatic damping. It models stages in the same way that they occur in reality. An FDM programme like FLAC may in some cases have advantages over finite element programme since they handle large grid distortions (geometric non-linearity) and non-linear material models in almost the same calculation time as small-strain linear problems. It simulates the behaviour of structures built of soil, rock or other materials that undergo plastic flow when their yield limits are reached. It includes evolution of progressive failure and collapse in hard rock mine and tunnel design and also time-dependent creep behaviour of viscous materials.

Transforming of the problems from a three-dimensional to a two-dimensional situation, is not either easy or correct when the materials are as complicated as rock masses.

Boundary condition and initial condition

A fixed boundary causes both stress and displacements to be underestimated, while a stress boundary does the opposite. The two types of boundary conditions bracket the true solution, so that it is possible to do tests with both boundaries and get a reasonable estimate of the true solution by averaging the two results (user's guide, pp 2-47).

In all the models used for both the projects, one stress boundary and five fixed boundaries have been used. Similarly, for initial condition, all the three principal stresses have been considered to be equal.

8.3 Case statement

Two tunnel cases have been considered for the modelling purpose. The first one is the case from the Khimti tunnel, a completed project. The second one is the case from the Melamchi tunnel, a planned project. Details about the projects are given in the previous chapters. Tunnel model shapes, input data, modelling results and discussions are given in the following sections.

8.4 Khimti tunnel modelling

8.4.1 Model set up and input data

A 24 m long tunnel section is represented in the model. A system of co-ordinate axes is defined with the origin in the centre of the tunnel; the z-axis points upward and the y-axis points along the axis of the tunnel. The model contains approximately 3,600 zones. The tunnel has been constructed in a weak Gneiss and Schist rocks and modelled as a Mohr-Coulomb material. As there is no rheological data available, time-effect is not included in the Khimti tunnel model. The tunnel was constructed with D-shape with curved portion on the top. Rock bolt (2.3 m in length and 20 mm in diameter) and shotcrete were the main tunnel support used in the Khimti tunnel. All the three principal stresses are assumed to be of same magnitude as that of the overburden pressure. A typical tunnel section used for the modelling is given in Figure 8.1.

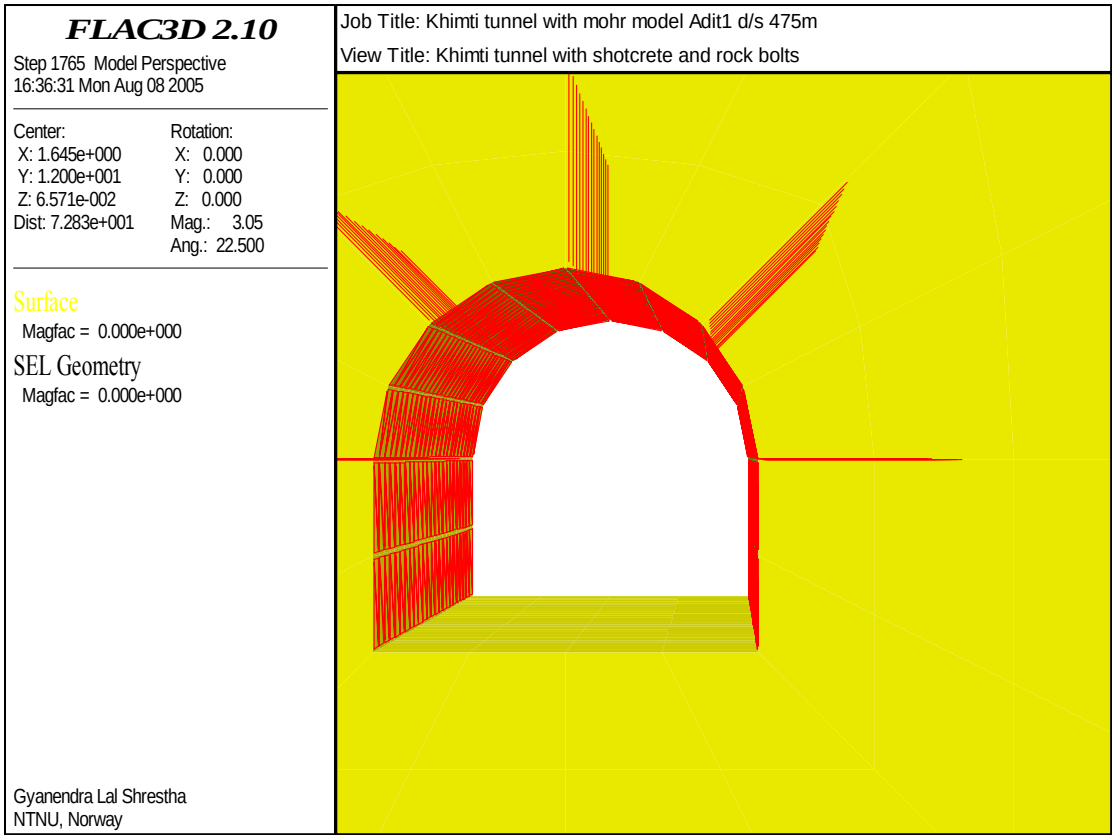

Figure 8.1 Tunnel model with rock bolt and shotcrete lining.

Input data have been obtained from the tunnel logs, registration of applied support and convergence measurement records. These three documents are the parts of the 'Khimti hydropower project: project completion report' (Statkraft Eng & BPC, 2001). Data given in the tunnel log has been used in 'RocLab' software to generate complete set of input data required for modelling in the FLAC^{3D} code.

Table 8.1 Input data for the numerical modelling of the Khimti tunnel. (Poisson's ratio 'υ' = 0.2 and density 'γ' = 0.026 MN/m^3).

Tunnel section	σ_o (MPa) with $\sigma_1=\sigma_2=\sigma_3$	Cohe-sion (MPa)	Frict-ion angle (degr-ee)	Tensile strength (MPa)	Defor-mation modul-us (MPa)	Shear modul-us (MPa)	Bulk modul-us (MPa)	Shotcr-ete lining (m)
Adit1 d/s 475	2.548	0.471	31.6	0.002	1000.0	416.6	555.5	0.10
Adit1 d/s 500	2.600	0.261	19.7	0.004	668.3	278.3	371.1	0.10
Adit1 d/s 515	2.600	0.210	17.5	0.003	446.7	186.1	248.1	0.20
Adit1 d/s 580	2.886	0.275	20.4	0.005	749.9	312.4	416.6	0.20
Adit1 d/s 665	2.912	1.739	32.5	0.010	2223.5	926.4	1235.2	0.05
Adit 2 d/s 441	3.276	3.173	37.9	0.028	5302.5	2209.4	2945.9	0.05
Adit 2 d/s 601	3.588	0.282	20.6	0.005	794.3	331.0	441.3	0.20
Adit 2 d/s 895	5.148	1.868	37.1	0.026	4881.6	2034.0	2712.0	0.10
Adit 2 u/s 1283	5.512	0.578	20.9	0.012	1189.9	495.8	661.1	0.10
Adit 2 u/s 1357	6.786	1.691	35.0	0.015	3262.6	1359.4	1812.5	0.10
Adit 2 u/s 1730	2.470	1.107	34.8	0.007	2241.4	933.9	1245.2	-
Adit 3 u/s 15	3.380	2.115	36.6	0.021	4188.3	1745.1	2326.8	0.10
Adit 3 u/s 59	4.108	1.967	35.1	0.014	3140.7	1308.6	1744.9	0.07
Adit 3 u/s 200	7.176	2.486	37.2	0.027	5023.8	2093.2	2791.0	0.10
Adit 3 u/s 210	7.176	2.205	37.5	0.026	4977.8	2074.1	2765.4	0.07

Adit 3 d/s 220	3.640	0.146	22.1	0.001	446.1	185.9	147.9	0.15
Adit 3 u/s 235	7.384	2.315	35.7	0.019	3767.3	1569.7	2092.9	0.07
Adit 3 u/s 340	7.800	1.679	31.9	0.008	1981.7	825.7	1100.9	0.15
Adit 3 u/s 345	7.800	0.976	32.2	0.005	1586.8	661.1	881.5	0.15
Adit 4 u/s 503	5.850	0.846	35.0	0.008	2307.0	961.2	1281.7	0.08
Adit 4 u/s 550	5.668	0.764	25.0	0.033	2663.9	1110.0	1479.9	0.07
Adit 4 u/s 852	2.964	2.451	36.9	0.025	4742.7	1976.1	2634.9	0.06
Adit 4 u/s 876	2.964	2.555	37.8	0.032	5636.8	2348.7	3131.5	0.10
Adit 4 u/s 974	2.912	0.195	28.8	0.001	421.2	175.5	234.0	0.20
Adit 4 u/s 1013	2.912	0.134	21.2	0.001	375.4	156.4	208.6	0.07
Adit 4 u/s 1045	2.912	0.389	28.8	0.001	595.7	248.2	330.9	0.08

Commands used in the modelling

A set of commands have been used to simulate each of the 26 tunnel sections. The input data used for the modelling are given in the Table 8.1. For the simplification in the modelling, rock bolts are provided in 1.5 m*1.5m pattern covering the arch portion only and shotcrete has been applied from invert to invert. However, only a set of commands used to generate and simulate the tunnel model with tunnel supports is given in Appendix C.

8.4.2 Modelling and stability indicators

In order to carry out the numerical modelling for the Khimti tunnel, 26 tunnel sections have been considered for which the tunnel convergence data are available. Model was run for each of the 26 tunnel sections. This numerical modelling has been carried out to compare the measured tunnel convergence and the convergence estimated by the modelling. In addition, other modelled indicators have also been evaluated to assess the stability.

There are several indicators that can be used to assess the state of the numerical model - whether the system is stable or unstable (*i.e.* in steady-state plastic flow). Unbalanced force ratio and gridpoint velocities are basic indicators to assess if the system is stable or in steady-state plastic flow. In stable state, both these indicators reduce to nearly zero values. Otherwise in steady-state plastic flow condition, it continues with non-zero values. Similarly, 'block state' indicates the yielding condition of the system. These indicators can be checked to assess the stability of the tunnel.

Histories for unbalanced force, displacement and gridpoint velocity are recorded at 12 m from the starting point of the tunnel. It is the mid section of the 24 m long tunnel section considered in the modelling. The unbalanced force, velocity, the extent of the plasticity region around the tunnel, tunnel convergence and stress condition are assessed. These results are discussed in the respective sections given below.

8.4.3 Maximum unbalanced force ratio

At equilibrium, the algebraic sum of the forces at each grid point is zero. It is assessed as a ratio of the maximum unbalanced force to the representative internal force. It is one of the indicators to assess the true equilibrium condition. This ratio of a value 1/100,000 is considered to be small enough to indicate that the system is in equilibrium condition.

For all the 26 tunnel sections, 'unbalanced force ratio' converged to 1/100,000, indicating that the tunnel system is stable. As an example, the Figure 8.2 shows the 'Unbalanced force' for the Khimti tunnel section at the Adit1 downstream chainage 475 m.

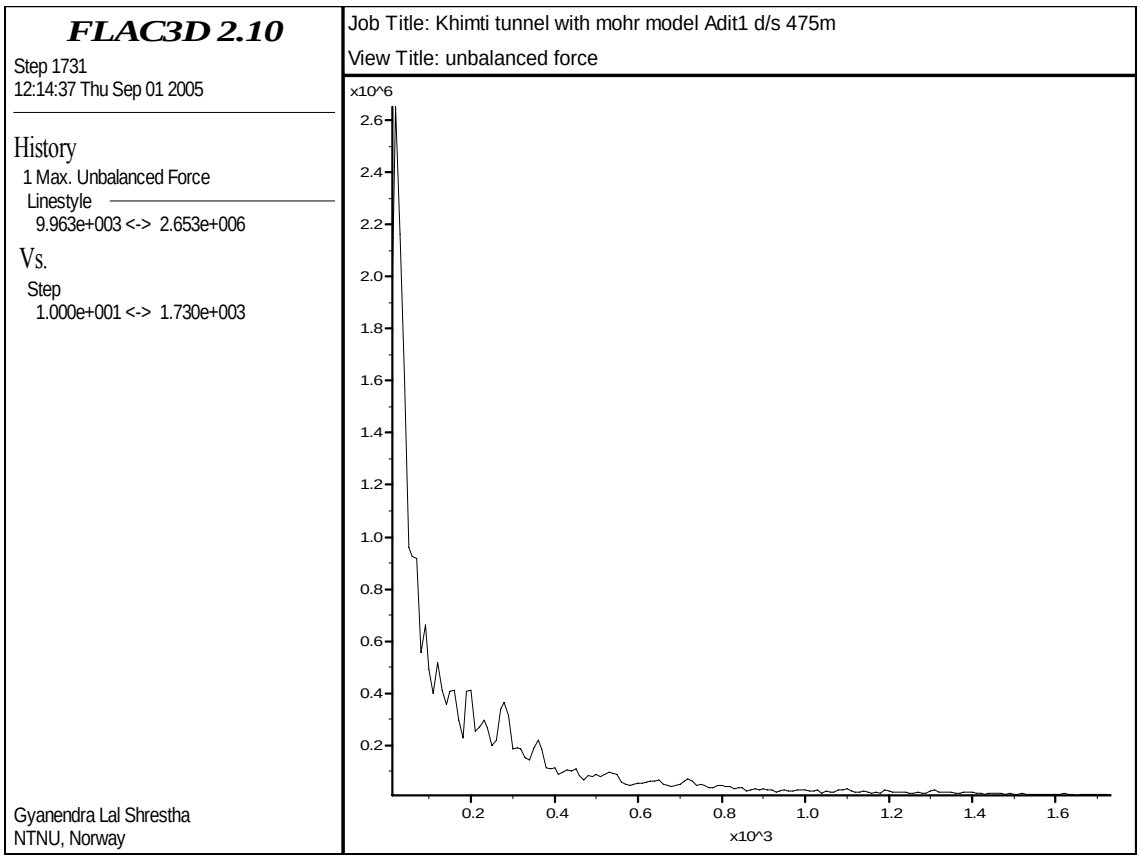

Figure 8.2 The maximum unbalanced force for the midsection of the Khimti tunnel.

8.4.4 Gridpoint velocity

In the modelling, grid velocities are assessed by selecting a certain point on the tunnel contour. If they have all converged to near-zero, then absolute equilibrium has occurred. If the velocity has converged to a nonzero value, then steady plastic flow is occurring at the gridpoint corresponding to that history.

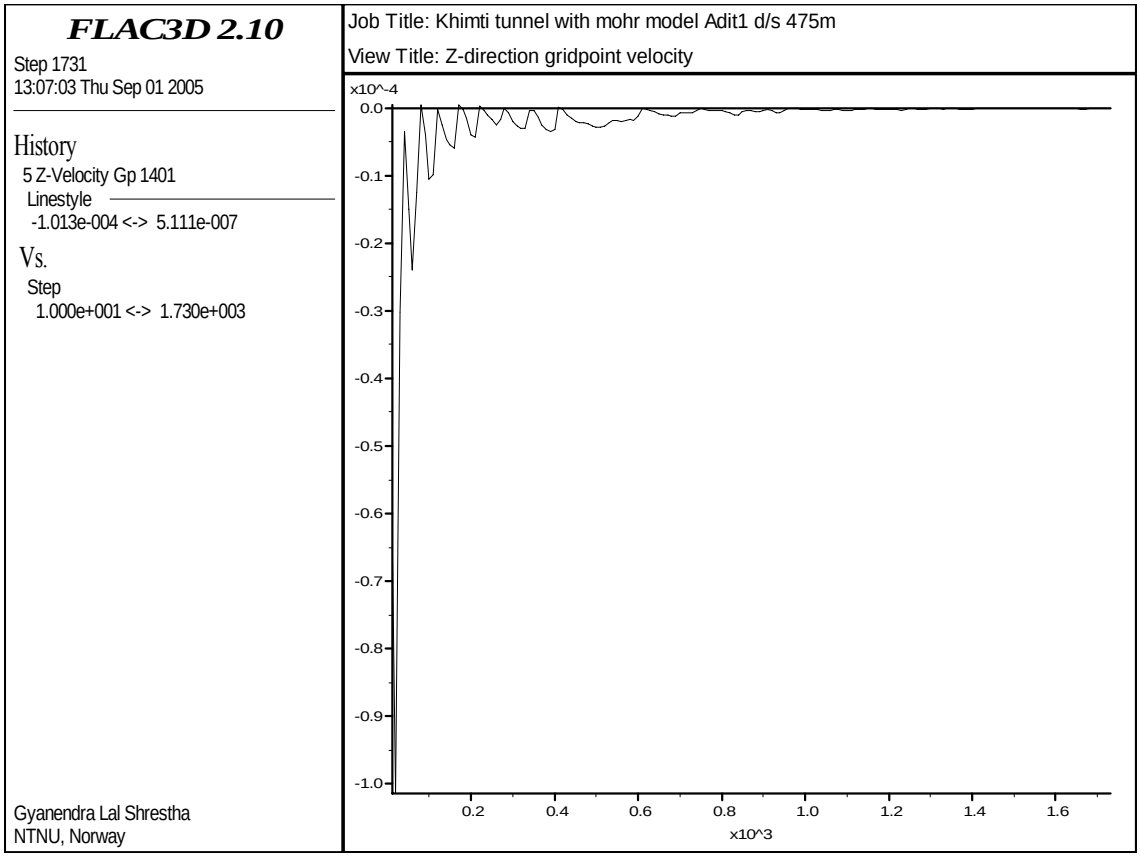

Figure 8.3 Z-direction gridpoint velocity at the tunnel crown at the middle of the 24 m long tunnel section.

A typical velocity convergence for a tunnel crown is presented in the Figure 8.3.

For all the 26 tunnel sections, 'z-direction gridpoint velocity' at crown came down to zero, indicating that the tunnel system is stable.

8.4.5 Block state

In FLAC^{3D} code, it is possible to check rock mass zones around the tunnel if the stresses satisfy the yield criterion. Such an indication usually denotes that plastic flow is occurring, but it is possible for an element simply to sit on the yield surface without any significant flow taking place. The diagnosis is confirmed if the velocity plot also indicates motion corresponding to the same mechanism.

In 12 out of the 26 tunnel sections, stress condition satisfied the yield criterion for some of the zones around the tunnel. However, the gridpoint velocity converged to near zero and the unbalanced force ratio converge to 1/100000 indicating that the tunnel systems were in equilibrium. So those zones in the 12 out of the 26 tunnel sections might be sitting on the yield surface without any significant flow taking place, indicating equilibrium condition (Figure 8.4).

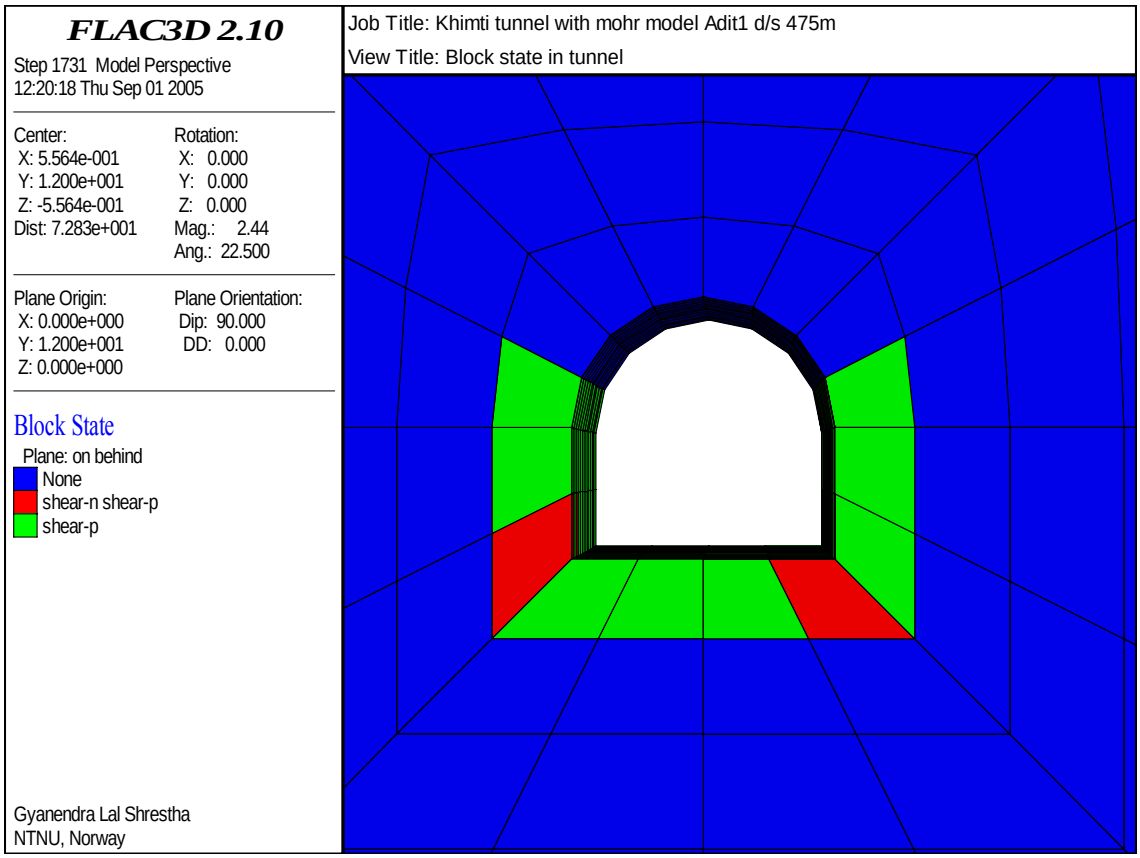

Figure 8.4 Block state in the tunnel indicating yield condition.

8.4.6 Tunnel convergence

There are some differences between input data used in the analytical and numerical modelling. Analytical methods do not use cohesion and tensile parameters, but the numerical modelling code, FLAC^{3D} uses cohesion and tensile strength. Inverted D-shaped tunnel has been considered for this modelling whereas circular tunnel section is considered in analytical methods. Thus the tunnel convergence given by analytical methods may be different from that given by the FLAC^{3D}. Tunnel convergence estimated by the modelling, particularly at Adit1 d/s 601, Adit3 d/s 220 and Adit4 u/s 1013 are much lower than those measured and analytically estimated values.

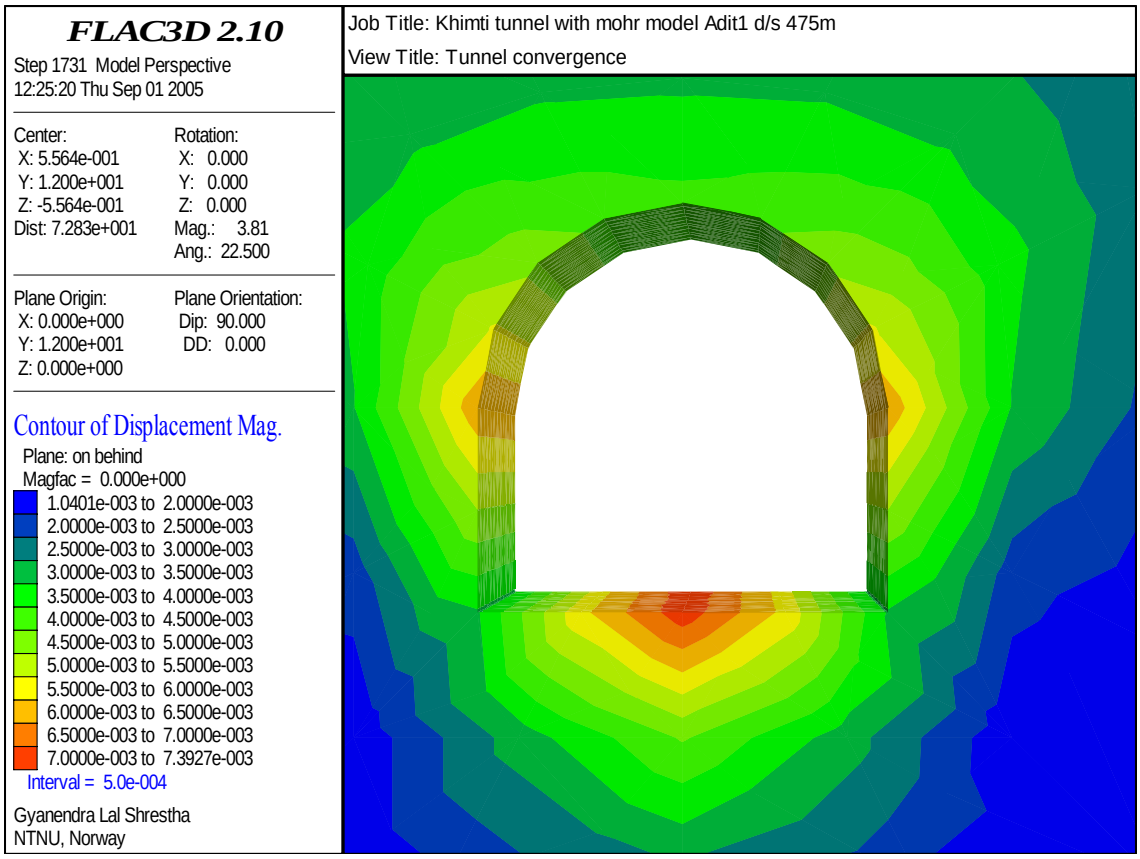

Figure 8.5 A typical figure showing tunnel convergence magnitude in contour.

Total tunnel convergence is obtained by adding deformations on both the tunnel side walls. That is 13 mm for the figure given above.

Simulation results for the tunnel convergence are given for all the 26 tunnel sections in Table 8.2.

Table 8.2 The tunnel convergence obtained by FLAC^{3D} modelling, calculated by analytical method (Duncan-Fama approach) and measured at the 26 tunnel sections.

Tunnel section	σ_o (MPa) with $\sigma_1=\sigma_2=\sigma_3$	Tunnel convergence by modelling (mm)	Tunnel convergence by analytical method (mm)	Tunnel convergence measured (mm)	Block state around tunnel	Maximum stress around tunnel (MPa)
Adit1 d/s 475	2.548	12	7.0	30.9	Yielding	4 at wall
Adit1 d/s 500	2.600	60	11.2	160.2	Yielding	3 at crown
Adit1 d/s 515	2.600	94	7.6	110.0	Yielding	2 at crown
Adit1 d/s 580	2.886	38	6.2	32.3	Yielding	3.5 at crown
Adit1 d/s 665	2.912	6	5.5	11.8	No Yielding	4.5 at wall
Adit 2 d/s 441	3.276	3	3.3	1.3	No Yielding	5.5 at wall
Adit 2 d/s 601	3.588	55	8.0	7.5	Yielding	3 at crown
Adit 2 d/s 895	5.148	5	4.0	11.5	No Yielding	8 at wall
Adit 2 u/s 1283	5.512	46	32.9	1.0	Yielding	6.5 at crown
Adit 2 u/s 1357	6.786	9	8.2	6.1	No Yielding	11 at wall
Adit 2 u/s 1730	2.470	6	5.3	11.6	No Yielding	4 at wall & crown
Adit 3 u/s 15	3.380	4	4.3	17.0	No Yielding	5.5 at wall
Adit 3 u/s 59	4.108	6	5.4	13.2	No Yielding	6.5 at wall
Adit 3 u/s 200	7.176	7	7.2	38.7	No Yielding	12 at wall
Adit 3 u/s 210	7.176	7	7.6	18.2	No Yielding	12 at wall
Adit 3 d/s 220	3.640	200	20.0	32.0	Yielding	2 at crown
Adit 3 u/s 235	7.384	9	10.5	62.0	No Yielding	12 at wall
Adit 3 u/s 340	7.800	16	18.1	14.0	No Yielding	13 at wall
Adit 3 u/s 345	7.800	19	24.0	9.0	Yielding	13 at wall

Adit 4 u/s 503	5.850	11	11.1	9.7	No Yielding	9.5 at wall
Adit 4 u/s 550	5.668	12	13.2	5.5	Yielding	8 at wall & crown
Adit 4 u/s 852	2.964	3	3.1	1.0	No Yielding	5 at wall & crown
Adit 4 u/s 876	2.964	3	2.6	9.7	No Yielding	5 at wall
Adit 4 u/s 974	2.912	32	13.5	7.9	Yielding	4 at wall
Adit 4 u/s 1013	2.912	188	48.5	47.7	Yielding	1.5 at crown
Adit 4 u/s 1045	2.912	19	15.9	4.0	Yielding	4.5 at wall

The tunnel convergence magnitudes obtained by modelling and analytical method have been found to be lower than that measured in the tunnel for 12 and 14 tunnel sections respectively (Table 8.2). In general, it should have been the case for all the 26 sections. That is justifiable too as the time effect was not considered in those methods whereas in reality time effect contributes for the additional convergence.

The horizontal tunnel convergence has been found to be larger than the vertical convergence.

8.4.7 Maximum principal stress location

The maximum principal stress is compressive; and the compression is indicated by a negative sign (Figure 8.6). In general, the tunnel sections in relatively stronger rock mass (with deformation modulus of about 1 GPa and above), have been found to have the maximum stress located in the side wall whereas in the relatively weaker rock mass, the maximum stress is located in the tunnel crown. Figure 8.6 is the typical graphical presentation showing the location and magnitude of the maximum principal stress. Location and magnitude of the maximum principal stress are given in Table 8.2.

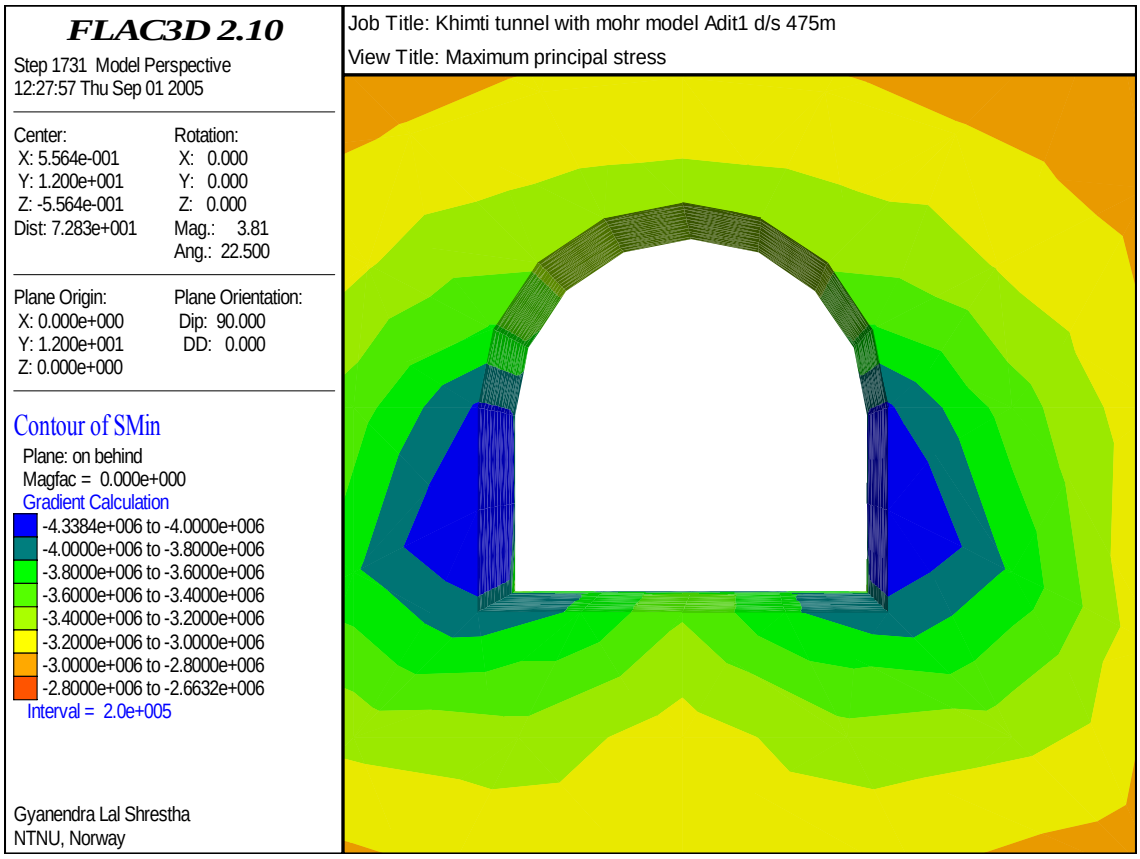

Figure 8.6 Location and magnitude of the maximum principal stress in rock mass. Compression is indicated by the negative signs.

8.4.8 Discussions on the Khimti modelling results

History records showed that for all the tunnel sections, unbalanced force ratio converged to 1/100,000 and gridpoint velocity converged to near zero value. Thus though some blocks around the 12 tunnel sections satisfied the yield criterion, they only indicated that they might be sitting on the yield surface without any significant flow taking place.

The tunnel convergence magnitudes obtained by modelling and analytical method have been found to be lower than the measured values in the tunnel for 12 and 14 tunnel sections respectively (Table 8.2). In general, it should have been the case for all the 26 sections. That is justifiable as the time effect was not considered in those methods whereas in reality time effect contributes for the additional convergence. However, the input data was obtained from the tunnel log and those data were the observational estimation without any laboratory tests or any in-situ instrumentation. Thus input data might have been far from the reality for the sections where the measured convergences are lower than the calculated and modelled values.

Here, the comparison has been made for the horizontal tunnel convergence as the field measurement was carried out for the horizontal convergence (Figure 8.7).

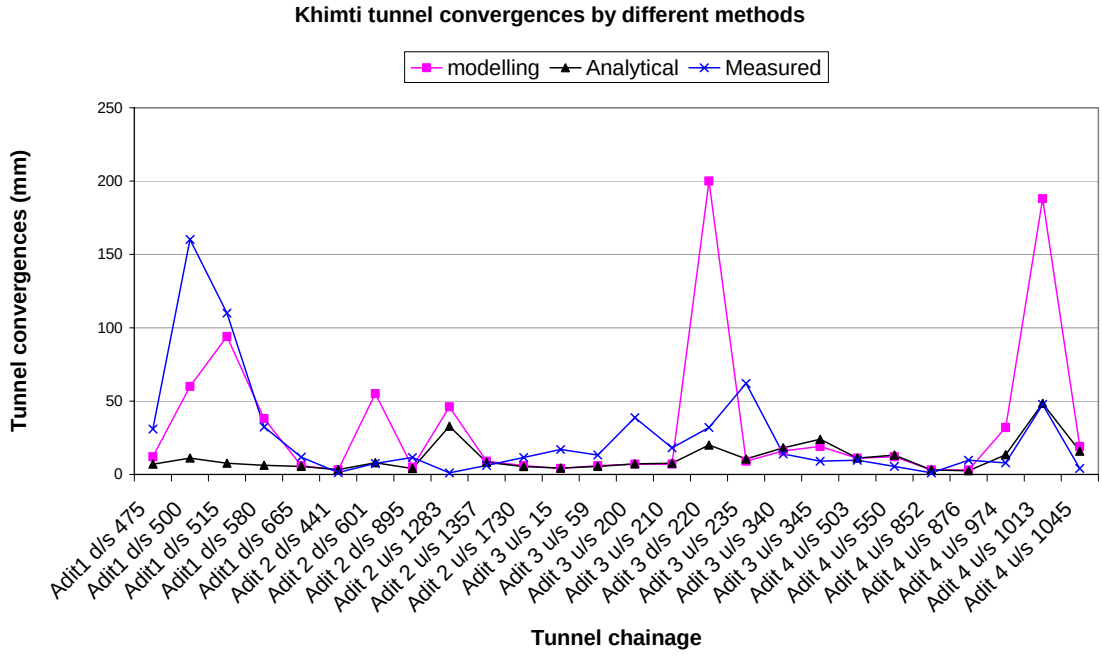

Figure 8.7 Khimti tunnel convergence obtained by FLAC^{3D} modelling, analytical method (Duncan-Fama) and field measurement.

It has been observed that the tunnel sections in relatively stronger rock mass, have been found with the maximum stress located in the side wall whereas in the relatively weaker rock mass, the maximum stress is located in the tunnel crown. In the weaker rock mass, because of the arch action, the maximum stress might have been sustained in the crown.

Numerical modelling gives locations where displacement and stress condition are critical, which are not possible by analytical methods. However, numerical modelling uses additional input data such as cohesion and tensile strength of the rock mass; and only reasonable values for these parameters can give realistic results.

8.5 Melamchi tunnel modelling

8.5.1 Model setup

Melamchi tunnel has been planned in a hilly terrain and thus overburden thickness above the tunnel level varies from few hundred metres to 1200 m. In this case, rock mass strength and the overburden thickness play important roles on the stability of the tunnel.

In modelling, excavation is assumed to be carried out at once. Rock mass is considered to be particulate that behaves as a continuous body. Therefore, FLAC ^{3D} code has been used to analyze stability of the unlined tunnel in this rock. Typical two sets of commands used to generate and simulate the Melamchi tunnel model (for GSI 45) with and without support are given in Appendix C. For the Melamchi tunnel, modelling was carried out by Sharma (2003) using Phase^2 code.

8.5.2 Input data

This numerical modelling has been carried out to assess stability of the tunnel. As used in the empirical and analytical designs (Chapter 7), circular tunnel has been used for this present modelling also. Following input data have been obtained from the lab test results (Chapter 6) on the drilled cores (EDCO, 2001) and 'Roclab' software:

Table 8.3 Input data for the numerical modelling of the Melamchi tunnel, generated from 'Roclab' software. (Poisson's ratio 'υ' = 0.21 and density 'γ' = 0.027 MN/m^3)

Rock mass	Cohesion (MPa)	Friction angle (degree)	Tensile strength (MPa)	Deformation modulus (MPa)	Shear modulus (MPa)	Bulk modulus (MPa)
GSI = 70	3.31	43.6	0.177	19748	8160	11349
GSI = 45	2.33	36.2	0.027	4683	1935	2691

Time effect has also been considered in the Melamchi tunnel model. In order to simulate time-dependent tunnel deformation, rheological parameters of the rock are needed. In order to correlate to the analytical calculation, instead of 7.5, 10 and 12.5 MPa, 8.1, 10.8 and 13.5 MPa in-situ stress values have been used in this modelling. The stress level and the respective calibrated rheological parameter values are same as given in Table 7.6 in chapter 7.

Creep test is not possible on the rock mass with discontinuities. Thus the time-dependent deformation modelled in this chapter, is supposed to be lower than that takes place in the rock mass with the discontinuities.

8.5.3 Modelling and stability indicators

In the Melamchi model, Mohr model has been used to simulate the tunnel excavation in the rock mass. It gives the tunnel deformation without considering the time-effect. Then the time-dependent deformation has been obtained by using 'Burgers' model. However, rheological parameters used in the 'burgers' model, have been obtained by carrying out creep tests on the intact rock samples only.

Six modellings are carried out without considering time effect and six others with the time effect. So in total, 12 simulations have been carried out. Histories for unbalanced force, displacement and gridpoint velocity are recorded at 12 m from the starting point of the tunnel. It is the mid section of the 24 m long tunnel section considered in the modelling. The unbalanced force ratio, velocity, the extent of the plasticity region around the tunnel, tunnel convergence and stress condition are assessed. These results are discussed in the respective sections given below.

8.5.4 Maximum unbalanced force ratio, gridpoint velocity and block state

For all the 12 simulations, 'unbalanced force ratio' converged to 1/100,000, indicating that the tunnel system is stable. Figure 8.8 shows the 'Unbalanced force' for the Melamchi tunnel with GSI 45 with in-situ stress 8.1 MPa .

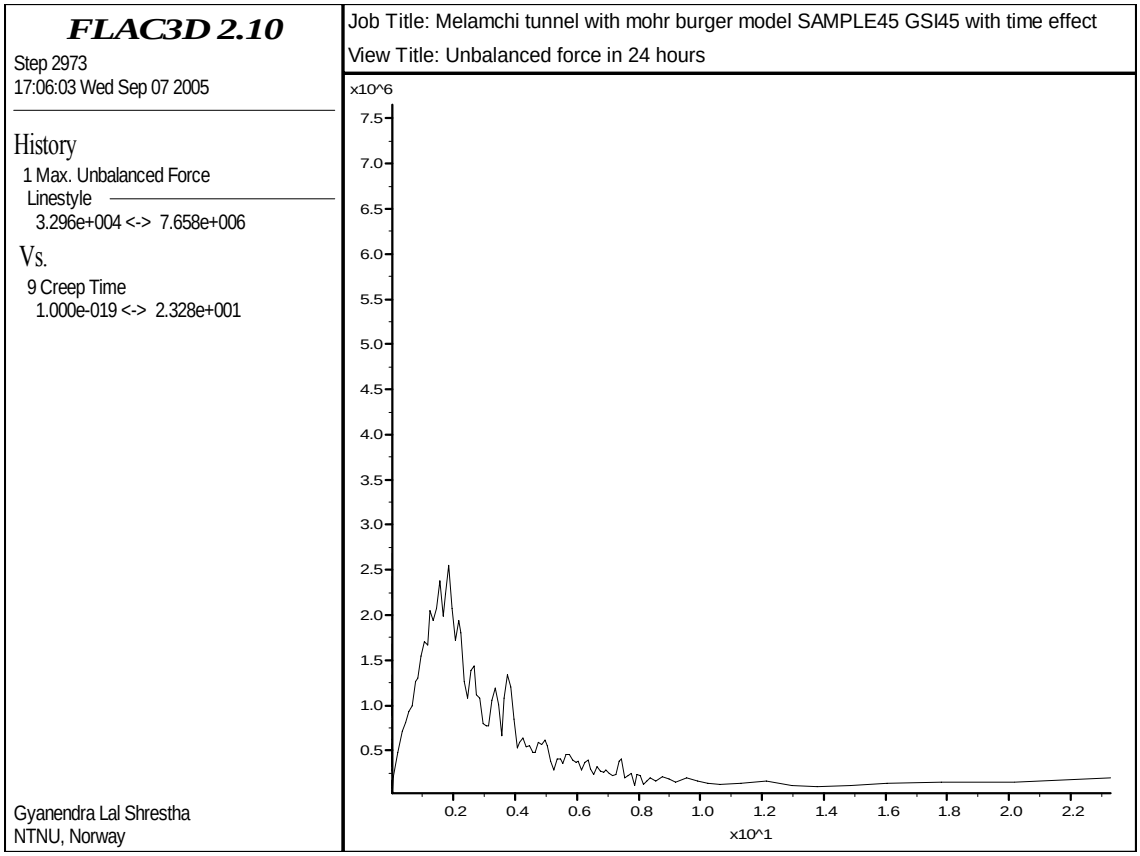

Figure 8.8 The maximum unbalanced force for the midsection of the Melamchi tunnel.

For all the 12 simulations, 'z-direction gridpoint velocity' at crown came down to near zero, indicating that the tunnel systems are stable.

A typical velocity convergence for a tunnel crown is presented in the Figure 8.9.

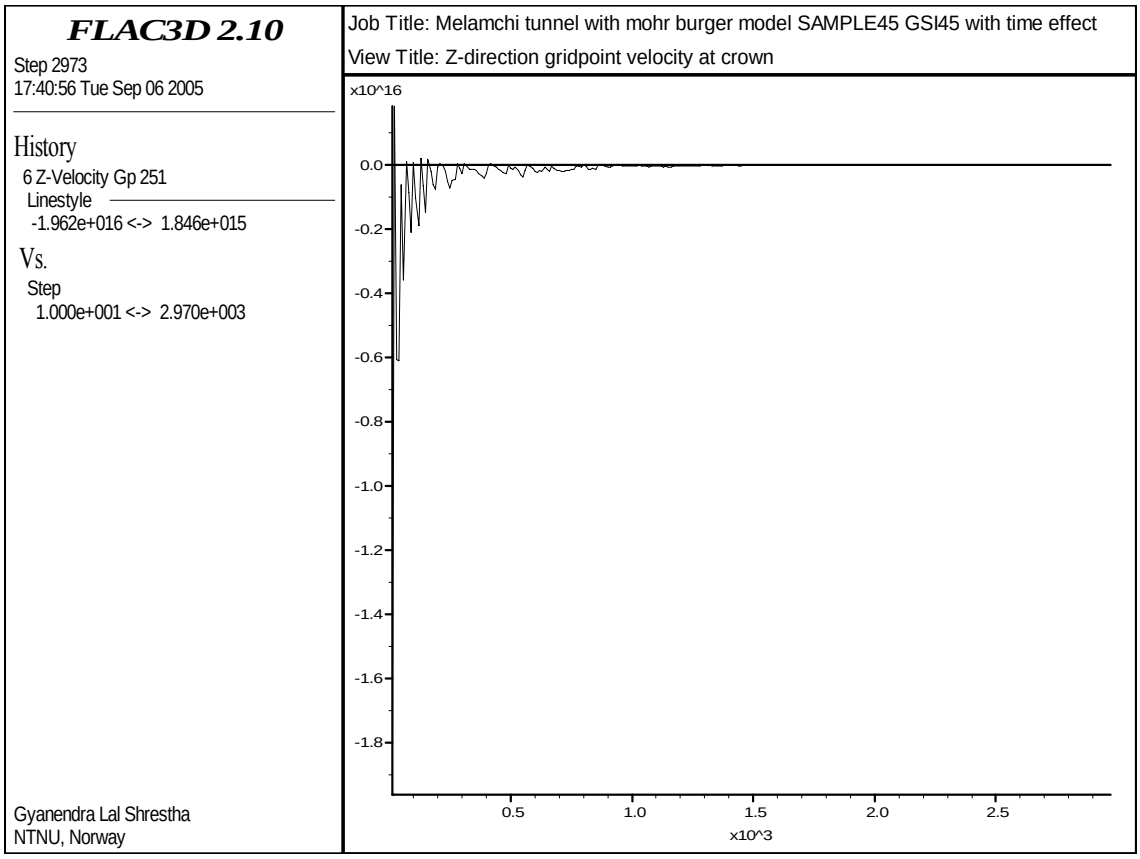

Figure 8.9 Z-direction gridpoint velocity at the tunnel crown.

In all the 12 simulations, yielding did not take place in none of the zones around the tunnel. A typical block state figure is given in the Figure 8.10.

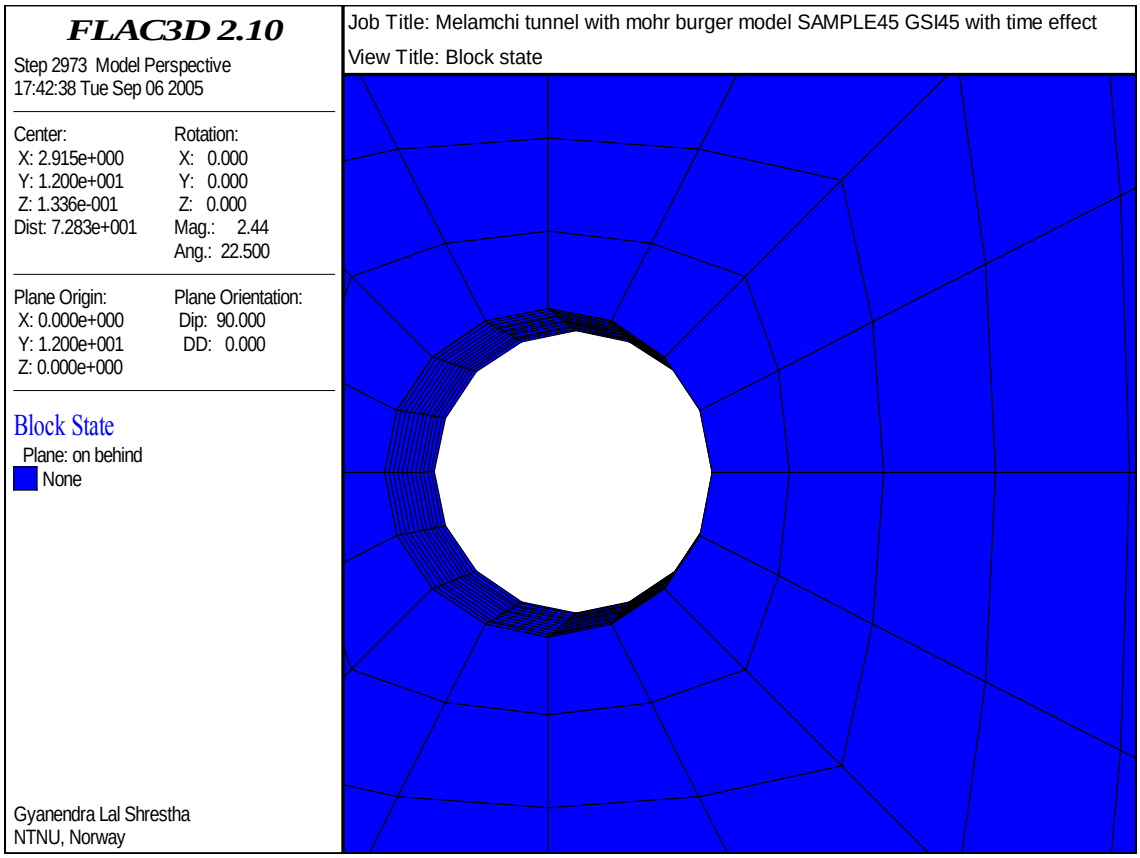

Figure 8.10 Block state around the tunnel with GSI 45 and in-situ stress 8.1 MPa.

8.5.5 Tunnel convergence with and without time effect

The numerical modelling code FLAC^{3D} uses cohesion and tensile strength but analytical methods do not use these parameters. Circular tunnel section has been considered for the both methods. For all the six simulations, tunnel deformations given by the analytical method and the FLAC^{3D} (without the time-effect) are found to be nearly equal.

The tunnel convergence magnitudes obtained by modelling (with no time effect) and analytical method have been found to be lower than that given by the modelling with time effect (Table 8.4).

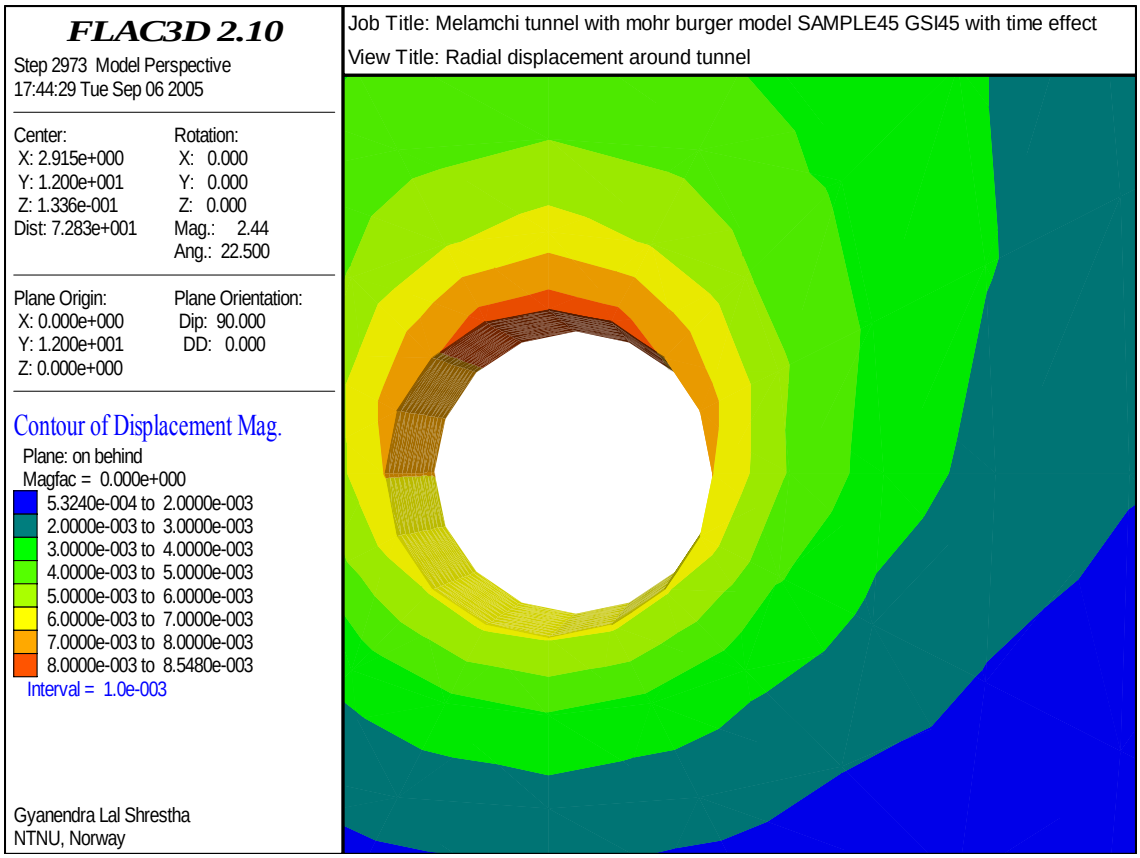

Figure 8.11 A typical figure showing the magnitude of the radial deformation in the Melamchi tunnel contour.

The maximum radial deformation is located in the tunnel crown in cases of all the 12 simulations carried out for the Melamchi tunnel. Results for the tunnel deformations for all the 12 simulations are given in Table 8.4.

Tunnel radial deformation pattern for 24 hours is shown in the Figure 8.12.

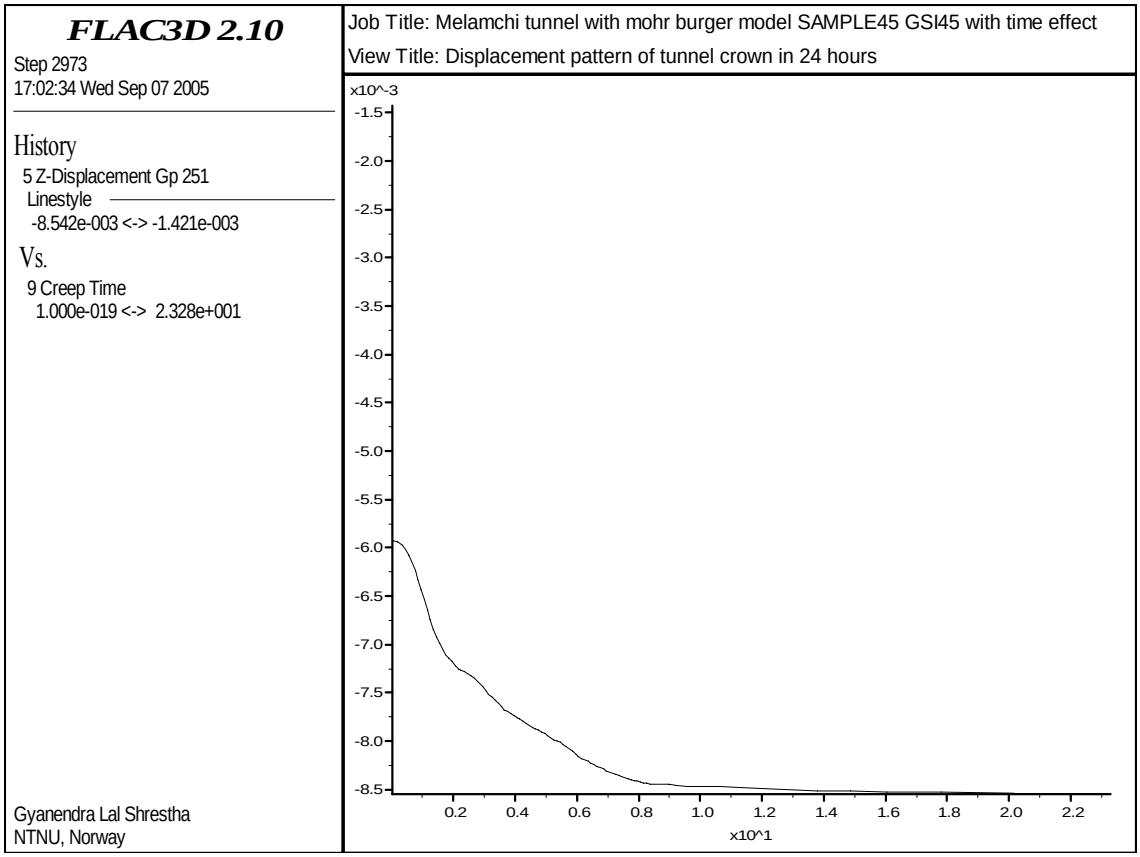

Figure 8.12 Displacement pattern of tunnel crown in 24 hours.

Table 8.4 Comparison of tunnel convergences calculated by the analytical method (Duncan-Fama approach) and obtained by FLAC^{3D} with and without time effect.

Rock mass condition	σ_o (MPa) with $\sigma_1=\sigma_2=\sigma_3$	Tunnel radial deformation (mm)			Block state around tunnel	Maximum stress (MPa) and location[2]
		modelling without time effect[1]	modelling with time effect for 24 hrs[1]	analytical method without time effect		
GSI 70	8.1	1.35	4	1.25	Not yielding	13.8
GSI 70	10.8	1.80	10	1.75	Not yielding	18.0
GSI 70	13.5	2.30	16	2.25	Not yielding	23.0
GSI 45	8.1	5.90	8	5.75	Not yielding	13.8
GSI 45	10.8	8.00	16	8.50	Not yielding	18.0
GSI 45	13.5	10.00	23	12.00	Not yielding	22.7

***Notes**: 1) The maximum deformation is found in the tunnel crown.*

2) The maximum principal stress is located around the whole tunnel contour.

8.5.6 Maximum principal stress location

The maximum principal stress is compressive. In all the 12 simulations, the maximum principal stress is located around the tunnel contour. Figure 8.13 is the typical graphical presentation showing the location and magnitude of the maximum principal stress.

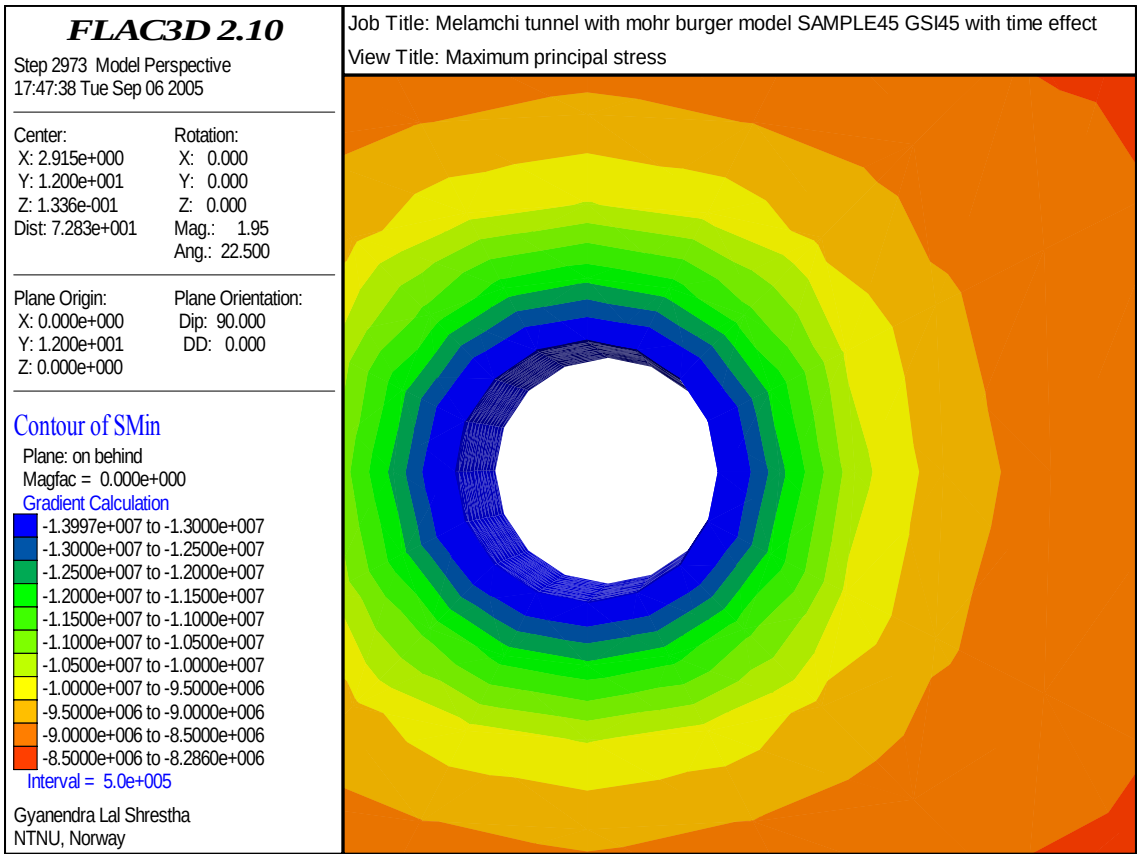

Figure 8.13 Location and magnitude of the maximum principal stress in rock mass. Compression is indicated by the negative signs.

8.5.7 Discussions on the Melamchi modelling results

History records showed that for all the 12 simulations, unbalanced force ratio converged to 1/100000 and gridpoint velocity converged to near zero value. None of the blocks around the 12 tunnel simulations satisfied the yield criterion. All these simulations indicate that the tunnel systems are stable. It is to be noted that time effect has been considered in the modelling by using rheological parameters. These parameters have been obtained based on the strain-time curves for the intact rock samples. As all the three applied stress levels are lower than the 'critical stress level', plastic condition did not take place around the tunnel.

The tunnel convergence magnitudes obtained by modelling (with no time effect) and analytical method have been found to be lower than that given by the modelling with

time effect. That is justifiable too as the time effect contributes for the additional convergence.

The deformation at the tunnel crown has been found to be largest in the tunnel section in all the 12 simulations. Figure 8.14 shows the three different radial deformations at tunnel crown for the same six tunnel conditions. One set of deformations was calculated by the analytical method and two sets obtained by the FLAC^{3D} modelling with and without time effect. Deformations calculated by the analytical method and those obtained by the FLAC^{3D} modelling without time effect, are almost equal. The analytical method and the numerical modelling, both consider the circular tunnel section. The analytical method calculates total deformation using only the rheological parameters based on the intact rock condition only. On the otherhand, the numerical modelling considered the rock mass condition with GSI 45 and 70 for the instantaneous deformation; and rheological parameters based on the intact rock condition for the time-dependent deformation. Thus the time-dependent deformations obtained by the analytical methods (final results for 24 hours in Table 7.5) are different from that obtained by the numerical modelling. However, deformation considering time effect increases with the increase in stress magnitude. It is to be noted that the deformation with time effect in the Figure 8.14, is only for the 24 hours time duration.

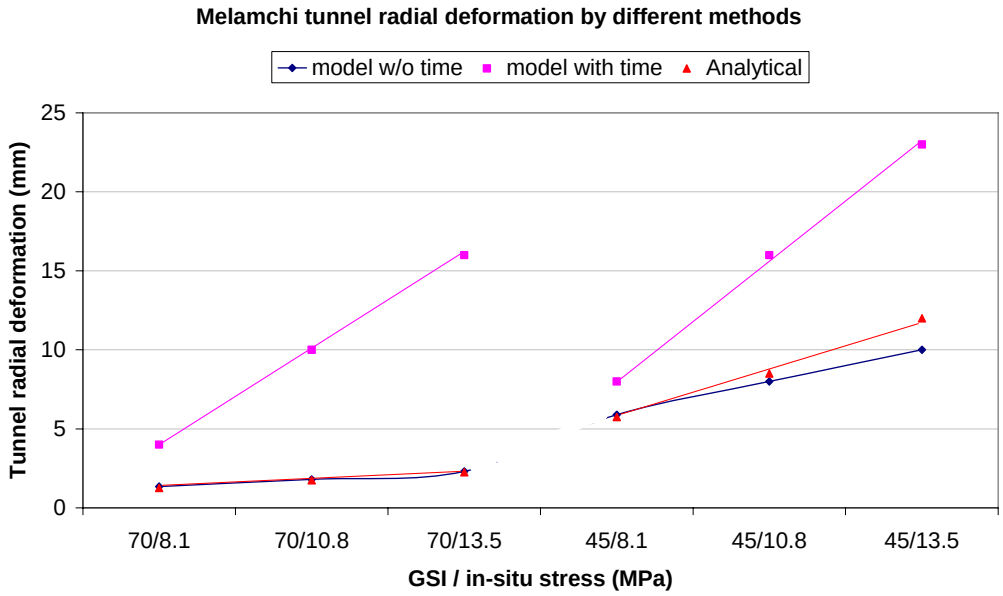

Figure 8.14 Three sets of the tunnel radial deformations: one set by the analytical method, two sets by the FLAC^{3D} with and without the time effect.

The maximum principal stress is around the tunnel contour. This may be because of the circular shape. Moreover, the rock mass condition around the tunnel might be strong enough and the arch action also might have contributed to sustain the maximum principal stress.

9 Conclusions and recommendations

9.1 Conclusions

Based on this thesis, the following conclusions can be made:

9.1.1 Tunnel stability analysis approaches and influencing rock mass properties.

1) There are two empirical and three semi-analytical approaches available for squeezing identification and tunnel support design. The available analytical approaches are not only for evaluating the squeezing potential in the tunnel. They are also applicable to general tunnel stability analysis. Based on the case study, Goel's (1994) empirical approach, Hoek-Marinos's (2000) semi-analytical approach and two analytical approaches by Duncan-Fama (1993) approach; and Carranza-Torres & Fairhurst (2000) are found to be convenient to use. Most of the approaches are based on the circular tunnel with hydrostatic stress condition. The results given by these approaches are however a very good start for tunnels with other shapes and stress condition as well.

2) Goel's (1994) empirical approach uses five parameters of the Q-method, tunnel size and overburden depth. Thus this approach is sensitive to these 7 parameters. Hoek-Marinos's (2000) semi-analytical approach uses three rock strength parameters namely, σ_{ci}, m_i and GSI. The σ_{ci}, is determined by laboratory test. There is not much variation for m_i value for a given rock type. GSI parameter is estimated by the visual observation and it has a significant effect on this approach. So care should be taken to estimate the value of this parameter. Carranza-Torres & Fairhurst (2000) analytical method is based on the Hoek-Brown criteria, so, it is convenient to use for jointed rock masses. However, values of many parameters are based on the GSI. Thus small mistakes in estimation of the GSI may lead to a significant difference in the results. Duncan-Fama (1993) analytical solution is more straight forward in case of less jointed or massive rock mass condition. It uses deformation modulus (E_{rm}), internal friction angle (φ), compressive strength (σ_c) and Poisson's ratio (υ). All these parameters can be directly determined by laboratory tests for a massive rock mass condition. However, for a jointed rock mass condition, all these parameters have to be estimated by using empirical method or 'RocLab' software.

3) Based on the 66 cases from 15 countries, it has been observed that weak rocks are more vulnerable to the squeezing even with small overburden depths, whereas stronger rocks sustain comparatively higher overburden before it squeezes. However, there are some squeezing cases in strong rocks with small overburden, and they might have been caused by the valley side effect of the topography.

4) Numerical modelling gives visual presentation of the stress and the deformation situation and their locations in the tunnel. Thus it is very useful to recognise the critical locations in the tunnel section.

9.1.2 Khimti squeezing tunnel

1) It was observed that squeezing is significantly larger in the weaker rocks (such as schist) than that in the stronger rocks (such as gneiss) though they have similar Q-values. Rock type (corresponding to rock mass strength) is not considered in the Q-system. However, it has been observed that squeezing is sensitive to the rock mass strength.

2) The 7.9 km long Khimti headrace tunnel have been analysed at the 26 tunnel sections from where tunnel convergences data have been available. Both, Singh et al. (1992); and Goel (1994) squeezing criteria, provided more than 80% accuracy in defining the non-squeezing tunnel sections. There is an agreement (difference within 10 mm) between the analytically calculated and the measured convergences in 14 out 26 tunnel sections. Significant differences (difference more than 50 mm) in convergences exist in three sections only. Thus good agreement has been observed in the convergences obtained by the analytical and measured values. Similarly, there is an agreement (difference within 10 mm) between the simulated and the measured convergences in 13 out 26 tunnel sections. Significant differences (difference more than 50 mm) in those convergences exist in four sections only. So these approaches have been used for the stability analysis and the support design of the Melamchi tunnel. Hoek and Marinos (2000) semi-analytical approach resulted with an agreement (difference within 10 mm) for 12 out 26 tunnel sections. Significant differences (difference more than 50 mm) in convergences exist in five sections. This approach has found to be comparatively conservative.

3) In the analysis of the Khimti tunnel squeezing, significant convergence took place in two sections where it was not suspected by both available squeezing prediction criteria. Moreover, the tunnel supports were provided in those sections. It had happened where the maximum topographical height was significantly higher than the vertical overburden above the tunnel. Thus it might have been caused by the valley-side effect of the topography. The valley side slope was 22˚ which is very close to the criteria for the rule of thumb for predicting stress induced problems.

9.1.3 Melamchi tunnel assessment

1) Melamchi tunnel stability assessment has been carried out by using empirical, semi-analytical and analytical approaches. The tunnel stability was also assessed by using the FLAC^{3D} numerical code. There is a very good agreement in tunnel deformation (without time-effect) obtained by the analytical and the modelling for all 6 stress conditions.

2) Based on the creep test results, the critical stress level for the Melamchi augen gneiss intact rock from the bore hole TDH1, has been found to be 20 MPa. The average UCS was 39 MPa. Thus the tangential stress above the critical level may lead to failure even if it does not exceed the rock mass strength.

3) The strain-time curves have been calibrated to obtain the rheological parameters. Based on these parameters, tunnel deformations have been estimated by FLAC^{3D} code including time-effect. The tunnel deformations obtained by FLAC^{3D} are larger than that obtained by the analytical method and numerical modelling when the time-effect was not considered.

4) An attempt was made to obtain a complete stress-strain curve for the Melamchi augen gneiss from the bore hole TDH1. However, such curve could not be obtained for the uniaxially loaded condition. It was therefore obtained with the confining pressures of 1.5 MPa and 3 MPa.

9.2 Recommendations

1) In order to assess the stability and to design support for a tunnel potentially subjected to squeezing, empirical, semi-analytical and analytical methods are recommended. As far as possible, more than one methods should be used so that results can be compared.

2) Carranza-Torres & Fairhurst (2000) analytical method is convenient for assessing the tunnel stability in a jointed rock mass. The Duncan-Fama (1993) analytical solution is recommended for assessing the tunnel stability in a less jointed rock mass as the rock mass parameters can be directly obtained from the laboratory test. Goel (1994) squeezing prediction criteria can be used for preliminary assessment of potential squeezing condition in tunnel.

3) For a big and other than circular tunnel, numerical method is strongly recommended to supplement the analytical calculations. The main advantage of this method is to recognise the critical locations in tunnel in terms of stress situation and deformation magnitude.

4) In the analysis of the Khimti tunnel squeezing, valley-side effect of the topography has been observed. The valley side slope was 22˚. This effect is not considered in none of the available squeezing prediction criteria. A further study is recommended to correlate the valley side slope and maximum topographical height with the stress increase in the tunnel.

5) Based on the 66 tunnel squeezing cases from around the world and the Khimti case study, in order to predict squeezing, rock mass strength should also to be considered in addition to the rock mass classification.

References

Anagnostou, G. and Kovari, K. 1993. Significant parameters in elastoplastic analysis of underground openings. *ASCE J. Geotech. Eng. Div.* 119(3), pp 401-419.

ASTM standard test method for Creep of cylindrical Hard Rock Core Specimens in Uniaxial Compression. 1985. D 4341-84.

Aydan, O., Akagi, T. and Kawamoto, T. 1993. The squeezing potential of rocks around tunnels; theory and prediction. *Rock Mech. Rock Engng*, 26(2), pp 137-163.

Aydan, O., Akagi, T. and Kawamoto, T. 1996. The squeezing potential of rock around tunnels: theory and prediction with examples taken from Japan. *Rock Mech. Rock Engng*, 29(3), pp 125-143.

Barla, G. 2001. Tunnelling under squeezing rock conditions. A paper available on website: www.polito.it. 96 p, 17/03/03.

Barla, G. 1995. Squeezing rocks in tunnels. *ISRM News Journal*, 3/4, pp 44-49.

Barton, N., Lien, R. and Lunde, J. 1974. Engineering classification of rock masses for the design of rock support. *Rock Mechanics*, Vol. 6, pp 189-236.

Bieniawski, Z. T. 1989. Engineering rock mass classifications. John Wiley and Sons, New York. 251p.

Brace, W. F. and Martin, R. J. 1968. A test for the law of effective stress for crystalline rocks of low porosity. *Int. J. Rock Mech. Min. Sci.* 5, pp 415-426.

Brady, B.H.G. and Brown, E.T. 1985. Rock mechanics for underground mining. George Allen & Unwin.

Brantmark, J and Stille, H. 1996. Prediction of squeezing pressure on the Uri Project, Kashmir, India. Proc. ISRM int.symp. Eurock 96., Vol. 2, pp 1025-1032., Turin.

Brantmark, J. 1998. Rock support in weak rock - A study based on the Uri project. Ph D thesis, Royal institute of technology, Sweden.

Broch, E. 1974. The influence of water on some rock properties. Proc. 3rd Congress, ISRM, Denver 74(2), Part A, pp 33-38.

Broch, E. and Sorheim, S. 1984. Experiences from the planning, construction and supporting of a road tunnel subjected to heavy rockbursting. *Rock Mech. and Rock Engng.*, Vol. 17, pp 15-35.

Broch, E. 1988. Site investigations. Norwegian tunnelling today, Tapir publication, Trondheim, Norway, pp 49-52.

Broch, E. 1996. Rock engineering projects outside Scandinavia. RIL K177-1996 Suomen Rakennusinsinoorien Liitto RIL r.y. pp 7-25.

Broch, E., Myrvang, A. M. and Stjern, G. 1996. Support of large rock caverns in Norway. *Tunnelling and Underground Space Technology*, Vol. 11, No. 1, pp 11-19.

Broch, E. 1999. The past, present and future of rock tunnelling. ITA open session, World Tunnelling Congress, Oslo, Norway.

Brown, E. 1981. Putting the NATM into perspective. *Tunnels and Tunnelling*, November, 1981, pp 13-17.

Butwal Power Company Pvt. Ltd.(BPC). 1993. Khimti Khola Hydroelectric Project, Nepal, Feasibility Study, Final Report, Vol. 1.

Butwal Power Company Ltd.(BPC). 1996. Technical Assistance to Melamchi Diversion Scheme, Bankable Feasibility Study. Final Report, Vol. 2, BPC Hydroconsult, Nepal.

Butwal Power Company Ltd.(BPC). 2001. Melamchi Diversion Scheme, Structural Geological Study Report.

Cai, M., Kaisar, P. K., Uno, H., Tasaka, Y. and Minami, M. 2003. Estimation of rock mass deformation modulus and strength of jointed hard rock masses using GSI system. *Int. J. Rock Mech. Min., Sci. Article in press*.

Carranza-Torres, C. and Fairhurst, C. 1999. The elasto-plastic response of underground excavations in rock masses that satisfy the Hoek-Brown failure criterion. *Int. J. Rock Mech. Min. Sci. 36*, pp 777-809.

Carranza-Torres, C. and Fairhurst, C. 2000. Application of the convergence-confinement method of tunnel design to rock masses that satisfy the Hoek-Brown failure criteria. *Tunnelling and underground space Technology*,15(2), pp 187-213.

Carranza-Torres, C. 2003. Dimensionless graphical representation of the exact elasto-plastic solution of a circular tunnel in a Mohr-Coulomb material subject to uniform far-field stresses. *Rock Mech. Rock Engng*, 36(3), pp 237-253.

CONSTRADO. 1983. Steel designers' manual. Granada: Constructional and steel research and development organisation.

Dalgic, S. 2002. Tunnelling in squeezing rock, the Bolu tunnel, Anatolian motorway, Turkey. *Engineering Geology*, (67), pp 73-96.

Desai, C. S. and Christian, J. T. 1977. Numerical Methods in Geotechnical Engineering. McGRAW-HILL.

Duncan Fama, M. E. 1993. Numerical modelling of yield zones in weak rocks. In: Hudson, J. A. (ed.), *Comprehensive Rock Engineering*, Pergamon Press, Oxford, Vol 2, pp 49-75.

Dusseault, M. B. and Fordham, C. J. 1993. Time-dependent behaviour of rocks. In: Hudson, J. A. (ed.), *Comprehensive Rock Engineering*, Pergamon Press, Vol 3, pp 119-149.

East Drilling Company Ltd. (EDCO). 2001. Melamchi Diversion Scheme, Geotechnical Investigation Report.

Gioda, G. and Cividini, A. 1996. Numerical methods for the analysis of tunnel performance in squeezing rocks. *Rock Mech. Rock Engng.* 29 (4), pp 171-193.

Goel, R. K. 1994. Correlations for predicting support pressures and closures in tunnels. Ph D thesis, Nagpur University, India.

Goel, R. K., Jethwa U. L. and Paithakan, A.G. 1995. Tunnelling through young Himalayas - a case history of the Maneri - Uttarkashi power tunnel. *Engng. Geol.*, 39, pp 31-44.

Goodman, R. E. 1989. Rock Mechanics. John Wiley & Sons, New York.

Grimstad, E. and Barton, N. 1993. Updating the Q-system for NMT. Proc. Int. Symp. On Sprayed Concrete, Fagernes, Norway 1993.

Grimstad, E. 2000. Squeezing in Lærdal tunnel surprised the tunnel experts (in Norwegian). Proc. FJELLSPRENGNINGSKONFERANSEN/ BERGMEKANIKKDAGEN/ GEOTEKNIKKDAGEN, Oslo, Norway. pp 36.1-36.11

Herget, G. 1988. Stresses in rock. A. A. Balkema, Rotterdam, 179 p.

Hoek, E. and Brown, E. T. 1980. Underground excavations in rock. The Institution of Mining and Metallurgy, London. 527 p.

Hoek, E., Kaiser, P. and Bawden, W. 1995. Support of underground excavations in hard rock. A A Balkema, p 215.

Hoek, E. and Brown, E. T. 1997. Practical estimates of rock mass strength. *Int. J. Rock Mech. & Min. Sci. & Geom. Abstracts. 34(8),* pp 1165-1186.

Hoek, E. and Marinos, P. 2000. Predicting tunnel squeezing problems in weak heterogeneous rock masses. *Tunnels and Tunnelling International*, part one-November, 2000, pp 45-51; part two -December, 2000, p 33-36.

Hoek, E. 2001. Big tunnels in bad rock. *ASCE Journal of Geotechnical and Geoenvironmental Engng, 2000 Terzaghi lecture, Seattle,* pp 726-740.

Hoek, E., Carranza-Torres, C. & Corkum, B. 2002. Hoek-Brown failure criterion – 2002 edition. In R. Hammah, W. Bawden, J. Curran & M. Telesnicki (eds.), Proceedings of NARMS-TAC 2002, Mining innovation and Technology. Toronto – 10 July 2002, pp 267-273. University of Toronto.

Huang, Z. 2001. Stabilizing of rock cavern roofs by rockbolts. A Doctor Ingeniør thesis, Department of Geology and Mineral Resources Engineering, NTNU, Norway. p260.

ISRM. 1999. Draft ISRM suggested method for the complete stress-strain curve for intact rock in uniaxial compression. *Int. J. Rock Mech. Min. Sci. 36*, pp 279-289.

ITASCA Inc. 2002. FLAC ^{3D} Fast Lagrangian Analysis of Continua in 3 dimensions. Version 2.1, FLAC ^{3D} manual.

Jaeger, J. C. and Cook, N. G. W. 1979. Fundamentals of rock mechanics, 3rd edition. Chapman and Hall, London.

John, M., Spondlin, D., Ayaydin, N., Huber, G., Westermayr, H. and Mattle, B. 2005. Means and methods for tunnelling through squeezing ground: A case history of the Strenger tunnel, Austria. Proc. RETC – 2005, USA.

Kitagawa, T., Kumeta, T., Ichijyo, T., Soga, S., Sato, M. and Yasukawa, M. 1991. Application of Convergence Confinement Analysis to the study of preceding displacement of a squeezing rock tunnel. *Rock Mech. Rock Engng*. 24 (1), pp 31-51.

Kobayashi, T., Sato, J. and Kusumoto, F. 2003. Design and excavation of large-scale tunnels in squeezing rock. Proc. (Re)Claiming the underground space, Saveur (ed.).

Kockar, M. K. and Akgun, H. 2003. Methodology for tunnel and portal support design in mixed limestone, schist and phyllite conditions: a case study in Turkey. *Int. J. Rock Mech. Min., Sci. Article in press*.

Kontogianni, V. and Stiros, S. 2002. Prediction and observations of convergence in shallow tunnels: case histories in Greece. *Engineering Geology*, Vol. 63, pp 333-345.

Kovari, K. 1994. On the existence of the NATM: Erroneous concepts behind the New Austrian Tunnelling Method. *Tunnel 1/94*, pp 16-25.

Kovari, K. and Staus, J. 1996. Basic considerations on tunnelling in squeezing ground. *Rock Mech. Rock Engng*., 29(4), pp 203-210.

Kovari, K. 1998. Tunnelling in squeezing rock. *Tunnel 5/98*, May, pp 12-31.

Kovari, K. 2000. Mastering of squeezing rock in the Gotthard Base. *Tunnels and Tunnelling International*, June, pp 234-238.

Ladani, B. 1993. Time-dependent response of rock around tunnels. In: Hudson, J. A. (ed.),*Comprehensive Rock Engineering*, Pergamon Press, Vol 2, pp 78-112.

Lama, R. D. and Vutukuri, V. S.1978. Mechanical properties of rocks, Vol 3. Trans Tech, Rock port, MA.

Lesotho Highlands Development Authority. October 1993. Sixth report of panel of experts, Lesotho Highlands Water Project. Kingdom of Lesotho.

Lesotho Highlands Tunnel Partnership. September, 1993. Lining for overstress – Ngoajane South Drive, Lesotho.

Lesotho Highlands Water Project (LHWP), Volume-1 November 1992. Shani Walis, LASERLINE, UK.

Lesotho Highlands Water Project (LHWP), Volume-3 May 1995. Shani Walis, LASERLINE, UK.

Li, C. C. and Marklund, P. I. 2004. Field tests of the cone bolt in mines of Boliden. Proc. FJELLSPRENGNINGSKONFERANSEN/ BERGMEKANIKKDAGEN/ GEOTEKNIKKDAGEN, Oslo, Norway. pp 35.1-35.12

Londe, P. 1988. Discussion on the determination of the shear stress failure in rock masses. *ASCE J. Geotech. Eng. Div.* 114(3), pp 374-376.

Malan, D. F. 1998. An investigation into the identification and modelling of time-dependent behaviour of deep level excavations in hard rock. Ph D thesis, University of Witwatersrand, South Africa.

Malan, D. F. 2002. Simulating the time dependent behaviour of excavation in hard rock. *Rock Mech. Rock Engng*. 33(4), pp 225-254.

MBT. 2003. Literature available on website of Master Builders Technology: www.ugc.mbt.com. pp 143-144, 10/10/03.

Muller, L. 1978. Removing misconceptions on the New Austrian Tunnelling Method. *Tunnels and Tunnelling*, October, 1978, pp 29-32.

Myrvang, A. M. 1970. Some experiences on the determination of creep properties of rock. Proc. 2nd congress, ISRM, Belgrade, 2-41.

Myrvang, A. M., Alnæs, L., Hansen, S. and Davik, K. 1997. Heavy spalling problems in road tunnels in Norway – long time stability and performance of sprayed concrete as rock support. Proc. International symposium on rock support, Lillehammer, Norway.

Myrvang, A. M. 2003. Class notes on rock stress, Norwegian University of Science & Technology, Trondheim, Norway.

NGI. 1997. Practical use of the Q-method. Norwegian Geotechnical Institute, Oslo, Norway.

Nilsen, B. and Palmstrom, A. 2000. Engineering geology and rock engineering. Handbook No. 2, Norwegian Group for Rock Mechanics (NBG), 249 p.

Norplan AS. 2002. Melamchi Diversion Scheme, Tender documents for tunnel contract. Draft vol. 5.1, section 11 Supplementary information - ground conditions.

Obert, L., and Duvall, W. I. 1967. Rock Mechanics and the design of structures in Rock. John Wiley and Sons, 650 pages.

Palmstrom, A. 2000. Recent developments in estimating rock support by the RMi. *Journal of Rock Mech. and Tunnelling Technology*, vol. 6, May 2000.

Palmstrom, A. and Broch, E. 2005. Use and misuse of rock mass classification systems with particular reference to the Q-system. Submitted for the publication in *Tunnelling and Underground Space Technology*.

Pan, Y. W. and Dong, J. J. 1991. 'Time-dependent Tunnel Convergence-I. Formulation of the model.' *Int. J. Rock Mech. & Min. Sci. & Geom. Abstracts. 28(6),* pp 469-475.

Panet, M. 1996. Two case histories of tunnels through squeezing rocks. *Rock Mech. Rock Engng*. 29(3), pp 155-164.

Park, R. G. 1993. Structural Geology, 2nd Edition. Chapman and Hall, Chapter 7, pp 71-79.

Rocscience, 2002. RocLab software program – free download from the Rocscience website www.rocscience.com.

Rowland, S. M. and Duebendorfer, E, M. 1994. Structural analysis and synthesis, 2nd edition. Blackwell scientific publications, 279 p.

Schubert, W. 1996. Dealing with squeezing conditions in Alpine tunnels. *Rock Mech. Rock Engng*., 29(3), pp 145-154.

Selmer-Olsen, R. and Broch, E. 1977. General design procedure for underground openings in Norway. Proc. Int. symp. ROCKSTORE – 77, Stockholm, pp 219-226.

Sharma, B. 2003. Squeezing assessment for the Melamchi water supply tunnel. Master of science thesis, NTNU, Norway.

Shrestha, G. L. and Thanju, R. 1997. Tunnelling through sheared zones in Likhu tunnel in Melamchi project. Proc. '2nd International course on small hydro development', November, 1997, Kathmandu, Nepal. International association for small hydro.

Shrestha, G., Panthi, K., Holmøy, K., Olsen, V. and Nilsen, B. 2003. Classification comparison; RMR vs Q vs RMi. *Tunnels & Tunnelling International*, May 2003.

Singh, B., Jethwa, J. L., Dube, A. K. and Singh, B. 1992. Correlation between observed support pressure and rock mass quality. *Tunnelling and Underground Space Technology*, 7, pp 59-74.

Singh, M. M. and Bortz, S. A. 1975. Use of special cements in shotcrete. In Use of shotcrete for underground structural support, pp 200-231. New York: American Society of Civil Engineers.

Statkraft Engineering AS and Butwal Power Company Ltd.(BPC). 2001. Khimti1 Hydropower Project, Project completion report.

Steiner, W. 1996. Tunnelling in squeezing rocks: case histories. *Rock Mech. Rock Engng*. 29(4), pp 211-246.

Stillborg, B. 1994. Professional users' handbook for rock bolting. Trans tech Publications.

Sulem, J., Panet, M. and Guenot, A. 1987. 'Closure analysis in deep tunnels' and 'An analytical solution for time-dependent displacement in a circular tunnel'. *Int. J. Rock Mech. & Min. Sci. & Geom. Abstracts. 24(3)*, pp 145-154 and pp 155-164.

Sunuwar, S., Shrestha, G. and O'Neill, B. 1999. Proc. Int. symp. on Engineering geology, hydrogeology, and natural disasters with emphasis on Asia organised by NGS and IAEG. Journal of Nepal Geological Society, 2000, Vol. 22, pp 227-236.

Terzaghi, K. 1946 (revised 1968, reprinted 1977). Rock tunnelling with steel supports. Commercial shearing Inc.

University of Saskatchewan. 2003. Course notes on 'creep' available on website: www.engr.usask.ca. pp 1-2, 07/04/03.

Wahlstrom, E. E. 1973. Tunnelling in rock. Elsevier, 250 p.

Wood, A. M. Muir. 1972. Tunnels for roads and motorways. *Q. J. Eng. Geol.* 5, pp 117-126.

Yamazaki, M., Hironaka, T., Ito, K. and Kato, T. 2003. Tunnelling and countermeasure design in unexpected squeezing rock zone. Proc. (Re)Claiming the underground space, Saveur (ed.).

Yassaghi, A. and Salari-Rad, H. 2005. Squeezing rock conditions at an igneous contact zone in the Taloun tunnels, Tehran-Shomal freeway, Iran: a case study. *Int. J. Rock Mech. Min. Sci. 42*, pp 95-108.

Yu, C. W., Chern, J. C. and Snee, C. P. M. 2000. Creep characteristic of soft rock and creep modelling of tunnel. AITES-ITA 2000 World Tunnel Congress. Durban, South African Institute of Mining and Metallurgy, 2000.

Yukio, K., Kazuyoshi, Y. and Motohiko, T. 2004. Supports for tunnelling in squeezing ground. WTC 2004. *Tunnelling and Underground Space Technology*, Vol. 19.

Appendix A: Rock type and overburden height for squeezing tunnels

S. No.	Country	Tunnel name	Min. overburden (m)	Max overburden (m)	Rock type	Length (m)	Type	Sources
1	Japan	Enrei		110	Mudstone	5994	Rail way	Aydan et al., 1996
2	Japan	Shirasaka-1		150	Mudstone	1296	Rail way	Aydan et al., 1996
3	Japan	Shirasaka-2		150	Mudstone	1765	Rail way	Aydan et al., 1996
4	Japan	Akakura		380	Siltstone, Mudstone	4220	Rail way	Aydan et al., 1996
5	Japan	Mikai		60	Mudstone	1000	Rail way	Aydan et al., 1996
6	Japan	Ibikijo		180	Mudstone	11350	Rail way	Aydan et al., 1996
7	Japan	Siekan		270	Andesite, Tuff, Mudstone	25000	Rail way	Aydan et al., 1996
8	Japan	Nabetachi yama		280	Mudstone	9117	Rail way	Aydan et al., 1996
9	Japan	Nakayama		400	Tuff	14830	Rail way	Aydan et al., 1996
10	Japan	Orizume		200	Tuff and mud stone	2300	Road way	Aydan et al., 1996
11	Japan	Fujishiro		260	Mudstone	1823	Road way	Aydan et al., 1996
12	Japan	Inari		140	Serpentinite, Shale	1441	Road way	Aydan et al., 1996
13	Japan	Komadome		300	Tuff	2000	Road way	Aydan et al., 1996
14	Japan	Shinfuku		200	Mudstone, Tuff	2400	Road way	Aydan et al., 1996
15	Japan	Myojin		250	Tuff, Shale	3700	Road way	Aydan et al., 1996
16	Japan	Eno		170	Andesite	955	Road way	Aydan et al., 1996
17	Japan	Kofuchi		280	Tuff, Serpentinite, Slate, Granite	4555	Road way	Aydan et al., 1996
18	Japan	Enasan		1000	Diorite	8489	Road way	Aydan et al., 1996
19	Japan	Nousie		79	Tuff, Mudstone	2992	Road way	Aydan et al., 1996
20	Japan	Mineoka		90	Shale, Tuff	735	Road way	Aydan et al., 1996
21	Japan	Nigamine II		400	Micaschist	3831	Road way	Aydan et al., 1996

22	Japan	Tagami tunnel: 10.5 m dia	350		Squeezing in 800 m section in sandstone with sandstone blocks.	6988	Rail way	Yamazaki et al., 2003
23	Japan	Fujikawa: 190m2	250	300	Squeezing in 100 m fault section in argillaceous (clayey) crushed zone. Host rocks are sandstone & volcanic tuff breccia.	4500	Rail way	Kobayashi et al., 2003
24	Japan	Jiyoshi	250		Squeezing in foliated and clayey Surpentinite rock with a fault.It had 90% clay minerals including 50% surpentinite.	2990	Road way	Yukio, et al., 2004
25	Austria	Arlberg	150	700	Gneiss (altered), Schist	14000	Road way	Kovari and Staus, 1996; Steiner, 1996
26	Austria	Karawanke	500	800	Schist			Kovari and Staus, 1996
27	Austria	Galgenberg	100	250	Phyllite			Kovari and Staus, 1996
28	Austria	Inntal		300	Phyllite			Kovari and Staus, 1996
29	Austria	Taurn	200	1100	Phyllite	6000	Road way	Kovari and Staus, 1996; Steiner, 1996
30	Austria	Strenger tunnel (twin). Total squeezing length is 2*1250 m.		800	Squeezing in 1250m section, caused sometimes by few meter thick fault and sometimes by schistocity. Host rock is phyllitic mica schist.	5800	Road way	John et al., 2005
31	Italy	Fleres		550	Gneiss (altered)			Kovari and Staus, 1996
32	Italy	San Vitale	50	150	Mudstone			Kovari and Staus, 1996
33	Switzerland	Furka, section 36 m2		1100	Gneiss (altered)	15000	Rail way	Kovari and Staus, 1996; Steiner, 1996
34	Switzerland	Gotthard	1050	1150	Gneiss (altered)			Kovari and Staus, 1996
35	Switzerland	Gotthard		300	Schist			Kovari and Staus, 1996
36	Switzerland	Vereina		700	Mudstone	20000	Rail way	Kovari and Staus, 1996; Steiner, 1996

37	Switzerland	Vereina	350	450	Serpentinite	20000	Rail way	Kovari and Staus, 1996; Steiner, 1996
38	France/Italy	Frejus width 11m	1000	1800	micaceous schist	12570	Road way	Panet, 1996
39	U S A (Utah)	Stillwater		600	Shale	12900	Aqueduct	Steiner, 1996
40	U S A (Colorado)	Moffat	300	350	Schist (sheared)	9830	Road way	Steiner, 1996
41	Algeria	Sidi Mezghiche, x-section 46 m2.		65	flyschs argilites	990	Rail way	Panet, 1996
42	Nepal	Khimti	100	130	Schist (sheared)	8000	Water way	Sunuwar, S., Shrestha, G. and O'Neill, B. 1999.
43	Nepal	Modi	70	90	Phyllitic schist,Quarzite (sheared)	2000	Water way	Author
44	Nepal	Kali Gandaki		620	Phyllite (sheared)	6000	Water way	Author
45	India	Chibro-Khodri Dia 3m.	280		crushed red shale with σcm =0.7 MPa. Strain 2.8%			Hoek, 2001
46	India	Giri-Bata tunnel. Dia 4.2m.	380		Slates with σcm =0.8 MPa.Strain 7.6%			Hoek, 2001
47	India	Giri-Bata tunnel. Dia 4.2m.	240		Phyllites with σcm =0.7 MPa.Strain 9%			Hoek, 2001
48	India	Loktak tunnel. Dia 4.8m.	300		Shale with σcm =0.7 MPa.Strain 7%			Hoek, 2001
49	India	Maneri Bhali stage II. Dia 7m.	410		Sheared metabasics with σcm =3 MPa. Strain 3%			Hoek, 2001
50	India	Maneri Bhali stage II. Dia 2.5m.	480		Metabasics with σcm =3 MPa. Strain 2.5%			Hoek, 2001
51	India	Uri tailrace	400	500	crushed graphitic Schist	2000	Water way	Brantmark, 1998
52	India	Uri tailrace	400	450	shale (eocene)	2000	Water way	Brantmark, 1998

53	India	Maneri-Uttarkashi	700	900	Metabasic (chlorite-schist). Strain 9%	8560	Water way	Goel et al., 1995
54	India	Maneri Bhali stage1		350	Fractured Quartzite. Strain 7.9%			Hoek, 2001
55	Taiwan	Pinglin (35-40 Mpa)	150	200	Argillite	40236	Rail way	
56	Taiwan	Maan headrace		200	Sandstone/Shale			Hoek, 2001
57	Taiwan	Maan Adit A		200	Sandstone/Shale			Hoek, 2001
58	Taiwan	Mucha tunnel		110	Sandstone/Shale			Hoek, 2001
59	Taiwan	Pengshan tunnel		140	Sandstone/Shale			Hoek, 2001
60	Venezuela	Yacambu-Quibor		600	Graphitic Phyllite			Hoek, 2001
61	Norway	Lærdal tunnel	1000		In 500 m thick fault zone with partly fresh and partly weathered Gneiss blocks and clay with 65-80% smectite giving swelling pressure upto 0.6 MPa.Host rock is Precambrian Gneiss.	24500	Road	Grimstad, 2000
62	Turkey	Bolu tunnel (twin): Elmalik Thrust	60	70	Squeezing in clayey fault gorges. Host rock is Flysoid series. Fault is 50m thick.	Approx 3250	Transit European Motor way	Dalgic, 2002
63	Turkey	Bolu tunnel (twin): Asarsuyu Thrust	200		Squeezing in clayey fault gorges and breccia. Host rock is combination of Metasedimentary (Shale & phyllite) & Metacrystalline (Amphibolite & Gneiss). Fault is 150m thick.	Approx 3250	Transit European Motor way	Dalgic, 2002
64	Iran	Taloun service tunnel	300		Squeezing in contact zones of Andesite-basalt & Tuff rocks, mainly in altered and foliated tuff. No Fault. Contact zone is 10m thick but squeezing section is 100m long.	5000	Free Motor way	Yassaghi & Salari-Rad, 2005
65	Greece	Patras by-pass tunnel 1. Dia 10m	20	45	In Soil. Poor qualilty argillaceous marls with sandy intercalation & Ground water. GSI <<20 to 20.	270	By-pass road, Completed 1999	Kontogianni & Stiros, 2002

66	Greece	Patras by-pass tunnel 2. Dia 11m	30		In Soil. Poor qualilty marls with sand & silt. GSI <20.	150	By-pass road, Completed 1998	Kontogianni & Stiros, 2003
67	Canada	Myra Falls Mine		1020	Squeezing occurred upto 60 cm in altered Rhyolite. The section was 60 m from the nearest mining stope.	60 m from stope	Transport drift tunnel	Li & Marklund, 2004

Appendix B: Calibration of strain-time curve for rheological parameters

TDH1 lot2 Sample 412 (79 mm) was tested from December 7 to 8 of 2004 in creep test set up. It was loaded under 20 MPa constant stress level and broke by creeping after 12 hours. The following is the summary of the test results and calculation to calibrate the creep curve for rheological parameters.

Time (Hour)	Micro Strain	q(assimtote-strain line)	Trend line	Calibrated strain line(μ)
0.000	0			3424.684
0.001	3707.595	2212.461	2488.915	3435.824
0.216	4151.899	1776.754	1252.099	4681.201
0.299	4222.785	1709.205	959.0503	4977.576
0.660	5416.456	529.97	302.5692	5648.464
1.159	5913.924	52.4767	61.31749	5909.663
1.660	5965.823	20.63082	12.34929	5978.662
2.159	6013.924	-7.45094	2.493778	6008.514
2.659	6037.975	-11.4821	0.503586	6030.502
3.159	6043.038	3.474126	0.101693	6050.902
3.659	6092.405	-25.8846	0.020554	6070.969
4.159	6062.025	24.51466	0.004151	6090.983
4.659	6103.797	2.762002	0.000838	6110.984
5.159	6127.848	-1.26913	0.000169	6130.982
5.658	6169.62	-23.0329	3.42E-05	6150.969
6.158	6177.215	-10.6083	6.91E-06	6170.967
6.658	6212.658	-26.0319	1.39E-06	6190.964
7.158	6239.241	-32.5947	2.82E-07	6210.962
7.658	6249.367	-22.7129	5.69E-08	6230.948
8.158	6265.823	-19.1491	1.15E-08	6250.946
8.658	6274.684	-7.99034	2.32E-09	6270.944
9.157	6303.797	-17.0959	4.69E-10	6290.93
9.657	6313.924	-7.20297	9.48E-11	6310.928
10.157	6329.114	-2.37335	1.91E-11	6330.925
10.657	6345.57	1.190451	3.86E-12	6350.923
11.157	6367.089	-0.32016	7.81E-13	6370.909
11.657	6384.81	1.977818	1.58E-13	6390.907
12.157	6415.19	-8.38243	3.18E-14	6410.905

Calibration was carried out by following the procedure given by Goodman (1989). By using the data in the table given above, following two curves have been plotted (Figures B1 and B2) and rheological parameters have been calculated.

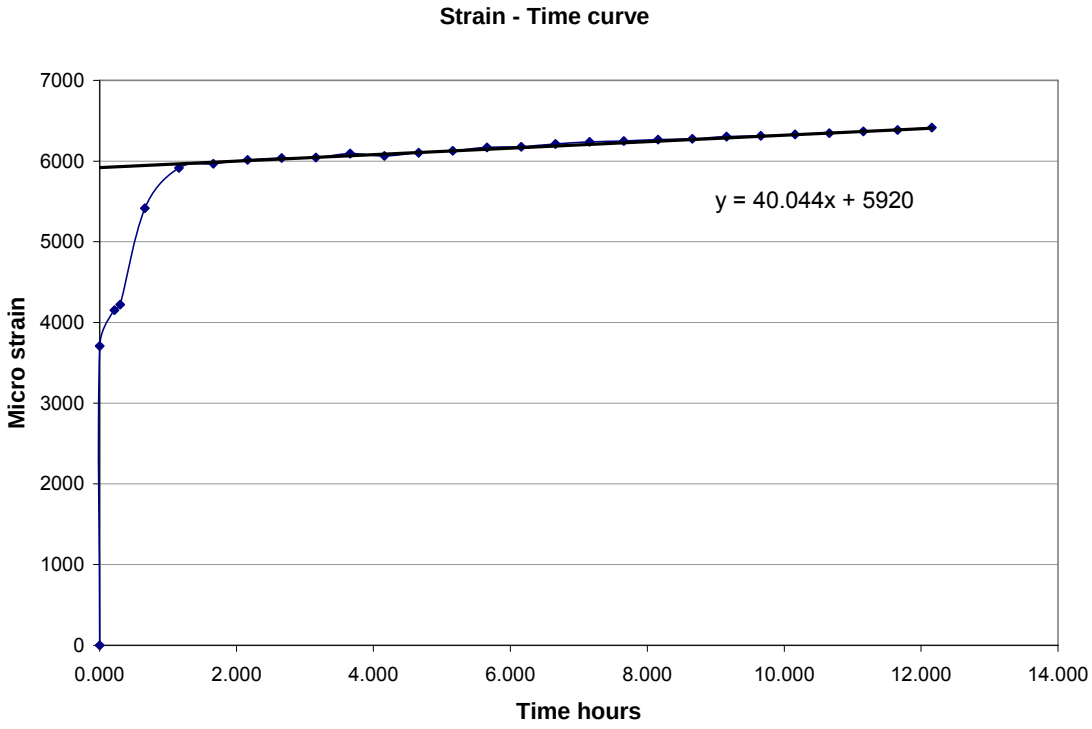

Figure B1 Strain – Time curve with asymptote line to the straight portion of the curve.

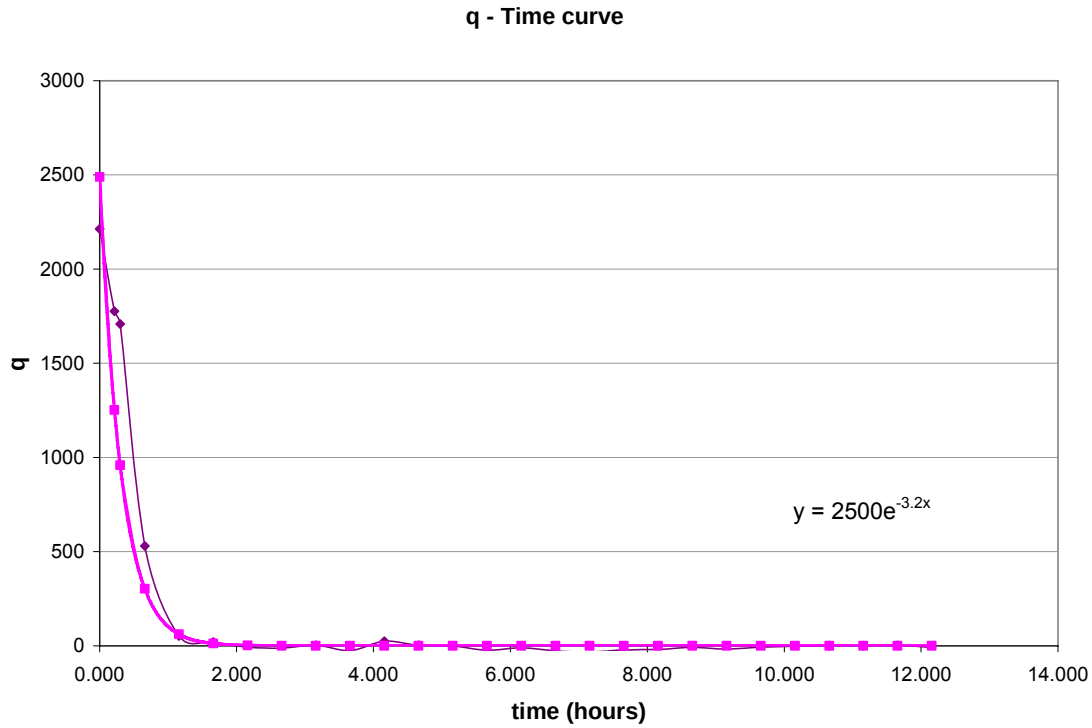

Figure B2 q – Time curve, a part of the calibration of the rheological parameters.

Calculations for the calibration are as follow (with σ_1 = 20 MPa):

1) Assymtote to straight portion of the Strain-Time curve is

y = 40.044x+5920

as the slope of the line is $\sigma_1/3\eta_2$,

$\eta_2 = 1.6648*10^{11}$ Pa.hr

2) We have $q = \frac{\sigma_1}{3G_1} e^{-\frac{G_1 t}{\eta_1}}$ and from the q-Time curve,

$q = 2500\ e^{-3.2x}$

Thus, $\sigma_1/3G_1 = 2500$ giving $G_1 = 2.6667*10^9$ Pa

and $G_1/\eta_1 = 3.2$ giving $\eta_1 = 0.8333*10^9$ Pa.hr

3) We also have $\frac{\sigma_1}{3G_2} = \varepsilon_B - \sigma_1\left(\frac{1}{3G_1} + \frac{2}{9K}\right)$ and $K = 1.925*10^{10}$ Pa (calculated from E = 33.5 10^9 Pa and $\upsilon = 0.21$),

By using the above mentioned equation, we get $G_2 = 2.0871*10^9$ Pa

Using the calibrated values for Rheological parameters, G_1, G_2, η_1 & η_2, Strain-Time curves are drawn and found to be similar to the true curve showing good calibration.

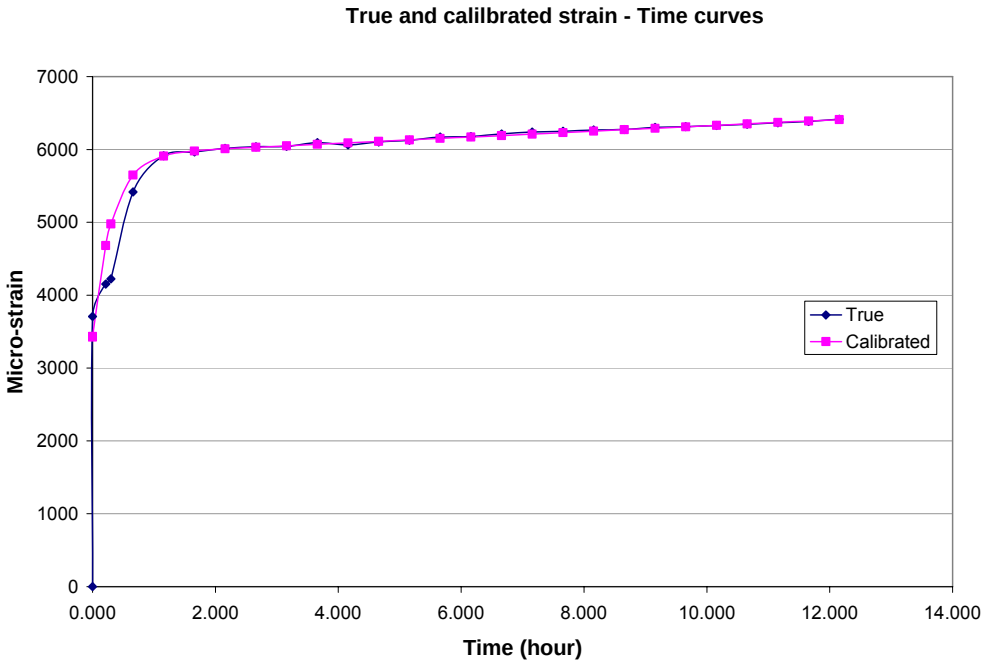

Figure B3 True and calibrated Strain – Time curves.

Appendix C: Data files for FLAC^{3D} Commands

1) Data file for Khimti tunnel without considering time-effect.

```
;Khimti tunnel stability analysis by FLAC 3D version 2.1
;Its geometry includes 2 blocks and reflection. It analyses lined tunnel with mohr model
;only
;
title 'Khimti tunnel with mohr model Adit1 d/s 475m'
;
;Generating lower part of the tunnel - rectangular
gen zone radtun p0 0 0 0 p1 0 0 -22 p2 0 24 0 p3 22 0 0 &
size 2 24 2 8 ratio 1 1 1 1.2 dim 2 2 fill
plot surf yellow
;
;Generating upper part of the tunnel - circular
gen zone radcyl p0 0 0 0 p1 22 0 0 p2 0 24 0 p3 0 0 22 &
dim 2 2 2 2 ratio 1 1 1 1.2 size 2 24 4 8 fill
gen zone reflect dip 90 dd 90
;
range name recttun x=-2,2 y=0,24 z=-2,0
group circtun range cyl end1 0,0,0 end2 0,24,0 rad 2
;mohr model to see immediate effect after excavation
mod mohr
prop shear 0.416e9 bulk 0.555e9 coh 0.47e6 fric 31.6 ten 0.002e6
pause
;boundary and initial conditions
apply szz -2.55e6 range z 21.9 22.1
pause
fix z range z -22.1 -21.9
fix x range x -22.1 -21.9
fix x range x 21.9 22.1
fix y range y -0.1 0.1
fix y range y 23.9 24.1
ini sxx -2.55e6 syy -2.55e6 szz -2.55e6
hist n=10
hist unbal
hist gp xdis 2,12,0
hist gp zdis 2,12,0
hist gp zdis 0,12,2
hist gp zvel 0,12,2
hist zone szz 2.1,12,0
hist zone szz 4,12,0
solve
pause
;
```

```
;Excavate 24m long tunnel
model null range recttun
model null range group circtun
pause
;
;Lining information
sel shell id=1 range cyl end1 0 0 0 end2 0 24 0 rad 2
sel shell prop iso=(30.0e9,0.25) thick=0.1
sel node fix y xr zr range y -0.1 0.1
sel node fix y xr zr range y 23.9 24.1
sel liner id=2 range x=1.9,2.1 y=0,24 z=-2,0
sel liner id=3 range x=-2.1,-1.9 y=0,24 z=-2,0
sel liner prop iso=(30.0e9,0.25) thick=0.1
sel node fix y xr zr range y -0.1 0.1
sel node fix y xr zr range y 23.9 24.1
pause
sel cable beg 2,1.5,0 end 4.3,1.5,0
sel cable beg 1.41,1.5,1.41 end 3.04,1.5,3.04
sel cable beg 0,1.5,2 end 0,1.5,4.3
sel cable beg -1.41,1.5,1.41 end -3.04,1.5,3.04
sel cable beg -2,1.5,0 end -4.3,1.5,0
;
sel cable beg 2,3,0 end 4.3,3,0
sel cable beg 1.41,3,1.41 end 3.04,3,3.04
sel cable beg 0,3,2 end 0,3,4.3
sel cable beg -1.41,3,1.41 end -3.04,3,3.04
sel cable beg -2,3,0 end -4.3,3,0
;
sel cable beg 2,4.5,0 end 4.3,4.5,0
sel cable beg 1.41,4.5,1.41 end 3.04,4.5,3.04
sel cable beg 0,4.5,2 end 0,4.5,4.3
sel cable beg -1.41,4.5,1.41 end -3.04,4.5,3.04
sel cable beg -2,4.5,0 end -4.3,4.5,0
;
sel cable beg 2,6,0 end 4.3,6,0
sel cable beg 1.41,6,1.41 end 3.04,6,3.04
sel cable beg 0,6,2 end 0,6,4.3
sel cable beg -1.41,6,1.41 end -3.04,6,3.04
sel cable beg -2,6,0 end -4.3,6,0
;
sel cable beg 2,7.5,0 end 4.3,7.5,0
sel cable beg 1.41,7.5,1.41 end 3.04,7.5,3.04
sel cable beg 0,7.5,2 end 0,7.5,4.3
sel cable beg -1.41,7.5,1.41 end -3.04,7.5,3.04
sel cable beg -2,7.5,0 end -4.3,7.5,0
;
sel cable beg 2,9,0 end 4.3,9,0
```

```
sel cable beg 1.41,9,1.41 end 3.04,9,3.04
sel cable beg 0,9,2 end 0,9,4.3
sel cable beg -1.41,9,1.41 end -3.04,9,3.04
sel cable beg -2,9,0 end -4.3,9,0
;
sel cable beg 2,10.5,0 end 4.3,10.5,0
sel cable beg 1.41,10.5,1.41 end 3.04,10.5,3.04
sel cable beg 0,10.5,2 end 0,10.5,4.3
sel cable beg -1.41,10.5,1.41 end -3.04,10.5,3.04
sel cable beg -2,10.5,0 end -4.3,10.5,0
;
sel cable beg 2,12,0 end 4.3,12,0
sel cable beg 1.41,12,1.41 end 3.04,12,3.04
sel cable beg 0,12,2 end 0,12,4.3
sel cable beg -1.41,12,1.41 end -3.04,12,3.04
sel cable beg -2,12,0 end -4.3,12,0
;
sel cable beg 2,13.5,0 end 4.3,13.5,0
sel cable beg 1.41,13.5,1.41 end 3.04,13.5,3.04
sel cable beg 0,13.5,2 end 0,13.5,4.3
sel cable beg -1.41,13.5,1.41 end -3.04,13.5,3.04
sel cable beg -2,13.5,0 end -4.3,13.5,0
;
sel cable beg 2,15,0 end 4.3,15,0
sel cable beg 1.41,15,1.41 end 3.04,15,3.04
sel cable beg 0,15,2 end 0,15,4.3
sel cable beg -1.41,15,1.41 end -3.04,15,3.04
sel cable beg -2,15,0 end -4.3,15,0
;
sel cable beg 2,16.5,0 end 4.3,16.5,0
sel cable beg 1.41,16.5,1.41 end 3.04,16.5,3.04
sel cable beg 0,16.5,2 end 0,16.5,4.3
sel cable beg -1.41,16.5,1.41 end -3.04,16.5,3.04
sel cable beg -2,16.5,0 end -4.3,16.5,0
;
sel cable beg 2,18,0 end 4.3,18,0
sel cable beg 1.41,18,1.41 end 3.04,18,3.04
sel cable beg 0,18,2 end 0,18,4.3
sel cable beg -1.41,18,1.41 end -3.04,18,3.04
sel cable beg -2,18,0 end -4.3,18,0
;
sel cable beg 2,19.5,0 end 4.3,19.5,0
sel cable beg 1.41,19.5,1.41 end 3.04,19.5,3.04
sel cable beg 0,19.5,2 end 0,19.5,4.3
sel cable beg -1.41,19.5,1.41 end -3.04,19.5,3.04
sel cable beg -2,19.5,0 end -4.3,19.5,0
;
```

```
sel cable beg 2,21,0 end 4.3,21,0
sel cable beg 1.41,21,1.41 end 3.04,21,3.04
sel cable beg 0,21,2 end 0,21,4.3
sel cable beg -1.41,21,1.41 end -3.04,21,3.04
sel cable beg -2,21,0 end -4.3,21,0
;
sel cable beg 2,22.5,0 end 4.3,22.5,0
sel cable beg 1.41,22.5,1.41 end 3.04,22.5,3.04
sel cable beg 0,22.5,2 end 0,22.5,4.3
sel cable beg -1.41,22.5,1.41 end -3.04,22.5,3.04
sel cable beg -2,22.5,0 end -4.3,22.5,0
;
sel cable prop emod 210e9 ytens 1e5 xcarea 3.14e-4 &
gr_coh 2e5 gr_k 33e6 gr_per 1.0
solve
pause
;plotting results
plot hist 2,3 4
plot set title text '2 displacements at sidewall and 1 at crown'
pause
plot hist 1
plot set title text 'unbal force ratio'
pause
plot hist 5
plot set title text 'z-displacement velocity at crown'
pause
plot hist 6,7
plot set title text 'stress zz at side wall & same at 4m inner'
```

2) Data file for Melamchi tunnel without considering time-effect.

```
;MDS tunnel (with GSI 45) stability analysis by FLAC 3D version 2.1
;Its geometry includes 1 block and double reflection.
;It analyses creep effect for unlined circular tunnel with mohr model only.
;
title 'Melamchi tunnel with mohr model SAMPLE45 GSI45 with no time effect'
;
;Generating the tunnel - circular
gen zone radcyl p0 0 0 0 p1 22 0 0 p2 0 24 0 p3 0 0 22 &
dim 2.5 2.5 2.5 2.5 ratio 1 1 1 1.2 size 2 24 4 8 fill
plot surf
gen zone reflect dip 0 dd 90
gen zone reflect dip 90 dd 90
;
group circtun range cyl end1 0,0,0 end2 0,24,0 rad 2.5
;mohr model to see immediate effect after excavation
mod mohr
prop shear 1.935e9 bulk 2.691e9 coh 2.33e6 fric 36.21 ten 0.027e6
pause
;boundary and initial conditions
apply szz -8.1e6 range z 21.9 22.1
pause
fix z range z -22.1 -21.9
fix x range x -22.1 -21.9
fix x range x 21.9 22.1
fix y range y -0.1 0.1
fix y range y 23.9 24.1
ini sxx -8.1e6 syy -8.1e6 szz -8.1e6
hist n=10
hist unbal
hist gp xdis 2.5,12,0
hist gp xdis -2.5,12,0
hist gp zdis 2.5,12,0
hist gp zdis 0,12,2.5
hist gp zvel 0,12,2.5
hist zone szz 2.55,12,0
hist zone szz 5,12,0
solve
pause
;
;Excavate 24m long tunnel
model null range group circtun
solve
pause
;plotting results
plot hist 1
```

```
plot set title text 'Unbalanced force'
Pause
plot hist 2,3
plot set title text 'Tunnel wall displacements after null'
pause
plot hist 4 5
plot set title text 'z-displacement at wall and crown after null'
pause
plot hist 6
plot set title text 'z-dispvelocity at crown after null'
pause
;checking creep causing vertical stresses
plot hist 7 8
plot set title text 'stress zz at wall and 2.5m inside after null'
```

3) Data file for Melamchi tunnel with time-effect.

```
;MDS tunnel (with GSI 45) stability analysis by FLAC 3D version 2.1
;Its geometry includes 1 block and double reflection.
;It analyses creep effect for unlined circular tunnel with mohr & burger model.
;
title 'Melamchi tunnel with mohr burger model SAMPLE45 GSI45 with time effect'
;
config creep
;Generating the tunnel - circular
gen zone radcyl p0 0 0 0 p1 22 0 0 p2 0 24 0 p3 0 0 22 &
dim 2.5 2.5 2.5 2.5 ratio 1 1 1 1.2 size 2 24 4 8 fill
plot surf
gen zone reflect dip 0 dd 90
gen zone reflect dip 90 dd 90
;
group circtun range cyl end1 0,0,0 end2 0,24,0 rad 2.5
;mohr model to see immediate effect after excavation
mod mohr
prop shear 1.935e9 bulk 2.691e9 coh 2.33e6 fric 36.21 ten 0.027e6
pause
;boundary and initial conditions
apply szz -8.1e6 range z 21.9 22.1
pause
fix z range z -22.1 -21.9
fix x range x -22.1 -21.9
fix x range x 21.9 22.1
fix y range y -0.1 0.1
fix y range y 23.9 24.1
ini sxx -8.1e6 syy -8.1e6 szz -8.1e6
hist n=10
hist unbal
hist gp xdis 2.5,12,0
hist gp xdis -2.5,12,0
hist gp zdis 2.5,12,0
hist gp zdis 0,12,2.5
hist gp zvel 0,12,2.5
hist zone szz 2.55,12,0
hist zone szz 5,12,0
hist crtime
solve
pause
;
;Excavate 24m long tunnel
model null range group circtun
solve
pause
```

```
;plotting results
plot hist 1
plot set title text 'Unbalanced force'
Pause
plot hist 2,3
plot set title text 'Tunnel wall displacements after null'
pause
plot hist 4 5
plot set title text 'z-displacement at wall and crown after null'
pause
plot hist 6
plot set title text 'z-dispvelocity at crown after null'
pause
plot hist 7 8
plot set title text 'stress zz at wall and 2.5m inside after null'
pause
;burger model to see time-dependent deformation (creep effect)
mod burger
prop bu 19.25e9
prop mshear 3.027e9 mvisc 22.425e11
prop kshear 5.4054e9 kvisc 63.593e8
plot surf
pause
;once prop is changed excavation to be done again
model null range group circtun
solve
pause
;reset velocities to zero
ini xvel 0 yvel 0 zvel 0
;viscous behaviour
set creep lfob=1e-4 ufob=5e-4 lmul=1.1 umul=0.9 min=1e-2 max=5
set creep dt auto on
solve age=24
;as viscosity unit is in pa hour, age (t) will be in hour
;
;plotting results
plot hist 2,3 vs 9
plot set title text 'X-displacements of tunnel wall after creep'
pause
plot hist 1 vs 9
plot set title text 'Unbalanced force'
pause
plot hist 4,5 vs 9
plot set title text 'Z-displacements of tunnel wall & crown after creep'
pause
plot hist 6 vs 9
plot set title text 'Z-dispvelocity of crown after creep'
```

```
pause
;checking creep causing vertical stresses with time
plot hist 7,8 vs 9
plot set title text 'Stress zz at wall and 2.5 m inside after creep'
```